DESIGN OF SECONDARY VOLTAGE AND STABILITY CONTROLS WITH MULTIPLE CONTROL OBJECTIVES

A Dissertation
Presented to
The Academic Faculty

by

Yang Song

In Partial Fulfillment
of the Requirements for the Degree
Doctorate of Philosophy in the
School of Electrical & Computer Engineering

Georgia Institute of Technology
August 2009

DESIGN OF SECONDARY VOLTAGE AND STABILITY CONTROLS WITH MULTIPLE CONTROL OBJECTIVES

Approved by:

Dr. Miroslav Begovic, Advisor
School of Electrical & Computer Engineering,
Georgia Institute of Technology

Dr. Ronald Harley
School of Electrical & Computer Engineering,
Georgia Institute of Technology

Dr. Deepak Divan
School of Electrical & Computer Engineering
Georgia Institute of Technology

Dr. Jeff S. Shamma
School of Electrical & Computer Engineering
Georgia Institute of Technology

Dr. Shijie Deng
School of Industrial and Systems Engineering
Georgia Institute of Technology

Frank Lambert
School of Electrical & Computer Engineering
Georgia Institute of Technology

Date Approved: May 21st, 2009

ACKNOWLEDGEMENTS

Through my Ph.D education at Georgia Tech, I have built a solid foundation for my future professional life. My five years of Ph.D study is fully sponsored by NEETRAC (National Electric Energy Testing Research and Applications Center) and directed by my advisor Dr. Miroslav Begovic.

I would like to express my deep gratitude for my advisor Professor Miroslav M. Begovic, who has spent great amount of time and energy in advising my research directions, reviewing my articles, encouraging my study progress. Through the time spent with him, I gained more thorough vision of the power industry, learned how to think creatively and analytically, built the confidence to tackle complex engineering problems. I would also like to extend my gratitude to Professor Ronald G. Harley and Deepak M. Divan for serving on my PhD defense committee and for their valuable suggestions.

I am extremely grateful for the support from all the NEETRAC personnel, especially Mr. Frank Lambert and Dr. Caryn Riley. Because of their unconditional support, I have gained valuable experience through all kinds of industrial research and development projects. I appreciate the supervisory from Mr. Frank Lambert and Dr. Caryn Riley during my work in NEETRAC. I owe my special thanks to Mr. Ray Hill, Larry Coffeen, Boyd Pettitt, and David Harwell for their help during my work in NEETRAC, and above all their friendship. My appreciate Mr. Robert C. Boozer, Al W.

Turner for their management of my status in NEETRAC. I have been so proud and will always remember that I was a member in NEETRAC**.**

Most of all, I would like to thank all my family members, including my Parents, my wife Line Xu, my lovely son Nathan J. Song, my in-laws for their unconditional love, understanding, and encouragement. I will always keep the precious friendship received from Dr. Wei Zhou, Wei Qiao, Jean Carlos, Harjeet Johal, Yi Yang, Yi Du, Yao Duan, Pinjia Zhang.

TABLE OF CONTENTS

Page

LIST OF TABLES

Page

LIST OF FIGURES

Page

SUMMARY

The purpose of the proposed research is to design a Decentralized Voltage/Stability Monitoring and Control System to counteract voltage violations and the impact of disturbances/contingencies on power system voltage stability. A decentralized voltage and stability control system is designed to coordinate the controls of the local secondary voltage control devices and necessary load shedding without requiring information about the rest of the system.

A brief review of the voltage stability monitoring and control applications in power systems is presented. The existing secondary voltage control applications rely on the automatic/manual control of individual secondary voltage control devices whose time constants are approximately three minutes in length. The design of a fast secondary voltage/stability control system is important to mitigate the impact of disturbances on system stability. A literature survey of the applications in the Wide Area Measurement System (WAMS) is performed. Based on the infrastructure of the WAMS, upgrades in voltage and stability controls are one of the most important options.

The voltage/stability control can be formulated as a multi-objective optimization problem. The control objectives include, but are not limited to: minimization of system active/reactive losses; maximization of the system stability margin; and minimization of the control actions. The constraints of the optimization problem depend on the specifications of the actual system components.

For the first time, margin sensitivities of the control actions are included in the control formulation. The concept of using margin sensitivity to evaluate the post-control load margin is presented as a fast and accurate way to assess potential voltage and stability control options. A system decomposition procedure is designed to define the disturbance-affected zone as an independent control subsystem. A normal constraint algorithm is adopted to identify the most suitable control solution in a shorter timeline than the typical utility voltage-control practice. Both steady-state and dynamic simulations are performed to compare the proposed system with typical utility control practices.

CHAPTER I

INTRODUCTION

The electricity demands of industry and residents have increased greatly over the past decades and are expected to grow even faster in the future. Under the economic pressure on the electricity market, the trend in power system planning utilizes tight operating margins, with less redundancy. Although the trend of deregulation has been emphasized on system efficiencies, cost reductions and power quality and profitability, more concerns should be placed on system stability. A constant and reliable power supply is becoming more and more essential for society, while blackouts [1] are becoming more and more costly, whenever they occur.

Currently, the secondary voltage control practices in many power utilities aim at maintaining voltage magnitude within the required band. The monitoring and optimizing of the voltage stability margin has not commonly been associated with the routine secondary voltage controls. The secondary voltage control applications rely on the automatic/manual control of individual secondary voltage control devices.

The automatic operation of LTCs, an important secondary voltage control device, has been known as a potential source of deterioration of the voltage stability margin. The conventional manual control operations of shunt capacitor banks are performed based on the operator's past experience or rigid operation manual. When a system encounters disturbances/contingencies under stressful conditions, fast and regionally coordinated

control decisions need to be made within limited time frame. The design of a fast secondary voltage/stability control system is important to mitigate the impact of disturbances on power system stability.

Advanced communication technology and measurement synchronization have made the design of real-time system-wide protection possible. The phasor measurement unit (PMU) can provide us with accurate and near real-time data which provides new possibilities for wide-area monitoring. New application of voltage/stability controls could be considered as one of the most important functions in the wide area measurement system (WAMS). The performance of an online voltage stability monitoring technique—the voltage instability oredictor (VIP) is studied under different system conditions (such as load ramping, fast dynamics etc). The criteria of choosing VIP parameters (such as sampling frequency, window size and forgetting factors) are presented to enhance the accuracy and adaptability of the VIP. A dynamic VIP method is presented to adaptively adjust the VIP parameters according to the changes of system conditions.

Based on the combination of monitoring data from SCADA and PMUs at critical nodes, the proposed voltage/stability monitoring and control system is in a decentralized structure. The system aims at providing fast and coordinated secondary control decisions in the time range from several seconds to a few minutes. Such secondary level control decisions can also be integrated into a tertiary level suboptimal control decision. Instead of performing control analysis based on the entire system model, the control region of the voltage/stability control system is designed to be adaptive to different disturbances. By separating the control zone from the rest of the system, an independent subsystem model

could be constructed. The secondary voltage/stability control problem can be formulated based on the subsystem model.

The voltage/stability control can be formulated as a multi-objective optimization problem. The control objectives in a local control zone may include, but are not limited to, minimum system active/reactive losses, secondary control actions and load shedding and maximum stability margin. The margin sensitivities of secondary voltage controls and load shedding are utilized to assess the performance of different control combinations in achieving the objective of maximum stability margin. The constraints of the optimization problem include equality constraints corresponding to AC power flow balance equations, and inequality constraints specified by the capacity of the actual system components. Depending on different system conditions, such as normal low voltage condition, emergency low voltage and voltage drop condition, extreme unsecured contingency condition, different combinations of control objectives and constraints can be conveniently adopted to obtain the suitable voltage and stability control solution. The performance of the decentralized voltage and stability solutions are compared with conceptual utility control solutions and optimal power flow (OPF) solutions.

1.1 THESIS OVERVIEW

Chapter II introduces the definition of voltage stability problems, the voltage and voltage stability controls in power utilities, and the research on wide-area stability monitor and controls.

Chapter III reviews the local voltage stability monitoring approaches, focusing on the dominant technique—the Voltage Instability Predictor (VIP). The performances of

different VIP methods (the Least Square method and recursive method) are studied under quasi-steady state and dynamic environments. The selection of appropriate VIP method and the associated parameters are suggested based on the analysis of simulation results. A dynamic VIP routine is designed to enhance the accuracy and sensitivity of the VIP in time-domain application, where the interference of disturbances/contingencies needs to be addressed.

In Chapter IV, the margin sensitivities of the secondary voltage control devices, as well as emergency load shedding control, are computed by adopting Dobson's algorithm and benchmarked with the actual margin sensitivity computed by iterative power flow method. The linear combination of the margin sensitivities of different control resources will enable the direct estimation of the increased load margin. The redundant or insufficient stability controls should be avoided. Benchmark simulations are conducted on the 39-bus system to compare the margin sensitivities obtained by Dobson's algorithm with the conventional iterative power flow analysis. It has been assessed that the margin sensitivities of the shunt capacitor banks controls and load shedding can be accurately estimated by Dobson's algorithm.

Chapter V presents the problem formulation to solve for stability constrained secondary voltage control solutions. The formulation of the security constrained reactive resource planning (RRP) is reviewed and solved for the IEEE 39-bus system. The voltage and stability control of a power system is formulated as a multiple-objective optimization problem. Normal constraint algorithm is adopted to explore the Pareto solutions of the multiple-objective optimization problem. According to the optimal control solutions, the

majority of secondary voltage controls are performed in the vicinity of buses with voltage violations when the objective of minimum control actions is restricted.

Chapter VI presents the idea of decentralized voltage and stability control. The introduction of the framework of the decentralized control system is followed by the description of the function entities, including system decomposition, control formulation and optimization. The identification of the disturbance-affected zone is decided by the propagation of voltage changes caused by disturbances/contingencies. A tier-wised network model is presented to explain the propagation of a local reactive disturbance. Three types of boundary models (PV, PQ and Voltage-controlled models) are adopted on the boundary of the disturbance-affected zone to terminate the disturbance-affected zone from the external network, which resemble the original propagation pattern of the detected disturbances/contingencies. The performance of the proposed decentralized voltage and stability control solutions are compared with typical utilities control solutions and OPF solutions in solving voltage control problems under different system conditions, such as normal low voltage condition, emergency low voltage and voltage drop condition, and unsecured instability condition.

Chapter VII summarizes the accomplishments and contributions.

In the Appendix, more simulation examples are presented to demonstrate the superiority of the decentralized voltage and stability control system in solving voltage and stability control problems under different system conditions.

CHAPTER II

VOLTAGE AND VOLTAGE STABILITY CONTROLS IN POWER SYSTEM

2.1 INTRODUCTION

The major responsibility of power utilities is to provide customers with constant and reliable electricity. Not only does the quality of electricity need to be assured, but also the stability of the entire power delivery system needs to be monitored and maintained. Voltage is the key factor of both the quality of the deliverable service and the stability analysis. Specific acceptable operational voltage ranges for both the service side and the utilization side are enforced by the ANSI C84.1-1995 standard.

The reliability councils of power utilities have developed rules that transmission utility operators should follow at all times. The fundamental principle for setting the rules is [2] that a power system should always be operated in such a way that no credible contingency could trigger cascading outages or other forms of instability. Since the faults and failures are unavoidable and unpredictable, all power systems should be able to endure them without inconveniencing consumers. The only solution to avoid blackouts is to operate the system with a sufficient stability margin.

In Chapter 2, the background of voltage-stability problems and remedial-control practices in utilities is reviewed.

2.2 VOLTAGE STABILITY PROBLEMS IN POWER SYSTEMS

Voltage stability is the ability of a system to maintain voltages so that when the load admittance is increased, the load power is also increased. Both the load power and the voltage on the load are controllable.

Voltage collapse is a process in which voltage instability leads to the degradation of the voltage profile in a significant part of the system.

A system enters a state of voltage instability when a disturbance, such as the increase in load or a contingency, causes the voltages to drop quickly or drift downward while the available means of controls fail to halt the decay.

These definitions of voltage stability, voltage instability, and voltage collapse can be found in [3].

Voltage-stability problems are far more complicated than the voltage control problems. Only a few types of voltage controls, such as the controls of switched capacitor banks and generator set points, can help improve voltage stability. Since voltage collapse usually occurs along with voltage constraint violations (such as low voltages and voltage drops), the voltage magnitudes on a set of important nodes are usually monitored by some utilities as the indicators to initialize voltage-stability controls. However, there are two limitations in using the voltage magnitudes as the indicators of the voltage-stability condition:

(1) Voltage collapse could occur at high voltage levels, when the voltage indicator is blind to the hazardous voltage-stability margin.

(2) The remedial stability controls driven by the voltage monitoring may not be sufficient to provide the controlled system with sufficient voltage-stability margin.

2.2.1 Background of the voltage stability problems

Voltage instability stems from the attempt of load dynamics to restore power consumption beyond the capability of the combined transmission and generation systems [3]. Loads are the driving forces of voltage instability. The limited capacity of a transmission system marks the onset of voltage instability. Accurate modeling of generators and their controllers is important for assessing voltage stability, although a generator is not an ideal voltage source.

Power system stability problems can be classified based upon two criteria: the time scale and the driving force of the instability. According to the time scale criterion, short-term and long-term stability problems can be distinguished. The driving forces of instability include the generator and the load. Short-term generator-driven instability problems can be solved by controls of automatic voltage regulators (AVR), excitation systems, turbines, and governors. Short-term generator-driven instability problems are related to frequency instability caused by active power imbalance between loads and generators in an island area. In a short-term time scale (a few seconds), there is no clear-cut separation between a generator-driven and a load-driven instability problem. In a long-term time scale (several minutes), a voltage-instability problem needs to be identified by analyzing the entire network model. A generator-driven instability problem can be identified by analyzing the generator-related models only. Generator-driven

instability problems are not of interest in this dissertation. The problem of voltage-stability usually refers to a load-driven stability problem, which could occur in several seconds up to a few hours.

2.2.2 Voltage collapse in a power system

Voltage collapse is defined as a process in which voltage instability leads to a very low voltage profile in a significant part of the system. A power system is defined as voltage stable if the voltages on loads approach post-disturbance equilibria after being subjected to a certain disturbance. The possible causes of voltage collapse include the following:

(1) Generator or line outages.

When a disturbance from a generator or line outage occurs, the load power absorption will drop because of a dip in voltage profile, but the load power absorption will be restored by voltage-control devices, such as load tap changers (LTCs). The reactive loss in the system will increase in response to the restoration of the load power. If the reactive support from generators and capacitive compensation resources cannot provide sufficient reactive support in time, voltage collapse may occur because of the propagation of the disturbance to more buses. The blackout of the Swedish system in 1983 was caused by line outages in the northern area, which constrained the generation support to the southern area.

(2) Load demand increases.

Since a voltage stability problem is load driven, the increase in the load demand will gradually push the stability margin in a system to zero. When the reactive power sources (such as generators and SVCs) reach their output limits, the voltage profile will decline, which may further reduce the reactive compensation from the capacitor banks. The control of the LTCs may cause additional reactive losses and reduce the stability condition. The blackout in Japan in 1987 was caused by the increase of the load demand during peak hours, which exhausted the reactive support from the available resources.

To prevent voltage collapse, the following approaches are usually taken by utilities around the world [4]:

A. Application of reactive power compensation devices.

Adequate stability control resources can be assured by planning the reactive power resources in terms of their sizes, ratings, and locations.

B. Control of both the network voltages and reactive outputs of generators.

An example of this type of approach is the voltage control system used by the EDF (France) and the ENEL (Italy).

C. Coordination of protections/controls.

Separation of a disturbance affected system from the rest of the system could mitigate the impact of disturbances on voltage stability. Adaptive or intelligent control methods need to be developed to facilitate this type of approach.

D. Controls of load tap changers (LTCs).

LTCs can be used for emergency stability control purposes either locally in automatic mode or centrally by manual coordination. Emergency LTC controls include tap blocking, tap locking, and tap reversing.

E. Under-voltage load shedding.

For unplanned or extreme situations, load shedding may be necessary to prevent voltage collapse. However, load shedding should be considered as the last step of voltage-stability control to avoid inconvenience to customers.

2.3 THE VOLTAGE STABILITY ANALYSIS APPROACHES

A power system can be described as a dynamic model with time-variant state variables and parameters. The state variables include voltage magnitudes and angles, rotor angles and torque, and excitation current. The parameters refer to the slow changing or constant quantities, such as the active and reactive load demands. The stability of a power system can be explained by the bifurcation theory. Bifurcation occurs when small and smooth changes made to the parameters of a system cause a sudden “qualitative” or topological change in its long-term dynamical behavior.

Three types of bifurcation scenarios that can lead to instability—saddle node bifurcation (SNB), Hopf bifurcation, and higher order bifurcation. A Hopf bifurcation occurs when the system reaches an equilibrium point with a pair of purely imaginary eigenvalues [3]. The consequence of the Hopf bifurcation is either steady-state oscillations or a growing oscillatory transient. Since voltage collapse does not show any

oscillatory characteristic, the Hopf bifurcation is not considered in the voltage-stability analysis. The mechanism of the SNB can be used to explain the phenomenon of voltage collapse.

2.3.1 Saddle node bifurcation and voltage collapse

A SNB is a collision and disappearance of two equilibria in dynamic systems. Considering a dynamic power system model in (2-1), x is the vector of state variables, while λ is the vector of slow changing parameters:

$$\dot{x} = f(x, \lambda) \qquad x \in R^n \quad \lambda \in R^m . \tag{2-1}$$

Assuming a bifurcation occurs at (x^*, λ^*), if the Jacobian matrix $f_x(x^*, \lambda^*)$ has a zero eigenvalue, the bifurcation is an SNB. If the eigenvalue is purely imaginary, the bifurcation is a Hopf bifurcation. At the SNB point, the stability equilibrium disappears because of an unstable type one equilibrium point on the stability boundary [3]. Once an SNB point is reached, any small perturbation in a system parameter will lead the system to instability. Therefore, the stable equilibrium at the closest SNB point can be considered as the stability boundary.

Although the transition from a stable equilibrium to a SNB point is a dynamic process, power-flow-based static analysis methods are usually relied on to evaluate the stability condition of a system. Power-flow analysis provides “snap-shots” of the system states (voltage magnitudes and angles) under different operation conditions. Load flow analysis reveals how a system equilibrium varies with changes in parameters and controls.

Disturbances with high probabilities, such as load increase and certain contingencies, can be simulated offline with power-flow analysis to discover their impact on the voltage stability. The total active power load is usually adopted as the measure to evaluate the distance to the closest SNB point. The available approaches to compute the closest SNB point are introduced as follows:

(1) Direct methods

The shortest distance from the current system parameter λ^0 (such as the loading factor) in the parameter space to λ^* corresponding to a SNB can be used as the direct measure of the voltage stability margin. The perpendicular direction to the hypersurface of a SNB point can be pointed by $w^* f_\lambda$, where w^* is the left eigenvector of the system-associated Jacobian matrix, while f_λ is the parameter-associated Jacobian matrix. Therefore, the norm of the shortest distance $\left\|\lambda^* - \lambda^0\right\|$ is the estimated stability margin. The convergence of the direct methods depends on a "good" initial guess close to the hypersurface of a SNB point.

(2) Iterative methods

The idea of the iterative method is to repetitively solve the bifurcation problem with the augmented parameter vector λ until a convergence criterion is met. Starting from the current system parameter λ^0 and an initial guess of the moving direction n^0, the new parameter vector will be $\lambda^0 + l\, n^0$, where l is the step size of the variation in the parameter vector. The parameter vector will be updated iteratively until the direction of the

parameter variation converges to $w^* f_\lambda$.—the perpendicular direction to the hyperspace of a SNB point.

Both the direct methods and the iterative methods rely on picking a close initial guess. Different initial guesses may lead the two types of methods to a locally closest bifurcation point.

(3) Continuation methods [5]

The continuation methods use load flow equations to locate the closest bifurcation point. Conventional power-flow algorithms require the evaluation of the Jacobian matrix, which will become singular when the SNB is reached. Therefore, the lower part of the solution path in the active power vs. voltage magnitude plane (PV curve) will not be accessible. The continuation power flow (CPF) method overcomes this problem by reformulating the load flow equations so that they remain well-conditioned at all possible loading conditions. CPF uses a combination of an adjustable predictor step and a corrector step to evaluate the critical loading parameter (as shown in Figure 1). Starting from an initial known state (x^0, λ^0), the algorithm uses the predictor step to approximate the next solution ($\hat{x}^i$, $\hat{\lambda}^i$) along the tangential direction to the solution path. The correction step uses the Newton-Raphson algorithm to locate the closest actual operation point (x^i , λ^i). At a SNB point, the tangential direction vector is zero and soon turns to be negative.

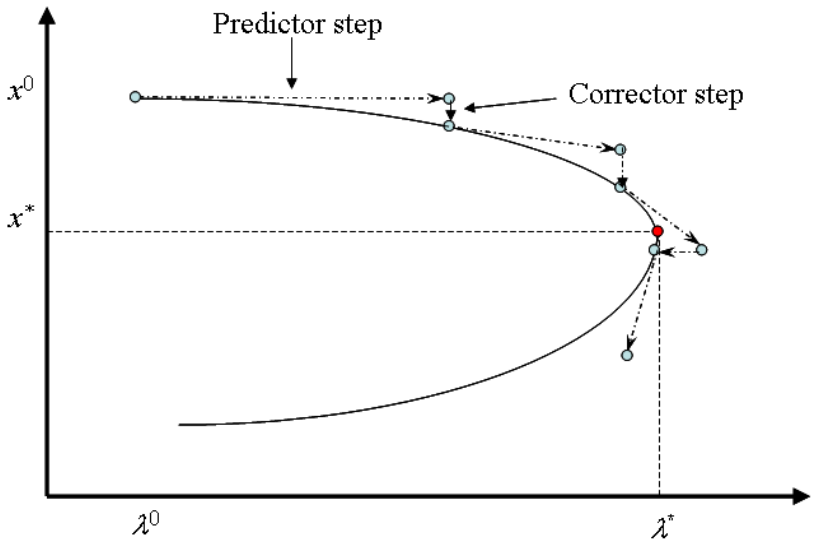

Figure 1. Predictor steps and corrector steps of the continuation method.

The advantage of the CPF is that the quality of the initial guess does not impact the accuracy of the algorithm. However, the predictor and correction factors need to be tuned in order to maintain the stability of the CPF algorithm. Because of its comparatively fast calculation speed, CPF is adopted by some utilities as an offline tool to explore the PV curves.

PV curves can be used for the conceptual analysis of voltage stability. A simple two-bus system (Figure 2) is used to illustrate the stability analysis based on PV curves. The voltage performance of this simple system is qualitatively similar to that of a practical system with many voltage sources, loads, and transmission lines.

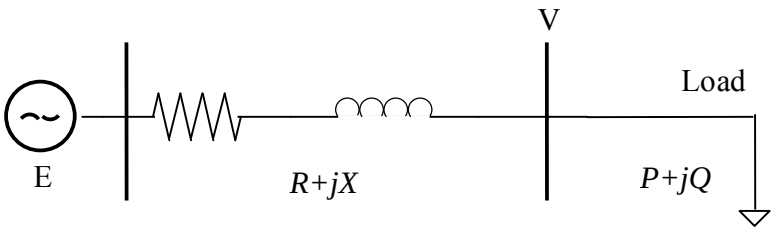

Figure 2. A two-bus system.

Actual values are assigned to the parameters in the two-bus example. Let *R=0, X=0.1j, P=1.5 p.u.*, $Q = P\tan\theta$, where $\cos\theta$ is the power factor of the load. The PV curves in Figure 3 are obtained by applying CPF. Each PV curve corresponds to a load with different power factor.

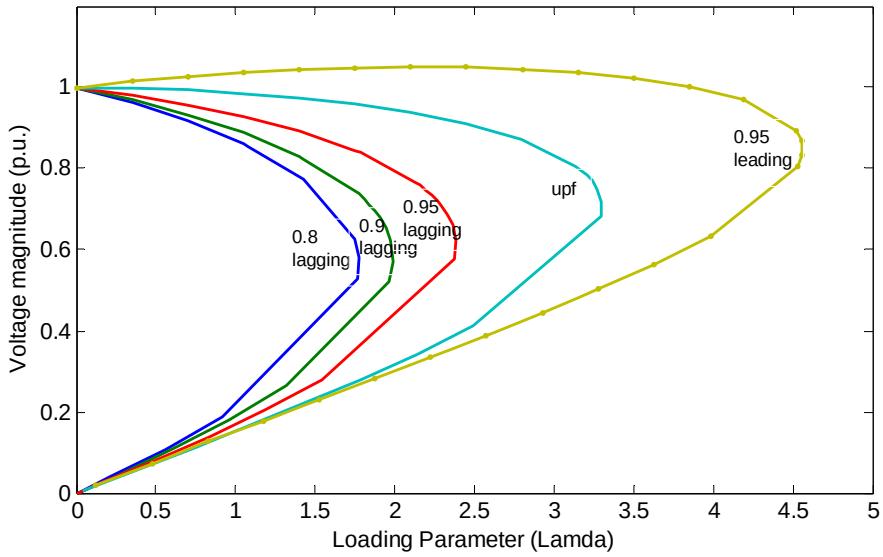

Figure 3. PV curves for the two-bus test cases with different power factors.

As the load becomes more and more compensated (transition from a lagging power factor to a leading power factor), the critical loading factor (the maximum loading factor at the SNB point) increases. However, the magnitude of the critical voltage corresponding to the nose point of the PV curve also increases. This situation is dangerous in a sense that voltage collapse could occur when voltages are still normal. For an over-compensated load (leading power factor), there is a portion of the upper PV curve along which the voltage increases with the load power. Thus, the more active power consumed, the more reactive power produced by the load.

2.3.2 Wide area stability monitoring and protection control

Many countries, including the United States, Mexico, China, and several European countries, have already started investigating and developing the wide area measurement system (WAMS). Currently, the major features of the WAMS-based functions [6] include real-time voltage and current monitoring, basic analysis, and automatic warning of abnormal conditions. More advanced functions could be developed based on the WAMS infrastructure.

Starting from the moment of voltage instability, which usually occurs after cascaded contingencies or faults, the transition to a voltage collapse only takes several seconds up to several minutes [7]. Under the constraint of such a short time frame, the voltage stability control problem is hard to handle by the steady-state control function in most of the supervisory control and data acquisition/energy management systems (SCADA/EMS). The transient stability monitoring function of WAMS, designed with fast response to changes in voltage and stability conditions, could possibly be upgraded to predict voltage collapse.

Some advanced functions, such as generator status monitoring, low-frequency oscillation analysis, and state estimation, have been proposed [6] to form a portfolio of applications in WAMS.

Many researchers from all over the world have presented many different approaches to tackle the topic of wide area protection [1, 6-12]. Although the actual WAMS system has not been defined explicitly, the expected functions and theoretical studies have been widely discussed. Publications [8, 9] provide a thorough generalization of the functions in WAMS. Voltage stability assessment is one of the most important functions in WAMS.

There are generally two typical voltage-stability control approaches presented by researchers. The first approach relies on the regulation of power generation through power system stabilizers (PSS) and exciters to improve the voltage-stability condition of a power system [9, 10, 12, 13]. This approach generally requires formulating the dynamic differential equations for the generation system. The amount of calculation effort can be considerable given a medium or large multi-machine system. Since time delay is critical for voltage-stability control, the possible long calculation time is the drawback of this approach.

The second approach uses PMU measurements to evaluate stability margin [14-16]. This approach applies the classic maximum power transfer theory to predict the proximity to voltage instability. When a certain stability threshold is reached, local load shedding will be suggested to a system operator to avoid a blackout. However, load shedding should be considered as the last step to avoid a voltage collapse. If alternative stability controls could be provided in time, load shedding could be avoided. Publication [16] suggests placing PMU on both sides of a transmission corridor to achieve more accurate and reliable monitoring of the stability condition. The evaluation process is similar to the studies of [14, 15] with a few variations. However, the suggested variations will bring redundancy to the monitoring system and require extra communication channels.

2.3.3 The voltage and stability controls in power utilities

Voltage-stability controls vary among power utilities. Common approaches include the shifting of setting groups and parameters for different protection and control devices,

LTC tap adjustment, switching of shunt capacitors, and load shedding. Many utilities use voltage limits and transfer limits as the indicators to evaluate the voltage stability condition of a power system. The voltage stability control practice in a few large power utilities is summarized as follows:

(1) Pennsylvania-New Jersey-Maryland Interconnection LLC (PJM) [17]

PJM is the reliability coordinator for the PJM regional transmission organization (RTO) and is responsible for all regional reliability coordination as defined in the North American Electric Reliability Corporation (NERC) and regional standards and applicable PJM operating manuals. The voltage and stability operation guidelines can be found in the PJM transmission operation manual [17]. PJM operates the PJM RTO considering voltage and stability-related capacity limits, including voltage limits, MW transfer limits across interfaces, and limits on voltage angle differences. If a limit violation develops, the voltages in the system should be regulated within the normal continuous voltage limits or emergency voltage limits for the simulated loss of the next most severe contingency. The PJM voltage operation guidelines for the actual and simulated voltage violations are shown in Table 1 and Table 6 respectively.

Table 1. PJM voltage operation guidelines for an actual voltage violation.

Voltage limit exceeded	If actual voltage limits are violated	Time to correct (minutes)
High voltage	Use all effective non-cost and off-cost actions.	Immediate
Normal low	Use all effective non-cost actions, off-cost actions, and emergency procedures except load dumps.	15 minutes
Emergency low	All of the above plus, shed load if voltages are decaying.	5 minutes
Load-lump low	All of the above plus load loading, if analysis indicates the potential for a voltage collapse.	Immediate
Transfer-limit warning point (95%)	Use all effective non-cost actions. Prepare for off-cost actions. Prepare for emergency procedures except load shedding.	Not applicable
Transfer limit	All of the above plus load shedding, if analysis indicates the potential for a voltage collapse.	15 minutes or less depending on the severity

Table 2. PJM voltage operation for a post-contingency simulated violation.

Voltage limit exceeded	If actual voltage limits are violated	Time to correct (minutes)
High voltage	Use all effective non-cost and off-cost actions.	30 minutes
Normal low	Use all effective non-cost and off-cost actions.	Not applicable
Emergency low	Use all effective non-cost actions, off-cost actions, and emergency procedures except load shedding.	15 minutes
Load dump low	All of the above plus load shedding, if analysis indicates the potential for a voltage collapse.	5 minutes
Voltage drop warning	Use all effective non-cost actions.	Not applicable
Voltage drop violation	All effective non-cost and off-cost actions plus load shedding, if analysis indicates the potential for a voltage collapse.	15 minutes

The PJM dispatcher uses the PJM real-time monitoring data and the security analysis as the primary tools to evaluate the current and future stability conditions of the PJM extra-high voltage (EHV) system. The following approaches are adopted to control voltage and stability: switching capacitors and reactors, adjusting voltage set points of static VAR compensators (SVC), operating synchronous condensers, changing transformer tap positions, adjusting MW outputs from generators, curtailing transmission transactions, adjusting phase angle regulators (PARs), and switching transmission facilities.

EHV (Extra-High Voltage) load tap changers (LTCs) are not operated in automatic control mode to regulate voltages, but are manually controlled by the system dispatcher to coordinate with all other voltage control devices. The voltage controls in the PJM RTO are coordinated in an attempt to minimize capacitor switching operations and transformer tap changes. The PJM dispatcher monitors the system voltage profile and the transfer capability of the PJM RTO and requests capacitor switching or transformer tap changes in a timely manner. PJM coordinates with the local control centers to execute the control decisions for all the 230 kV and 500 kV capacitors. The local conditions may

require some deviations from the control decisions made by the system dispatcher. The 500 kV LTC transformer taps should be adjusted to control the system voltage regardless of the capacitor's in or out-of-service status.

(2) ENTERGY [18]

Two major load centers in Entergy are identified as areas with potential voltage stability concerns. These two areas are located at the down stream of the Gypsy area (DSG), including the city of New Orleans, and the western region of the Entergy system located in the southeastern part of Texas, between Beaumont and Houston. Two 300 MVAr SVCs are installed at these load centers. Along with the SVC implementation, for the first time, a coordinated capacitor-bank switching has been implemented at the Entergy using the SVC controls and SCADA system. Frequent capacitor bank switching in the western region has led to several capacitor-bank failures and switching device malfunctions in the past few years. These capacitor banks were mainly switched by the operators using supervisory control without any coordination.

During light and intermediate load conditions when the total load in the system is 900 MW or lower, the full reactive capacity of the SVC could be used to replace the capacitor VARs in order to reduce the switching operations of the capacitor banks. When the total load reaches 1200 MW and higher, the static capacitor banks will have to be switched on to maintain the voltage profile in this area, while the SVC output will be limited to 0 MVAr. The saved reactive reserve of the SVC can be used for dynamic VAr compensations.

The SVC's 300 MVAr rating is derived from two wye-connected 75 MVAr Thyristor Switched Capacitors (TSCs) and one delta-connected 150 MVAr TSC. The voltage controller switches the TSCs in response to voltage changes by calculating the difference between the reference voltage and the actual voltage, $\Delta V = V_{ref} - V_{act}$. If ΔV exceeds the dead band, the SVC will switch the TSC branches in or out as needed. If ΔV stays within the limits of a dead band, the voltage controller (V-controller) of the SVC is stabilized. The Q-controller, however, tries to maintain the output of the SVC at a pre-determined VAr level which is not voltage dependant. The SVC compares the reactive power set-point Q_{ref} to the reactive power output Q_{SVC} and derives a difference value, $\Delta Q = Q_{ref} - Q_{SVC}$. The Q-controller is regulated by the sign of ΔQ. In the Porter SVC, Q_{ref} is set to 300MVAr when the system is lightly loaded, and it is adjusted in 75 MVAr steps according to the changes in the system load. The slow Q-controller has a time constant (usually several seconds) that is many times greater than the voltage regulator. This means that the Q-controller does not react to a fast transient. The Q-controller can command TSC switching regardless to ΔV. If $\Delta Q \neq 0$ and no external capacitor banks are available for switching, the Q-controller will attempt to switch TSC branches by adjusting the value of V_{ref}. V_{ref} is updated by integrating the value of ΔQ over time and adding to the original setting of V_{ref}. The Q-controller can adjust the VAr output as long as the actual system voltages are within the range from 0.9 to 1.05 pu. When $\Delta Q \neq 0$ and the external capacitor banks are available for switching, the SVC will send a switching request to control modules of the external capacitor banks and block the V_{ref} adjustment by fixing the integrator output to zero. By blocking the V_{ref} adjustment, the controller is enabling the switching of the external capacitor banks based solely on the sign of ΔQ.

The SVC will continue to hold the switching request until ΔV is outside of the control dead-band, at which point the fast voltage controller will raise or lower the system voltage by switching TSC branches. This process is repeated until either Q_{SVC} is approximately equal to Q_{ref} or no further capacitor banks are available for switching.

(3) Independent Electricity System Operator (IESO)

Because of the large geographic area covered by the IESO, excessive voltage declines and voltage instability become challenging issues for the operation of the IESO-controlled grid (ICG). At present, approximately 40 voltage security interfaces have been identified in Ontario. In deriving the operating security limit for a voltage security interface, the interface flow is increased step by step with all recognized contingencies simulated at each step. The maximum flow level without violating the security criteria represents the operating security limit. The pre-contingency voltages at all critical buses must be within acceptable bands that are in accordance with equipment capabilities, customer requirements, and system characteristics. If the system exhibits voltage instability, the operating limit must be dropped by at least 10% from the marginally stable case (i.e., the nose point on the PV curve). After the voltage security limits for the normal system (with all elements in service) are established, the next step is to derive the limit penalties for single outages that are deemed critical. Once the operating security limits and the associated penalties have been derived, these limits will be converted into linear constraints to be used in optimal generation pre-dispatch calculations and online voltage security monitoring.

The Control Room Operator (CRO) relies on the following control measures to secure the IESO controlled grid and to prevent voltage instability or excessive post-contingency voltage decline.

A. Specification of dynamic VAR requirements.

Dynamic VARs provided by the generators at key locations play a very important role in maintaining voltage security, especially in the post-contingency period.

B. Under-load transformer tap changing.

Tap positions on LTCs can be adjusted manually under the direction of the CRO to maintain a desirable voltage profile across the Ontario power grid.

C. Switching of shunt capacitors or reactors.

Shunt capacitors can be switched in or out under the direction of the CRO to control transmission voltage levels at various locations.

D. Special protection schemes (SPS).

The IESO relies on several types of pre-defined special protection schemes (SPSs) to improve the voltage security of the power grid, especially for stabilizing the system during a post-contingency period.

E. Voltage reduction.

Voltage reduction is usually applied to mitigate generation deficiency in Ontario under extreme weather and multiple outage conditions.

F. Generation re-dispatch.

If the power flow on a voltage security interface is approaching or exceeding its maximum operating security limit (OSL), then it may be necessary to re-dispatch generation on both sides of the interface in order to bring the interface flow below its operating security limit.

G. Other control measures, including load transfers, switching of transmission lines, transmission loading relief (TLR) etc.

In the IESO, operating security limits are derived offline assuming the worst system conditions (i.e., maximum primary demand, maximum interface flows, etc.). Therefore, the operating security limits are usually more conservative than the capability of the actual system. In order to improve market efficiency, the operating security limits need to be more accurate in reflecting the actual system conditions. A project has been undertaken by the IESO to provide the CRO with online operating security limits.

(4) ELECTRICITE DE FRANCE (EDF) [19]

Voltage controls on the French EHV (extra-high voltage) network are operated at three different levels, which are temporally and spatially independent. The so-called "pilot buses" are selected in local control zones. The voltage of a pilot bus is representative of the voltage profile of its local zone. The voltage profile at the pilot buses are monitored by the system operator as a measure of the system condition. The sensitivities of the voltages on the pilot buses to the control variables (such as the stator voltages) are utilized in evaluating the voltage control solutions. Details of the three-level voltage control system applied by the EDF are introduced as follows:

Primary-level control devices, with response time of a few seconds, consist of the automatic voltage regulators (AVR) installed on generators. The primary voltage controls are performed automatically to compensate the rapid variations in the EHV voltages.

Secondary-level voltage controls (SVC), with response time of approximately three minutes, are executed by both slow and fast VAr compensation devices (capacitors and condensers) and LTCs. These devices are considered to have longer operating time intervals (slow control devices) than the primary-level control devices. The original SVC relies on automatic controls of the LTCs and shunt capacitor banks for the purpose of voltage regulation. A more advanced secondary control system—the coordinated secondary voltage control, or CSVC— has been in service in western France for a few years and is expected to eventually replace the existing SVC system. The CSVC system adjusts the voltage profile over the entire system by controlling the voltages on all the pilot buses. In a closed-loop mode, the CSVC refreshes the set points of the primary control devices in 10-second intervals.

The purpose of tertiary-level controls [20, 21] is to determine an optimal voltage profile of the entire network and to coordinate the secondary controllers according to the safety and economic criteria. The control variables include the active power outputs of the generators, power flows in the transmission lines, set points of the AVRs on the synchronous generators, amount of reactive power compensation, and tap positions of the LTCs. The tertiary-level control solutions are generated by solving an optimization problem with the objective of optimizing the voltage profile. Tertiary controls are currently performed manually. The timeline of tertiary-level controls in automatic mode is around 15 minutes.

(5) Midwest independent system operator (MISO) [22]

The Midwest ISO is an independent, nonprofit organization that supports the constant availability of electricity in 15 U.S. states and the Canadian province of Manitoba. Besides the responsibility as a market operator, MISO also acts as a reliability coordinator to manage and monitor voltage and reactive power.

The voltage and reactive power controls by MISO are schedule through day-ahead and real-time assessments. Off-line PV analysis and reactive reserve calculations are performed for the next-day using projected peak loads with the scheduled transfers and expected generation pattern.

The off-line PV analysis uses incremental transfers from a pre-defined source to a pre-defined sink across the study area to stress the model and determine the maximum transfer level. At each transfer step, contingency analysis is performed on a subset of contingencies that are most limiting for the area. The stability limit is determined by the resultant flow on the proxy interface at the last stable operating point. The calculated limit is used by the real-time operations staff as an alarm to indicate any flow limits being approached.

The off-line reactive reserve analysis are performed to assure enough static reactive resources (such as shunt capacitor banks) and dynamic reactive resources (such as SVCs) are in place to maintain the voltage profile within the required post-contingency voltage limits.

The real-time voltage assessments performed by MISO include the following:

a. Voltage monitoring and alarming function of SCADA

If a normal voltage violation is identified, MISO will manually control the capacitor banks and LTCs and request coordinate nearby generators to increase reactive outputs. If a normal voltage violation is identified, MISO will initial congestion management, re-dispatch generation, or curtail relevant transmission contracts.

b. Real time contingency analysis (RTCA)

MISO RTCA utilized data from State Estimator (SE) and performs a full AC contingency analysis. Same control actions will be taken for any identified normal or emergency voltage violations as described in (a).

c. Real-time PV analysis

The Midwest ISO performs routine voltage assessment of specific areas using P-V analysis with a snapshot of the state estimator solution. The P-V analysis involves subjecting the real-time snapshot to a series of incremental transfers from a pre-defined source area to a pre-defined sink area. At each transfer level contingency analysis is performed for a subset of contingencies that are most limiting for the area. Voltages and line flows are monitored for various locations in the study area. The limit is determined by the final operating point at which the power flow case solves for base and contingency conditions. If the monitored flow exceeds the calculated stability limit, a voltage stability constraint will bind and generation re-dispatch will be requested.

d. Real-time reactive reserve analysis

MISO monitors the difference between the available reactive capabilities and total reactive output in real-time, and compare the difference with the defined reserve margin. If the analysis indicates insufficient reactive reserve, capacitor controls will first be

manually conducted followed by transmission contract curtailment, and eventually load shedding depending on the severity of the voltage stability constraint.

2.4 CONCLUSION

In this chapter, the background of the voltage-stability problems and the remedial control practices in utilities is reviewed. A voltage-stability problem is load-driven, taking several seconds up to a few hours. Voltage collapse is usually caused by insufficient reactive power support after the severe contingencies or load increases. The theory of the saddle node bifurcation can be used to explain the phenomenon of voltage instability. Proximity to voltage instability can be predicted by assessing the distance from the current operation equilibrium to the closest SNB point.

The wide area measurement system (WAMS) provides a convenient platform for new online stability monitoring and control applications. The voltage-stability assessment function has been presented as an important tool in the WAMS. The introduction of innovative real-time applications into the WAMS has been recognized by many researchers as a prevailing topic.

The two representative voltage and stability control procedures from PJM and EDF are introduced. PJM utilizes post-contingency analysis to decide the voltage and stability controls in the PJM RTO. The control timeline ranges from 15 to 30 minutes for normal and emergency low-voltage constraint violations. The timeline for conducting emergency load shedding is 5 minutes. The control coordination among control zones are organized by the system dispatcher, who is in charge of the EHV LTCs and capacitors. When a

severe disturbance occurs, the operator has to rely on his/her own past experience to control these EHV LTCs and capacitors.

The three-level voltage control system in the EDF has realized coordinated voltage controls among different control zones. The automatic generator controls from the first-tier deal with fast disturbances in the system. The secondary-voltage-control (SVC) tier only relies on the automatic controls of the LTCs and shunt capacitor banks to correct local voltage violations. The timeline of the original SVC is approximately 3 minutes, depending on the time constants of the LTCs. The CSVC coordinates the controls of the generators (voltage set-points and reactive power output) from different control zones. Tertiary-level controls are performed manually to optimize the voltage profile of the entire system. The SVC could be upgraded to include more voltage control resources in a coordinated manner, such as the LTCs and shunt capacitor banks.

CHAPTER III

ON THE PERFORMANCE OF THE VOLTAGE INSTABILITY PREDICTOR

3.1 INTRODUCTION

According to the background study in Chapter II, a voltage-stability problem can be viewed as a load-driven stability problem in a long time frame. Electricity deregulation and transmission competition may stress part of the bulk transmission network closer to stability boundary, while emphasize on economic benefits. Increased power transfers and reduced transmission margins can lead to overloads and voltage security problems. Voltage instability is closely related to the notion of the maximum loadability of a transmission network. In some power utilities in the U.S., stability protection and control schemes are designed to cope with anticipated disturbances. The uncertainties in the transmission network, such as load changes, scheduled outages, disturbances, and weather impacts can all disqualify the predefined control and protection schemes. The conventional power-flow-based methods [3, 23] rely on PV or QV curves and sensitivity analysis to estimate the stability condition of a system. In order to reduce computational burden and the risk of dispersing load-flow calculations, continuation power flow (CPF) is widely accepted by utilities to evaluate the margin to voltage collapse. Because CPF requires system-wide information to conduct stability analysis, the accuracy and timeline are the main limitations of the CPF.

With the emerging technology of the online synchronized measurement, local stability monitoring methods [14, 15, 24-27] have become more and more interesting to many researchers and utilities. Although the algorithms behind these local methods are different, their main ideas are similar—extracting sufficient information from local monitoring devices (such as the phasor measurement units, PTs and CTs) to detect locations in a system that are prone to voltage collapse. The local stability monitoring methods rely on local measurements from one or a few buses in the system to detect the changes in stability condition. The advantages of the local methods can be justified by their fast speed, simplicity, and low investment. Therefore, local methods could be applied in real-time system monitoring and protection.

Vu and Begovic [15] presented the application of the voltage instability predictor (VIP) as a fast and real-time voltage-stability monitoring approach. The VIP continuously tracks a Thevenin-like equivalent model of the system, as seen from a load bus, and the apparent power load on the same bus. According to the maximum power transfer theorem, the maximum power transfer from the Thevenin-like source to the load bus, corresponding to the point of voltage collapse, will occur when the magnitudes of the Thevenin-like impedance and load impedance are equal.

Mirosevic and Begovic [14] further upgraded the VIP algorithm to generate a stability index as the indicator to generators' reactive-power reserve. By adopting the proposed recursive identifications of the Thevenin equivalents, the impact of transients on VIP can be reduced. Therefore, the VIP can be applied in the environment where slow transients could be encountered. The performance of the recursive VIP method is yet to be justified by comparing it with the original least square (LS) identification method.

Besides the studies on the VIP algorithm, the authors also demonstrated the impact of nonlinear load in a monitored system on the stability-margin evaluated by VIP. By tracking just the portion of load with constant-power demand, the recursive VIP algorithm can still accurately capture the changes in stability conditions.

After the presentation of VIP, many researchers and utilities further implemented the algorithm of VIP for practical applications. Since 1997, a research project [24] has been conducted jointly by American Electric Power (AEP) and ABB to study the applicability of the VIP algorithm on the AEP network. The idea of adopting VIP in predicting stability margin over a critical transmission interface is verified by dynamic simulations [24] on the 2002 winter-peak 7000-bus case used by AEP in planning studies.

A joint R&D project between Statnett, ABB and Sintef [28] applied VIP as a distributed stability monitor and trigger for coordinated reactive control in the actual Norwegian transmission system. The performance of VIP in tracking the changes in system stability condition has been tested and demonstrated by abundant steady-state and dynamic simulations during the progress of the project. Since spring 2004, the prototype VIP and coordinated secondary voltage control have been implemented and installed in the Norwegian transmission system.

Verbiˇc and Gubina [29] proposed a stability index by tracking the apparent power injection into a load bus. The basic validation assumption for this method is that the line losses increase faster than the actual delivered power to the load at the proximity to voltage collapse. At the point of voltage collapse, a majority of increased power demands are due to line losses. The drawback of this method lies in the uncertainty of reactive losses at different loading levels.

Holen [26] and Sachdev [30] suggested the extension of the VIP in monitoring power exchanges and stability conditions in mesh networks. The authors demonstrated in their simulation studies that the accuracy and robustness of the VIP algorithm can be enhanced by including more measurement data from neighboring buses and lines. The limitation in communication infrastructure and the complexity of network topology could be the constraints of the proposed enhancement to VIP.

Smon and Verbiˇc [31] extended the idea of VIP but applied Tellegen's theorem in identifying the parameters of the Thevenin equivalent model. At the point of voltage collapse, the Thevenin impedance equivalent can simply be evaluated by the ratio between the changes in voltage and current phasors. Therefore, by tracking this ratio, the condition of proximity to voltage collapse can be identified. The authors did not provide information about the choosing of step size for calculating changes in voltage and current phasors. This one-step identification method could be ideally used in systems where the fast dynamics need to be carefully analyzed.

Corsi and Taranto [32] presented an innovative real-time adaptive identification method to track the Thevenin equivalents of the VIP. The proposed identification method takes into account the estimation errors in the Thevenin equivalents as the trigger to start new iteration of parameter identification. The step-size of the iterative adjustments on the Thevenin source is conservatively decided by comparing multiple options, including a user-defined step change, maximum step change allowed by the Kirchhoff's law, and the maximum step change allowed by load flow. The definition of a step-size is critical to the stability and efficiency of any iterative algorithm. The sampling rate of phasor

measurements is another variable that could change the estimation of Thevenin equivalents.

The VIP algorithms and their variations represent the mainstream of local stability monitoring methods. The status of the research on VIP-related methods can be summarized as follows:

(1) The critical loading factor estimated by VIP and power-flow methods has been compared. The VIP can be used to track the changes in stability margin caused by load changes.

(2) The studies on the VIP variations with different parameter identification methods, including recursive method, one-step method according to the Tellegen's theorem, adaptive step-size method, have been presented to modify the VIP technique for better reliability and accuracy.

(3) The impact of nonlinear load on voltage stability margin can be tested by VIP. By decomposing the load into a nonlinear portion and a constant-power portion, a recursive VIP algorithm can be adopted to capture the changes in voltage stability.

(4) The VIP-based stability index, estimating the time to reach reactive generation limits or critical loading factor, is presented as an online indicator to activate remedial and emergency controls.

(5) VIP has been prototyped and simulated in the transmission systems of a few utilities [24, 28]. Positive feedback has been received on the performance of VIP.

Compared with the conventional time-consuming system-wide stability analysis approaches, such as iterative and continuation power flow methods, the advantage of VIP lies in its less computation effort and therefore shorter response time. The potential

applications of VIP include voltage stability and emergency control, network equivalents for dispatch and modeling purpose. However, the applicable boundary of VIP has not been defined, because of the complex operation environment of the power systems. Because VIP use a static Thevenin-like equivalent model to represent a system as seen from a load bus, the parameter identification of the Thevenin-like equivalent model will be impacted by various internal (VIP algorithms and choices of parameters) and external sources (transients and disturbances). A summary of the necessary studies on VIP are presented as follows:

(1) The first point is the selection of suitable VIP methods under different application environments. Different VIP approaches utilize different numerical methods to identify the Thevenin-like equivalents. The identification accuracy varies with a few external factors, such as the time interval between adjacent measurements (sampling rate), or the window size of the measurements to be included in the parameter identification, the assignment of weight factors for the measurements included in the window (or the forgetting factor for the recursive method). In other words, VIP needs to be tuned to be more adaptively deployed in complex application environment.

(2) The second point is the accuracy and sensitivity of the VIP equivalent model in representing a time-variant system. The boundary of VIP applications needs to be defined. The VIP only provides information about the difference between the load impedance and the Thevenin impedance. Such information could be translated into a stability index, which can be picked up directly by remedial and emergency control devices. Since the VIP is a real-time technique, the VIP-based stability index could be quantified by not only the margin to critical load, but also the estimated time to reach

critical load or maximum reactive reserve of certain generators. The impact of disturbances/contingencies and discontinuous controls (such as LTC and capacitor banks), as well as the associated fast dynamics, on the performance of the VIP need to be discovered. The VIP only represents the external network as a static Thevenin equivalent model, without considering the detailed dynamic components. Therefore, the VIP may not be an appropriate tool when the monitored system experiences fast dynamics. The ability of the VIP in providing propositional information during dynamic processes needs to be studied.

3.2 REVIEW OF THE VIP ALGORITHMS

A VIP device should be installed on a load bus, where changes in voltage and hence stability condition can be conveniently detected. Located on the load bus, without knowing the actual external operations, the VIP assumes the external system to be an equivalent model. By taking advantage of frequent voltage and current measurements, the parameters of the assumed equivalent model can be identified through parameter identification methods. The basic idea of VIP is to calculate the difference between the measured load impedance and the estimated network impedance. When the two impedances are close in magnitude, the maximum power transfer limit of the system is also close, and therefore a voltage collapse may happen. In fact, voltage instability may occur before reaching the point of maximum power transfer. Reactive power generation limits on generators can cause discontinuous changes in stability margin and rapidly lead the system to instability.

Any load bus of a complex power network can be represented as an equivalent load Z_{app} and the Thévenin equivalent of the rest of the system, as shown in Figure 4.

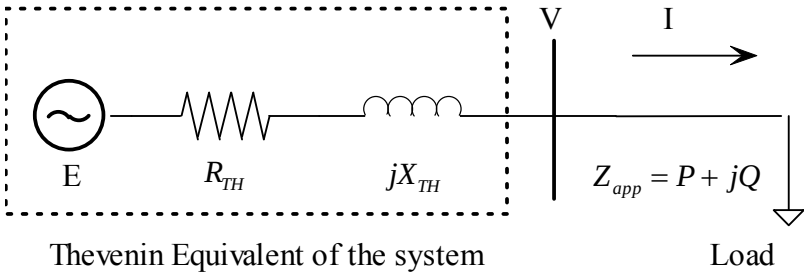

Figure 4. Illustration of a local bus and the Thévenin equivalent of the rest of the system [15].

The derivation of the least square VIP algorithm is presented byVu and Begovic [15]. The voltage phasor $\bar{V}\angle\delta$ and current phasor $\bar{I}\angle\theta$ on the load bus can be measured by the local PMU installed on the same bus. Therefore, the load impedance can be calculated by (3-1).

$$Z_{app} = \frac{\bar{V}\angle\delta}{\bar{I}\angle\theta} \tag{3-1}$$

The system equation can be written as:

$$\bar{E}\angle\varphi = \bar{V}\angle\delta + \bar{I}\angle\theta * Z_{eq} \tag{3-2}$$

The model to be identified is given in (3-2). The complex nonlinear equation (3-2) can be converted to a linear equation group in (3-3),

$$\begin{bmatrix} 1 & 0 & -g & h \\ 0 & 1 & -h & -g \end{bmatrix} \times \begin{bmatrix} E_r \\ E_i \\ R_{eq} \\ X_{eq} \end{bmatrix} = \begin{bmatrix} u \\ w \end{bmatrix} \tag{3-3}$$

where $\bar{V}\angle\delta = u + jw$ and $\bar{I}\angle\theta = g + jh$.

In (3-3), $\begin{bmatrix} E_r & E_i & R_{eq} & X_{eq} \end{bmatrix}^T$ can be defined as the unknown parameter vector θ. Since there are four unknowns and only two linear equations, it requires at least two

measurements to estimate θ. Using two adjacent measurements to identify θ, the following discrete dynamic system can be modeled:

$$y(k-1)=\begin{bmatrix}u(k-1)\\ w(k-1)\end{bmatrix}=\phi^T(k-1)\theta(k)$$

$$y(k)=\begin{bmatrix}u(k)\\ w(k)\end{bmatrix}=\phi^T(k)\theta(k)$$

$$z(k)=y(k)+v(k)$$

$$\phi^T(k-1)=\begin{bmatrix}1 & 0 & -g(k-1) & h(k-1)\\ 0 & 1 & -h(k-1) & -g(k-1)\end{bmatrix} \tag{3-4}$$

where *z(k)* and *v(k)* are the measured output and zero-mean modeling error respectively. The minimum least square of the error in discrete parameter estimation can be formulated in (3-5).

$$\text{Min } J(\theta,k)=[z(k-1)-\phi^T(k-1)\theta(k)]^T[z(k-1)-\phi^T(k-1)\theta(k)]+$$
$$[z(k)-\phi^T(k)\theta(k)]^T[z(k)-\phi^T(k)\theta(k)] \tag{3-5}$$

By setting $\frac{\partial J(\theta,2)}{\partial\theta(k)}=0$, the least square estimation of the unknown vector can be obtained in (3-6).

$$\hat{\theta}(k)=\left[\phi(k-1)\phi^T(k-1)\right]^{-1}\phi(k-1)z(k-1)+\left[\phi(k)\phi^T(k)\right]^{-1}\phi(k)z(k)$$
$$=\left[\Phi_k\Phi^T{}_k\right]^{-1}\Phi_k Z_k \tag{3-6}$$

$$\Phi^T{}_k=\begin{bmatrix}1 & 0 & -g(k-1) & h(k-1)\\ 0 & 1 & -h(k-1) & -g(k-1)\\ 1 & 0 & -g(k) & h(k)\\ 0 & 1 & -h(k) & -g(k)\end{bmatrix} \text{ and } Z_k=\begin{bmatrix}u(k-1)\\ w(k-1)\\ u(k)\\ w(k)\end{bmatrix}.$$

In order for (3-6) to be valid in online applications, the inverse of $\Phi_k \Phi^T{}_k$ must not be singular, which implies that the difference between two phasor measurements should be large enough for a change in system state to be identified. When the system is running in steady state, the difference between adjacent measurements is negligible. To circumvent this problem, a recursive version of the least square method, known as the recursive least square method (RLS), can be applied. The basic idea of the RLS algorithm is [33], rather than repeatedly solving (3-6) with the risk of encountering singular matrix, to compute the parameter estimate $\hat{\theta}(k)$ by adding a correction term to the previous estimate $\hat{\theta}(k-1)$ when new measurement becomes available.

Begovic [15] applied RLS with infinite window size and a forgetting factor λ. The least square cost function is formulated in (3-7).

$$\text{Min } J(\theta,k) = \sum_{j=1}^{k} \lambda^{k-j} \left[z(j) - \phi^T(j-1)\theta(k)\right]^T \left[z(j) - \phi^T(j-1)\theta(k)\right] \tag{3-7}$$

The derivation of the recursive solution to (3-7) can be referred to many textbooks and papers [14].

$$\hat{\theta}(k) = \hat{\theta}(k-1) + G(k)\left[y(k) - \phi^T(k-1)\theta(k)\right]$$

$$G(k) = P(k)\phi(k) = P(k-1)\phi(k)\left[\lambda + \phi^T(k)P(k-1)\phi(k)\right]^{-1}$$

$$P(k) = \left[I - G(k)\phi^T(k)\right]P(k-1)\lambda^{-1} \tag{3-8}$$

$P(k)$ is called the power function [14]. The initial condition $P(0)$ should be large enough to initiate the correction step. The function of $G(k)$ is to define the correction step from the previous estimation based on new measurement. The coefficient λ is called the forgetting factor. The forgetting factor λ acts as a weight factor for the historic data.

The range of λ is usually set in the range from 0.95 to 0.99 to avoid the possible error in new measurement. During transient system state, the voltage measurements may contain errors and oscillate around the next stable equilibrium. The RLS method could sooth the impact of errors in measurement by putting more weight on historical data.

3.3 PRELIMINARY STUDIES ON VIP

As a local stability monitoring device, the basic function of the VIP is to track the changes in stability condition. A good evaluation of the tracking function is to benchmark with the power flow based stability analysis method, which is well-acknowledged by many utilities. The basic idea is to use power flows at different load levels to obtain a "PV" curve for a load bus, and compare the curve with the tracking result of the VIP. The interests of comparison include the predicted critical loading factor and the trend of stability margin as load changes from base level to critical level. The relevant simulations are performed on the IEEE 39-bus system model.

This IEEE 39-bus system is well known as the 10-machine New-England Power System. It represents a greatly reduced model of the power system in New England. The 39-bus system model includes 10 generators, 19 loads, 36 transmission lines and 12 transformers. Operational limitations relating to the generator reactive limits, the voltage magnitudes, and the capacity of transmission lines are defined. Dynamic data for the generators, turbine governors and exciters are given in [34]. The complete information about the IEEE 39-bus system is provided in Appendix I. Figure 5 shows the one-line diagram of the 39-bus New England System.

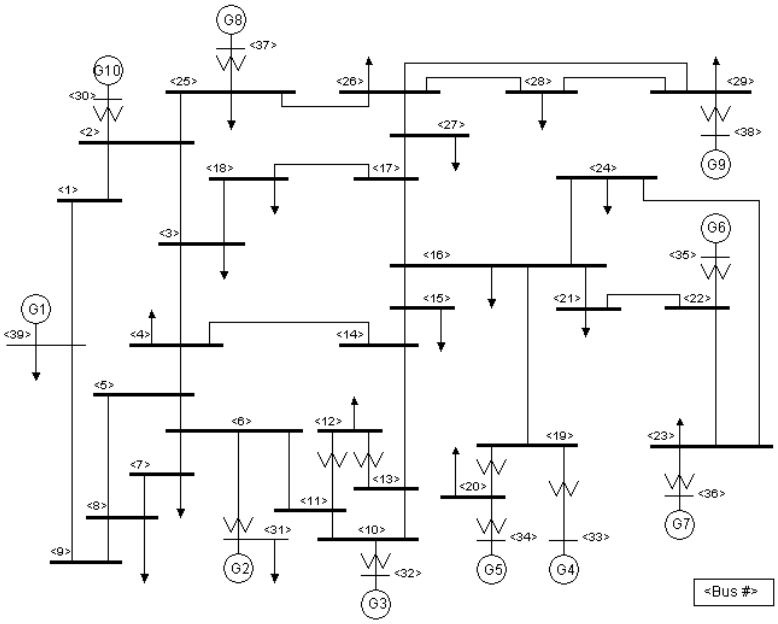

Figure 5. IEEE 39 bus New England system.

Before applying the VIP method, power flow test is used to check for voltage stability analysis and find the critical loading parameters. Using the original 39-bus power flow model as the base case, the detailed procedures of the power flow based analysis are as follow:

a. Increased the system loading level in steps of 1%. The added power demand is proportionally distributed to the generators' active power outputs. The loads and generator outputs in the system can be updated by (3-9):

$$\Delta P_L(i) = 0.01 P_L^{base}(i),\ \Delta P_G(j) = \frac{P_G(j)\sum_{i=1}^{n}\Delta P_L(i)}{\sum_{j=1}^{m} P_G(j)} \tag{3-9}$$

$$P_G^{New}(j) = P_G(j) + \Delta P_G(j),\ P_L^{New}(i) = P_L(i) + \Delta P_L(i)$$

where $P_L(i)$ is the active load demand on load bus *i*, $P_G(j)$ is the active power generation on generator bus *j,* the superscript *'base'* represents the corresponding parameter is obtained from the base case mode (without the added loads). *n* and *m* are the total number of load and generator buses respectively.

b. Run a power flow on the updated system model. If the power flow converges, the voltage phasors of the load buses are recorded as $\overline{V}_i(k)$ and $\delta_i(k)$, where $\overline{V}_i(k)$ and $\delta_i(k)$ are the voltage magnitude and phase angle on load bus *i* when the system loading factor is $\left(1+{}^{k}\!/_{100}\right)$, where *k* is the total steps of 1% load increases. Return to step *a* until the power flow result does not converge, in which case the critical loading parameter has been reached. Record the corresponding loading parameter as the critical loading parameter $\lambda_{critical}$.

When executing step *b*, the reactive generation limits of generators need to be considered. When the reactive power limits of generation is reached, the corresponding bus is converted from a PV bus to a PQ bus with the reactive power output set at its limit. At the same time, the active and reactive generation of the corresponding generator bus is regarded as a negative load. Using the power flow method, the critical loading factor is 2.2 when the reactive generation limits are not considered. When the reactive generation limits are considered, the critical loading factor is 1.65.

Figure 6 shows the reactive power output from the slack bus and a set of PV buses. For generators on slack bus 31 and PV buses 33, 34, their reactive generation limits are not reached throughout the simulation. However, for generators on buses 30, 32, 35 and 36, their reactive generation limits will be reached at increased loading levels. Table 3

listed the reactive generation limits of all the generators and their status during the load ramping simulation.

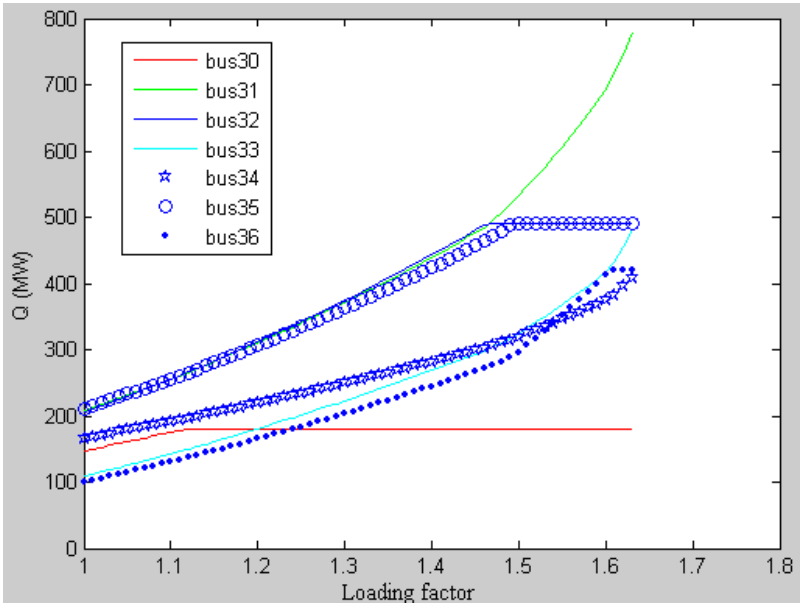

Figure 6. Reactive power output of a set of generators in the 39-bus system.

Table 3. Status of the reactive generation limits during the 39-bus simulation

Generator Location	Reactive generation limit	Status of reactive limit
Bus 30	180 MVAr	Active
Bus 31	1000 MVAr	Inactive
Bus 32	490 MVAr	Active
Bus 33	470 MVAr	Inactive
Bus 34	460 MVAr	Inactive
Bus 35	490 MVAr	Active
Bus 36	420 MVAr	Active
Bus 37	400 MVAr	Inactive
Bus 38	620 MVAr	Inactive
Bus 39	750 MVAr	Inactive

For a load bus *i*, any adjacent two sets of voltage phasors (from iteration *k* and *k+1*) from the power flow procedures mentioned above can be transformed to:

$$\overline{V}_i(k)\angle\delta_i(k) = u_1 + jw_1,\ \overline{V}_i(k+1)\angle\delta_i(k+1) = u_2 + jw_2; \tag{3-10}$$

The current phasor on load bus I can be calculated by:

$$\bar{I}_i(k)\angle\theta_i(k) = \left(1+\frac{k}{100}\right)\left(\frac{P_L^{base}(i)+jQ_L^{base}(i)}{\bar{V}_i(k)\angle\delta_i(k)}\right)^* = g_1 + jh_1; \quad (3\text{-}11)$$

$$\bar{I}_i(k+1)\angle\theta_i(k+1) = \left(1+\frac{k+1}{100}\right)\left(\frac{P_L^{base}(i)+jQ_L^{base}(i)}{\bar{V}_L^{\,i}(k+1)\angle\delta_i(k+1)}\right)^* = g_2 + jh_2;$$

By inserting the values of u_1, u_2, w_1, w_2, g_1, g_2, h_1, h_2 into (3-6), the estimates for $\overline{E}$ and Z_{TH} on load bus *i* can be obtained and recorded as $\overline{E}_i(k)$ and $Z_{TH}^i(k)$.

Using the calculated load and equivalent impedances on bus 24 as an example, the magnitudes of voltage across the identified Thevenin impedance *vs.* corresponding loading factor are shown in Figure 7 with a solid curve, while voltage magnitudes on load impedance are shown with a dashed curve. The simulation scenarios are considered—with vs. without considering the reactive generation limits.

Theoretically, the point at which V_{TH} and V_{24} meet each other corresponds to the critical loading parameter. The discontinuities of the Z_{TH} curve correspond to the PV—PQ transitions of different PV buses. After each transition, the entire system will settle down at a new state with different network equivalent impedance as seen from a load bus. The critical loading factor is 1.65 when the reactive limits are considered or 2.2 when the reactive limits are not considered. The PV curves by the power flow based analysis indicate the same critical loading factors for both of the two simulation scenarios.

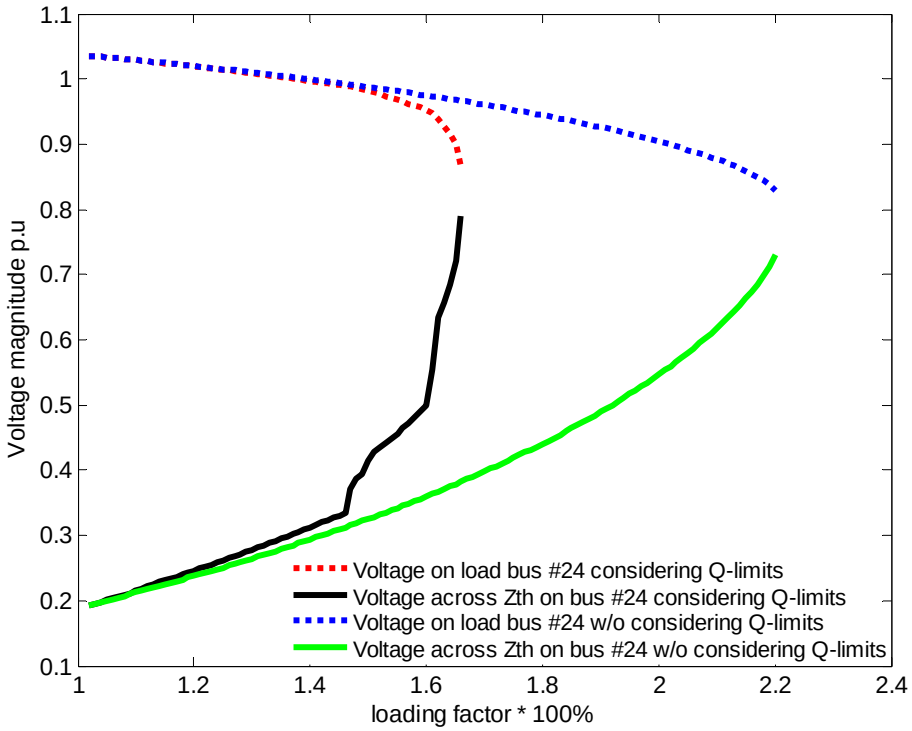

Figure 7. V_{TH} and V_{24} curves for bus 24.

3.4 SELECTION OF THE VIP ALGORITHMS AND THE IMPORTANT PARAMETERS

When the LS algorithm is applied in non-stationary environments, e.g. system identification and parameter estimation in the presence of unknown parameter changes, forgetting factor or finite length sliding window techniques have been widely used in association with the RLS. The finite sliding window technique also has an inherent advantage to keep the computational complexity to a fixed level by replacing the growing dimension in Φ_k with a fixed lower dimension matrix.

The power system is a time-variant system with complex abrupt and/or gradual changes in system state. The RLS with forgetting factor will weigh down the impact of the new changes in system state on the parameter estimation results. By choosing a sliding window with either infinite or fixed size (such as the recursive least square method), the changes in system states may not be grasped effectively since the measurements corresponding to the previous state are still left in the sliding window. For time-invariant systems, the longer the window length, the higher the estimation accuracy. However, for time-variant system, the longer the window size, the less the estimation sensitivity to system changes.

For slow changes in the system states, such as load variations, the size of the sliding window needs to be enlarged in order to avoid stationary error from the least square method. For recursive least square method, the window size is controlled by the forgetting factor. A unity forgetting factor will set equal weights for all measurements within the window, and better stabilize the estimation result by sacrificing the sensitivity to state changes. Therefore, the less the forgetting factor, the more sensitive of the algorithm to state changes, and the higher risk of the encountering stationary errors will be. The sampling rate of a PMU is usually in the range of 20Hz to 30Hz. Inputting too frequent measurements to the VIP algorithms will cause similar stationary problem encountered by choosing too small a window size.

The performance of VIP in dealing with system conditions (such as load ramping, fast dynamics, etc.), and choice of VIP parameters (such as sampling frequency, window size, forgetting factors) are still open issues in designing VIP-based applications. These open issues can be expanded to the following questions:

- How often should the VIP be monitored to track the changes in the system using only local measurements.
- Which VIP algorithms possess better performance? What are the strengths and limitations of each technique?
- How can the parameters for the VIP algorithms (such as sampling rate, window size, and forgetting factor) ne optimized, so that the VIP can be applied to estimate stability margin?

In conclusion, the tradeoff between sensitivity and stability of different VIP algorithms could be optimized by choosing appropriate window size, forgetting factor, and sampling rate. In order to answer the above questions, comparison studies are performed by quasi-steady state simulations. The LS and RLS VIP algorithm are compared for their performance in tracking stability changes with different speeds. The simulations are conducted in the IEEE 39-bus system. Similar simulations can be extended to larger system models without losing generality.

Under steady-state simulation environment, the load across the entire test system will be ramped up starting from 150% of the base load to the critical loading level (165.5%) at different ramping speeds (based on initial load to collapse ramping in 10, 30 and 60 minutes respectively) corresponding to three simulation scenarios. For each simulation scenario, power flow will be performed along with the ramping load to generate voltage and current phasors at monitored load buses. We choose to ramp the system load non-linearly with regard to time in the following form, in which "*Ramp_time*" is the time to reach load peak; t is the simulation time.

$$\text{When } t \geq Ramp\_Time,\ \text{Load\_factor} = 1.5 + 0.158 * \sin\left(\frac{\pi}{2} * \frac{\text{t}}{\text{Ramp\_Time}}\right)$$

When $1.3Ramp\_Time > t > Ramp\_Time$,

$$\text{Load\_factor} = 1.5 + 0.158 * \cos(\frac{\pi}{8} * \frac{\text{t - Ramp\_Time}}{0.3 * \text{Ramp\_Time}}),$$

The above load ramping format is designed to resemble the behavior of the system load reaching the peak load. For each simulation scenario, power flow will be performed along with each step of the load changes to generate voltage and current phasors at monitored load buses (load bus 4 is the monitored bus). Based on the voltage and current phasors, VIP with different approaches (least square method or recursive least square method), different sampling rates (20Hz, 2Hz and 1Hz) and different forgetting factors (0.95 or 0.8) are applied in parallel to find the best combinations of parameters for different simulation scenarios. The simulation results are shown in Figure 8 through Figure 11. Differences among the V_{TH} curves in Figure 9 to Figure 11 are produced by different parameters or different algorithms only. Reactive power limits of generators are considered during any simulation process.

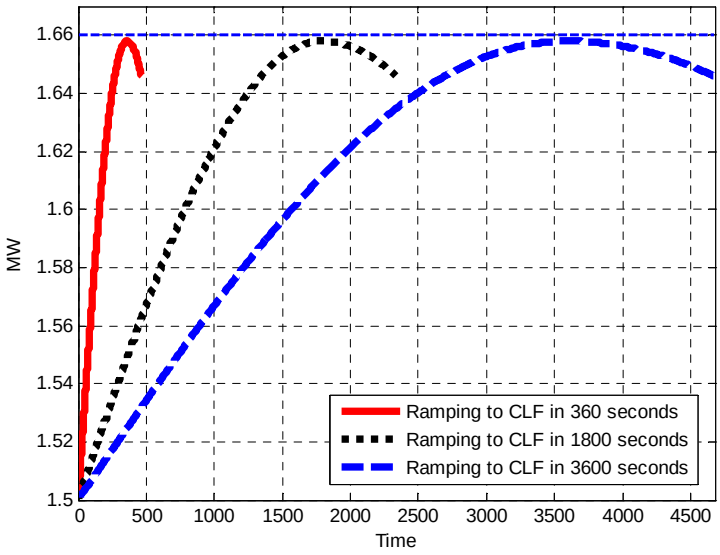

Figure 8. Load disturbances at different ramping rate (360, 1800 and 3600 seconds ramping to Critical Loading Factor).

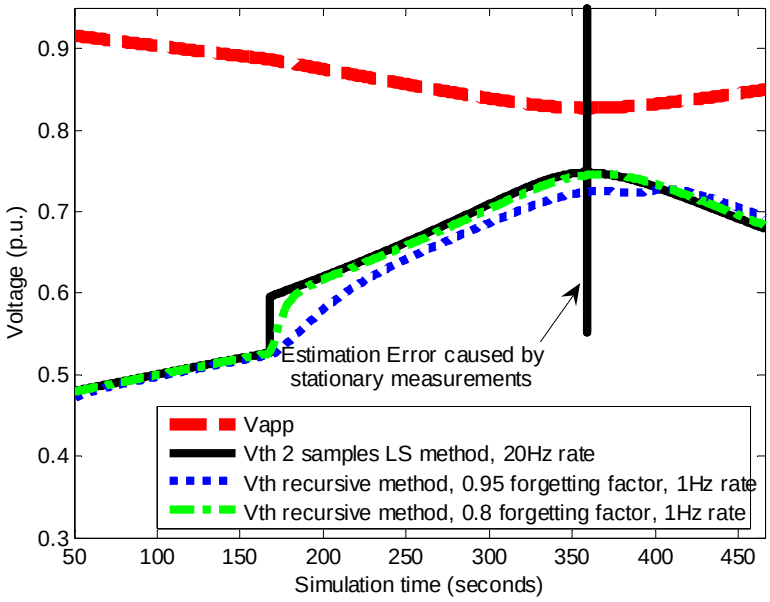

Figure 9. Load disturbances at different ramping rate (360, 1800 and 3600 seconds ramping to Critical Loading Factor).

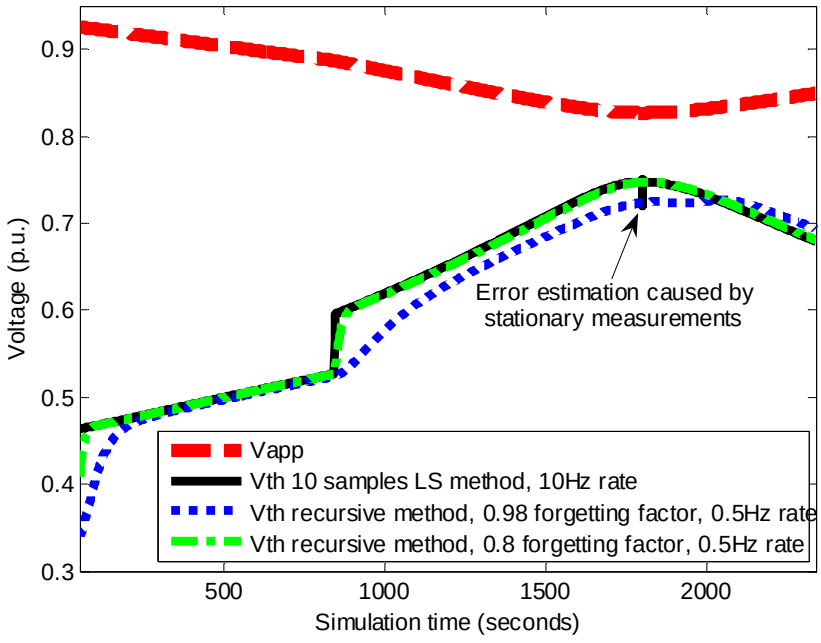

Figure 10. Load disturbances at different ramping rate (360, 1800 and 3600 seconds ramping to Critical Loading Factor).

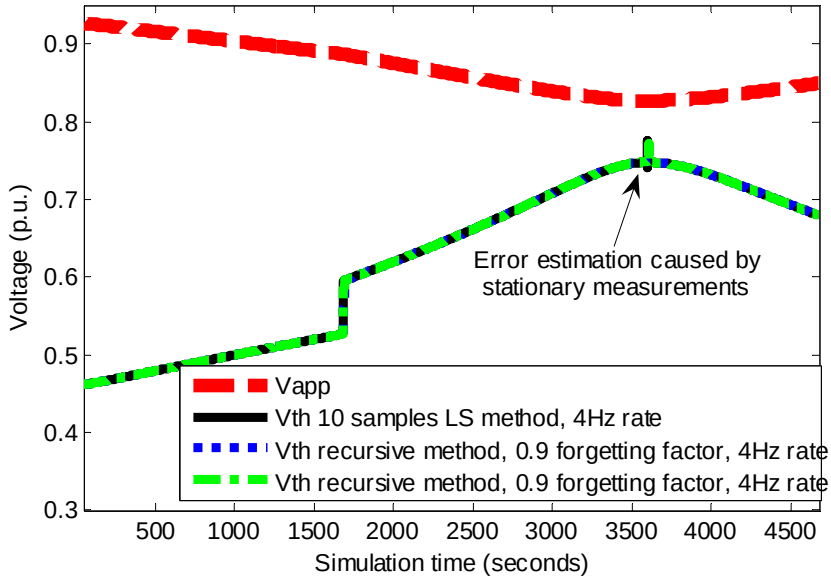

Figure 11. Load disturbances at different ramping rate (360, 1800 and 3600 seconds ramping to Critical Loading Factor).

More simulations are performed with different combination of the important factors (sampling rate, window size and forgetting factor). The performance matrices for the LS and recursive VIP algorithm are listed in Table 4 and Table 5, respectively. The meaning of the codes in the performance matrices are as follows:

Code 0: No appreciable error is discovered in simulations.

Code 1: Stationary estimation errors are discovered in the vicinity of load peark.

Code 2: The parameters of the identified VIP model are lower than the other cases.

According to the performance matrices, the suggested parameters for the LS and recursive algorithm are introduced in Table 6.

Table 4. Performance matrices of the recursive VIP algorithm considering different sampling rate and forgetting factor

Rate	20Hz			10Hz			4Hz			2Hz			1Hz			0.5Hz			0.2Hz			0.1Hz		
Case	1	2	3	1	2	3	1	2	3	1	2	3	1	2	3	1	2	3	1	2	3	1	2	3
λ=0.98	0	0	0	0	0	0	2	0	0	2	0	0	2	0	0	2	2	0	2	2	2	2	2	2
λ=0.95	0	0	0	0	0	0	0	0	0	0	0	0	2	0	0	2	0	0	2	2	0	2	2	2
λ=0.9	0	0	1	0	0	0	0	0	0	0	0	0	0	0	0	2	0	0	2	0	0	2	2	0
λ=0.8	0	0	1	0	0	0	0	0	1	0	0	0	0	0	0	0	0	0	2	0	0	2	0	0
λ=0.7	0	0	1	0	0	0	0	0	0	0	0	0	0	0	0	0	0	0	2	0	0	2	0	0
λ=0.6	0	1	1	0	0	0	0	0	1	0	0	0	0	0	0	0	0	0	0	0	0	2	0	0
λ=0.5	0	0	1	0	0	1	0	0	0	0	0	0	0	0	0	0	0	0	0	0	0	2	0	0
Note: λ is the forgetting factor. Code 0: no appreciable error. Code 1: Stationary error. Code 2: low estimation.																								

Table 5. Performance matrices of the LS VIP algorithm considering different sampling rate and window size

Rate	20Hz			10Hz			4Hz			2Hz			1Hz			0.5Hz			0.2Hz			0.1Hz		
Case	1	2	3	1	2	3	1	2	3	1	2	3	1	2	3	1	2	3	1	2	3	1	2	3
N=2	1	1	1	0	1	1	0	1	1	0	0	1	0	0	1	0	0	0	0	0	0	0	0	0
N=4	0	1	1	0	1	1	0	1	1	0	0	1	0	0	0	0	0	0	0	0	0	0	0	0
N=10	0	1	1	0	1	1	0	0	1	0	0	0	0	0	0	0	0	0	0	0	0	2	0	0
N=20	0	1	1	0	1	1	0	0	0	0	0	0	0	0	0	0	0	0	2	0	0	2	0	0
N=30	0	0	1	0	0	1	0	0	0	0	0	0	0	0	0	0	0	0	2	0	0	2	0	0
N=40	0	0	1	0	0	0	0	0	0	0	0	0	0	0	0	2	0	0	2	0	0	2	2	0
N=50	0	0	1	0	0	1	0	0	0	0	0	0	0	0	0	2	0	0	2	0	0	2	2	0
Note: N is the window size. Code 0: no appreciable error. Code 1: Stationary error. Code 2: low estimation.																								

Table 6. Summary of quasi-steady state simulation results for VIP algorithms.

Rate / Ramp	20Hz		10Hz		2Hz		1Hz		0.5Hz	
	N_{LS}	λ_{RLS}	N_{LS}	λ_{RLS}	N_{LS}	λ_{RLS}	N_{LS}	λ_{RLS}	N_{LS}	λ_{RLS}
360 seconds	*4*	*0.95*	***2***	*0.95*	***2***	***0.95***	***2***	***0.9***	***2***	***0.8***
1800 seconds	***30***	*0.95*	***30***	*0.95*	***2***	*0.95*	***2***	*0.95*	***2***	***0.95***
3600 seconds	***>50***	*0.95*	***40***	*0.95*	***10***	*0.95*	***4***	*0.95*	***2***	***0.95***
Note	**N_{LS} is the recommended window size for least square method. λ_{RLS} is the recommended value for the forgetting factor used in the recursive least square method.**									

Based on the simulation results, the following conclusions can be drawn.

1) In general, the numerical difference between Zapp and Z_{TH} estimated by RLS method is larger than by LS method under the same system conditions. In the absence of fast

transients, simple LS method with low sampling rate is sufficient to track the changes in a monitored system.

2) With the increase in sampling rate and decrease in speed of load disturbance, the window size of the LS method need to be enlarged to avoid stationary estimation errors.

3) The forgetting factor λ of the RLS algorithm needs to be lowered with the decreasing of sampling rate in order to maintain the sensitivity of the RLS algorithm. For example, when the sampling rate is 0.5 Hz, the recommended λ for the 10-minutes load ramping case is 0.8 or less.

3.5 VOLTAGE STABILITY INDEX BASED ON VIP

Based on the ability of the VIP in tracking stability changes, more advanced application of the VIP can be designed, such as the estimation of stability margin. Since the VIP relies on time-domain measurements of the system states (voltage and current phasors), the Thevenin equivalent model embedded in the VIP can be used to represent the external network as seen by a monitored load bus. Therefore, the entire system model can be reduced to a 2-bus model (as shown in Figure 4). The power flow equation of this 2-bus system model can be represented by (3-12).

$$V^4 + V^2[2(R_{TH}P_L + X_{TH}Q_L) - E^2] + Z_{TH}{}^2(P_L^2 + Q_L^2) = 0 \tag{3-12}$$

The solution to the voltage on load bus V can be solved by (3-13).

$$V^2 = \frac{-[2(R_{TH}P_L + X_{TH}Q_L) - E^2] \pm \sqrt{[2(R_{TH}P_L + X_{TH}Q_L) - E^2]^2 - 4Z_{TH}{}^2(P_L^2 + Q_L^2)}}{2} \tag{3-13}$$

The discriminant of (3-13) should be positive in order to ensure feasible solutions for V^2:

$$[2(R_{TH}P_L + X_{TH}Q_L) - E^2]^2 \geq 4Z_{TH}{}^2(P_L^2 + Q_L^2) \tag{3-14}$$

At the nose point of the PV curve, a single solution of (3-13) will be converged. The following equation will be satisfied:

$$2(R_{TH}P_L + X_{TH}Q_L) - E^2 = \pm 2|Z_{TH}|(P_L^2 + Q_L^2) \tag{3-15}$$

Assuming the ratio between active and reactive loads is fixed, which can be expressed by $P_L = mQ_L$; (3-15) becomes (3-16).

$$2(R_{TH}P_L + mX_{TH}P_L) - E^2 = \pm 2|Z_{TH}|\sqrt{P_L^2 + m^2P_L^2} = \pm 2|Z_{TH}|P_L\sqrt{1+m^2} \tag{3-16}$$

Therefore, the active load demand P_L can be evaluated by (3-17).

$$P_L = \frac{E^2}{2(R_{TH} + mX_{TH}) \pm 2|Z_{TH}|\sqrt{1+m^2}} \tag{3-17}$$

Considering $P_L>0$ and $E^2>0$, then (3-18) should hold;

$$2(R_{TH} + mX_{TH}) \pm 2|Z_{TH}|\sqrt{1+m^2} > 0 \tag{3-18}$$

Equation (3-18) can be decoupled into (3-19) and (3-20). Satisfying either one of (3-19) and (3-20) will lead to a feasible solution for P_L.

$$2(R_{TH} + mX_{TH}) + 2|Z_{TH}|\sqrt{1+m^2} > 0 \tag{3-19}$$

$$2(R_{TH} + mX_{TH}) - 2|Z_{TH}|\sqrt{1+m^2} > 0 \tag{3-20}$$

Obviously, (3-19) is true at all circumstances, because the signs of all terms are positive. Supposing (3-20) is true, we can get (3-21):

$$4(R_{TH} + mX_{TH})^2 > 4|Z_{TH}|^2(1+m^2)) \tag{3-21}$$

By expanding (3-21), (3-22) can be obtained eventually:

$$2mR_{TH}X_{TH} > m^2 {R_{TH}}^2 + {X_{TH}}^2 \tag{3-22}$$

Since (3-22) is false, (3-20) is also false. Therefore, the critical load based on VIP equivalent model can be estimated by:

$$P_L^{Max} = \frac{E^2}{2(R_{TH} + mX_{TH}) + 2|Z_{TH}|\sqrt{1+m^2}} \tag{3-23}$$

Assuming index of most recent measurement is *k*, the current and previous measurements on real load are $P_L(k)$ and $P_L(k-1)$, the estimated time to reach critical load is:

$$t_{critical}(k) = \frac{P_L^{Max} - P_L(k)}{P_L(k) - P_L(k-1)} \Delta t_{measure}, \tag{3-24}$$

where $\Delta t_{measure}$ is the time interval between measurement *k* and *k-1*.

Estimating the rate of change in load based on two measurements is not a reliable and accurate method. Since the load changes can be linearized in a small time window, the slope of the linearized load changes can be estimated by a linear regression algorithm with a small sliding window. Let the linear relation between load and time be:

$$P_L = \alpha + \beta T \tag{3-25}$$

Let the regression window size be W samples. The least square estimation of the slop β can be calculated by (3-26)

$$\hat{\beta}(k) = \frac{\sum_{i=k-W}^{k} (T_i - \overline{T}_k)(P_{L,i} - \overline{P}_{L,k})}{(T_i - \overline{T}_k)^2} \tag{3-26}$$

where $\overline{T}_k$ and $\overline{P}_{L,k}$ is the average of time and load measurements within the regression window.

Since $\hat{\beta}(k)$ is estimated based on load measurements, the updating of $\hat{\beta}(k)$ should only be done only when the load changes are appreciable. Otherwise, small estimations in $\hat{\beta}(k)$ could lead to unreasonable prediction in stability margin. The low-speed load changes usually happen during either steady-state or load peaks. For either situation, the corresponding stability margin is approximately static. A simple update mechanism for $\hat{\beta}(k)$ can be formulated in (30):

$$\begin{cases} \hat{\beta}(k) \geq \varepsilon \quad update \quad \hat{\beta}(k) \quad u\sin g \quad (3-26) \\ \hat{\beta}(k) < \varepsilon \quad \hat{\beta}(k) = \hat{\beta}(k-1) \end{cases} \tag{3-27}$$

Therefore, the aforementioned formulations for predicting stability margin can be reformulated as:

$$t_{critical}(k) = \frac{P_L^{Max} - P_L(k)}{\hat{\beta}(k)} \tag{3-28}$$

Similar to the sliding window of the VIP algorithm, the choice of window length for linear regression can also have an impact on the estimation error. Even if the estimation error is within a high confidence interval with long window length, a high sampling rate can still cause unreasonable answers. Through the load ramping simulations, a window length of 10 samples has been tested to be sufficient when the sampling rate is lower than 4Hz. Further increasing the window length will not appreciably reduce the estimation error. However, with the regression window fixed to be 10 samples, the sampling rates for the three scenarios need to be no higher than 4Hz, 1Hz and 0.5Hz, respectively, in order to avoid stationary errors in the vicinity of load peaks.

Applying the proposed margin estimation algorithm on the VIP results from Figure 8 through Figure 11, the time-domain stability margins for different load-ramping scenarios can be evaluated (as shown in Figure 12). When the estimated time to instability is close to "0", remedial stability controls scheme should be considered.

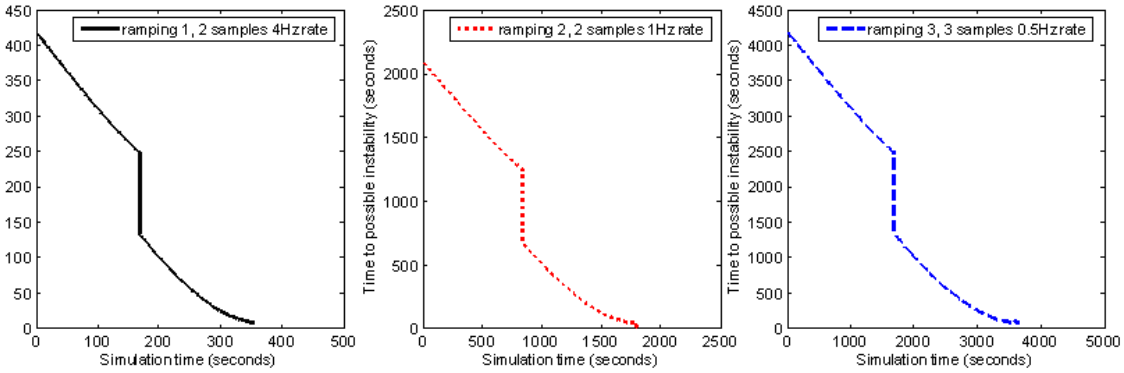

Figure 12. Time to reach critical load for different load ramping speeds.

In Figure 12, the discontinuous changes in the stability margin correspond to the PV~PQ transients of the generator on bus 37. Since the risk of instability associated with the PV-PQ transitions can only be evaluated by performing system-wide analysis, the best usage of a local method is to predict the occurrence of a possible PV~PQ event. For each interconnected generator, the estimated time to reach its reactive generation limit can be calculated by (3-29):

$$t_{Limit,i}(k) = \frac{Q_{Limit,i} - F_{Shift,i} Q_L(k)}{\hat{\beta}(k)}, \tag{3-29}$$

where $F_{Shift,i}$ is the shift factor for generator i to the local load measurements; $Q_{Limit,i}$ is the reactive generation limit for generator i.

Therefore, the estimated time to possible system instability is as following:

$$t_{collapse}(k) = \min\left\{t_{critical}(k), t_{Limit,i}(k)\right\},\ i \in [1,n] \tag{3-30}$$

where n is the number of interconnected generators.

From the preliminary studies of the VIP, we have observed that voltage collapse could happen as a discontinuous transition. As a result, the stability margin estimated by the VIP may not be fast enough to capture the transition to voltage collapse. A good way to calibrate the VIP stability index is to use the margin estimation from the continuation power flow as a reference. Using the same formulation as described in (3-28) to (3-30), the critical loading factor estimated by CPF can be regarded as P_L^{Max} to predict the time to reach instability. The results from the CPF based method and the VIP method are compared in Figure 13. In order to eliminate the gap between the two curves in Figure 13, a simple correction factor can be used to correct the VIP result. After adopting a correction factor of 0.6, the calibrated VIP result is compared with the CPF based method in Figure 14.

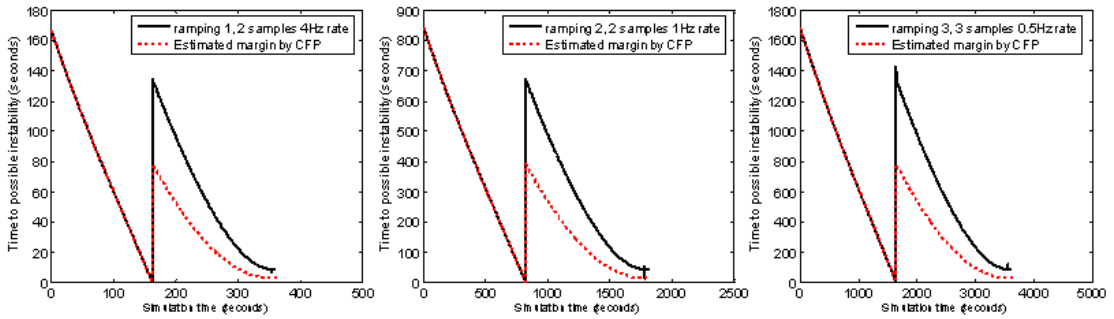

Figure 13. The time to reach instability estimated by the VIP and CPF.

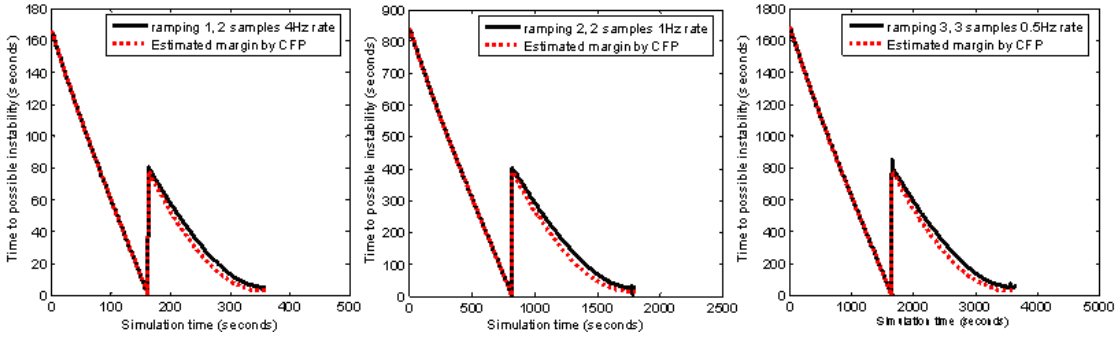

Figure 14. The time to reach instability estimated by the calibrated VIP and CPF.

In Figure 14, the calibrated VIP result matched with the CPF method in predicting the time to reach the critical load. The above simulation studies focus on the sensitivity and accuracy of the VIP at the proximity to instability. During routine operation conditions, the VIP will face load changes from base level to peak level, as well as multiple PV-PQ transitions from different generators. In addition, the precision of load measurement could have an impact on the VIP results. In the following case study, a load ramp from base level to peak level with 1% uniform-distributed random measurement errors is generated by (32) (illustrated in Figure 15). The sources of measurement errors include the measurement devices and losses through communication channels. The load will be settled around the peak level (165% loading factor) then start decreasing to the proximity to instability.

$$\text{Load\_factor} = 1 + 0.65 * \sin(\frac{\pi}{2} * t * 1.01) + 0.01 * random\_noise(0,1) \quad (3\text{-}31)$$

Using the same correction factor of 0.6, the calibrated VIP results are compared with the results from the CPF based method in Figure 16.

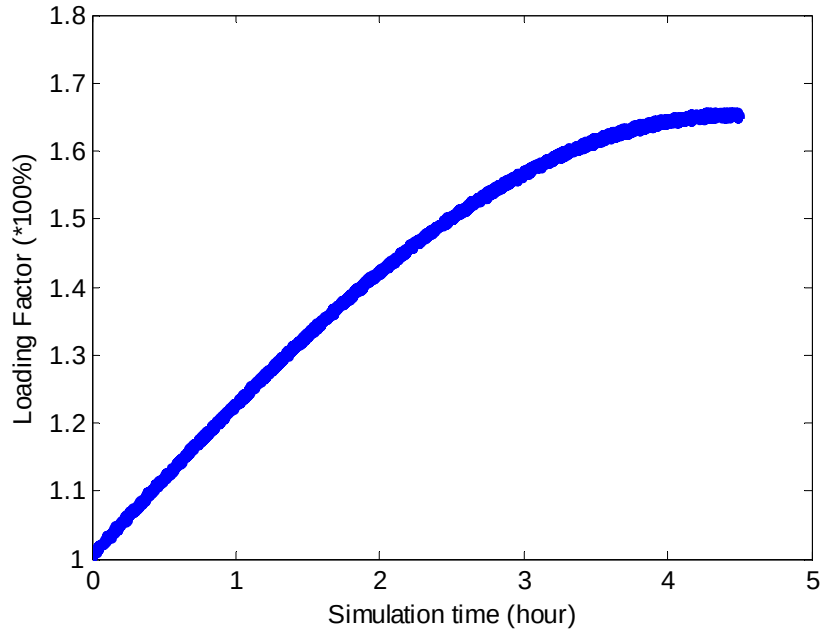

Figure 15. A simulated load ramp from base level to peak level with 1% uniform-distributed random measurement errors.

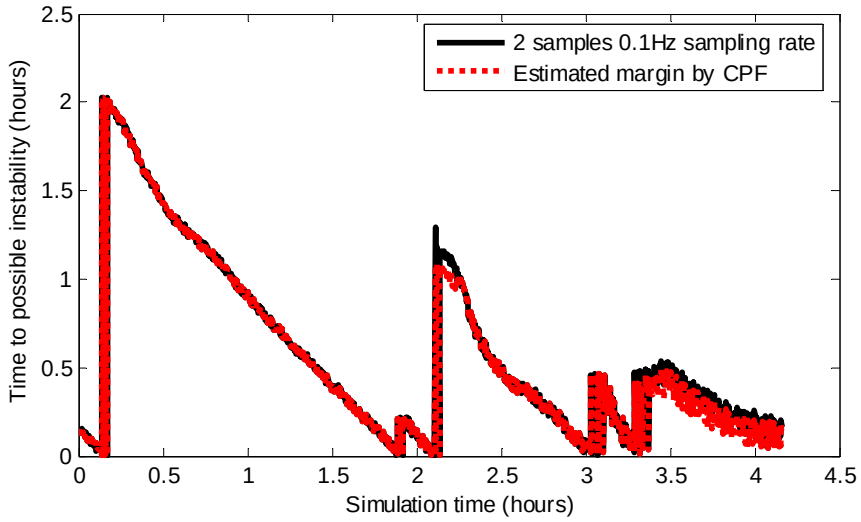

Figure 16. The time to reach instability estimated by the calibrated VIP and CPF considering errors of load measurement and multiple PV-PQ transitions.

In Figure 16, every time the two curves reach the x-coordinate, a PV-PQ transition occurs. The random errors in the load measurements will cause slight impact on the margin estimation results from both methods. The differences between the VIP and

CPF stability index near the load peak (after 3.5 hours) lie in the range from zero to 6.08 minutes, with a mean value of 3.32 minutes. The differences between the VIP and CPF stability index before the load peak (0~3.5 hours) lie in the range from zero to 13.03 minutes, with a mean value of 0.23 minutes. The maximum difference is observed at 2.11 hours after a discontinuous PQ-PV transient. In general, the results of the calibrated VIP method matched with the CPF method in predicting the time to reach the critical load.

3.6 USE ONLINE VIP EQUIVALENT MODEL TO CAPTURE THE CHANGES IN STABILITY CONDITION UNDER DYNAMIC ENVIRONMENT

When the power system is running under steady-state, the VIP evaluation should be paused since the difference between any two adjacent measurements is negligible. On the other hand, if a disturbance or contingency event is detected, the resulting dynamic process may cause substantial error for the VIP evaluation. The discontinuous controls, such as the controls of LTCs and over excitation limiter (OXLs), can also cause short dynamics processes. All of these dynamic processes could be magnified by the voltage-sensitive components in the system. In order to adapt the VIP to real-time operation environment, Milosevic [14] presented the idea of using recursive method to update the VIP results. By adopting the recursive VIP method, the output of the VIP can be stabilized because of the weighting effect over historical measurements. It has been shown in the previous section that both the LS and recursive method can be tuned to capture the changes in stability condition following load ramping.

The performance of the LS method is better than the recursive method in capturing slow changes in stability condition. Both of the VIP algorithms require a set of

voltage and phasor measurements covering similar system conditions but with appreciable difference. If the differences among the measurements are negligible, the sampling rate needs to be reduced in order to avoid static error. Since the recursive method has the advantage of using forgetting factor to control the window size, the risk of evoking static error could be reduced.

On the other side, if the effective window of any VIP algorithm covers the measurements from different system conditions (such as pre- and post-contingency states), the VIP result could become inaccurate or infeasible. The VIP algorithms assume the identical Thevenin model applied to all system states sampled within the sliding window. If there are multiple distinct system conditions included in the sliding window, the existence or validity of the unique applicable Thevenin model for all included system conditions is not guaranteed.

Besides the discontinuous changes, the subsequent transients may also cause error in the VIP result. During a transient process, the system state varies quickly from one transient state to another. If the VIP algorithm absorbs the measurements crossing multiple transient states, the credibility of the VIP result could be reduced. Moreover, the errors caused by a dynamic process could accumulate over time and eventually alter the steady-state VIP result.

Figure 17 demonstrates the limitation of the recursive VIP algorithm in handling abrupt changes and transients. The time-domain simulation is performed on the IEEE 39-bus dynamic model. The forgetting factor for the RLS algorithm is set to be 0.95 or 0.99 for two simulation scenarios represented by a dotted black curve and a solid blue curve, respectively. The discontinuous changes in the voltage measurements correspond to the

following events: N-1 contingencies (at 100 seconds and 250 seconds), automatic OXL controls (at 120 seconds, 170 seconds and 390 seconds), and automatic LTC control (at 175s and 190 seconds). During discontinuous changes and subsequent dynamic processes, the VIP reacts by showing overshoot and subsequent over-damping. It is difficult to extract any constructive information about the changes in the voltage stability condition from Figure 17.

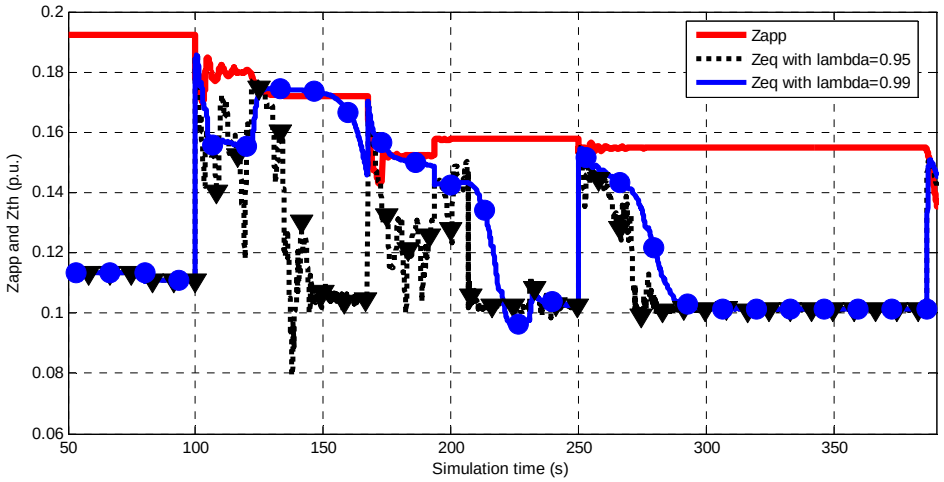

Figure 17. VIP evaluation using recursive approach for time-domain application.

The overshoot during the dynamic process cause a temporary instability signal from the VIP (at 100 seconds and 250 seconds). After the discontinuous changes and dynamic processes, the VIP result recovers from the overshoot but indicates optimistic estimation of the stability margin. The increases in stability margin implied by the VIP result can not be justified by the actual contingencies events experienced by the system.

Since the discontinuous changes and dynamic processes are the causes of false VIP results, a blocking trigger for VIP should be the identification of the onset and ending time for such events. A transient monitor with signal processing packages (such as wavelet toolbox) could be adopted to fulfill the task. Between the time frames of such

events, special procedures should be designed to evaluate the trend of stability condition with reduced error. The scheduling of the transient monitor is shown in Figure 18.

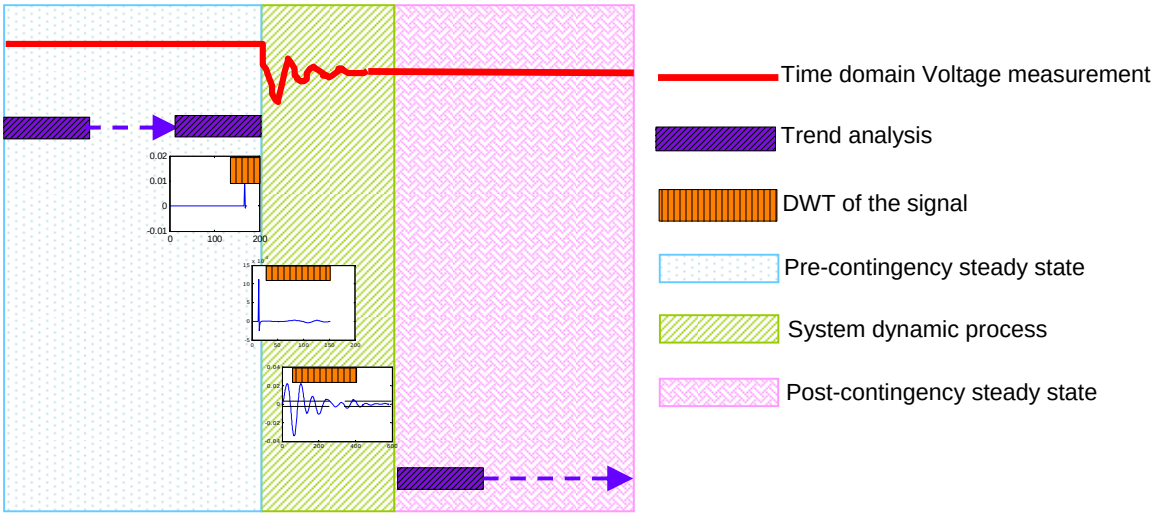

Figure 18. The design of the transient monitor.

In Figure 18, the transient monitor relies on 3-level Discrete Wavelet Transform (DWT) to detect the starting and ending of a dynamic process. The details of the DWT algorithm can be found in [35]. Among the family of mother wavelets, Haar wavelet resembles a step function, which is similar to a discontinuous change. By adopting the Haar wavelet as the mother wavelet, the 2^{nd} and 3^{rd} level detail components of the wavelet transform on the voltage and current measurements show the discontinuity precisely (as shown in Figure 18). The ending time of a dynamic process can also be identified by applying a few logic rules:

If $D(t) > \varepsilon_1$ Report the starting of a dynamic process and set Flag = 1;

If Flag=1 and $D(t) \le \varepsilon_2$, Report the end starting of a dynamic process and set Flag=0.

where *D(t)* is the coefficient of the 2nd level detail component obtained at time *t*; ε_1 and ε_2 are small positive real numbers.

During steady-state operation conditions, linear regression can be applied to estimate the trend of the voltage measurement within a sliding window. Since the only interest is to detect the slow changes in voltage measurement, a simple regression model in the similar form of (26) may be adopted.

According to the study in the previous section, the LS algorithm performed at a low frequency (0.5-2Hz) produces accurate VIP results for tracking slow changes in system states. When a trend in voltage measurements is detected, the LS VIP algorithm with appropriate parameters can be adopted. If the trend in voltage measurements disappears, the most recent VIP result should be carried on until either another trend or a discontinuous change is detected. When a discontinuous change is detected, the VIP should be reactivated to evaluate the stability condition after the discontinuous change. There are two possible system conditions following a discontinuous change—a dynamic process or a new steady state. For either possibility, the recursive VIP algorithm is a better choice than the LS VIP algorithm. The recursive VIP algorithm has the advantages of soothing the impact of noise and reducing the risk of static error. However, since the VIP is not a dynamic model, measurements during server dynamics should be screened from entering the VIP algorithms. Using the most recent VIP results from the previous system condition before the discontinuous change as the initial guess, the recursive VIP algorithm will soon converge to a new state reflecting the stability condition after the discontinuous change. Summarizing all of the above considerations, a synthetic time-

domain VIP routine can be presented. The flow chart of the proposed VIP routine is shown in Figure 19.

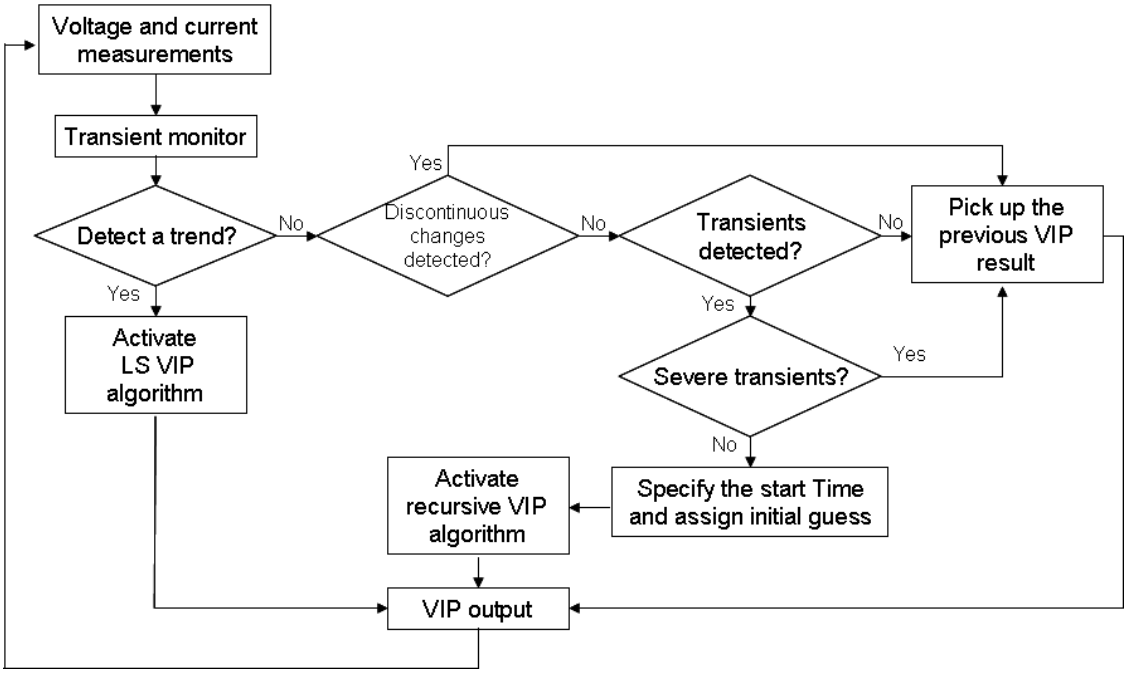

Figure 19. The flowchart of the proposed time-domain VIP routine.

In the previous section, the performances of the VIP algorithms have been justified by the power flow based stability analysis. The accuracy of the VIP algorithm under dynamic environment will be demonstrated by the following simulation examples. The dynamic modeling, contingency events, and data extraction are performed in PSS/E.

2-bus Example:

Considering the 2-bus system as shown in Figure 20, bus 1 is the slack bus with a constant voltage phasor of $1\angle 0$, while bus 2 is a PQ bus connecting a constant power load (120 MW and 48 MVAr). There are three identical lines connecting between bus 1 and bus 2. Two N-1 contingencies are simulated at 50 seconds and 100 seconds

respectively by tripping one line at a time. The snapshot following each N-1 contingency is shown in Figure 20. The accuracy of the VIP algorithm can be evaluated by comparing the identified Thevenin impedance with the actual line impedance. Following the proposed VIP routine, two discontinuous changes are detected. The recursive VIP algorithm is reactivated twice. The comparison between the identified Thevenin impedance and the actual line impedance is shown in Figure 21(a). Because of the "memory" of past measurements, the error of the recursive algorithm is in an opposite direction to the changes in stability margin. A multiplier can be adopted to compensate the error in the estimated Thevenin impedance (as shown in Figure 21(b)). The actual line impedance and the identified Thevenin impedance by the dynamic VIP algorithm are compared in the Cartesian plane (as shown in Figure 21(c)).

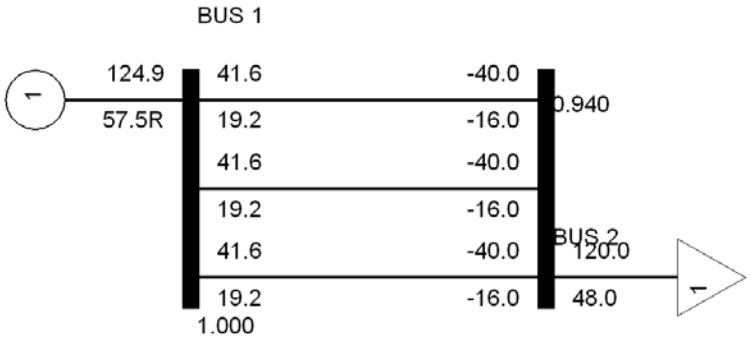

(a) Base case

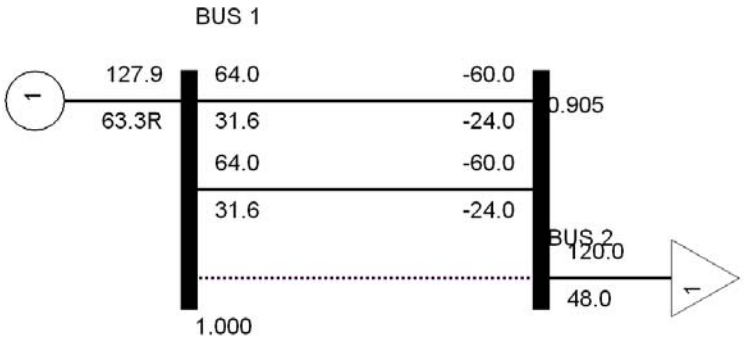

(b) After first N-1 contingency

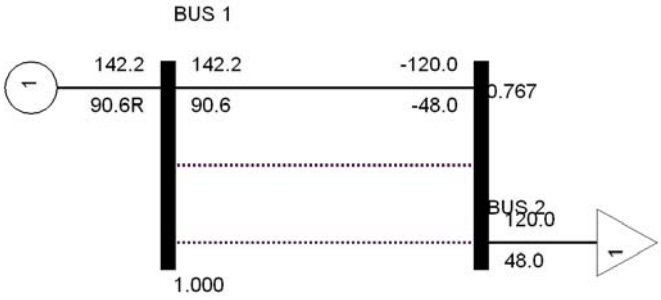

(c) After second first N-1 contingency

Figure 20. 2-bus dynamic system.

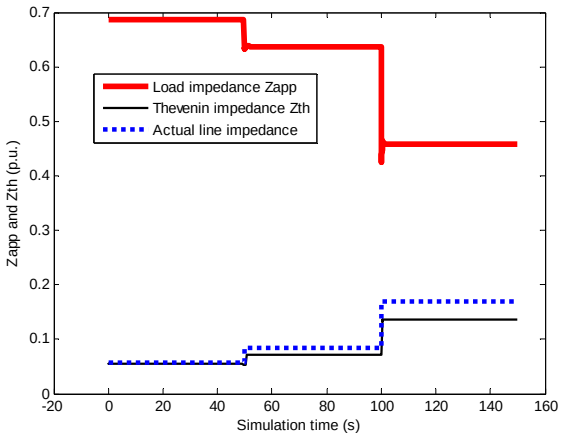

(a) Original VIP result

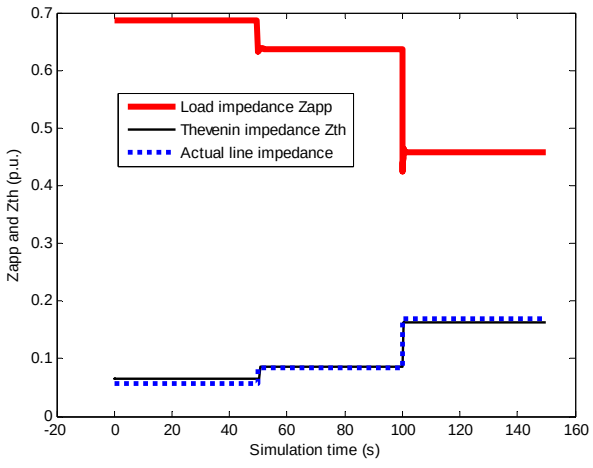

(b) Calibrated VIP result

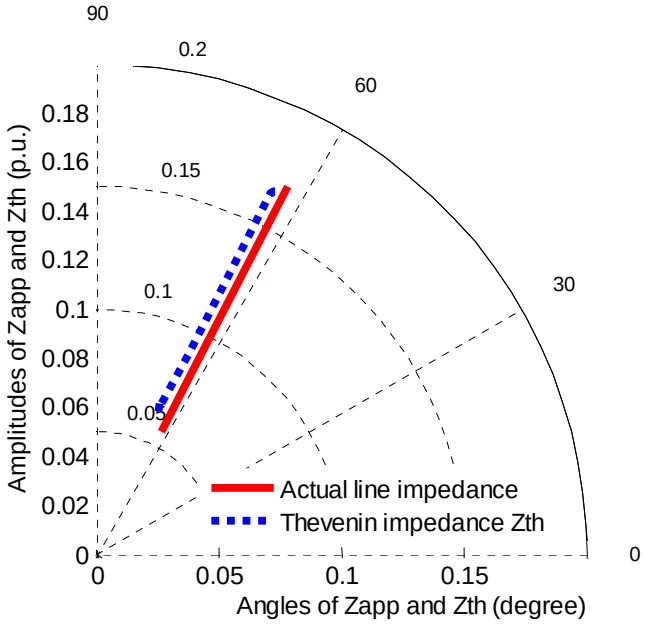

(c) Polar plot of the line impedance and equivalent Thevenin impedance

Figure 21. Compare the Thevenin impedance with the line impedance for the 2-bus system.

In Figure 21, the identified Thevenin impedance by the proposed dynamic VIP algorithm matches with the actual line impedance closely. The changes in the line impedance are captured immediately following the detection of the discontinuous changes caused by the line contingencies at 50 seconds and 100 seconds. The VIP model is sensitivity to the changes in stability condition caused by contingencies in the 2-bus system.

IEEE-39 bus time-domain simulation:

Dynamic simulations are performed based on the 39-bus test system modeled in PSAT. The adopted dynamic components include 10 generators, governors and excitation stabilizer. The parameters of the dynamic components can be found in [34]. Using the given parameters, the base case of the dynamic 39-bus system is tested to be stable. The

goal of the dynamic simulation is to test the performance of the proposed dynamic VIP routine, as well as examine the accuracy of the VIP equivalent model.

During the dynamic simulation, the aggregated system load is set to be 120% of the base case loading level in order to exaggerate the impact of the later applied line contingencies. The virtue VIP device is installed on load bus 8, which is prone to voltage instability. Two line contingencies (line 21-22 and line 2-3) are applied at 100 seconds and 200 seconds respectively. The VIP is expected to track the changes in the local stability condition after each line contingency. The transient monitor detects the starting time of the discontinuous change and ending time of the severe dynamic process (as shown in Figure 22). In Figure 22, DWT(V) is the discrete wavelet transform of the time-domain voltage measurement. The dashed lines represent the cutoff magnitude for the identification of severe dynamic processes.

Since there is no comparable online method that can be used to calibrate the time-domain VIP results, the previous studied quasi-steady state VIP algorithm is adopted to benchmark the dynamic VIP algorithm. At each system state, such as pre- and post-contingency states, offline simulations using the quasi-steady state VIP is performed. The idea is to estimate the variables of the Thevenin equivalent model offline, then compare with the result from the online dynamic VIP. During the offline VIP analysis, the aggregated system load is ramped to the online operation load level to facilitate the quasi-steady state VIP algorithm. The offline VIP only requires two measurements sampled at low frequency of 1Hz for accurate estimation of the stability condition. To achieve best accuracy in the offline analysis, multiple offline VIP calculations with different load ramping rate is recommended. The parameters adopted for the online VIP

algorithms are 2 Hz sampling rate, 0.8 forgetting factor for the recursive algorithm, and a window size of 2 samples for the LS algorithm. The results from the offline and online VIP methods are compared in Figure 23. Table 7 lists the detailed actions of the proposed dynamic VIP algorithm in response to different system conditions.

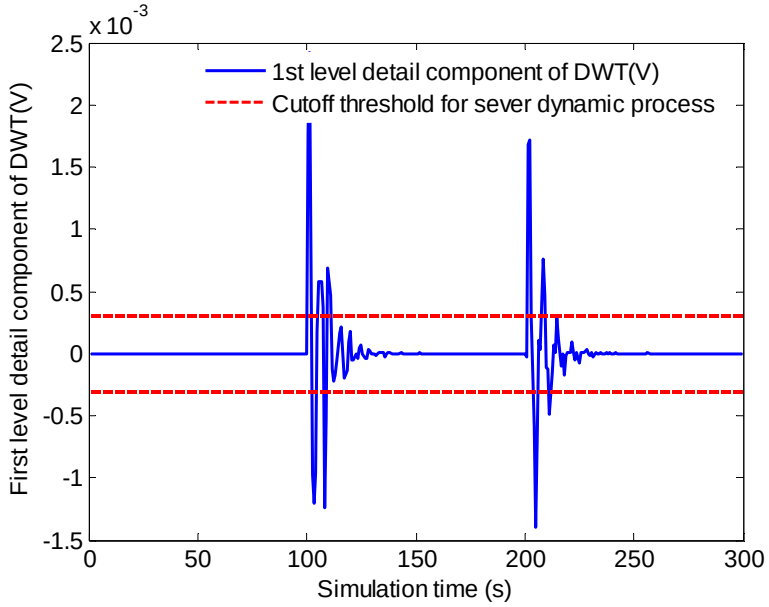

Figure 22. The window of the transient monitor for screening severe transients.

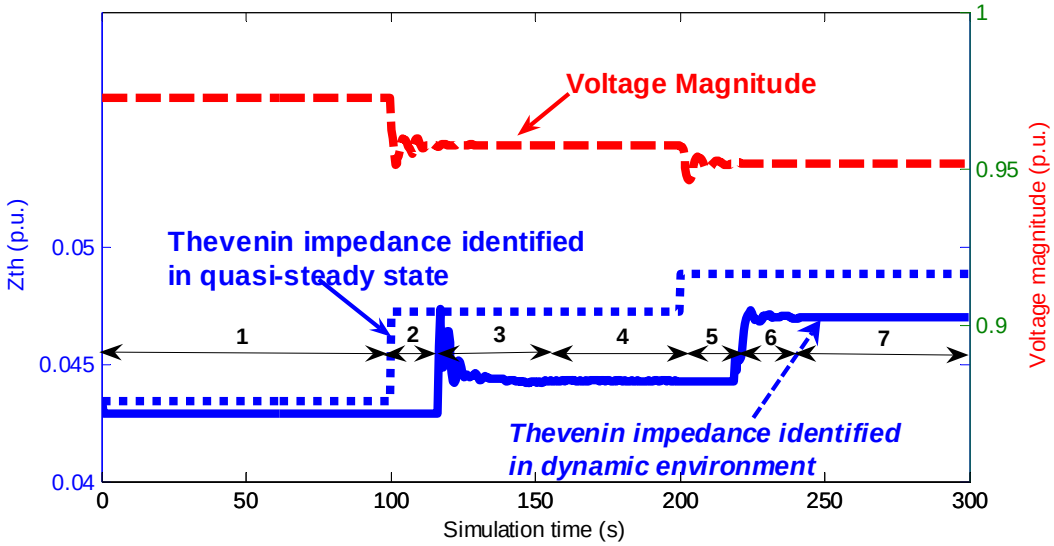

Figure 23. VIP results from the online dynamic VIP routine and the offline quasi-steady state VIP algorithm.

Table 7. VIP actions corresponding to different system condition during the time-domain simulation

Period ID	System conditions	VIP actions
1	Steady state	No evaluation and report the last calculation results.
2	Discontinuous changes and transient	VIP calculation blocked.
3	Subsequent transients	Use LS algorithm to obtain initial guess, then use recursive algorithm to updated VIP results.
4	Steady state	No evaluation and report the last calculation results.
5	Discontinuous changes and transient	VIP calculation blocked.
6	Subsequent transients	Use LS algorithm to obtain initial guess, then use recursive algorithm to updated VIP results.
7	Steady state	No evaluation and report the last calculation results.

In Figure 23, the estimated Thevenin impedance from the dynamic VIP routine matches well with the offline VIP results. The small quantitative difference (no more than 5% relative error) is caused by the "averaging effect" of the recursive method. The measurements during severe dynamic processes are screened from entering the VIP during periods two and five to minimize the impact on the accuracy of the VIP algorithms. Recursive VIP algorithm is adopted during periods three and six, when subsequent transients present after severe transients. During steady-states in period one and seven, VIP algorithms are halted since no change is detected in system state, while the most recent calculated VIP model are adopted. In order to estimate the stability condition during the dynamic process, certain signal reconstruction techniques may be adopted to transform the dynamic measurements into nearly quasi-steady measurements. The interest of this research is to verify the ability of the VIP in observing the voltage stability condition and serving as an equivalent model for stability control analysis. The

possible applications of the VIP in dynamic modeling and transient stability monitoring are beyond the scope of this dissertation.

3.7 CONCLUSION

The Voltage Instability Predictor (VIP), a local stability analysis method, relies on discrete measurements to identify the equivalent Thevenin circuit of the entire power system connected to a load. The ability of the VIP in tracking changes in stability conditions, as well as serving as a time-variant equivalent model, are both novel features to be further extended for online application in voltage stability monitoring and control. However, the performance of VIP in dealing with different system conditions (such as load ramping, fast dynamics etc), and choice of VIP parameters (such as sampling frequency, window size, forgetting factors) are still open issues in designing VIP-based applications.

In this chapter, benchmark tests and simulations of VIP were conducted to fully appreciate the performance of the VIP algorithms. The study in this chapter aims at defining the boundary of the VIP for potential applications in the area of stability monitoring and network equivalent modeling. Through quasi-steady-state and time-domain simulations, the limitation of the VIP algorithms can be summarized as follows:

(1) Severe transients will cause numerical stability problems for the VIP algorithms.

(2) Stationary estimation errors are observed at the load peaks when higher sampling rates are adopted, whereas the sensitivity of the VIP algorithms are maintained.

(3) The sensitivity of the VIP algorithms may not be sufficient when lower sampling rates are adopted, whereas the stationary errors are eliminates.

Using the examples of the IEEE 39-bus system with different load-ramping speed, the tradeoffs between the two representative VIP algorithms—the LS and recursive algorithms were discovered.

- The Least-Square based VIP Algorithm is more sensitive and accurate than the recursive algorithm in tracking the slow changes in the voltage stability condition. However, the risk of encountering static errors increases with the decreases in the load-ramping speed. A wider window size and slower sampling rate can be adopted in the LS algorithm to avoid the static error, without losing accuracy in tracking stability condition.
- The recursive VIP algorithm can be applied in both steady-state and dynamic environment. The sensitivity and accuracy of the recursive VIP are compromised by the low risk of encountering static errors and interference from transients. Such tradeoff can be tweaked by choosing the suitable combination of the forgetting factor and sampling rate.
- The VIP equivalent model can be used to represent the external network of a load bus as a generator bus and a radial line. The maximum power transfer (MPT) of the 2-bus radial model can be predicted by tracking the determinant of the quadratic power flow equation. The voltage stability margin, in terms of the distance and time to reach the MPT point or the exhaustion of generator reactive support, can be evaluated in real time. A simple linear calibration can help to match the VIP stability index with the stability margin estimated by CPF.

Based on the characteristics of different VIP algorithms, a synthetic time-domain VIP routine is presented to adapt the VIP in more complex operation environment, where abrupt changes in system state and complex dynamic processes could present. The

proposed approach relies on the actual system condition (steady or dynamic state, slow changes or discontinuous changes) to activate or switch between the VIP algorithms. The VIP routine is paused during severe dynamic processes when the VIP model is not valid. The performance of the dynamic VIP is examined by comparing with the result of quasi-steady state VIP algorithm. Dynamic 2-bus and 39-bus examples presented in Chapter 3 prove that the dynamic VIP can reflect the impact of severe disturbances (load increase or line tripping) on stability in dynamic environment. The relative error of the dynamic VIP is less than 5% bench-marked by the quasi-steady VIP when no transients are considered.

Since the voltage stability condition can be assessed by the VIP or similar approaches, it is possible to coordinate the local stability monitoring devices to form a defensive frontier to counteract any locally initiated disturbances. Moreover, the VIP equivalent model could be adopted to represent a potion of network where the relevant system information is not accessible. In Chapter 6, the possibility of using the VIP model as a equivalent network model will be discussed.

CHAPTER IV

SENSITIVITY OF SECONDARY VOLTAGE CONTROLS AND EMERGENCY CONTROLS TO STABILITY MARGIN

4.1 INTRODUCTION

Voltage instability arises when load dynamics attempts to establish power consumption beyond the capability of the combined transmission and generation system. Loads are the most important parameters of voltage instability. Starting from a particular operation point, the amount of additional load in a specific known pattern of load increase that would cause a voltage collapse is called the load margin. Since voltage collapse could be associated with a saddle point bifurcation (SNB) point, load margin is adopted as the fundamental measure of the proximity to instability. In section 2.2, the existing methods of assessing the load margin corresponding to the nearest SNB point have been summarized. A stability control action corresponds to the change of a specific control parameter, such as switching of a capacitor bank, changing the tap position of an LTC transformer, or shedding load on a portion of the system. The changes in control parameters are expected to cause an increase in load margin.

4.2 THE FORMULATION OF THE MARGIN SENSITIVITY WITH RESPECT TO THE CHANGE OF ANY CONTROL PARAMETER

Dobson and Alvarado [5] presented an algorithm for computing the margin sensitivity with respect to any power system stability-control parameter. The estimated

margin sensitivity can be used to quickly assess the quantitative effectiveness of various control actions to maintain a sufficient load margin to voltage collapse. The derivation of first-order (linear) sensitivity of load margin L with respect to a parameter p is introduced in the follow text.

The equilibrium of the power system satisfies the power balance (power flow) equations:

$$f(x,\lambda,p)=0,\ f:R^n\to R^n \qquad (4\text{-}1)$$

where:

$x\in R^n$ —vector of the state variables,

$\lambda\in R^m$ —vector of the active and reactive loads,

$p\in R^P$ —vector of the control variables.

Let λ_0 be the vector of real and reactive load at the operating equilibrium. With a specified pattern of load increase $\hat{k}$, the load at the SNB point can be presented by:

$$\lambda^*=\lambda_0+\hat{k}L \qquad (4\text{-}2)$$

where L is the load margin to voltage collapse. If $\hat{k}$ is equal to λ_0, it follows that $L=\lambda^*/\lambda_0-1$. Linearization of the operation equilibrium at the bifurcation point (x^*,λ^*,p^*) yields:

$$f_x|_*\Delta x+f_\lambda|_*\Delta\lambda+f_p|_*\Delta p=0 \qquad (4\text{-}3)$$

The suffix '$|_*$' means that the quantity is evaluated at the SNB point (x^*, λ^*, p^*). Since the Jacobian matrix f_x is singular at the SNB point, there must exist a zero eigenvalue and the corresponding left eigenvector $\omega(x, \lambda, p)$ such that:

$$\omega(x_*, \lambda_*, p_*) f_X(x_*, \lambda_*, p_*) = 0 \tag{4-4}$$

Pre-multiplication of $\omega(x^*, \lambda^*, p^*)$ with (4-3) yields

$$\omega f_\lambda|_* \Delta\lambda + \omega f_p|_* \Delta p = 0 \tag{4-5}$$

Considering $\Delta\lambda = \hat{k}\Delta L$, the margin sensitivity of parameter p can be calculated by:

$$L_p|_* = \frac{\Delta L}{\Delta p} = \frac{-\omega f_p|_*}{\omega f_\lambda|_* \hat{k}} \tag{4-6}$$

where：

f_x —partial derivative of power flow equations to x

f_λ — partial derivative of power flow equations to λ

f_p —partial derivative of power flow equations to p

The same formula holds for multiple parameters in vector p, in which case $-\omega f_p|_*$ is a vector. This is helpful when approximating the combined effects of changes in several parameters.

The estimations of margin sensitivities require calculation of only one SNB point, which could be obtained numerically by the iterative or continuation power flow methods.

However, the Jacobian matrix evaluated close to the SNB point by the power flow methods is therefore not strictly singular. Consequently, the term $\varpi f_x|_* \Delta x$ is nonzero, which could introduce a constant error in the estimated margin sensitivity $L_p|_*$. In addition, the first-order margin sensitivity estimation ignores the quadratic and higher order terms, which could result in additional inaccuracy in the estimates. These errors could be reduced by including a correction term in (4-6) to compensate the impact of nonzero $\varpi f_x|_* \Delta x$ on the calculation of $L_p|_*$.

$$L'_p|_* \approx \frac{\Delta L}{\Delta p} = -\frac{\varpi f_x|_*}{\varpi f_\lambda|_* \hat{k}} \frac{\Delta x}{\Delta p} - \frac{\varpi f_p|_*}{\varpi f_\lambda|_* \hat{k}} \tag{4-7}$$

Therefore, the linear estimation error of the margin sensitivity can be calculated by:

$$\Delta L_p \approx L'_p|_* - L_p|_* = -\frac{\varpi f_x|_*}{\varpi f_\lambda|_* \hat{k}} \frac{\Delta x}{\Delta p} \tag{4-8}$$

Assuming a linear relation between Δx and Δp within a small control range, the term $\frac{\Delta x}{\Delta p}$ can be considered to be constant. Therefore, the estimation error ΔL_p is nearly constant. With a step change of Δp, the corresponding changes in the state variable Δx can be easily calculated by performing an additional power flow calculation in the vicinity of the same critical SNB point referred by the margin sensitivities.

The formulations for calculating the margin sensitivity in (4-6)~(4-8) also hold for multiple control parameters, in which case Δp, Δx, $\varpi f_p|_*$ are vectors. If the margin sensitivities of different control parameters are independent to each other, the combined effects of the changes in several control parameters on stability margin can be simply

evaluated as a linear combination of the impact on stability margin caused by the changes of all involved control parameters.

If the relation between the changes in parameter p and the resulting changes in stability margin is highly nonlinear or even discontinuous, the margin sensitivity for p would only be valid in a small range around the value of p for which the margin sensitivity is calculated. In the next section, the margin sensitivities of the secondary voltage controls and load shedding controls will be calculated and examined in the IEEE-39 bus system.

4.3 MARGIN SENSITIVITIES OF SECONDARY VOLTAGE AND STABILITY CONTROLS

Some utilities [36, 37] use pre-contingency controls to increase the stability margin in anticipation of certain severe contingencies. The off-line contingency analysis uses the most recent state estimation results to evaluate the post-contingency system conditions following each monitored contingency. Certain contingencies could possibly take the system directly into instability, where the post-contingency stability margin is small enough or even negative to evoke immediate attention of the system dispatcher. The margin sensitivities of the potential control actions can be evaluated and updated in parallel with the monitoring of system conditions. When an instability-inducing contingency is detected either by on-line monitoring system or off-line simulations, the margin sensitivities of the voltage control devices can be used by the system operator as a quick reference to assess the stability control options. In this section, the IEEE 39-bus

system is adopted as the platform to examine the accuracy of the margin sensitivities for the secondary voltage controls.

The Dobson's margin sensitivity algorithm can be conveniently applied to calculate the margin sensitivity of the secondary voltage control devices, such as shunt capacitor banks and LTCs. The term $\omega f_\lambda|_* \hat{k}$ in (4-7) is not related to and parameter *p*. Therefore, the same value of $\omega f_\lambda|_* \hat{k}$ can be adopted to evaluate the margin sensitivities with respect to any parameter *p*.

Define *C* as the vector containing the MVAr capacity of the shunt capacitors switched on all buses installed with shunt capacitor banks. The partial derivative of the power flow balance equations with respect to the changes in C evaluated at the critical loading level can be calculated by:

$$C = [Q_1 \quad Q_1 \quad \cdots \quad Q_m]$$

$$f_C|_* = \frac{\partial f(x, \lambda, C)}{\partial C}|_* = -diagonal(V_1^2|_*, V_2^2|_*, \cdots, V_m^2|_*) \tag{4-9}$$

where:

Q_i —MAVr capacity of the shunt capacitor banks at bus *i*,

m—number of buses equipped with shunt capacitor banks.

Define *T* as the vector containing tap positions of all branches equipped with LTCs. The calculation of the partial derivative $f_T|_*$ is much more complex than the calculation of $f_C|_*$, which can be expressed as a matrix with the number of rows as the Jacobian matrix $f_x|_*$. For an LTC across bus *i* and *j*, the partial derivative of the active and

reactive power injections on bus i and j with respect to the tap position TAP_{ij} can be calculated by:

$$f_T(i,j)\big|_* = \frac{\partial P_i(x,\lambda,T)}{\partial TAP_{ij}}\big|_* \;;\; f_T(i+N_{pqv},j)\big|_* = \frac{\partial Q_i(x,\lambda,T)}{\partial TAP_{ij}}\big|_* \tag{4-10}$$

$$f_T(j,j)\big|_* = \frac{\partial P_j(x,\lambda,T)}{\partial TAP_{ij}}\big|_* \;;\; f_T(j+N_{pqv},j)\big|_* = \frac{\partial Q_j(x,\lambda,T)}{\partial TAP_{ij}}\big|_*$$

where $P_i(x,\lambda,C)$ and $Q_i(x,\lambda,C)$ are the active and reactive power injections on bus i; $P_j(x,\lambda,C)$ and $Q_j(x,\lambda,C)$ are the active and reactive power injections on bus j; N_{pqv} is the total number of PQ and PV buses in the system.

The calculations of the margin sensitivities of the shunt capacitor banks and LTCs can be demonstrated on the platform of the 39-bus system. The total active load in the original 39-bus system is considered as the base load. In the future 39-bus case studies, system load and stability margins are estimated as the percentages of the base load. The loads on load buses are assumed to increase proportionally from the base load until voltage collapse. The load increase is distributed to all generators proportional to their capacities. Assuming a single contingency in line 21~22, the 39-bus system collapses at 142% loading level (evaluated by iterative power flow method). The increases in loading margin as the result of any voltage control action can be evaluated either by iterative power flow method or the margin sensitivity of the same control action directly.

According to the formulation of margin sensitivity, the margin sensitivities should be evaluated at the vicinity of the SNB point corresponding to 142% load level. The margin sensitivities of the secondary controls are evaluated by Dobson's method and iterative

power flow method. By using the iterative power flow method, the nearly accurate load margin with respect to the change of any control parameter can be obtained. Considering load margin as a linear combination of the settings on any individual voltage control devices, the slope of the linear function provides an estimation of the overall margin sensitivity. In Table 8, the margin sensitivities evaluated by Dobson's algorithm and the iterative power flow method for a set of stability-sensitive secondary voltage control devices are compared.

Table 8. Comparison of the estimated margin sensitivity by Dobson's algorithm and iterative power flow analysis for selected stability-sensitive secondary voltage control devices (margin sensitivity evaluated with 0.01 p.u. change of control parameters).

Voltage control device	Margin sensitivity estimated by Dobson's algorithm	Margin sensitivity by power flow analysis
Capacitor bank on bus 4	0.0001	0.00009
Capacitor bank on bus 7	0.00006	0.00007
Capacitor bank on bus 8	0.00006	0.00006
Capacitor bank on bus 12	0.00008	0.00008
Capacitor bank on bus 15	0.00019	0.00018
Capacitor bank on bus 20	0.00005	0.00005
Capacitor bank on bus 21	0.00023	0.00021
Capacitor bank on bus 23	0.00064	0.00061
Capacitor bank on bus 24	0.0003	0.0003
Capacitor bank on bus 25	0.00007	0.00007
Capacitor bank on bus 27	0.00014	0.00013
Capacitor bank on bus 28	0.00006	0.00006
Capacitor bank on bus 29	0.00004	0.00004
LTC 19~33	0.0055	0.0052
LTC 25~37	0.0029	0.0024
LTC 10~32	0.0027	0.0025
LTC 20~34	0.0021	0.0021
LTC 6~31	0.0021	0.0021
LTC 23~36	***-0.0034***	***0.0048***
LTC 22~35	***-0.0075***	***-0.0027***

From Table 8, close matches between the margin sensitivities evaluated by the Dobson's algorithm and the power flow analysis can be observed, especially when assessing the control of the shunt capacitor banks. However, larger mismatches in the estimated margin sensitivities are discovered for the LTCs 23~26 and 22~35. A close observation of the relations between the control settings of different control devices and the corresponding critical loading factors are shown in Figure 24 and Figure 25. Figure 24 illustrates that the load margin is usually in linear relation to the capacity of the applied shunt capacitor bank. Since an applied shunt capacitor bank can be treated as a negative reactive load, added load margin is expected to be in linear relation to the capacity of the applied negative load unless over-compensation occurs. Overcompensation rarely happens because of limited capacity of reactive resources in the system and minimum VAr control objective adopted by many utilities. The system dispatchers in PJM coordinate the voltage controls to avoid redundant transmission level VAr and LTC controls. The margin sensitivity of a shunt capacitor can be considered to be constant within the control range of the capacitor bank.

In Figure 25, the tap changes of the LTC 6~31, LTC 19~33 and LTC 29~38 also exhibit nearly linear relations to the load margin. However, the impact of the controls in the LTCs 22~ 35 and 23~36 on the load margin are highly non-linear. The margin sensitivity according to Dobson's algorithm is evaluated in the vicinity of the SNB point. Applying a constant margin sensitivity over the entire control range of a LTC with highly non-linear impact on the load margin will lead to substantial error, which may also cause an unexpected decrease in the load margin. In order to avoid such an undesirable

situation, the control of such type of LTCs should be frozen or limited within a narrow range.

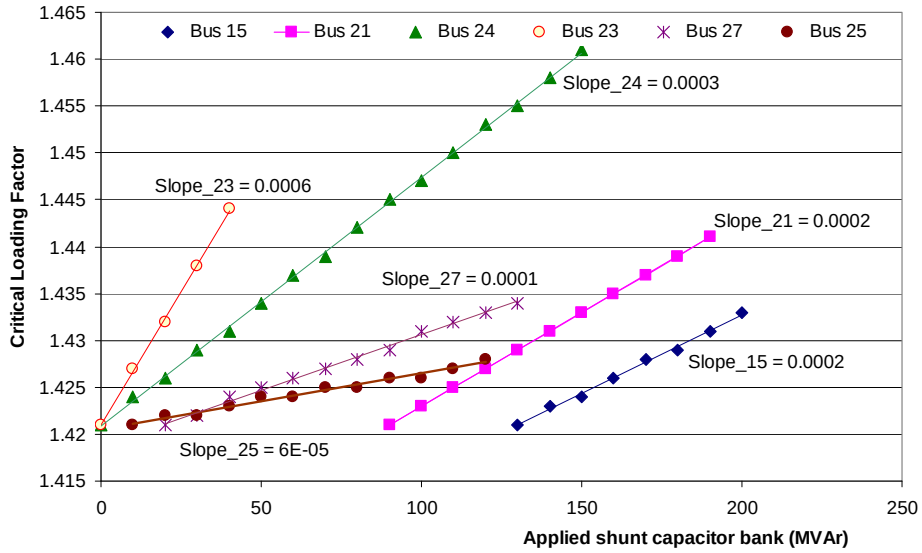

Figure 24. The impact of the shunt capacitor banks on the load margin can be represented by linear functions.

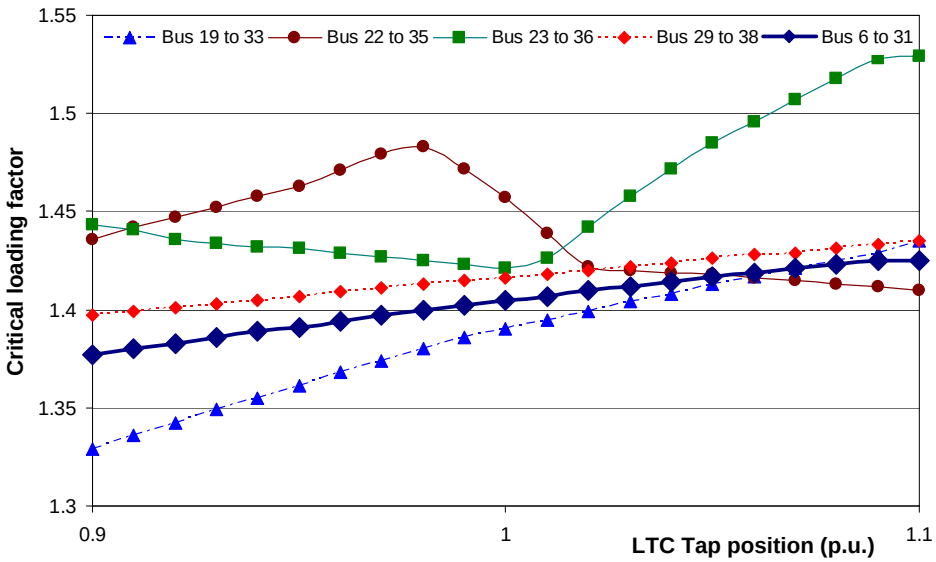

Figure 25. The impact of the LTC tap positions on the load margin.

In order to examine the accuracy of margin sensitivities with respect to combined impact of the shunt capacitor controls, 1000 comparative simulations are performed using both power flow method and margin sensitivities to evaluate the changes in stability margin. In each of the 1000 simulation cases, the capacity of the added shunt capacitor banks changes randomly (following normal distribution) and independently from different buses within the total installed capacity. The comparison of the increased stability margin estimated by power flow method and margin sensitivity analysis for the 1000 simulation cases is shown in Figure 26. Treating the results obtained by power flow method as the accurate results, the relative error in the results obtained by margin sensitivity analysis can be calculated and fitted by a cumulative distribution function (as shown in Figure 27).

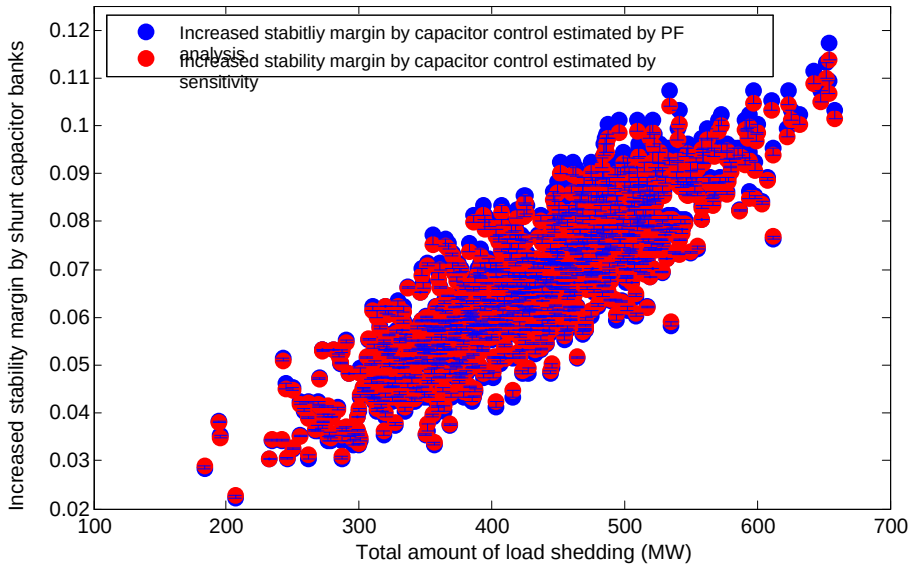

Figure 26. Comparison of the increased stability from reactive controls estimated by power flow method and margin sensitivity analysis.

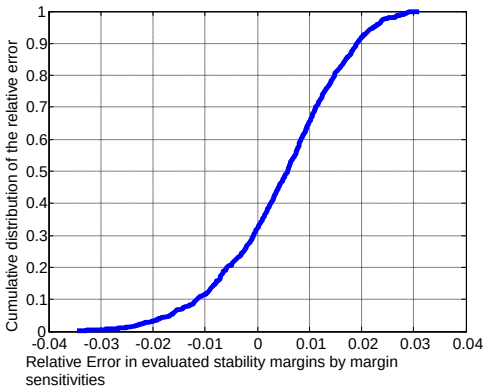

Figure 27. Cumulative distributions of the errors in the estimations of the combined impacts on stability margin from shunt capacitor banks using margin sensitivity analysis.

The relative errors in the stability margins estimated by margin sensitivity analysis lie in the range of $\pm 3\%$. Since the difference in stability margins evaluated by power flow method and margin sensitivity analysis are close (within $\pm 3\%$ relative error), margin sensitivity analysis can be considered as an on-line stability assessment tool with similar accuracy as the off-line power flow method.

4.4 CALCULATE THE MARGIN SENSITIVITIES OF EMERGENCY LOAD SHEDDING

Load shedding (LS) is the only solution to maintain the stability of a system when all the other control options, such as secondary voltage controls, transmission loading relieve (TLR), and generation re-dispatch, have been exhausted. LS has been applied as a measure of last resort to prevent power systems blackouts [38]. Since 2000, the implementation of *LS* programs in California has been complemented by creation of interruptible users that have voluntarily reduced the power demands during summer peaks (53 GW) by almost 1.5 GW in 2003. In the State of New York, approximately 1.8 GW interruptible loads have been increased in both the day-ahead energy market and the

proper interruptible services market. Because of the increased operation flexibility by the interruptible loads, the total load curtailment has increased by more than 0.7GW during the summer peak periods in 2003. In South Korea, in comparison to a load annual peak of about 49 GW, the *LS* program has been accepted by interruptible users of about 4 GW in 2003. However, the criteria for assessing load shedding in the LS programs are usually simple [39-41], such as using low voltage or frequency deviation as the activating trigger. The amount of load shedding in the LS program is usually defined in fixed steps corresponding to the severity of voltage or frequency violations. Optimal power flow (OPF) is adopted by some utilities (such as IESO) to find out the minimum amount of load shedding solution that can sufficiently preserve the system stability. Feng [42] and Alfonso [43] both used participation factors to identify the most adequate buses for load shedding purposes in their customized OPF formulation. However, the active and reactive load participation factors do not provide a direct relation between the changes in stability margin and load shedding. By adopting the load participation factors (LPF), only the buses with pronounced LPFs will be considered as the candidate locations for performing load shedding.

Greene and Dobson [5, 44] presented the margin sensitivity algorithm to quantify the impact of load shedding on stability margin. The authors have demonstrated that the increases in stability margin as a result of load shedding on a single load bus can be accurately predicted by the margin sensitivity of load shedding on that bus.

Similar to the formulation of margin sensitivity in (4-6), the sensitivity of load shedding can be formulated as follows:

$$L_{SP}|_* = \frac{-\omega f_{LS,P}|_*}{\varpi f_\lambda|_* \hat{k}} \tag{4-11}$$

$$L_{SQ}|_* = \frac{-\omega f_{LS,Q}|_*}{\varpi f_\lambda|_* \hat{k}}$$

where $f_{LS,P}|_*$ and $f_{LS,Q}|_*$ represents the partial derivatives of the active and reactive power injections with respect to the active and reactive load reductions on each load bus respectively.

Assuming a constant power factor on each load bus, the combined margin sensitivity from (active and reactive) load shedding L_{SC} can be calculated in (4-12).

$$L_{SC}|_* = L_{SP}|_* + kL_{SQ}|_* \tag{4-12}$$

where *k* is the vector of fixed power factors of the load buses.

The margin sensitivities with regard to load shedding can be calculated for the same IEEE 39-bus example with a single contingency in line 21~22, as introduced in section 4.2. Figure 28 shows margin sensitivities of load shedding controls applied to a few heavily loaded buses (bus 4, 15, 21, 27) evaluated by Dobson's algorithm, and separately, iterative power flow method. Similar comparison results are also observed when load shedding is applied on the other load buses. The margin sensitivities evaluated by the two methods match each other very well. The small discrepancy in the load margins evaluated by the two methods is caused by the slight non-linearity of the actual margin sensitivities.

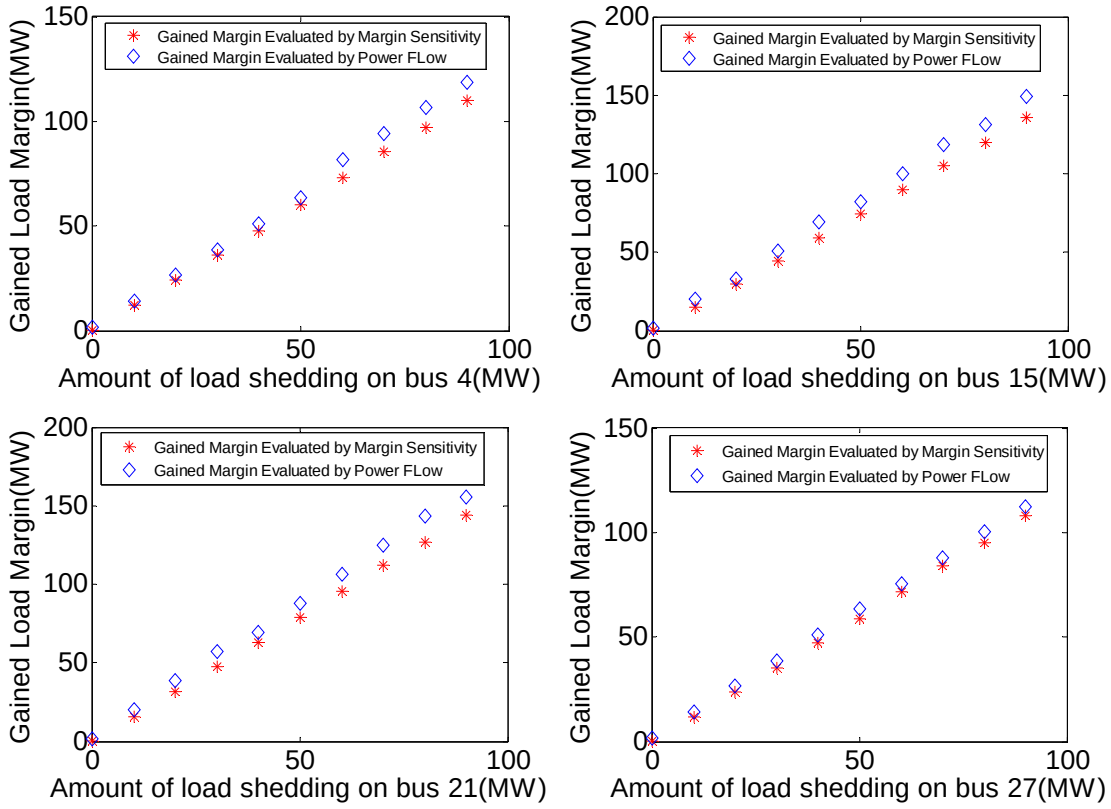

Figure 28. Comparison of the margin sensitivities of load shedding on critical load buses in the 39-bus system evaluated by Dobson's algorithm and iterative power flow method.

In order to examine the accuracy of margin sensitivities with regard to combined impact of the load shedding at different buses, 1000 comparative simulations are performed using both power flow method and margin sensitivities to evaluate the changes in stability margin. 10 buses with the highest margin sensitivities are considered as the candidate buses for load shedding. The portion of the interruptible load on the 10 buses is assumed to be in the ranges of 0~10%, 10%~20%, 20%~30%, or 30%~40% of the total pre-shedding load level in five case studies, respectively. In each case study, 1000 simulations are conducted. In each simulation, the amount of load shedding changes randomly (following normal distribution) and independently on the 10 load

buses within the corresponding capacity of the interruptible load. The comparisons of the increased stability margin estimated by power flow method and margin sensitivity analysis for the first and fourth case studies (0~10% and 30~40% interruptible load) are shown in Figure 29. Assuming the results obtained by power flow method as accurate, the absolute and relative errors in the results obtained by margin sensitivity analysis can be calculated and fitted by a cumulative distribution functions (as shown in Figure 30).

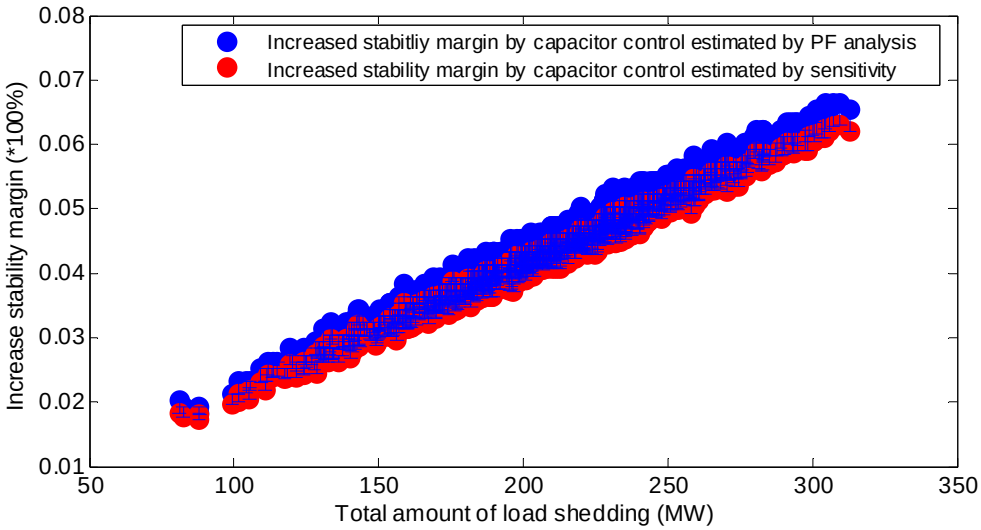

(a) Case 1: 0~10% load shedding

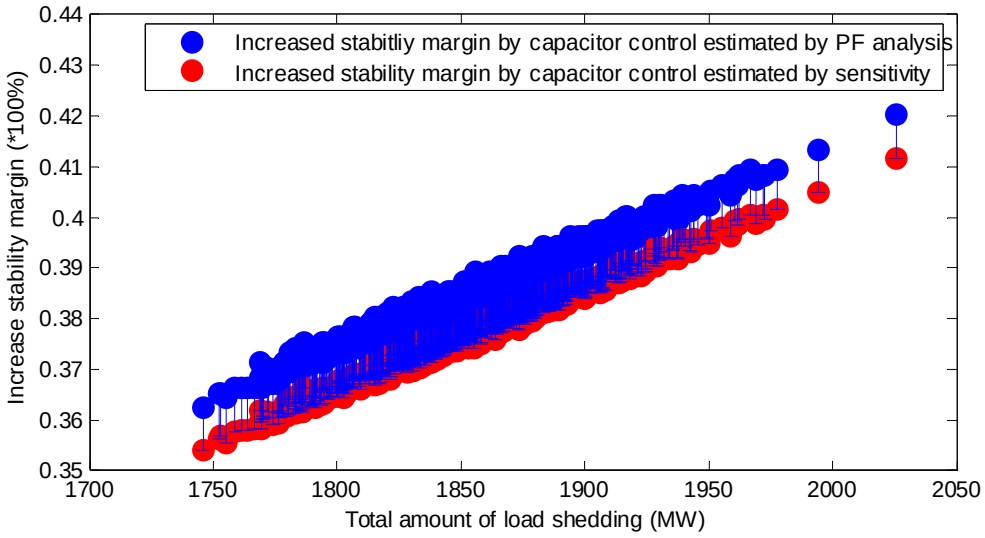

(b) Case 4: 30~40% load shedding

Figure 29. Comparison of the increased stability from load shedding estimated by power flow method and margin sensitivity analysis.

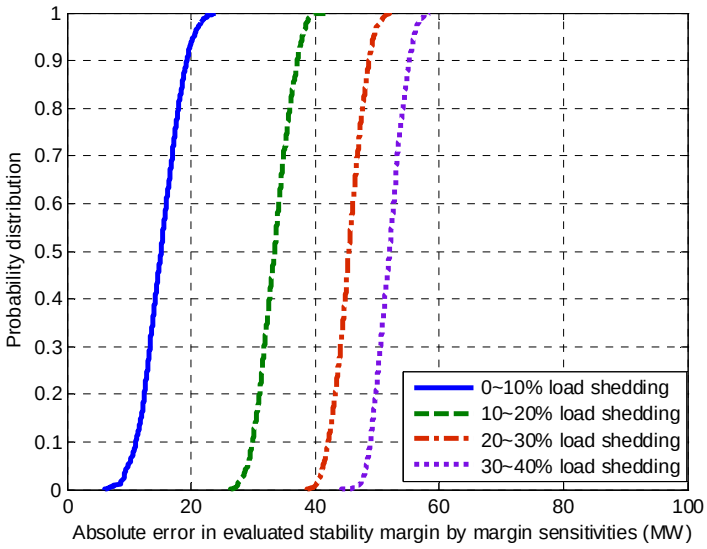

(a) Cumulative probability distribution of the absolute errors

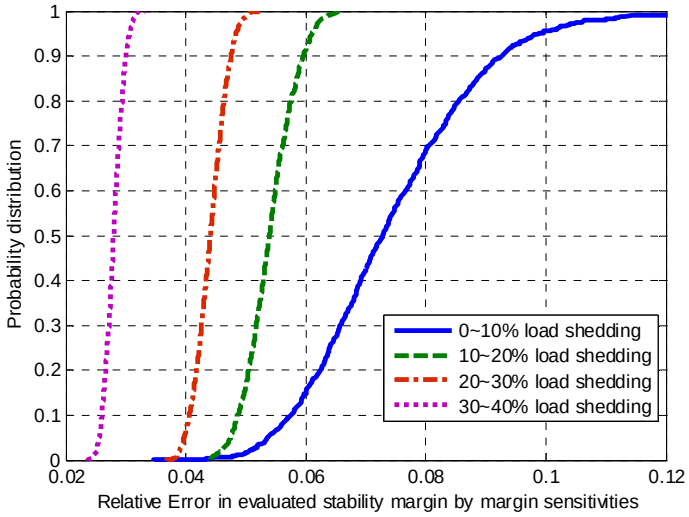

(b) Cumulative probability distribution of the relative errors

Figure 30. Cumulative distributions of the errors in the estimations of the combined impact on stability margin from load shedding using margin sensitivity analysis.

With the increasing amount of load shedding from case 1 to case 4, the absolute errors in the estimated stability margin by margin sensitivity analysis increase (as shown in Figure 30a). Because the slight non-linearity of the actual margin sensitivities, the increases in the absolute error is also slightly non-linear to the increase in load shedding. Consequently, the relative errors in the estimated stability margin by margin sensitivity analysis decrease with the increasing amount of load shedding from case 1 to case 4 (as shown in Figure 30b).

The largest relative error in the stability margins estimated by margin sensitivity analysis is 12% in case 1, while 95% of the errors are less than 10%. The largest absolute error in the stability margins estimated by margin sensitivity analysis is 58.6 MW out of 2460 MW total amount of interruptible load in case 4.

Since the difference in stability margins evaluated by power flow method and margin sensitivity analysis is small, margin sensitivity analysis can be utilized to compare load shedding options with similar accuracy as the off-line power flow method.

4.5 CONCLUSION

The concept of using margin sensitivity to evaluate the post-control load margin is presented as a fast and accurate way to assess potential voltage and stability control options. The linear combination of the margin sensitivities of different control resources will enable the direct estimation of the increased load margin. The redundant or insufficient stability controls should be avoided. Benchmark simulations are conducted on the 39-bus system to compare the margin sensitivities obtained by Dobson's algorithm with the conventional iterative power flow analysis. It has been assessed that the margin sensitivities of the shunt capacitor banks controls and load shedding can be accurately estimated by Dobson's algorithm. However, the high non-linearity of the margin sensitivities of a few LTCs limits their usage for stability control purpose. The increased stability margin by combined shunt capacitor controls, as well as combined load shedding on different buses, can be accurately predicted by margin sensitivity analysis without performing additional power flow analysis. Margin sensitivities of the voltage stability controls could be introduced as additional objective into the OPF or other optimization-based control formulations to achieve faster and more comprehensive evaluation of the control solutions for stability considerations.

CHAPTER V

STABILITY CONSTRAINED SECONDARY VOLTAGE CONTROLS

5.1 INTRODUCTION

In a power utility control center, operators monitor the voltage profile of the entire system according to data from SCADA. The collected data, including switch status, voltage and current magnitudes, are updated every several seconds. A state estimator evaluates state variables of the entire system and identifies possible error (bad) measurements from local monitoring devices. Off-line power flow analysis is performed by some utilities to identify severe contingencies, which could produce (if they happen) violations of voltage constraints or even stability issues. When an actual or simulated violation of voltage constraint is discovered, various voltage controls are initiated according to the severity of the voltage constraint violation. Table 9 summarizes the typical voltage controls used by different utilities.

Table 9. Voltage control approaches adopted by utilities.

Control Devices	Time Frame (s)	Traditional Control	EDF control	PJM control
AVR, Excitation, Governor	1~30	Automatic	Primary control: Automatic	Automatic
LTC and Shunt Capacitor bank	20~180	Automatic	Secondary control: automatic	Half manual Half automatic
Coordinated Control	> 300	Optimal power flow	Tertiary control: coordinated	Optimal power flow

The generator controls are performed continuously in response to any dynamic process following an actual disturbance. Because of the fast control time frame, EDF defines the continuous generator controls as primary controls. Set-points of the generators are also included in the coordinated controls, such as OPF and tertiary control, to achieve different control objectives. A coordinated control decision, corresponding to an optimal solution, is expected to optimize the available control resource so as to meet all security and stability criteria. If the coordinated controls do not satisfy the control objectives, emergency controls (such as load shedding and line tripping) may be considered. Such emergency controls would normally inconvenience the end customers.

The control of LTC and shunt capacitor banks are defined as the Secondary Voltage Control (SVC) by EDF because of their longer time constants compared with the primary control. Secondary voltage control (SVC) are usually performed by utilities [17] as a non-cost solution to correct voltage violations, such as low voltage and voltage drop. The Coordinated Secondary Voltage Control (CSVC) approach, under development by EDF [19, 45], aims at coordinating voltage supports from primary voltage control devices (such as AVRs) and secondary voltage control devices (such as LTCs and capacitor banks) to more effectively control the voltage profile. In PJM, the controls of capacitor banks and LTCs at major transmission lines are coordinated by the system dispatcher. The control decision is either rigidly in accordance with a pre-defined control scheme or in line with the past experience of the system dispatcher.

The voltage controls in most utilities do not include voltage stability margin as a control objective or constraint. In fact, according to WECC criterion, the remaining load margin following the most severe N-1 contingency is required to be 5% or more. The

need of stability consideration when deploying voltage controls tends to be more pronounced during emergency conditions when the system is operating in proximity of stability boundary. Only a few utilities rely on the objective of minimum reactive power losses in OPF as an indirect measure for increasing stability margin. The link between stability margin and voltage controls is indirect. Hence, it is difficult to quantify the increased stability margin resulting from voltage controls.

Furthermore, major goal of OPF is to re-dispatch the generation and control set-points to minimize the lumped sum of operation costs. Adopting stability objective into OPF may cause both economical and regulatory conflicts.

Since the secondary voltage control (by shunt capacitor banks) is considered as a no-cost voltage control approach, the system dispatcher is naturally given the flexibly of utilizing secondary voltage control to counteract the impact of disturbances/contingencies on system stability. In this chapter, the allocation of reactive resources (shunt capacitor banks) considering security and stability constraints is performed to form the basis for secondary voltage and stability controls. Secondly, an algorithm for estimating sensitivity of secondary voltage control to load margin is introduced. By absorbing the objective of maximizing load margin as a control objective, a multiple-objective secondary voltage and stability control formulation is presented. A normalized constrained optimization algorithm is adopted to solve for a set of optimal secondary control solutions. Finally, a 39-bus example is given to demonstrate the proposed secondary voltage and stability control routine.

5.2 SECURITY AND VOLTAGE STABILITY CONSTRAINED REACTIVE RESOURCE PLANNING

Optimal allocation of VAr sources, such as capacitor banks, Static Var Compensators (SVC), and STATic COMpensators (STATCOM), is a critical task in reactive resource planning (RRP). Expensive SVC and STATCOM are only used in critical nodes or interfaces where very fast controls are absolutely needed. The control of switched capacitor banks is the most economic and efficient voltage control approach. If operated properly, switched capacitor banks can change the system's critical operation state and increase stability margin.

Optimal Power Flow (OPF), PV and QV analysis are usually performed by utilities to seek a suitable VAr compensation scheme to achieve economic benefits through loss reduction as well as to meet security and stability requirements. According to WECC criterion [46], the system load serving capability is defined as the lower of either 2.5% below the knee of category C outage (the worst N-2 contingency or loss of two transmission lines) PV curve or 5% below the knee of category B outage (the worst N-1 contingency or loss of one transmission line, and N-1-1 contingency or loss of two consecutive sections of the same transmission line) PV curve.

The conventional way of performing RRP is to estimate the capacity and locations of the VAR sources by engineering judgment, by identifying buses with possible voltage violations. Recent research has addressed RRP as a complex optimization model with multiple objectives defined according to operation conventions of different utilities. Due to the complicated objective functions, constraints, and solution algorithms that arise, RPP is considered as one of the challenging problems in power systems.

The objective function of an RPP may be set to achieve economic benefit or enhance operation security, including minimizing VAr installation and operation cost, real power loss cost, and/or fuel cost, and deviation from a given schedule of a control variable (such as voltage). The combinations of different objectives will lead to a multi-objective (MO) model. The system planner can compare the Pareto solutions of the MO model by different measures to identify the most suitable allocation of the VAr sources.

Conventional constraints in RPP are mostly capacity related, such as power flow limits under normal and contingency state. Recently, the voltage stability limit under contingency state has also been included by some operation administrators (such as WECC [46]). In general, the RRP models, classified by the different constraints that they adopt, include optimal power flow (OPF) model, security-constrained OPF (SCOPF) model, and SCOPF with voltage stability constraints (SCOPF-VS)—the present state-of the-art RPP model.

Security-constrained optimization was introduced in the 1960 seconds and early 1970 seconds. Alsac and Stott in 1974 modeled the SCOPF and solved the model with AC power flow equations [47]. The continuation of the research in [47] led to further implementation of the SCOPF in [47-50]. The SCOPF model is applied to RPP in [51-55]. With the development of the SCOPF model, the goal of RPP is extended to determine a minimum cost allocation plan of new Var resources in terms of size and location so as to guarantee feasible operation both under normal conditions and after contingencies. SCOPF minimizes the base case and the pre-contingency objective functions while observing both the pre- and post-contingency constraints. In other words, SCOPF determines an optimal operating point, such that in the event of any contingency

of a given list, the post-contingency states will remain secure (within operating limits). The formulation of the SCOPF model can be established as follows:

$$\text{Minimize } P_{Loss} = \sum_{k \in Nc} \sum_{l \in N_l} P_{Loss,l}^{k}(V^k, \theta^k)$$

$$\text{Subject to } \sum_{k=1}^{N_b} \left| Q_k^{Post} - Q_k^{\Pr e} \right| \le Q_c$$

$$P_{gi}{}^k - P_{li} \; - P_i^k(V^k, \theta^k) = 0$$

$$Q_{gi}{}^k + Q_i \; - Q_{li} \; - Q_i^k(V^k, \theta^k) = 0$$

$$P_{gi,\min}^k \le P_{gi}^k \le P_{gi,\max}^k$$

$$Q_{gi,\min}^k \le Q_{gi}^k \le Q_{gi,\max}^k$$

$$V_{i,\min}^k \le V_i^k \le V_{i,\max}^k$$

$$\tau_{l,\min}^k \le \tau_i^k \le \tau_{i,\max}^k$$

$$Q_{i,\min} \le Q_i \le Q_{i,\max}$$

$$\left| LF_l^k \right| \le LF_{l,\max}^k$$

$$VSM^k(Q_i) \ge VSM_{\min}^k$$

$P_{gi}{}^k$ —generator active power output on bus *i* for contingency *k*

$Q_{gi}{}^k$ —generator reactive power output on bus *i* for contingency *k*

$P_{li}{}^k$ —load active power on bus *i*

$Q_{li}{}^k$ —load active power on bus *i*

$P_i^k(V^k, \theta^k)$ —real power injection into bus *i*

$Q_i^k(V^k, \theta^k)$ —reactive power injection into bus *i*

V_i^k —voltage on bus i for contingency *k*

V_i^k —voltage on bus i for contingency *k*

τ_l^k —LTC tap position in branch l for contingency *k*

Q_i —VAr source installed at bus *i*

Q_c —the maximum available capacity of the VAr sources in the system

$VSM^k(Q)$ —the voltage stability margin after contingency *k* with current allocation of Var source

A set of base case states corresponding to different load levels needs to be modeled in order to identify a reactive allocation solution, which is optimal for any given load conditions. For each base case, the sensitivity of the objective function with regard to the suggested Q_c capacity should be studied in order to estimate the suitable amount of VAr source, which is sufficient to provide voltage support and economically reduce the active power losses. The security-constrained minimum voltage stability margin could be considered as the filter to screen the undesired optimal solutions for the peak-load base case. The detailed procedure of allocating the reactive resources is as follows:

Step 0: Construct a few base cases with different load levels, and solve the load flows for the base cases. The maximum load level in the 39-bus system is assumed to be 140%, because the maximum loading factor is 142% following a sever contingency in line

21~22. Therefore, five base cases, corresponding to 100%, 110%, 120%, 130% and 140% load levels, are constructed. Select one base case and proceed to Step 1;

Step 1: Start with the minimum capacity of VAr source which leads to a feasible solution. Increase VAR capacity by a small step and solve the aforementioned problem formulation to obtain an allocation solution.

Step 2: Repeat Step 1 until the convergence criterion is satisfied: $\left|P_{Loss}^{j} - P_{Loss}^{j-1}\right| \leq \varepsilon$, where P_{Loss}^{j} and P_{Loss}^{j-1} are the reactive losses corresponding to solution j and j-1.

Step 3: Collect all the allocation solutions and the corresponding Var capacities to construct a two-dimensional Pareto front and discard dominated solutions.

Step 4: Go to Step 0 until all the base cases are analyzed.

Step 5: Select one allocation solution on the descending slope of the Pareto front for the peak-load base case, which leads to at least 10% stability margin after the most severe N-1 contingency. Treat this solution as the base solution.

Step 7: Select one allocation solution on the descending slope of the Pareto front for all the other base cases, with less capacity than the base solution.

Step 8: Compute the superset and subset of the combination of all the allocation solutions picked out in Step 7 and 8. Define the superset as the final allocation solution, while the subset is the allocation of the fixed capacity bank.

The above introduced RRP algorithm is applied to the IEEE 39-bus system. The one-line diagram of the 39-bus system can be found in Figure 5. Five base cases are generated corresponding to different load levels, including 100%, 110%, 120%, 130%, and 140% of the total load in the original system model. Following the eight-step allocation procedure, a set of Pareto fronts can be constructed for each base case. Figure

31 shows the Pareto solutions for allocating reactive resources under 100% load condition labeled as blue diamonds. The red square corresponds to a desired allocation solution, which results in 18 MW of reduction in active power losses with the installation of 595 MVAr shunt capacitor banks. Similarly, Pareto solutions for allocating reactive resources under 140% load condition are plotted in Figure 32 labeled as blue diamonds. Treating the 140% load level as the peak load level, the desired voltage stability limit can be set at 150% load level, since some extra margin on top of the 5% WECC standard can help to meet the stability criterion under certain unexpected outages.

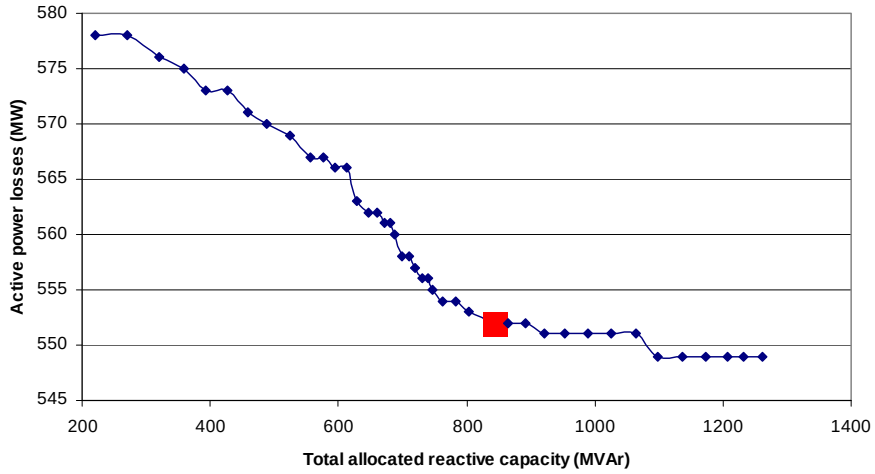

Figure 31. Pareto solutions for allocating reactive resources under 100% load condition.

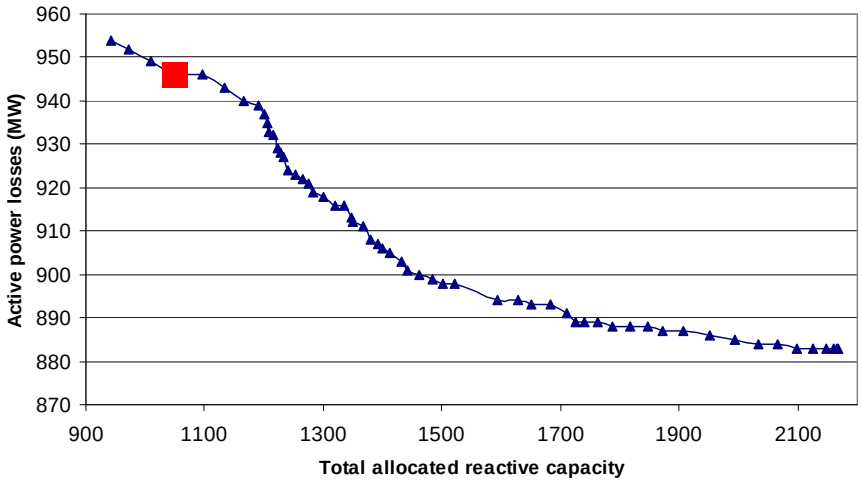

Figure 32. Pareto solutions for allocating reactive resources under 140% load condition.

In Figure 33, the voltage stability limits corresponding to the Pareto allocation solutions under 140% load condition is compared. Any solution that leads to a 1.5 (150%) or higher critical loading factor satisfies the desired voltage stability limit. Therefore, a desired solution for 140% load base case can be picked out by observing Figure 32 and Figure 33. The desired solution, represented by a red square, satisfies the stability constraint and leads to efficient active power reduction with the minimum amount of allocated VAR source.

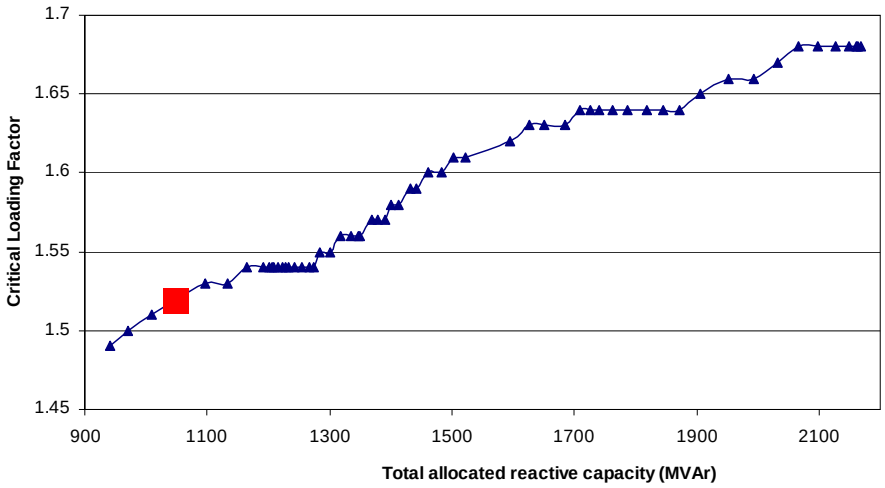

Figure 33. Voltage stability limits vs. total allocated reactive resource under 140% load condition.

By overlapping the desired Pareto solutions selected from each base case, the final reactive resource allocation scheme can be obtained (as shown in Table 10). The capacity of each block of a capacitor bank is assumed to be 10 MVAr, and each capacitor bank may contain multiple blocks. In Table 10, rounded superset is obtained by taking the maximum capacity of the installed capacitor bank on each bus, while rounded subset is obtained by taking the minimum capacity of the installed capacitor bank on each bus. The rounded superset is the suggested capacitor allocation solution, while the rounded subset is the suggested solution for fixed capacitor banks.

Figure 34 shows the one-line diagram of the 39-bus system equipped with the shunt capacitor banks according to the final allocation scheme. The number under each capacitor bank indicates the suggested installation capacity. This allocation scheme will be adopted in the 39-bus simulation examples of the subsequent chapters.

Table 10. Synthesis of the desired allocation solutions for the base cases (all units in MVAr).

Bus	Load levels of the base cases					Rounded Superset	Rounded Subset
	1.4	1.3	1.2	1.1	1.0		
1	0	0	0	0	0	0	0
2	0	0	0	0	0	0	0
3	0	0	0	0	0	0	0
4	163	161	162	150	84	160	80
5	0	0	0	0	0	0	0
6	0	0	0	0	0	0	0
7	63	73	92	86	39	90	40
8	77	93	118	116	58	120	60
9	0	0	0	0	0	0	0
10	0	0	0	0	0	0	0
11	0	0	0	0	0	0	0
12	21	44	75	71	29	70	20
13	0	0	0	0	0	0	0
14	0	0	0	0	0	0	0
15	200	200	184	142	132	200	130
16	0	0	0	0	0	0	0
17	0	0	0	0	0	0	0
18	0	0	0	0	0	0	0
19	0	0	0	0	0	0	0
20	0	0	0	9	0	10	0
21	129	187	139	118	91	190	90
22	0	0	0	0	0	0	0
23	0	0	35	7	0	40	0
24	147	80	0	0	0	150	0
25	116	63	61	59	11	120	10
26	0	4	0	0	0	0	0
27	133	114	85	51	20	130	20
28	0	0	11	0	0	10	0
29	0	0	9	33	0	30	0
30	0	0	0	0	0	0	0
31	0	0	0	0	0	0	0
32	0	0	0	0	0	0	0
33	0	0	0	0	0	0	0
34	0	0	0	0	0	0	0
35	0	0	0	0	0	0	0

36	0	0	0	0	0	0	0
37	0	0	0	0	0	0	0
38	0	0	0	0	0	0	0
39	0	0	0	0	0	0	0
SUM	1049	1020	970	843	464	1320	450

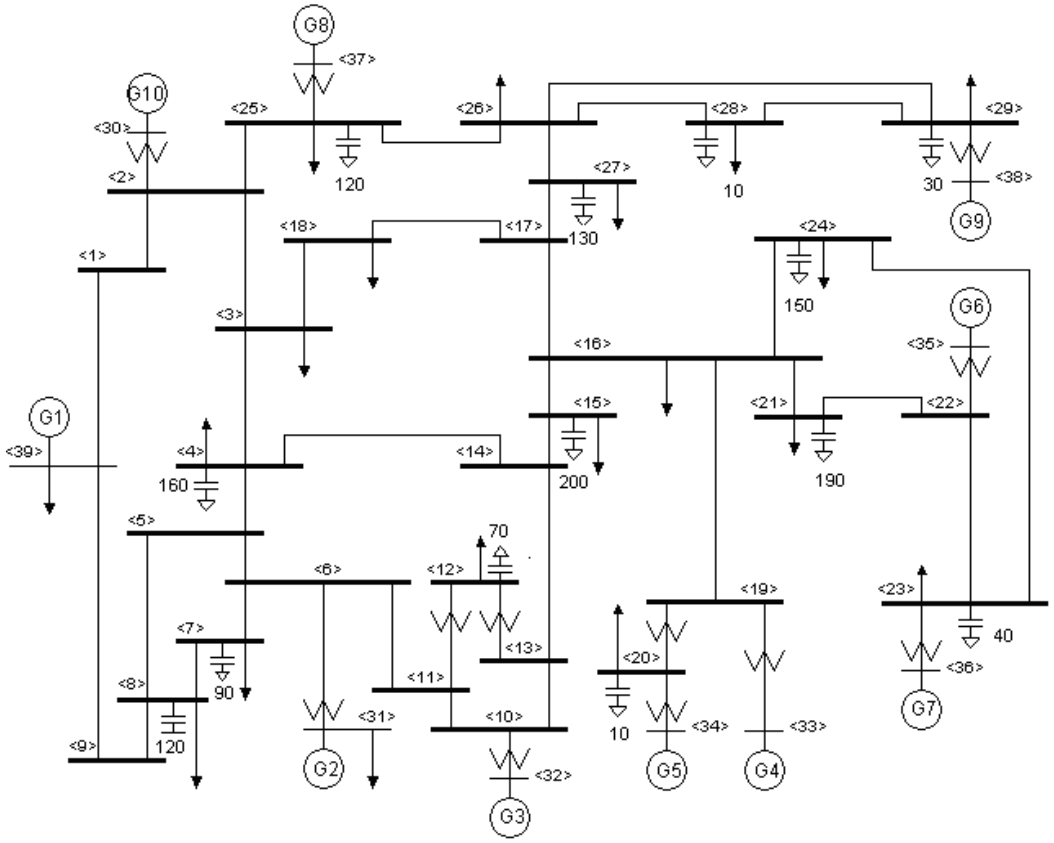

Figure 34. The final reactive resource allocation scheme for the 39-bus system.

5.3 OPTIMAL SECONDARY VOLTAGE AND STABILITY CONTROL FORMULATION

On top of the hierarchical voltage control portfolio, the alternative system-wide optimal control approach is based on the optimal power flow (OPF) function. Although the control emphasis of OPF is economic dispatch or VAr planning, the formulation of

OPF can be used as the reference to stability control modeling by choosing relevant objective functions. For voltage stability control purposes, the following four control objectives would be suitable:

1) Maximize the voltage stability margin.

2) Minimize reactive power generation.

3) Minimize reactive power losses.

4) Minimize control actions.

Minimization of reactive power generation and reactive losses are closely related to each other, since they have the common goal of achieving maximum reactive reserve. The amount of reactive reserve is highly related to the system stability margin. A more direct stability-related objective is to maximize voltage stability margin by applying secondary voltage controls.

A power system can be modeled as a nonlinear time varying system. The secondary voltage stability control problem can be formulated as a multiple-objective optimization problem. The objectives of the control formulation can be any combination of minimum reactive power losses, maximum stability margin and minimum control actions. The control variables could include the set-point for AVRs, LTC tap positions, and capacitor banks switching status (on/off). The nonlinear system power flow equations are the equality constraints of the optimization problem. The capacities of components in transmission and generation networks, such as generator, lines and transformer, are the inequality constraints in the control formulation.

5.3.1 Nonlinear equality constraints

The general format of power flow equations can be written as $g(x,u,p)=0$, where g is the set of power flow equations, x is the state vector, u is the control vector, and p is the parameter vector. The state vector can be further expanded as $x=\lfloor x_1 \quad x_2 \quad \cdots \quad x_{N_b} \rfloor$. Let $k \in [1, N_b]$. If bus k is a PQ bus, then $x_k = \lceil V_k \quad \theta_k \rceil$ is the set of positive sequence phasors represented in polar coordinates. Otherwise, if bus k is a PV bus, then $x_k = \lceil \theta_k \rceil$ since V_k is fixed. Similarly, the control vector can be further expanded as $u=\lfloor u_1 \quad u_2 \quad \cdots \quad u_{N_b} \rfloor$. Let $k \in [1, N_b]$, such that the control vector u_k consists of settings of different control devices at bus k, such as voltage setting V_k, if bus k is a PV bus, capacitor bank shunt susceptance b_k, and off-nominal transformer tap position τ_{km} (from bus k to interconnected bus m). The parameter vector p_k for bus k, including admittance and conductance for branches, load and generator operation limits, is known before performing power flow.

The set of power flow equations for bus k can be written as:

$$P_{gk} - P_{dk} = V_k^2 \left[g_k + \sum_{m \in M(k)} (g_{km} + g_{skm}) \right] - V_k \sum_{m \in M(k)} \left[g_{km} \cos(\theta_{km}) + b_{km} \sin(\theta_{km}) \right] V_m$$

$$Q_{gk} - Q_{dk} = -V_k^2 \left[b_k + \sum_{m \in M(k)} (b_{km} + b_{skm}) \right] - V_k \sum_{m \in M(k)} \left[g_{km} \sin(\theta_{km}) - b_{km} \cos(\theta_{km}) \right] V_m$$

P_{gk}, Q_{gk} = Active and reactive generation at bus k (5-1)

P_{dk}, Q_{dk} = Active and reactive demand at bus k

g_k, b_k = Shunt conductance and susceptance at bus k

g_{km}, b_{km} = Conductance and susceptance of the line between bus k and bus m

g_{skm}, b_{skm} = Shunt conductance and susceptance of the same line

θ_{km} = Voltage phase angles difference between bus k and m

V_i, δ_i = Voltage magnitude and angle at bus i (i=k,m)

$M(k)$ = Set of buses connected to bus k

If bus k and bus m are connected by an off-nominal tap transformer with the tap ratio of $\tau_{km}:1$ between bus k side and bus m side, then the shunt admittances of the regulating transformer model (b_{skm1} on bus k side and b_{skm2} on bus m side) can be calculated based on a model of regulating transformer (see Figure 24):

$$b_{skm1} = (1-\tau_{km})y_{km},\ b_{skm2} = (\tau_{km}{}^2 - \tau_{km})y_{km} + \tau_{km}{}^2 y_{skm},$$

The susceptance between bus k and bus m can be calculated by:

$$b_{km} = \tau_{km} y_{km},$$

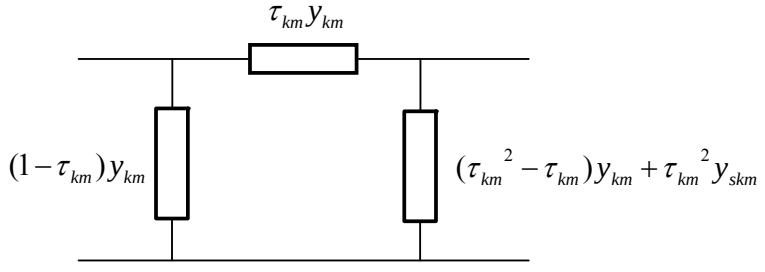

Figure 35 simplified single-phase tap transformer model [56].

where y_{km} and y_{skm} are the equivalent series and shunt admittances of the simplified single-phase tap transformer, respectively.

5.3.2 Inequality constraints

Limited control resource and operation limits of the control devices can be regarded as inequality constraints. The set of inequality constraints, many of which are capacity constraints, can be listed as follows:

$$V_{i,\min} \le V_i \le V_{i,\max},\ i = 1,\cdots,N_b .$$

$$P_{gi\_\min} \le P_{gi} \le P_{gi\_\max},\ i = 1,\cdots,N_g$$

$$Q_{gi\_\min} \le Q_{gi} \le Q_{gi\_\max},\ i = 1,\cdots,N_g$$

$$\tau_{km\_\min} \le \tau_{km} \le \tau_{km\_\max},$$

$$b_{i,\min} \le b_i \le b_{i,\max},\ i = 1,\cdots,N_b$$

$$S_{km} \le S_{km\_\max}$$

where $V_{i\_\min}, V_{i\_\max}$ are the lower and upper bounds on the voltage magnitude at bus *i;* $P_{gi\_\min}, P_{gi\_\max}$ are the lower and upper bounds on the active generation at generator *i;* $Q_{gi\_\min}, Q_{gi\_\max}$ are the lower and upper bounds on the reactive generation at generator *i;* $\tau_{km}, \tau_{km\_\min}, \tau_{km\_\max}$ are the current, lower and upper bound of the tap ratio for the transformer between bus *k* and bus *m;* $b_i, b_{i,\min}, b_{i,\max}$ are the current, lower and upper bound of the shunt susceptance on bus *i;* $S_{km}, S_{km\_\max}$ are the current and maximum allowable apparent power flow in branch between bus *k* and bus *m;* and N_g N_b are the total number of generators and buses in the system.

5.3.3 Objective functions

a. Maximization of stability margin

The stability margin of a power system can be evaluated by the maximum loading margin, the difference between the critical loading level λ_c and the base case loading level. Therefore, when the system is running at critical condition, the real and reactive loads at bus *k* can be approximated by linear increase of the load: $P_{dk\_c} = (1+\lambda_c)P_{dk}$ and $Q_{dk\_c} = (1+\lambda_c)Q_{dk}$. The equality constraint should still be valid by substituting P_{dk} and Q_{dk} with P_{dk_c} and Q_{dk_c}. The objective function for maximizing the stability margin is; Maximizing λ_c. Suppose the increased stability margin as a result of secondary voltage controls is λ_a, the objective of maximizing stability margin can be re-formulated to Maximize λ_a. Applying the vector of margin sensitivity as introduced in section 4.2, λ_a can be formulated as:

$$\lambda_a = \sum_{k=1}^{N_b} SC_k (b_k^{Post} - b_k^{\Pr e}) + \sum_{k=1}^{N_L} ST_k (\tau_k^{Post} - \tau_k^{\Pr e}),$$

$b_k^{\Pr e}$, b_k^{Post} —the pre- and post-control shunt susceptance at bus *k* corresponding to online shunt capacitor banks,

$\tau_k^{\Pr e}$, τ_k^{Post} —the pre- and post-control tap positions of the LTC in branch *k,*

N_b N_L—the number of buses and lines in the system,

SC_k, ST_k—the margin sensitivity with respect to capacitor and LTC controls.

Since load shedding is performed separately after the other voltage and stability controls, the linearity assumption of the margin sensitivity of load shedding is still valid. However, the evaluation of the increased stability margin by load shedding needs to take the impact of the other controls into account. Suppose the increased stability margin as a result of load shedding is λ_S, the objective of maximizing stability margin can be re-formulated to Maximize λ_S. Applying the vector of margin sensitivity as introduced in section 4.2, λ_S can be formulated as:

$$\lambda_S = \sum_{k=1}^{N_b} SL_k (P_k^{Post} - P_k^{\Pr e}),$$

$P_k^{\Pr e}$, P_k^{Post} —the pre- and post-control active power load at bus *k*,

N_b—the number of buses and lines in the system,

SL_k—the margin sensitivity with respect to load shedding on bus *k*.

b. Minimization of the active and reactive losses.

The objective function for minimizing the sum of active and reactive losses can be formulated as:

$$\text{Minimize: } Q_{Loss} = \sum_{k=1}^{N_L} [-b_k V_{k,s}^2 \tau_k^2 - 2b_k V_{k,s} V_{k,r} \tau_k \cos(\theta_k) - b_k V_{k,r}^2];$$

$$\text{Minimize: } P_{Loss} = \sum_{k=1}^{N_L} [g_k V_{k,s}^2 \tau_k^2 - 2g_k V_{k,s} V_{k,r} \tau_k \cos(\theta_k) + g_k V_{k,r}^2];$$

where:

P_{Loss} , Q_{Loss} —the total active and reactive power loss in the system,

N_L —the total number of branches,

g_k , b_k —the conductance and susceptance of the branch *k*,

$V_{k,s}$, $V_{k,r}$ —the voltage magnitudes on the sending and receiving buses of branch *k*,

θ_k —the angle difference between the sending and receiving buses of branch *k*,

c. Minimization of the control actions

Fewer control actions will lead to shorter control time and thus a higher possibility of avoiding collapse. The objective function for minimizing the capacity of switched shunt capacitor banks and tap changes of LTCs can be written as:

Minimize: $\sum_{k=1}^{N_C} \frac{\left| b_k^{Post} - b_k^{\Pr e} \right|}{B_k}$; Minimize: $\sum_{k=1}^{N_L} \left| \tau_k^{Post} - \tau_k^{\Pr e} \right|$;

where:

$b_k^{\Pr e}$, b_k^{Post} —the pre and post-control shunt susceptance at bus *k* corresponding,

to the online shunt capacitor banks,

B_k—the shunt susceptance corresponding to one block of shunt capacitor installed on bus *k*,

$\tau_k^{\Pr e}$, τ_k^{Post} —the pre- and post-control tap positions of the LTC in branch *k*,

N_c, N_L—the number of buses and lines in the system.

It can be observed that the fundamental idea of the stability control formulation is similar to the Optimal Power Flow function in the EMS. In practice, the time interval between two OPF calculations is about 10 minutes [57] due to the delay caused by updating system information, which precludes its application in real-time voltage and stability control.

5.4 NORMALIZATION OF THE CONTROL OBJECTIVES

The voltage stability control problem can be viewed as a multiple-objective optimization problem, in the following format:

$$\text{Minimize } f(x,u,p) \qquad f: R^N \to R^k \tag{5-2}$$

$$\text{Subject to } g(x,u,p)=0, \qquad g: R^N \to R^n$$

$$h(x,u,p) \geq 0 \qquad h: R^N \to R^m$$

where:

$f(x,u,p)=\left[f_1(x,u,p) \quad f_2(x,u,p) \quad \cdots \quad f_k(x,u,p)\right]$—contains a partial or full set of objective functions presented in section 4.2.3,

$g(x,u,p)$—the set of equality constraints presented in section 4.2.1,

$h(x,u,p)$— contains the set of inequality constraints presented in section 4.2.2,

x,u,p—the vector of the state variables, the vector of the control variables, and the vector of the constant parameters of the system model.

The generally accepted solution of a multiple-objective optimization problem is said to be Pareto optimal, or a Pareto solution. A Pareto solution is one for which any improvement in one objective can only take place if at least one other objective worsens. Since there may exist multiple Pareto solutions, the system operator needs to make tradeoffs between the disparate and conflicting objectives (such as the tradeoff between loss reduction and control effort). A thorough discovery of the entire Pareto front is only necessary for long time-frame coordinated controls (such as OPF). For secondary voltage controls and emergency stability controls, the selection of an acceptable control decision is dictated by the short control time-frame. The exploration of the entire Pareto front is not practice, but a general assessment of the available control options is necessary to discover a suitable control decision. To obtain a general idea about the Pareto front within the time-frame of secondary voltage controls (3 minutes or less), a suitable algorithm needs to be designed. The difficulties for designing such a multiple-optimization algorithm can be summarized as follows:

(1) Short control time-frame.

Considering the necessary time delay caused by data collection and communications (up to 30 seconds), the remaining time for control computation is about 150~180 seconds.

(2) Numerical difference among the objectives

The numerical different among the objective values could be larger. For example, the stability-relate objective value is usually in the range from -0.10 to 0.15, while the loss-related objective is typically in the range from 2000 to 3000 for the 39-bus system. Depending on the practical control intentions, the control objectives need to be discriminated to emphasize the more important ones. The designed algorithm needs to

normalize the control objectives such that the desired control intention can be well expressed.

(3) The congestion of the optimal solutions

When the discovered optimal solutions locate close to each others and concentrate on a portion of the Pareto front, the efficiency and performance of the optimization algorithm is affected by the congestion problem. The designed algorithm should generate close to evenly distributed Pareto solutions which sparsely cover the entire Pareto front.

Osyczka and Kundu [58] emphasized the importance of the objective formulation in achieving a direct optimal solution. However, choosing the weight factors could be an iterative process, which could easily be complicated by different scales of the objectives. Das and Dennis [59, 60] use an aggregate objective function (AOF) with different sets of scalar weights of the objective to obtain an evenly distributed set of Pareto solutions. The designer can pick out an acceptable solution from the Pareto solutions by making the appropriate tradeoffs.

Messac and Ismail [61] presented a normal constraint method for generating a set of evenly-spaced solutions on the Pareto front. The proposed algorithm provides a convenient procedure for normalization and linear mapping of the objectives.

(1) Anchor points.

The anchor points f_i^* can be obtained by solving a set of single-objective optimization problems in minimizing $f_i(x,u,p)$, $i \in [1,k]$. The plane comprising all the anchor points is defined as a Utopia hyper-plane [61].

(2) Objectives mapping/normalization.

Define a Utopia point and a Nadir point in the following:

$$f^u = \left[f_1(x^{1*}) \quad f_2(x^{2*}) \quad \cdots \quad f_k(x^{k*}) \right]^T ; \; f^N = \left[f_1^N \quad f_2^N \quad \cdots \quad f_k^N \right]^T ;$$

where: $f_i^N = \max\left[f_i\ (x^{1*}) \quad f_i\ (x^{2*}) \quad \cdots \quad f_i\ (x^{k*}) \right]^T$

(3) Define a distance vector L in the following:

$$L = f^N - f^u ;$$

Therefore, the normalized design metrics can be obtained by the following:

$$\bar{f}_i = \frac{f_i - f_i(x^{i*})}{L(i)}, \; i=1,2,\ldots,n$$

(4) Generate points on the Utopia hyper-plane.

The convex combinations of the anchor points will yield a set of points on the Utopia hyper-plane.

$$\overline{X}_{pj} = \sum_{i=1}^{k} \alpha_{ij} \bar{f}_i^* , \; 0 \le \alpha_{ij} \le 1 \text{ and } \sum_{i=1}^{k} \alpha_{ij} = 1$$

The value of α_{ij} will decide the weight for the objective $f_i(x,u,p)$. If α_{ij} is set to be close to 1, the generated Utopia point $\overline{X}_{pj}$ will be close to the anchor point $\bar{f}_i^*$.

(5) Utopia plane vectors.

Define the direction $\overline{N}_i$ from $\bar{f}_i^*$ to $\bar{f}_k^*$ in the following:

$$\overline{N}_i = \bar{f}_k^* - \bar{f}_i^* , \; i = 1,2,\ldots,k-1$$

(6) Pareto solution generation.

Starting from a Utopia point $\bar{X}_{pj}$, the mapping to a Pareto solution $\bar{f}_j^*$ can be obtained by solving the following single objective optimization problem:

Minimize $\bar{f}_n(x,u,p)$ $\qquad f: R^N \to R$ (5-3)

Subject to $g(x,u,p)=0$, $\qquad g: R^N \to R^n$

$h(x,u,p) \geq 0 \qquad h: R^N \to R^m$

$\bar{N}_i(\bar{f}-\bar{X}_{pj})^T \leq 0 \qquad i = 1,2,\ldots,k\text{-}1$

where $\bar{f}=\{\bar{f}_1 \quad \cdots \quad \bar{f}_k\}$

The mechanism of generating a Pareto solution in a two-dimension solution space is illustrated in Figure 36.

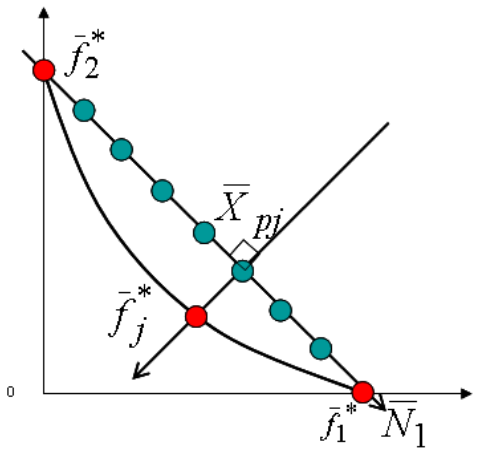

Figure 36. Use of the normal constraint method to generate a Pareto solution [61].

In Figure 36, the blue dots are the starting Utopia points, while the red dots are the Pareto solutions. $\bar{f}_1^*$ and $\bar{f}_2^*$ are the anchor points projected on the horizontal and

vertical coordinates respectively. Starting from a Utopia point $\overline{X}_{pj}$, by solving the optimization problem in step 6, a Pareto solution $\bar{f}_j^*$ can be generated. If the generation of Pareto solutions with large population is desired, step 6 can be repeated but with different starting Utopia point. The selected Utopia point should evenly cover the entire Utopia hyper-plane. Step (7) can be used to evenly distribute the Utopia points on the k-dimensional Utopia hyper-plane.

(7) Normalized increments.

Interpolate m_i points evenly along the vector $\overline{N}_i$. The normalized increments along the direction of $\overline{N}_i$ can be calculated by:

$$\delta_i = \frac{1}{m_i - 1},\ i = 1,2,\ldots,k\text{-}1$$

With a specified number of points m_1 along the vector $\overline{N}_1$, the number of points along $\overline{N}_i$ can be calculated as:

$$m_i = \frac{m_1 \left\| \overline{N}_i \right\|}{\left\| \overline{N}_1 \right\|}$$

Therefore, the number of points along $\overline{N}_i$ should increase with the length of the vector $\overline{N}_i$. After generation of candidate solutions, the existence of non-Pareto solutions is not guaranteed, since part of the solution space could be concave. It is necessary to apply a Pareto filter to eliminate all the non-Pareto solutions. Only the globally optimal Pareto solutions should remain in the Pareto front [61].

Definition 1: A design metric vector f^* is globally Pareto optimal if there does not exist another design metric vector f such that $f_i \leqslant f_i^*$ for all $i \in \{1, 2, ..., n\}$, and $f_j < f_j^*$ for at least one index of j , $j \in \{1, 2, ..., n\}$ in the feasible design space.

The Pareto filter is an algorithm that tests the Pareto optimality of each candidate solution in a given set of points and discards all the non-Pareto solutions.

The following example illustrates how the normal constraint method, introduced above, could be applied to obtain the Pareto front of an optimal capacitor bank control problem.

The example is based on the IEEE 39-bus system with 145% of the base load. A snapshot taken under this load condition is shown in Figure 37. According to the problem formulation introduced in Section 4.3, a combination of the following control objectives can be selected:

$$\text{Minimize: } Q_{Loss} = \sum_{k=1}^{N_L} [-b_k V_{k,s}^2 \tau_k^2 - 2 b_k V_{k,s} V_{k,r} \tau_k \cos(\theta_k) - b_k V_{k,r}^2];$$

$$\text{Minimize: } P_{Loss} = \sum_{k=1}^{N_L} [g_k V_{k,s}^2 \tau_k^2 - 2 g_k V_{k,s} V_{k,r} \tau_k \cos(\theta_k) + g_k V_{k,r}^2];$$

$$\text{Minimize: } \sum_{k=1}^{N_C} \frac{\left| b_k^{Post} - b_k^{\Pr e} \right|}{B_k}.$$

The initial allocation of the capacitor banks is performed in order to optimize reduction in active power losses, and maintain acceptable voltage profile and stability margin under normal and contingency conditions. The detailed capacitor bank allocation procedures were introduced in section 4.1.

Both equality and inequality constraints introduced in section 5.2.1 and 5.2.2 are considered. The post-control voltages on all the buses should be maintained within their specified range. The maximum allowable shunt susceptance on each bus is the total allocated capacity of the capacitor banks on the bus. The limits of reactive power output from the generators are also considered.

AMPL [62], developed by Bell Laboratories as a powerful optimization modeling software, is adopted to customize the normal constraint algorithm for solving the secondary voltage control problem. An interface is designed to link between AMPL and MATLAB in which the remainder of the model is written, so that the AMPL model can be executed as a subroutine in MATLAB. AMPL also provides convenient interface with a variety of solvers for linear and nonlinear programming. From the available optimization solvers, MINOS is chosen to solve the secondary voltage and stability control problem. MINOS is a Fortran-based computer program designed to solve large-scale linear and non-linear optimization problems [63]. MINOS uses linearly constrained Lagrangian method to solve non-linear optimization problems. The designed AMPL model will be applied in the 39-bus example later. For systems with similar or larger scale than the 39-bus system, the same AMPL model can be adopted to generate Pareto control solutions.

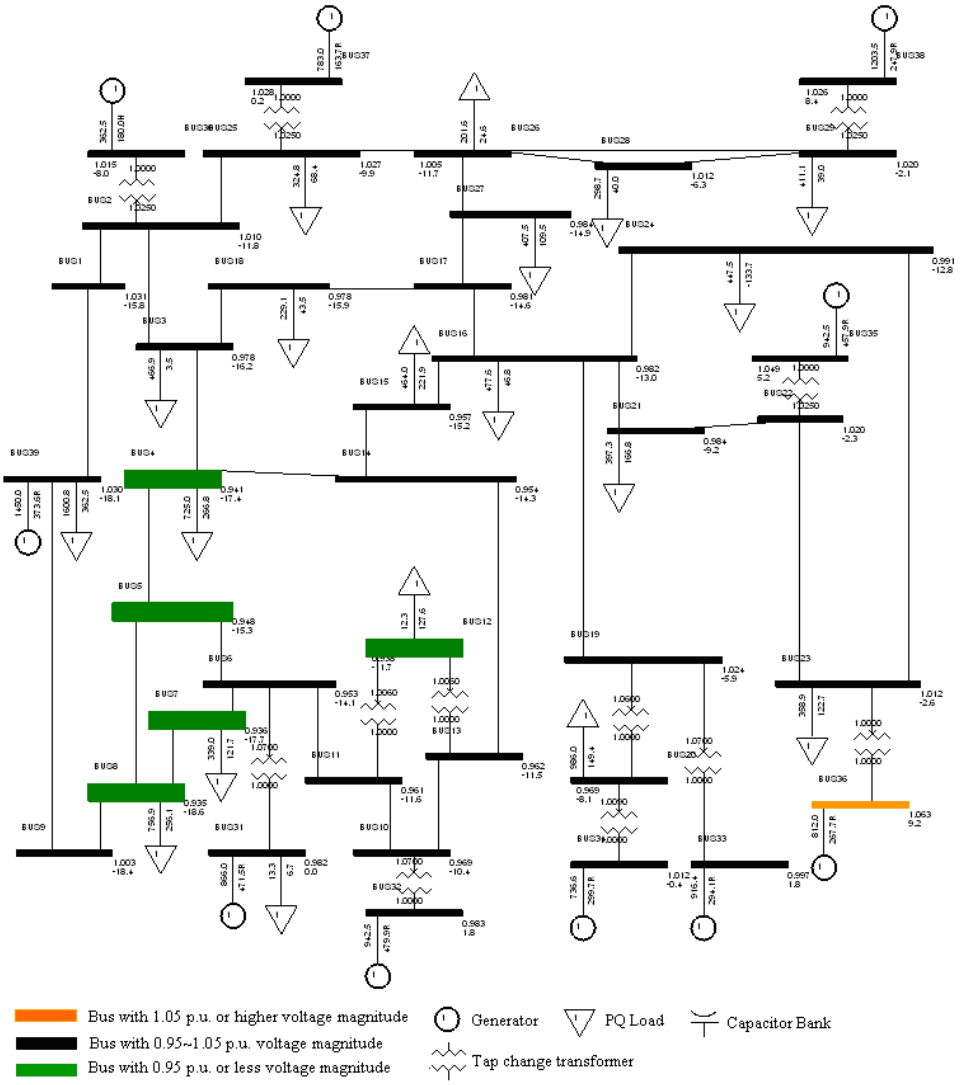

Figure 37. Snapshot of the IEEE 39-bus system under 145% loading.

The Pareto fronts obtained by adopting different populations of the initial Utopia points are compared in Figure 39 and Figure 40. If a short control time is strictly demanded, a fast and suboptimal control solution can be picked out from the six Pareto solutions shown in Figure 39. The Pareto solutions in Figure 39 are generated in 11.64 seconds using a desktop computer with 1.6 GHz core duo chip and 1 GB memory, which adequately fits the time frame for secondary voltage stability controls. The 121 Pareto

solutions represented by the red dots in Figure 40 are generated after 59.4 seconds. The computation time would be much short if the high performance computers in the control centers of the utilities were utilized. Moreover, if weights of the objective functions could be accurately determined based on the actual system conditions, it only takes about 2.3 seconds for the normal constraint method to generate one control solution.

A more thorough search of the Pareto front can be achieved by solving a set of two-objective sub-problems decoupled from the original three-objective problem formulation. When solving one two-objective sub-problem, one of the original three objectives (e.g. the objective of minimum capacitor control) is set as a fixed value within its feasible range. The formulation of the decoupled two-objective optimization problem is as follows:

Minimize active power losses: $P_{Loss} = \sum_{k=1}^{N_b} P_{G,k} - P_{L,k}$

Minimize reactive power losses: $Q_{Loss} = \sum_{k=1}^{N_b} Q_{G,k} - Q_{L,k}$

Subject to: $\sum_{k=1}^{N_C} b_k^{Post} = B_c,\ 0 \le B_c \le \sum_{k=1}^{N_C} b_{k,\max}$

Equality constraints introduced in section 4.2.1;

Inequality constraints introduced in section 4.2.2;

where B_c —Fixed capacity of the applied shunt capacitor banks;

$b_{k,\max}$ —Total installed capacitor of the capacitor banks on bus *k*.

By repetitively solving the two-objective problem with different fixed value for the third objective, the population of the Pareto solutions will gradually grow to cover a larger portion of the Pareto front. The dominated solutions need to be filtered out in order to ensure the optimality of the Pareto solutions. The flow chart of using the decoupled method to search for the Pareto front for the three-objective capacitor control example is shown in Figure 38.

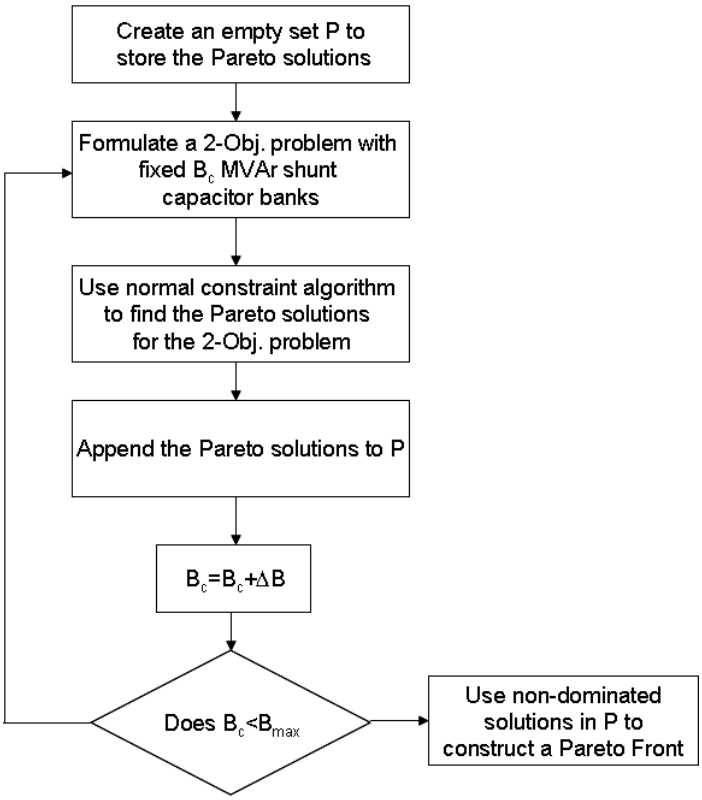

Figure 38. The flow-chart of the decoupled method.

The Pareto fronts obtained by solving the original three-objective problem and a set of decoupled two-objective problems are compared in Figure 40. When solving the decoupled two-objective problems, the capacity in the applied capacitor banks is increased by 1 MVAr for each problem formulation until the total installed capacity in the capacitor banks is reached. In Figure 40, the dense blue dots, with a population of

5344, correspond to the Pareto solutions obtained by the decoupled method. The red dots, with a population of 121, correspond to the Pareto solutions obtained by solving the original three-objective problem. The blue dots overlap with the red dots in most part of the projections to all three planes. Small discrepancies in active power losses can be detected when the capacity of the applied capacitor banks reaches close to the upper limit. The red dots are generated in less than one minute, while the blue dots are generated in 60 minutes with the same desktop computer. The blue dots provide more accurate and general exploration of the three-dimensional Pareto front, which is a spiral-shape narrow surface. For utilities interested in minimizing controls of capacitor banks, control solutions could be picked out from the lower part of the Pareto front corresponding to less control actions in capacitor banks. From Figure 39 and Figure 40, the advantages of applying the normal constraint algorithm in solving secondary voltage control problems can be summarized as follows:

(1) Short computation time. Instead of spending 60 minutes to discover the details about the Pareto front, a set of Pareto solutions representing different control interests can be obtained within 1 minute for systems with similar size to the 39-bus model. Depending on the actual control requirements, the sparsity of the Pareto solution can be conveniently changed to further shorten the computation time, such as the 6 Pareto solutions generated in 11.64 seconds as shown in Figure 39.

(2) High accuracy. In Figure 40, the red dots (a subset of Pareto solutions generated by the normal constraint algorithm) belong to the Pareto front formed by the blue dots (a more complete set of Pareto front). Therefore, the optimality of the Pareto solutions corresponding to the red dots is the same as the blue dots.

(3) High diversity and little congestion. The red dots in Figure 39 and Figure 40 evenly distribute on the Pareto front formed by the blue dots. Congestion of the red dots is not observed.

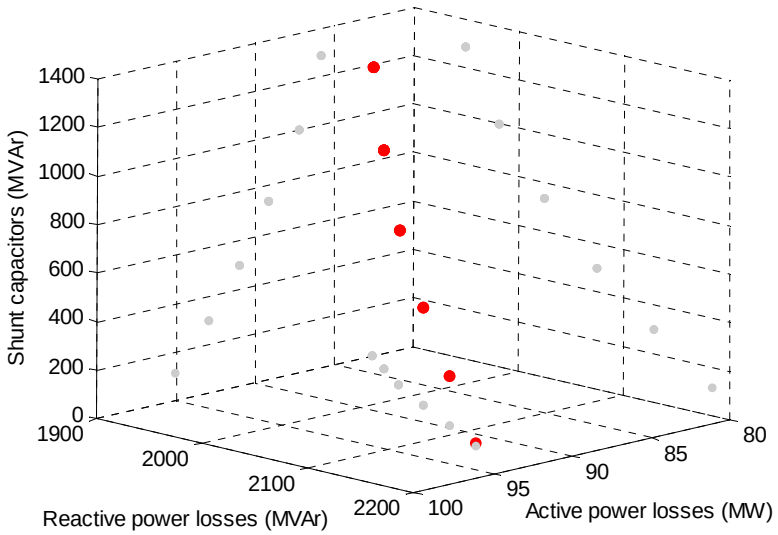

Figure 39. The Pareto front obtained in 11.64 seconds by the normal constraint algorithm with six initial Utopia points for the optimal capacitor banks control problem.

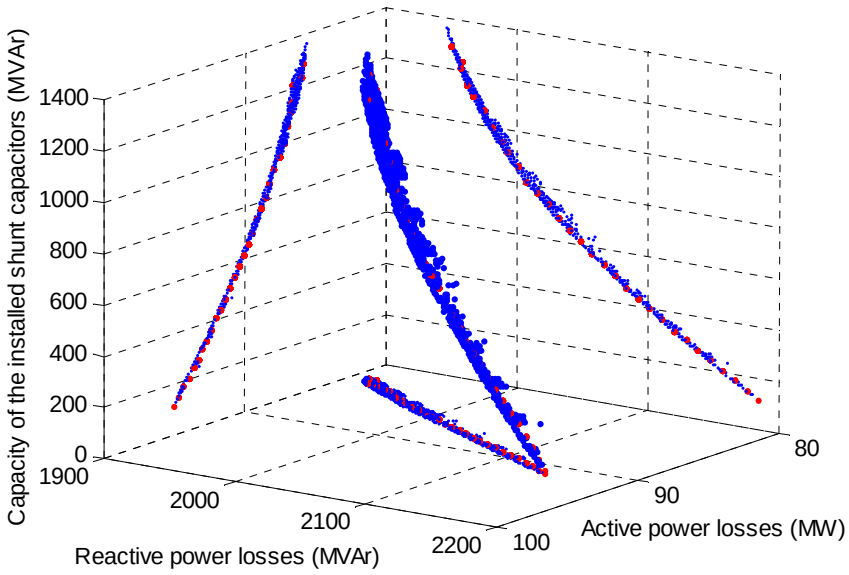

Figure 40. Comparison of the Pareto frontier obtained by solving the original three-objective optimization problem vs. decoupled two-Objective optimization problems.

The automatic secondary voltage controls are usually performed to improve local voltage profiles [19, 45, 64]. Manual and coordinated secondary voltage controls [17, 37] correct voltage violations of the local buses by controlling control devices in the vicinity. It can be concluded that the local secondary voltage control devices mainly participates in the voltage controls of the nearby buses. A thorough observation of the Pareto solutions discovered for the 39-bus example shows that the portion of controls applied in the vicinity of the buses with voltage violations varies the weight factors If the objective of minimum capacitor control is weighted heavily, the controls will be more restricted in the vicinity of the voltage-constrained buses in the purpose of solving voltage constraint violations. With small weight factor on minimum control objectives and thus more control actions, the controls will be more distributed system-wide to further reduce transmission losses. By studying the pattern of the optimal control solutions, one can determine the area setting the most control support for a given disturbance.

In Figure 41, a statistical analysis is performed on the entire population of the Pareto solutions obtained by the decoupled method. Three sets of buses are defined:

Set 1: the faulted buses only (bus 4, 5, 7, 8, 12),

Set 2: the faulted buses and the first tier of neighboring buses (bus 3, 4, 5, 6, 7, 8, 9, 10, 11, 12, 13, 14),

Set 3: the faulted buses and the next two tiers of neighboring buses (bus 2, 3, 4, 5, 6, 7, 8, 9, 10, 11, 13, 14, 15, 18, 31, 32, 39).

For a neighboring bus connected to an LTC, the bus on the other side of the LTC will also be included as a neighboring bus. The goal of this analysis is to compare the

capacity of the applied capacitor banks on the three sets of buses, when the total capacity of the applied capacitor banks in the system is constrained. For each constrained total capacity of the applied capacitor banks in the system, the maximum percentages of the capacity of the capacitor banks applied on the three bus sets are compared in Figure 41.

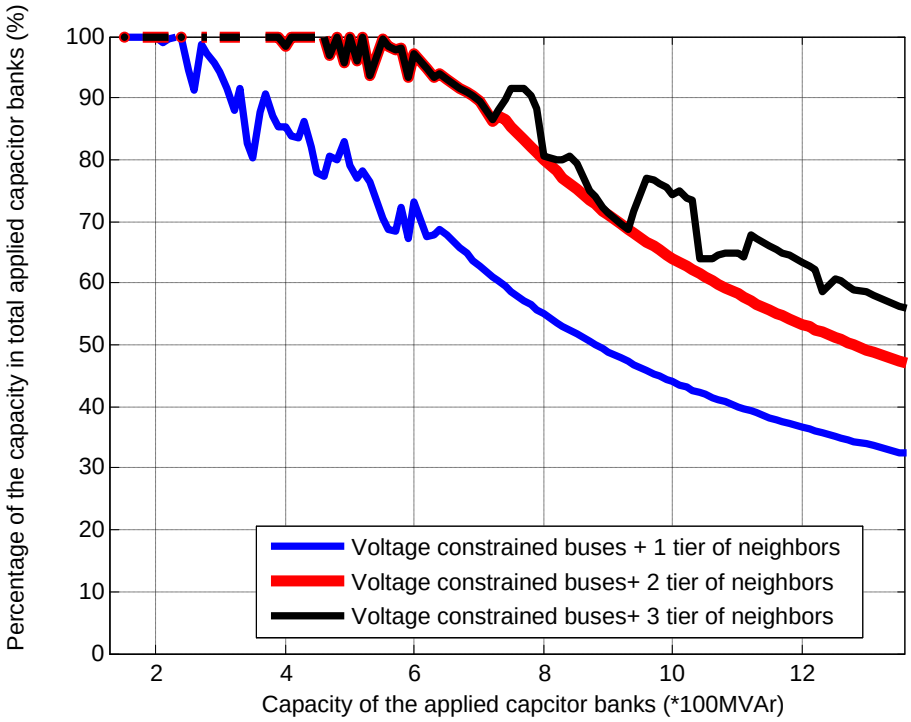

Figure 41. The percentage of the applied control capacity of the switched capacitor banks on faulted buses vs. faulted buses and the neighboring buses.

According to the reactive resource allocation scheme in Table 10, the total capacity of the allocated capacitor banks on the buses with voltage violations and the next two tiers of neighboring buses is 640 MVAr. When the total applied capacitor banks is constrained to be less than 640 MVAr, almost all of the optimal controls are performed within a local zone enclosing the buses with voltage violations and the next two tiers of neighboring buses. Only when the constraint on the total capacity of the applied capacitor

banks is relaxed, then the VAr resources from the rest of the system should be switched on to optimize the objectives. Utilities tend to constrain the controls on capacitor banks so as to avoid redundant switching. Following such control philosophy, it can be assumed that most of the secondary voltage controls can be optimized locally without involving the control devices from the external system, which are three or more tiers away from the buses with voltage violations. A collection of the local optimal control solutions will resemble a portion of the Pareto front obtained by evaluating the control solutions for the entire system.

5.5 CONCLUSION

In this chapter, the idea of utilizing secondary voltage control devices to solve voltage and stability constraints as well as optimize transmission losses was presented. The allocation of reactive resources is critical to the performance of secondary voltage and stability controls. The security and voltage stability constrained RRP approach is designed to boost the capability of the secondary voltage controls in meeting mixed control objectives without violating security limits.

The general formulation for a voltage and stability control problem is presented, which includes multiple control objectives, equality and inequality constraints, and variables representing the control settings of the secondary voltage control devices. Because of the short control time-frame (less than 3 minutes) required by secondary voltage controls and emergency stability controls, a suitable multiple-objective optimization algorithm is called for to a generate partially explored but representative Pareto front. A normal constraint algorithm [61] is adopted to provide a quick and sparse

exploration of the Pareto front of the multiple-objective voltage and stability control problem. Depending on the actual control interests, the sparsity of the Pareto solutions generated by the normal constraint algorithm can be conveniently adjusted to fit the requirement on the computation time. The partial Pareto front explored by the normal constraint algorithm matches with the Pareto front obtained by solving decoupled optimizations with an exhaustive search over one of the solution dimensions. The Pareto solutions generated by the normal constraint algorithm evenly distribute over the entire Pareto front with high accuracy and little congestion. A commercial optimization modeling software—AMPL [62] is adopted to customize the normal constraint algorithm for solving the secondary voltage control problem. For systems with similar or larger scale than the 39-bus system, the same AMPL model can be adopted to generate Pareto control solutions.

Further analysis of the Pareto solutions suggests that the optimal controls are usually conducted in the vicinity of the buses with voltage violations with higher priority than the buses located three tiers or farther to the buses with voltage violations. A voltage and stability control problem could possibly be evaluated locally with properly defined control zones which include only sensitive control devices.

CHAPTER VI

DECENTRALIZED SECONDARY VOLTAGE AND STABILITY CONTROL

6.1 MOTIVATION AND PROBLEM STATEMENT

Compared to the generator control components, such as excitation controller and AVRs, the controls of the shunt capacitor banks and LTCs have the characteristics of slower dynamics, and therefore may be considered as the secondary voltage control devices. The objective of the secondary voltage controls is to solve actual or simulated voltage constraint violations. The secondary voltage controls are either automatic (EDF) or manually coordinated (PJM).

Transmission level capacitor banks are typically in the capacity range between 120MVAr to 200 MVAr for a 230kV system, or between 30MVAr to 60 MVAr for a 115kV system. Normally, one or two switched capacitor banks are found in a substation. The controls of those capacitor banks are most commonly manual. On a daily basis, 230kV capacitor banks operate at least once daily to a maximum of three times daily, depending on the system loading level. Automatic capacitor control units are routinely used in distribution feeders and in the capacity range of up to several MVAr. The control of transmission level switch capacitor banks is performed only when the voltage magnitude at the controlled bus violates its regulation limits. Usually, the capacitor bank control is delayed until the LTC automatic tap adjustment finishes. The control time

interval for LTC ranges from 20 seconds to more than 100 seconds. When the controlled power system is under stressful or extreme loading conditions repetitively, LTC automatic tap adjustment could possibly deteriorate the system stability. Some power utilities rely on LTC emergency controls, such as tap locking (deactivating the automatic tap controls), tap blocking (restricting the automatic tap controls within a narrow band) or tap reverse control (conservative voltage reduction), to temporarily relax the stability constraint. Such LTC emergency controls allow the temporary violation of voltage regulation and can possibly delay the onset of voltage collapse. Certain remedial controls, such as generator control or capacitor bank switching, are needed immediately following the LTC emergency controls to radically solve the aftermath of voltage constraint violations. Since such control coordination between LTC and capacitor banks needs to be nearly instantaneous, existing centralized SCADA/EMS control structure is not sufficient to satisfy that requirement.

In the late 1980's, the French utilities EDF designed a hierarchical Voltage-Var control system [19-21, 45, 65] by coordinating regional, secondary and tertiary level controls to achieve real-time voltage regulation and stability control. The primary control level devices, with a response time of a few seconds, consist of Automatic Voltage Regulator (AVR) installed on generators. The secondary level voltage control, with a response time of about three minutes, is carried out by both slow and fast Var compensation devices (capacitors and condensers) and LTCs. These devices are considered to have a longer operating time interval (slow control devices). The purpose of the tertiary control level [20, 21] is to determine an optimal voltage profile of the network and to coordinate the secondary controllers according to safety and economic

criteria. The control objective variables include reactive generation and line flows, automatic voltage regulator (AVR) set points at synchronous generators, switching of reactive compensation devices and changing of LTC tap positions. The tertiary control is achieved by minimizing the sum of squared voltage deviations. The decision variables are the set-points of control devices. The flow chart of the French voltage control system is shown in Figure 23.

The advantage of this approach is the coordination of control devices and faster response of the hierarchical structure. State estimation is not necessary for this system since the only needed system information is the sensitivity matrix, which can be calculated promptly once the data of system states are collected. The sensitivity matrix can be calculated based on the state measurements and system topology. For simple coordination controls, no dedicated communication channels are needed, since only the critical buses are monitored.

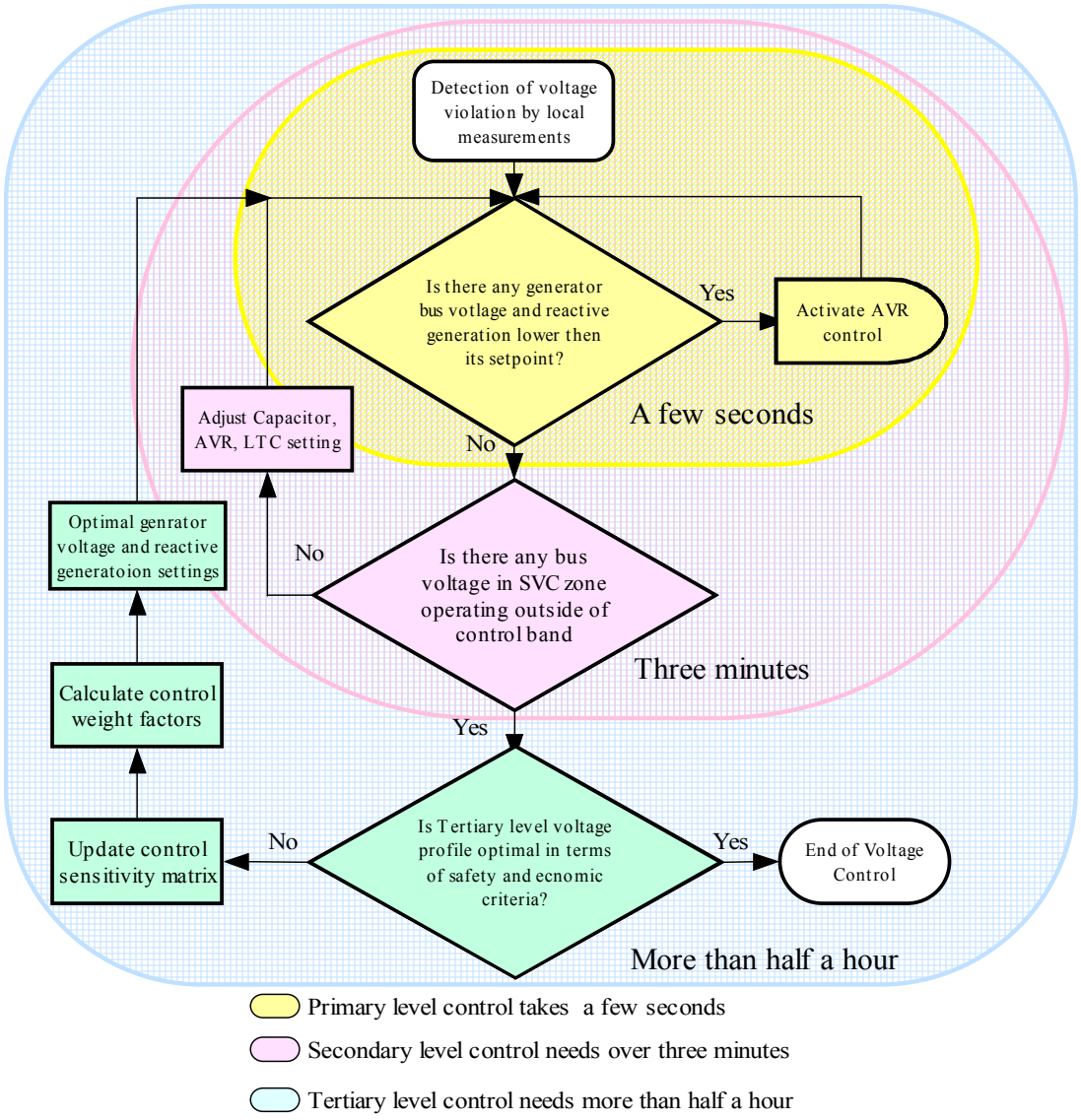

Figure 23. Flow chart of the voltage control system by EDF.

Currently, this three-tier hierarchical voltage control system is the most advanced and efficient voltage control system. However, there are still possible improvements for such a system to add stability monitoring and control abilities. In order to maintain system stability under extreme conditions such as high loading level or cascaded system disturbances, it would be ideal for the three minutes response time [20] of the secondary level control to be dramatically shortened and determined more analytically. Since the

conventional empirical capacitor bank control approach and automatic tap changes occupy most of the secondary level control response time, a deterministic control algorithm based on local time domain measurements may not only speed up the secondary level control but also take the control coordination of the secondary control devices into account.

Further implementation of the secondary level coordination [21] has been accomplished by monitoring the pre-defined fixed pilot points with pronounced voltage variations in different secondary systems. In order to make a secondary control zone more flexible, while taking into account different types of disturbances and emergency conditions, dynamic identification of the disturbance-affected zones or pilot points would be a better solution for stability considerations.

The tertiary level control takes the generation coordination into account by performing a fast system wide linear optimization. The reliability of this centralized tertiary level control depends on the accuracy of the SCADA data since the required sensitivity matrix and control weight factors are deduced from the system wide network status. By adopting the time-stamped PMU data, a continuous stability monitoring function becomes a possibility. Moreover, system decomposition based on the stability monitoring technique can be an alternative approach to avoid the time consuming system-wide information updating. An enhanced coordinated secondary level control evaluation can include not only the set-points of generator terminal voltages and reactive generation, but also the coordination of local voltage control devices such as LTCs and capacitor banks.

In Chapter 5, the secondary voltage and stability control has been formulated as a multiple-objective optimization model. The optimal control solutions can be considered as the centralized control decisions since the optimization model covers the entire system network. Simulation studies in section 4.4 reveal that with constrained control actions, the majority of the controls should be performed at the buses with voltage violations and the next one or two tiers of neighboring buses. The observation sheds light on the idea of relying on local secondary voltage controls to meet different control objectives.

With the emergence of advanced measurement technology such as PMU and fast communication networks, the next generation of the voltage control system can be implemented by incorporating the following ideas:

1) Decentralize the entire system into local control zones based on stability monitoring to achieve faster secondary level controls. The aggregated control solutions of all local control zones should lead to similar control objective values compared to the centralized (global) control solution. The arguments to support this idea include:

a. The system decomposition model needs to be designed to identify the disturbance affected region and separate from the rest of the system. The reduced system should represent the entire system equivalents accurately with respect to any given disturbance or system conditions.

b. Implement the system decomposition method to achieve the dynamic identification of the disturbance-affected zones. On the boundary of the disturbance-affected zone, external network can be represented by equivalent models. Therefore, the control of the entire system can be approximated by the control of the subsystem following the decomposition.

c. Controls of the external zones, which are less affected by the disturbances, contribute little to the disturbance mitigation. Therefore, the control solution from the disturbance-affected zones constitutes the major part of the remedial action. A comparison study between the global control solution and the aggregated local solutions needs to be performed to validate the proposed idea.

2) When the optimization formulation involves multiple variables and objectives, a set of suboptimal solutions meeting different control objectives need to be generated within the control time frame of the secondary control devices.

6.2 THE DECENTRALIZED VOLTAGE STABILITY CONTROL APPROACH

The conventional OPF method is not suitable for short-term secondary voltage stability control because it requires information about the entire system.

It is necessary to define a local control zone as an independent control area containing the observable area of a group of monitoring devices and connecting with external networks by suitable equivalent models. The allocation and observable areas of the monitoring devices are studied in section 4.3.1.

The decentralization of the entire controlled power network into separated local control zones can greatly reduce the dimension of the stability control formulation. Figure 25 illustrates the process of decomposing the entire system into two independent subsystems. The detailed system decomposition method will be introduced in section 4.3.2.

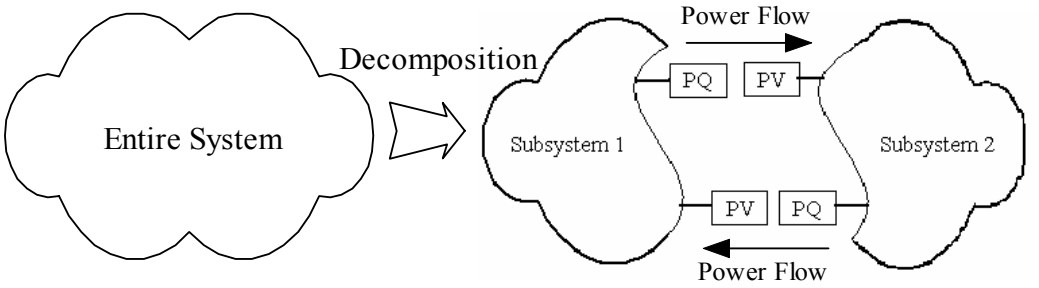

Figure 42. **Decomposition of the entire system into two subsystems**

According to the problem formulation from section 4.2, the general form of global voltage stability control can be written as follows:

$$\text{Minimize } f(x_G, u_G, p_G) \qquad f: R^{N_G} \to R^{k_G} \tag{6-1}$$

$$\text{Subject to } g(x_G, u_G, p_G) = 0, \qquad g: R^{N_G} \to R^{n_G}$$

$$h(x_G, u_G, p_G) \geq 0 \qquad h: R^{N_G} \to R^{m_G}$$

where x_G is the vector of voltage phasors on all buses in the system; u_G is the control settings (capacitors, taps, etc.) of the entire system; p_G is the network parameters (for lines, loads, generators) of the entire system; k_G, n_G, and m_G are the dimensions of objective functions *f*, equality constraints *g*, and inequality constraints *h* for the entire system model, respectively.

Supposing there are *d* subsystems after decentralization, subscript *G* and *L* refer to global and subsystem quantities, respectively. The general form of the global version voltage stability control formulation (6-1) can be approximated by the local version formulation (6-2).

$$\text{Minimize } f(x_{Li}, u_{Li}, p_{Li}) \qquad f: R^{N_{Li}} \to R^{k_{Li}} \tag{6-2}$$

$$\text{Subject to } g(x_{Li}, u_{Li}, p_{Li}) = 0, \qquad g: R^{N_{Li}} \to R^{n_{Li}}$$

$$h(x_{Li}, u_{Li}, p_{Li}) \geq 0, \qquad h: R^{N_{Li}} \rightarrow R^{m_{Li}}$$

where $i \in \{1,2,\cdots,d\}$ is the Subsystem index, x_{Li} is the voltage phasors on the buses in subsystem *i*, u_{Li} is the control settings (capacitors, taps etc) of subsystem *i*, and p_{Li} is the network parameters (for lines, loads, etc.) of subsystem *i*. k_{Li}, n_{Li}, and m_{Li} are the dimensions of objective functions *f*, equality constraints *g*, and inequality constraints *h* for the subsystem L_i, respectively.

Interface condition: define $\Gamma(x_{Li})$ as the portion of system (subsystem *i* without equivalent models). Similarly, $\Gamma(x_G)$ is the entire system network. Therefore, the interface condition between the global and local networks (6-3) should be satisfied:

$$\Gamma(x_G) = \bigcup_{i=1}^{d} \Gamma(x_{Li}) \bigcup_{i,j=1}^{d} T(x_{Li}, x_{Lj}) \tag{6-3}$$

where $T(x_{Li}, x_{Lj})$ is the tie line between subsystem L_i and L_j.

Validation check: let the combinational control decision made in all the local control zones be:

$$\hat{u}_G = u_{L1} \oplus u_{L2} \cdots \oplus u_{Ld} = \begin{bmatrix} u_{L1} & u_{L2} & \cdots & u_{Ld} \end{bmatrix}; \tag{6-4}$$

Then the following criterion should be satisfied:

$$\left\| f(x_G, u_G, p_G) - f(x_G, \hat{u}_G, p_G) \right\| < \varepsilon, \tag{6-5}$$

where ε is the validation threshold. A decentralized control solution should lead to similar objective values as the centralized control solution with the same control interests

does. The following criterions are adopted in evaluating the performance of the decentralized control solutions in the later case studies.

(1) MVA line consumption. A decentralized control solution may lead to 0.2% higher losses than the centralized control solution with the same control interests does.

(2) Stability margin: A decentralized control solution may lead to 0.5% higher or 0.5% lower stability margin than the centralized control solution with the same control interests does.

(3) Utilization of control resources. A decentralized control solution may lead to up to 10% more utilization of the control resources than the centralized control solution with the same control interests does. As a result of the possible excessive controls suggested by a decentralized control solution, additional benefits in the other objectives (such as minimum MVA line consumption and maximum stability margin) could be gained which make a decentralized control solution more conservative than the corresponding centralized control solution.

(4) Compared with the conventional utility control solution, such as automatically and manually coordinated voltage controls, the decentralized control solution should be made in shorter time frame and lead to better objectives values.

6.2.1 Observable zones based on the monitoring device allocation

For a given power network, define $N = \{n_1, n_2, ..., n_m\}$ as the set of nodes of the network. The set of branches (transmission lines) can then be defined as

$B = \{(n_{b1}, n_{c1}), (n_{b2}, n_{c2}), \cdots, (n_{bk}, n_{ck})\} \subseteq N \times N$, where k is the total number of branches. Let $N_P \subseteq N$ be the set of nodes equipped with monitoring devices. Then the set of observable nodes N_0 will be the superset of N_p. For $n_{o\_ij} \in N_0, 1 \le j \le l$, $n_{pi} \in N_p$, the remote nodes (nodes connected to far ends) of the branches $\{(n_{o\_i1}, n_{pi}), (n_{o\_i2}, n_{pi}), \cdots, (n_{o\_ij}, n_{pi})\}$, which all belong to *B*, represent the locations of the observable buses for which the pseudo-measurements of the voltage phasors are possible to be calculated from the measurements of line flows at the monitored location n_{pi}. The subscript *i* represents the i^{th} monitoring device, and *j* is the index of surrounding buses connected to the i^{th} monitored bus. Figure 26 illustrates the above definitions of the observable region.

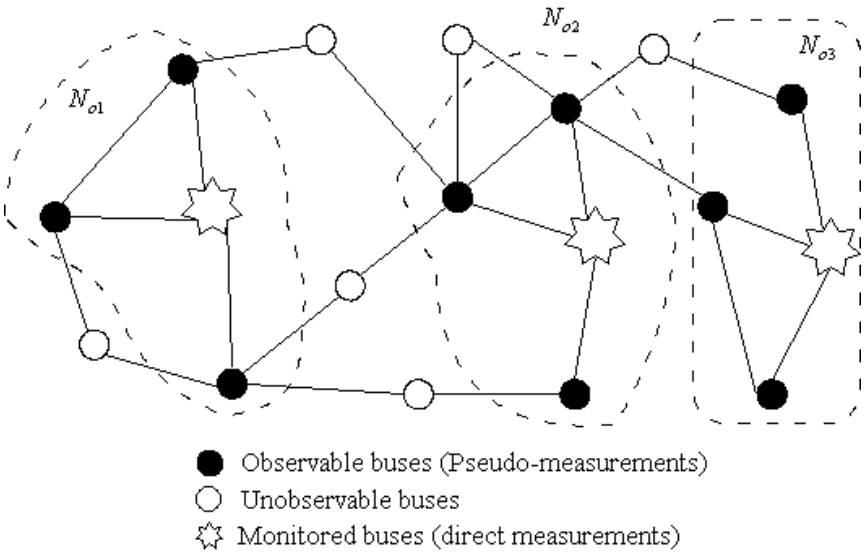

Figure 43. **Definition of the observable zone for decentralized control**

For a completely topologically observable system, the sufficient condition is $N_0 \equiv N$. For a completely observable *redundant* system, there must exist non-zero

intersections of $N_{oi} \cap N_{oj} \neq \phi$, $i \neq j$, such that the union of the observable sets of nodes covers the entire graph $N_{o1} \cup N_{o2} \cup \cdots \cup N_{ok} = N$.

An integral system can be divided into local observable zones by performing system decomposition (see section 4.3.2 for details). The placement of the monitoring devices should follow the rule of maximum observable zones with the minimum number of monitoring devices. Redundancies caused by overlapping of the observable zones are desirable to enhance the monitoring redundancy considering the possible occurrences of contingencies.

The complete topological observability of the entire system may not be necessary since many of the local buses may not be prone to voltage constraint violations. Therefore, the real-time monitoring devices (such as the PMUs) can be installed only at the buses with higher sensitivity to disturbances. The secondary voltage control system in EDF relies on monitoring of the "pilot buses" to perform control evaluation. The selection of the pilot buses is a large-scale combinational problem [66], taking into account the many factors such as the sensitivity of the pilot bus voltages to generator controls, as well as the observability of the system state. No exact solution technique exists to address such a problem [67]. Conejo [67] compared the greedy method and the global search method to select the pilot buses. The trade-off between these two methods lies in the efficiency and robustness.

Different from the secondary voltage system in EDF, the proposed decentralized secondary voltage stability control does not rely on the reference voltage and sensitivity of the pilot buses to evaluate control decisions. Since the control objective is to

counteract the impact of the disturbances/contingencies on voltage stability condition, the minimal requirement for the monitoring devices is the observability of the buses sensitive to disturbances and the lines associated with critical contingencies. The off-line transmission planning analysis, such as continuation power flow and contingency ranking, can be performed to determine the location of these sensitive buses. A fundamental approach to identify these sensitive buses can be designed as follows:

(1) Perform contingency ranking to identify the critical single contingencies with the largest impact on voltage profile.

(2) Prepare a set of base cases to include N-0 and all the critical N-1 contingencies.

(3) Freeze the controls of the LTCs and the capacitor banks. Perform power flow on the base cases at different loading levels. Identify the buses violating their voltage limits.

(4) Allocate monitoring devices to achieve complete topological observability of the buses identified in (3) and the line flows related to the critical N-1 contingencies. If some of the sensitive buses are interconnected with each other, the buses on the boundary of the interconnection have the higher priority for allocation.

The IEEE 39-bus system is used as an example to demonstrate the approach. The critical contingencies are defined for this example only as the top three N-1 contingencies with the largest impact on voltage profile. Starting from the initial level, loading is simultaneously and proportionally increased at all load buses in 10% steps until reaching 140% of the initial loading level. In addition, the limits of the reactive power generation are taken into account by activation of reactive limits on generators. The generator outages and two fatal N-1 line contingencies (line 16~19 and 19~20) are

assumed to be low probability events and are excluded from the contingency list. The top five critical N-1 contingencies identified at different loading levels are listed in Table 11.

Table 11. Critical N-1 contingencies with respect to voltage profile for the IEEE 39-bus system.

Loading level	Contingency Ranking				
	1	2	3	4	5
100%	15~16	21~22	2~3	26~27	3~4
110%	15~16	21~22	2~3	26~27	28~29
120%	15~16	21~22	2~3	26~27	28~29
130%	21~22	15~16	2~3	28~29	26~27
140%	21~22	15~16	2~3	28~29	8~9

The line contingency in the branch 21~22 is the most severe contingency which will lead the entire system to voltage collapse at around 140% loading level. The voltage sensitive buses, obtained by using (applying) the proposed approach, include buses 3-8, buses 10-18, bus 21, bus 22, bus 24, bus 27, bus 29, bus 32, and bus 36. In order to monitor the current in the lines related to the critical contingencies and all the sensitive buses, the monitoring device can be placed on buses {3, 6, 8, 10, 12, 15, 21, 23, 27, 29} as shown in Figure 44.

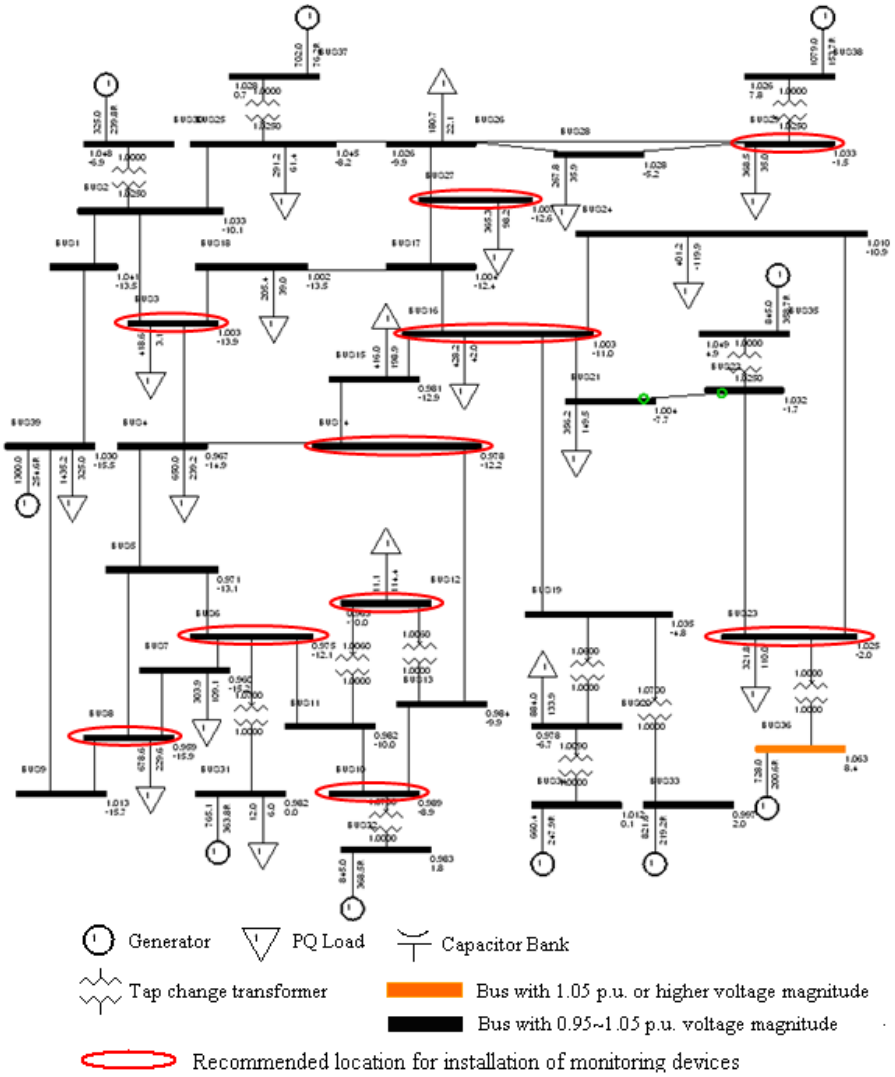

Figure 44. The allocation of the monitoring device for decentralized secondary control.

6.2.2 System decomposition

When a disturbance or contingency occurs, the buses electrically close to the disturbance will experience voltage drops. According to [68], if a contingency occurs which causes a change in bus voltage magnitudes, the change is the largest at the location where the fault has occurred and this change propagates through the system tier-wise. This conclusion is based on the assumption that the buses are partitioned into tiers and the electric network is a no-gain system to be defined shortly. The buses where the

disturbance is injected constitute tier 1 [68], the busses directly connected to tier 1 constitute tier 2, and so on. An electric network is said to possess the no-gain property [68] if and only if: a) the magnitude of the voltage between any pair of nodes in the network is less than or equal to the sum of the magnitudes of the voltages appearing across the independent sources, and b) the magnitude of the current flowing into each terminal of every element of the network is less than or equal to the sum of the magnitudes of the currents flowing through the independent sources.

For a no-gain system, localized voltage response [68] is caused by reactive disturbances such that the smallest voltage change in a lower ranking tier is larger or equal to the largest change in a higher-ranking tier. In publication [69], the authors further pointed out that system wide voltage responses can be encountered if part of the transmission line in the system does not possess the no-gain property as proved in [68]. In order to study the propagation property of the system-wide responses, the authors introduced the concept of an 'echelon structure', which differentiates the clusters of PV and PQ buses. Echelon 1 corresponds to the PV buses, while echelon 2 corresponds to the PQ buses directly connected to echelon 1. Analogically, echelon *i* corresponds to the PQ buses directly connected to echelon *i-1*. Starting from the disturbance originated echelon level, which coincides with the location of the disturbance, uniform voltage changes will be amplified in higher-ranking echelons, but attenuated in lower-ranking echelons.

According to the concept of echelon-structured network topology, the propagation of a reactive disturbance could be analyzed by observing the associated voltage drops on the buses surrounding the source of the disturbance. Depending on the structure of echelon in

a system network, a reactive disturbance could be attenuated or magnified along different propagation paths.

Spong [69] used the concept of a echelon-structured network model to explain the propagation of system-wide uniform reactive disturbances. The derivation of the echelon-structured network model can be extended to understand the propagation of local reactive disturbances. For a local reactive disturbance, the physical distances between different buses are as important as their topological distance to PV buses. A local reactive disturbance could be caused by a single contingency which may cause pronounced voltage drops in a few buses either physically or topologically close to the source of the disturbance. A disturbance-affected zone can be conveniently defined to enclose the buses with pronounced voltage drops. The VAR controls performed in the disturbance-affected zone can be regarded as reactive perturbation controls, which could also propagate in the disturbance-affected zone to counteract the impact of the disturbance.

6.2.2.1 The propagation of voltage disturbances caused by line contingencies

Without considering the conductance of the transmission lines, the reactive power injection at bus *i* can be formulated as:

$$Q_i = -V_i \sum_{k \in K_i} V_k c_{ik} \tag{6-6}$$

where K_i is the set of buses directly connected to bus *i* (including *i*) and

$$c_{ik} = B_{ik} \cos\theta_{ik}\,,\ i \neq k \tag{6-7}$$

$$c_{ii} = -(B_{is} + \sum_{\substack{k \in K_i \\ i \neq k}} (B_{ik} + B_{sik})$$

where B_{ik} and B_{sik} is the series and shunt susceptance of the line between bus *k* and *i*; B_{is} is the shunt susceptance at bus *i*.

Let $V_i = e^{x_i}$, the reactive power injection at bus *i* can be re-written as (6-8):

$$Q_i = -\sum_{k \in K_i} e^{(x_i + x_k)} c_{ik} \tag{6-8}$$

With a small reactive disturbance ΔQ_i, the voltage changes on bus *i* and *k* can be expressed by Δx_i and Δx_k.

$$\Delta Q_i = -\sum_{k \in K_i} e^{(x_i + x_k)} [e^{(\Delta x_i + \Delta x_k)} - 1] c_{ik} \tag{6-9}$$

Applying the Taylor expansion, the linear approximation of ΔQ_i can be written as:

$$\Delta Q_i = -\sum_{k \in K_i} (\Delta x_i + \Delta x_k) g_{ik} c_{ik} \ , \ g_{ik} = e^{(x_i + x_k)} \tag{6-10}$$

The above equation can also be expressed in matrix format:

$$-\Delta Q_i = H \Delta x \tag{6-11}$$

where

$$h_{ii} = -2[B_{is} + \sum_{\substack{k \in K_i \\ i \neq k}} (B_{ik} + B_{sik})] g_{ii} + \sum_{\substack{k \in K_i \\ i \neq k}} c_{ik} g_{ik} = -2Q_i - \sum_{\substack{k \in K_i \\ i \neq k}} c_{ik} g_{ik} \ , \tag{6-12}$$

$$h_{ik} = c_{ik} g_{ik}$$

With the dc load flow assumptions of small angles θ_{ik} and unity voltage magnitudes, the elements in H matrix can be approximated by (5-13):

$$h_{ii} \approx -2B_{is}^{'} - \sum_{\substack{k \in K_i \\ i \neq k}} B_{ik}\ ,\ h_{ik} \approx B_{ik} \tag{6-13}$$

where $B_{is}^{'} = B_{is} + \sum_{\substack{k \in K_i \\ i \neq k}} B_{sik}$.

Different from the pattern of uniform disturbances occurring on the buses of the same echelon, a reactive disturbance associated with an N-1 or N-1-1 contingency will cause voltage changes on a few buses topologically close to the contingency event. It can be assumed that the largest voltage drop is observed on bus *i* after a severe N-1 (tripping of single transmission line) or N-1-1 (tripping of single transmission line with two sections) contingency. To examine the propagation of the disturbance caused by the contingency, we define a tier-wise structure for the network under post-contingency condition. A load pocket of a bus set S is formed by one or a set of inter-connected PQ buses receiving generation support only from bus set S. The PQ buses directly connecting to bus *i* but not belonging to the load pocket of bus *i* is defined as tier 1; while the PQ buses connected to tier 1 but not belonging to the load pocket of tier 1 is defined as tier 2. Analogously, the PQ buses connected to tier *n-1* but not belonging to the load pocket of tier n-1 is defined as tier *n*. The tier-wise structure is shown in Figure 45. According to (5-11), the Q-V network equation for bus *i* and tier 1 can be formulated in (5-14).

$$h_{0,1}\Delta x_1 + h_{0,0}\Delta x = 0 \tag{6-14}$$

$$h_{1p,1p}\Delta x_{1p} + h_{1p,1}\Delta x_1 = 0$$

$$h_{1,0}\Delta x + h_{1,2}\Delta x_2 + h_{1,1p}\Delta x_{1p} + h_{1,1}\Delta x_1 = 0$$

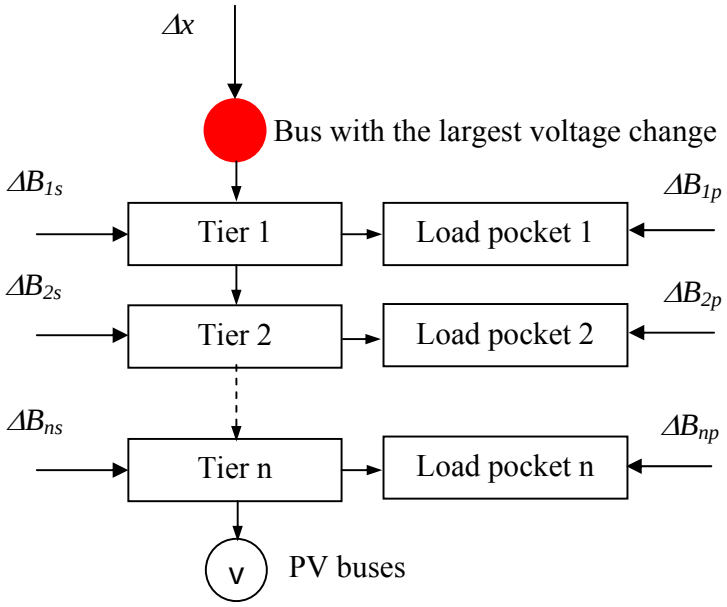

Figure 45. The propagation of the disturbance caused by a N-1 contingency in the tier-wise structured network.

Since tier *n* or lower are grouped by PQ buses, the reactive injections Q_i $(i \geq 2)$ into the PQ buses are non-negative with the assumption of capacitive shunt susceptance (in most cases). On the contrary, the signs of the terms B_{ik} $(i \neq k)$ are all negative with the assumption of reactive series susceptance in the transmission line between bus *i* and *k*. Considering the shunt susceptance on a bus is much less than the series susceptance of the lines connected to the same bus, the following condition will hold:

$$h_{0,0} = -2B_0 - B_{0,1} < -B_{0,1},\ h_{1p,1p} = -2B_{1p,1p} - B_{1p,1} < -B_{1p,1} \tag{6-15}$$

$$h_{1,1} = -2B_1 - B_{1,1p} - B_{1,2} - B_{1,0} < -B_{1,1p} - B_{1,2} - B_{1,0}$$

Derive (6-15) into (6-14), and (6-16) can be obtained.

$$|\Delta x_1| < |\Delta x|,\ |\Delta x_1| < |\Delta x_{1p}| \tag{6-16}$$

Combine (6-16) and the last equation in (6-14), and (6-17) can be obtained.

$$\Delta x_2 < \frac{h_{1,1} + h_{1,0} + h_{1,1p}}{-h_{1,2}} \Delta x_1 < \Delta x_1,\ \Delta x_1 \geq 0\ \ \Delta x_2 \geq 0 \tag{6-17}$$

$$\Delta x_2 > \frac{h_{1,1} + h_{1,0} + h_{1,1p}}{-h_{1,2}} \Delta x_1 > \Delta x_1,\ \Delta x_1 \leq 0\ \ \Delta x_2 \leq 0$$

Therefore, $|\Delta x_2|$ is smaller than $|\Delta x_1|$. Using the same derivation method for tier 2 and higher, equation (6-18) can be obtained:

$$|\Delta x_n| < |\Delta x_{n-1}| < \ldots\ldots < |\Delta x_3| < |\Delta x_2| < |\Delta x_1| < |\Delta x| \tag{6-18}$$

$$|\Delta x_i| < |\Delta x_{ip}| \quad (i = 1,2,\ldots,n)$$

Starting from tier *i*, if there exist multiple sub-tiers in load pocket *i*, it can be proved following the similar derivation as (6-17) that the voltage changes will be magnified in the sub-tiers of load pocket *i* away from tier *i*, such that $|\Delta x_i| < |\Delta x_{ip\_1}| < \ldots |\Delta x_{ip\_m}|$, where *m* is the count of the sub-tiers in load pocket *i*. Supposing a reactive perturbation (such as switching of shunt capacitor bank) is applied on bus *k* in tier *j* ($1 \leq j \leq n-1$) to counteract the impact of the contingency, the voltage change on bus k will be attenuated to bus k_1 in tier *j+1*, and propagate to bus *i* (the bus with the largest voltage drop because of contingency) through minimum *j* tiers. If the reactive perturbation is applied on bus k_1 in tier *j+1*, the voltage change on bus k_1 will

first be attenuated by passing to bus *k*. Starting from bus *k*, the reactive perturbation will propagate to bus *i* through a minimum of *j* tiers. Therefore, the reactive control performed on tier *j* is more effective than the reactive control performed on tier *j+1* ($1 \le j \le n-1$).

In conclusion, in the tier-wise structured network corresponding to a contingency, the voltage changes will be attenuated in the direction from a lower-ranking tier to a higher-ranking tier and amplified in the sub-tiers of a load pocket. In order to counteract the impact of the contingency, remedial voltage controls should first be considered in the lower-ranking tiers.

Based on the above conclusion, a system decomposition procedure can be designed. The basic idea is to identify the buses with voltage constraint violations and pronounced voltage drops and terminate the interface of these buses to the external system.

6.2.2.2 Identification of the disturbance-affected zones

According to the analysis performed in 6.2.2.1, the propagation of a local reactive disturbance (such as a N-1 contingency) will propagate tier-wise from a lower ranking tier to a higher ranking tier, and amplified in the sub-tiers of a load pocket. The reactive controls performed in the lower ranking tiers are more effective in mitigating the voltage constraint violations caused by the contingency event. Therefore, for the buses with higher tier ranking, the impact of the contingency on their voltages could have been greatly attenuated and the voltage controls performed there will provide limited mitigation of the voltage constraint violations.

Under post-contingency condition, starting from the buses with pronounced voltage changes (or voltage constraint violations), if the voltage change on a lower tier bus does not decrease by a threshold factor (such as positive real ε), then the lower tier bus should be considered as a disturbance-affected bus. A set of the disturbance affected buses forms the disturbance-affected zone. In order to represent the participation of the external network to the disturbance-affected zone, the interface needs to be designed in such a way that the propagation of the disturbance and the control perturbation within the disturbance-affected zone follows a similar pattern.

Assuming bus *j* is on the boundary of the disturbance-affected zone, bus *i* is adjacent to bus *j* in the disturbance-affected zone, while bus *k* is adjacent to bus *j* but outside the disturbance-affected zone. The reactive disturbance equation can be written as:

$$h_{jj}\Delta x_j + h_{ij}\Delta x_i + h_{kj}\Delta x_k = 0 \tag{6-19}$$

where $h_{jj} = -2Q_j - c_{kj}g_{kj} - c_{ij}g_{ij}$, $h_{kj} = c_{kj}g_{kj}$, $h_{ij} = c_{ij}g_{ij}$

Since bus *k* is outside the disturbance-affected zone, $|\Delta x_k|$ is less than $|\Delta x_j|$. A suitable interface model should not only represent the import/export power through the interface, but also the reasonable impact from the external network on the propagation of the voltage changes within the disturbance-affected zone. PQ and PV models are commonly applied as network equivalents with different approximation assumptions of either constant import/export or constant voltage. A PQ model could be directly connected to the boundary bus j to represent the import/export from bus j to the external network. A PV model may or may not be placed on bus j depending of the attenuation of the voltage changes on bus j. Combining the features of PQ and PV models as well as the

assumption of fixed voltage attenuation on bus k, a voltage controlled interface model (VC model) is presented. The PQ, PV and VC models are shown in Figure 46.

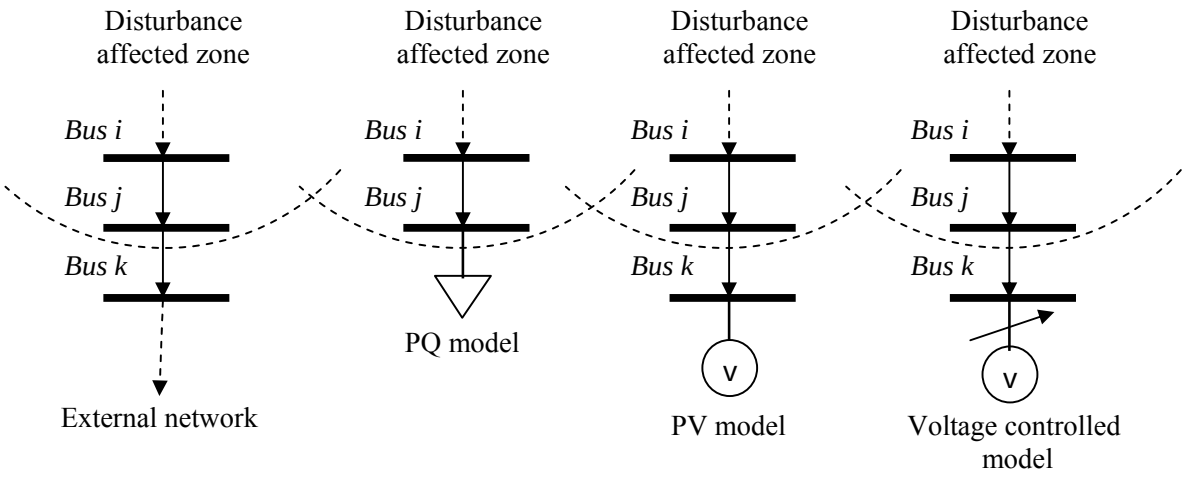

Figure 46. Design of the interface models to represent the external network.

The common feature of the PQ, PV and VC models is the assumption of fixed active power import/export. This assumption is valid since the active and reactive power flows can be decoupled, and the impact of reactive controls on real power flow is non-significant. By adopting an interface model on either bus j or k, the network equation (6-19) will change and therefore affect the voltage changes on the other buses in the disturbance-affected zone. The following analysis will define the applicable range of the PQ, PV and VC models based on their impacts on the disturbance network equations.

(1) PQ model on bus *j*

By assuming the active and reactive power flow from bus *j* to *k* as a PQ load, (6-19) can be transformed to (6-20):

$$h'_{jj}\Delta x_j + h_{ij}\Delta x_i = 0 \tag{6-20}$$

where $h'_{jj} = -2Q'_j - c_{ij}g_{ij} = h_{jj} + 2(B_{jk} + B_{jks})g_{jj} - c_{jk}g_{jk}$, $h_{ij} = c_{ij}g_{ij}$,

Equation (6-20) can be further expanded to (6-21).

$$[h_{jj} + 2(B_{jk} + B_{jks})g_{jj} - B_{jk}g_{jk}\cos\theta_{jk}]\Delta x_j + h_{ij}\Delta x_i = 0 \tag{6-21}$$

Deducting (6-19) from (6-21), (6-22) can be obtained:

$$\frac{\Delta x_k}{\Delta x_j} = \frac{2(B_{jk} + B_{jks})g_{jj} - B_{jk}g_{jk}\cos\theta_{jk}}{B_{jk}g_{jk}\cos\theta_{jk}} > 1 + \frac{2B_{jks}}{B_{jk}}g_{jj} \approx 1 \tag{6-22}$$

Since $|B_{jks}|$ is numerically much smaller than $|B_{jk}|$, the ratio $\frac{\Delta x_k}{\Delta x_j}$ needs to be close to unity for a PQ model to be applicable.

(2) PV model on bus *k*

Bus k can be considered as a PV bus. The voltage set-point of bus k is the post-contingency voltage magnitude on bus *k*. The active power output from bus k is the active power flow from bus k to *j*. The network equation following the PV model on bus *k* is formulated in (6-23).

$$h_{jj}\Delta x_j + h_{ij}\Delta x_i = 0 \tag{6-23}$$

where $h_{jj} = -2Q_j - c_{ij}g_{ij} - c_{kj}g_{kj}$, $h_{ij} = c_{ij}g_{ij}$. The validation condition for adopting a PV model is $|\Delta x_k| \approx 0$, or $\frac{|\Delta x_j|}{|\Delta x_k|} >> 1$. By ignoring the impact of Δx_k term, the ratio $\frac{\Delta x_i}{\Delta x_j}$

will be increased to $\frac{h_{jj}}{-h_{ij}}$, which implies faster disturbance attenuation from bus *i* to *j*. Therefore, in order to achieve the same amount of voltage change on bus *i*, more reactive controls would be needed on the buses other than bus *j* in the disturbance-affected zone. Since more reactive controls usually lead to more stability margin, the PV model would be useful to evaluate controls on the buses other than bus *i*. However, for the reactive control on bus *j*, (6-23) will still be valid, which dictates amplified voltage change on bus *i*. In summary, adopting a PV model on bus k could lead to conservative evaluation of the reactive controls in the disturbance-affected zone, given that $\frac{|\Delta x_j|}{|\Delta x_k|} >> 1$ and no control device on bus *j*.

(3) Voltage Controlled (VC) model

The common drawback of the PQ and PV models lies in the cancelation of the Δx_k term in (6-19). Instead of ignoring Δx_k (by using a PV model) or exaggerating Δx_k (by using a PQ model), the VC model assumes a near constant $\frac{\Delta x_k}{\Delta x_j}$ to preserve the impact of Δx_k on the propagation of reactive disturbance. The disturbance network equation for the VC model on bus *k* can be formulated in (6-24):

$$h_{jj}\Delta x_j + h_{ij}\Delta x_i + r_{kj}h_{kj}\Delta x_j = 0 \tag{6-24}$$

where $h_{jj} = -2Q_j - c_{kj}g_{kj} - c_{ij}g_{ij}$, $h_{kj} = c_{kj}g_{kj}$, $h_{ij} = c_{ij}g_{ij}$, $r_{kj} = \frac{\Delta x_k}{\Delta x_j}$.

The reactive controls on an arbitrary bus *m* in the disturbance-affected zone will only cause a small change in h_{mm}, since B_{ms} is usually much less than $-B_{mn}$ ($n \in M(m)$ and $M(m)$ is the set of buses connecting bus *m*). The ratio $\frac{\Delta x_m}{\Delta x_n}$ can be assumed to be nearly constant regardless of the reactive controls on bus *m*. Therefore, following the same assumption, r_{kj} in (6-24) can be assumed as a variant in the close vicinity of the $\frac{\Delta x_k}{\Delta x_j}\Big|_{Pre}$ calculated before the application of voltage and stability controls. The following inequality constraint represents the VC model in control formulation. A small positive value ε (in the range of 0~0.2) is adopted to limit the variation of r_{kj}.

$$\left| r_{kj} - \frac{\Delta x_k}{\Delta x_j}\Big|_{Pre} \right| \le \varepsilon$$

By adopting a VC model on bus k, the propagation pattern of the reactive disturbance within the disturbance-affected zone is preserved. The VC model can be adopted under the situation when both the PQ and PV models are inapplicable. With suitable interface models installed on the boundary of the disturbance-affected zone, a self-sustained control subsystem is constructed. The procedure of system decomposition can be done as follows:

1) Construct an internal zone to enclose all the buses with voltage constraint violations.

2) Identify the buses neighboring to the disturbance center zone with the voltage drops higher than ε times of the highest voltage drop in the internal zone (for example $\varepsilon = 30\%$). Expand the internal model to enclose all the buses identified so far.

3) For any bus j on the boundary of the internal zone and its external adjacent bus *k*:

a. If $\left|\frac{\Delta x_k}{\Delta x_j}\right| \approx 1$ (for example $1 < \left|\frac{\Delta x_k}{\Delta x_j}\right| < 1.25$), a PQ model can be installed on bus *j* to represent the external network including bus *k*. The size of the PQ model is equal to the active and reactive power flow from bus *j* to bus *k* under post-contingency condition.

b. If $|\Delta x_j|$ is much greater than $|\Delta x_k|$ (for example $\frac{|\Delta x_j|}{|\Delta x_k|} > 1.5$) and therefore no control device on bus *j*, a PV model can be installed on bus *k*. The voltage set-point of bus *k* is the post-contingency voltage magnitude on bus *k*. The active power output from bus k is the post-contingency active power flow from bus k to *j*.

c. If both PQ and PV models are unsuitable, a VC model can be installed on bus k. The ratio r_{kj} can calculated by monitoring Δx_k and Δx_j.

The proposed system decomposition method can also be applied to identify the control subsystem following slow load disturbances. The voltage changes during slow load disturbances can be evaluated by comparing the voltage monitoring data measured in short time intervals.

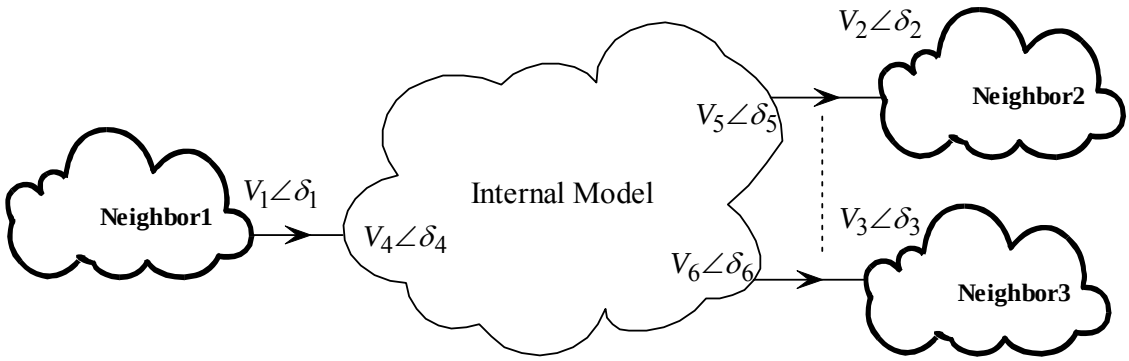

Figure 47. A disturbance-affected zone and the neighboring subsystems.

In **Figure 48**, an internal model connecting external networks is shown. The internal model is identified by monitoring the voltage drops on the buses neighboring to the buses violating voltage constraints. It can be assumed that the following conditions hold at the interfaces to three external networks:

$$(1)\ \frac{\Delta V_4}{\Delta V_1} > 1.5\,;\ (2)\ 1 < \frac{\Delta V_5}{\Delta V_2} < 1.25\,;\ (3)\ 1.25 < \frac{\Delta V_6}{\Delta V_3} < 1.5$$

According to the system decomposition procedure, a PV model can be adopted to represent Neighbor 1; while a PQ and VC model can be adopted to represent Neighbors 2 and 3, respectively. Therefore, an independent subsystem model containing all the disturbance affected buses can be obtained as shown in **Figure 48**.

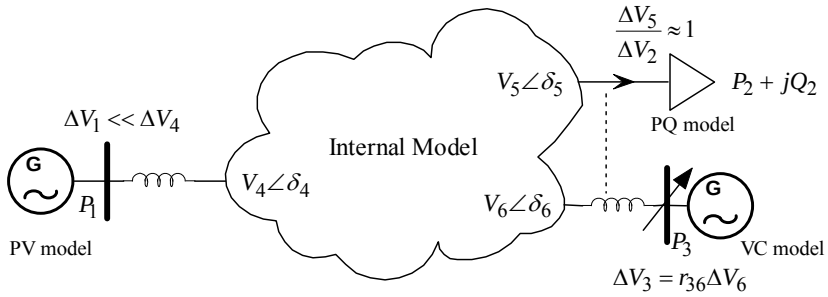

Figure 48. Use of equivalent models to represent the external networks.

Given the monitoring results of $V_n \angle \delta_n$ ($n = 1,2,\cdots,6$), the parameters of the equivalent models can be calculated as follows:

$$P_1 = V_1 V_4 (G_{14} \cos \delta_{14} + B_{14} \sin \delta_{14}) \tag{6-25}$$

$$P_2 = V_2 V_5 (G_{52} \cos \delta_{52} + B_{52} \sin \delta_{52})$$

$$P_3 = V_3 V_6 (G_{36} \cos \delta_{36} + B_{36} \sin \delta_{36})$$

$$Q_2 = V_2 V_5 (G_{52} \sin \delta_{52} - B_{52} \cos \delta_{52})$$

where G_{ij} and B_{ij} are the series conductance and capacitance of the transmission line between bus *i* and *j*, respectively.

The stability and control analysis can be performed on this independent subsystem model. Local stability monitoring and optimal controls can be conveniently performed without collecting the system-wide information.

Considering the example given in section 5.2, the three-objective optimal capacitor bank control problem can be solved by using the decentralized secondary voltage and stability control approach. By following the system decomposition procedure introduced in this section, an independent control subsystem can be constructed in Figure 49. The capacitor bank control problem can be formulated based on this fictitious subsystem. A set of Pareto solutions can be obtained by applying the normal constraint method introduced in section 5.3. The achieved objectives corresponding to the Pareto solutions (from the decentralized control and previously solved centralized control) are compared in Figure 50. The Pareto front obtained by the decentralized control solutions matches with the lower part of the Pareto front obtained by the centralized control solutions,

except for a small amount of discrepancy in minimizing the active power losses. The decentralized control only minimizes the active losses in the control subsystem. However, the impact of the secondary voltage controls on active power losses is less significant on reactive power losses. Therefore, the discrepancies in minimized active power losses corresponding to centralized control solutions and decentralized control solutions are very small (around 0.5 MW for the given example).

The decentralized control is limited to using the available local control resources, and therefore not able to provide as thoroughly control choices as the centralized control does. The advantages of the decentralized control approach lie in the short control time which enables the coordination of the secondary voltage control devices to achieve different control objectives.

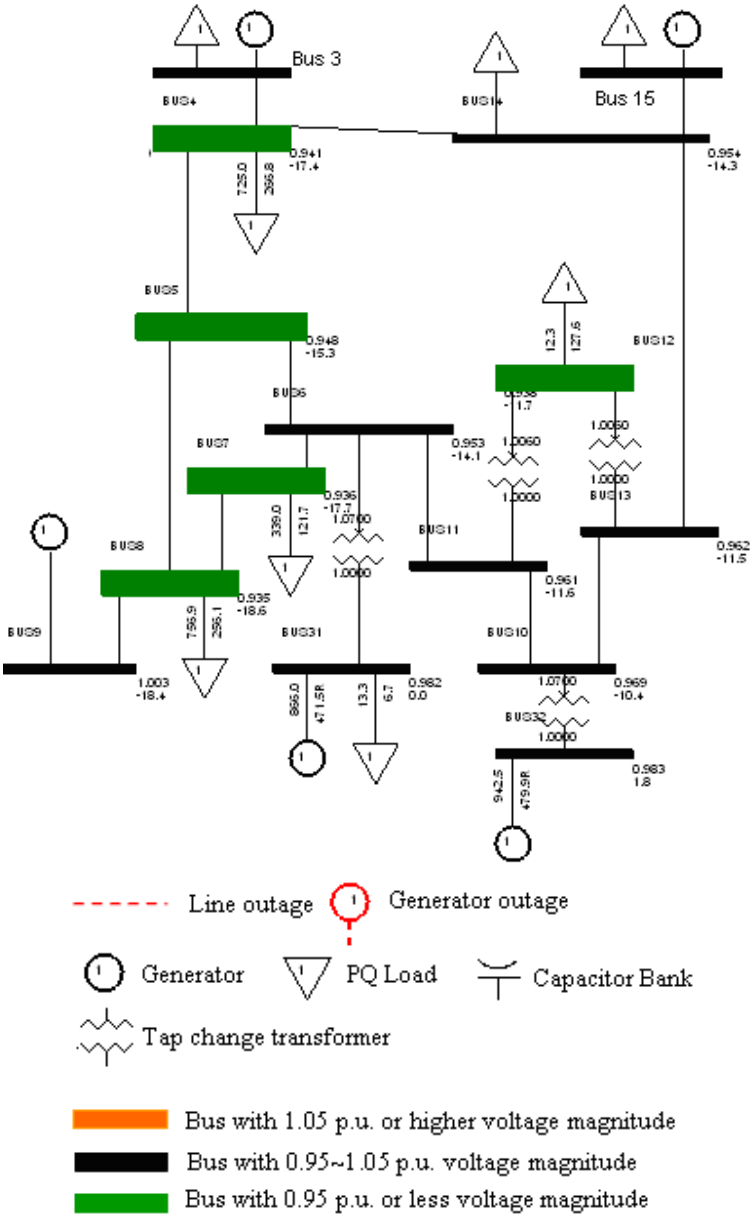

Figure 49. An independent control subsystem for decentralized voltage control.

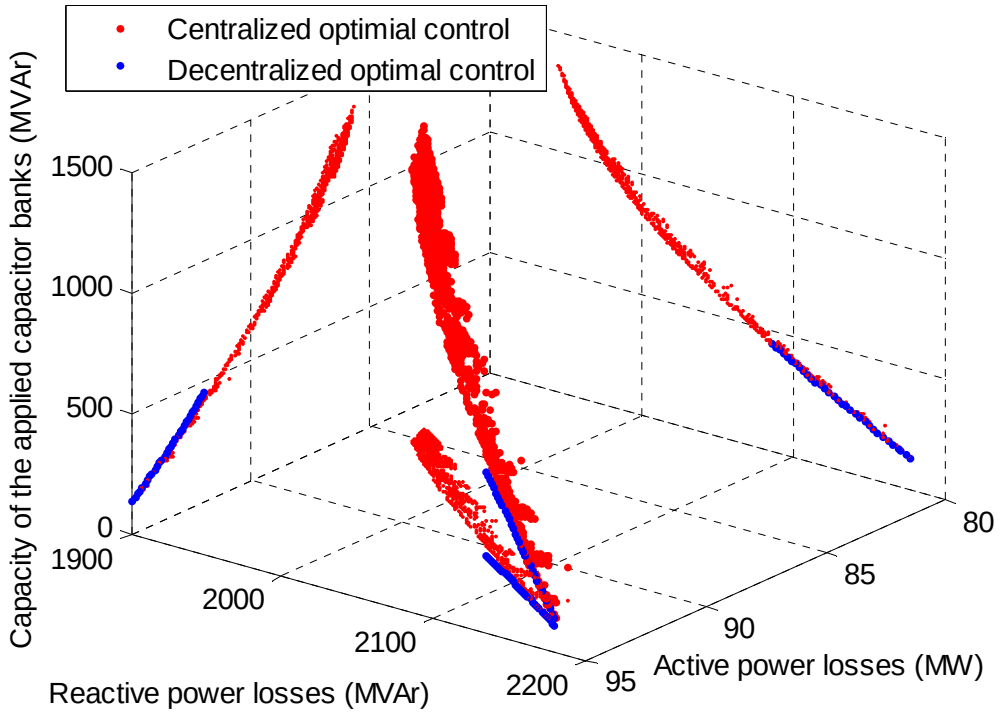

Figure 50. Comparison of the Pareto solutions obtained by solving the system wide secondary control and the decentralized secondary control problems.

6.2.3 Impact of line series impedance on the disturbance-affected zone

Besides relying on voltage controls to maintain power flow equilibrium, the control of series line impedances is an effective way to alter the pattern of power flows. Since the current flow in a line depends on the line impedance, the power flow in the line can be increased/decreased by inserting a series capacitor/inductor. Flexible AC transmission systems (FACTs), such as thyristor-switched series capacitor (TSSC), thyristor-controlled series capacitor (TCSC) or static series synchronous sompensation (SSSC), are the typical control devices adopted by utilities in critical transmission corridors. However, the applications FACTs devices are limited by their high cost, low reliability and complex customization. Divan et al. [70] presented the concept of Distributed

FACTS (D-FACTS), not only reserving the dynamic control capability of the FACTs devices, but also improving reliability and reducing cost because of the distributed structure. Distributed series impedance (DSI), is part of the so called distributed FACTS devices (D-FACTS). Like the Thyristor controlled series compensator (TCSC), it modulates the series line impedance, adding reactive or capacitive impedance depending on the applied control. A schematic diagram of the device is shown in Figure 51, [71]. S_M is an electromechanical switch which is normally closed, thereby bypassing the transformer. When it is open, switching on switch S_1 allows a reactive reactance X_M+X_L to be injected in series with the line, while switching on S_2 injects a capacitive reactance X_M-X_C. A distributed series reactance (DSR) only has the series reactance with the switched series capacitor being excluded. A distributed static series compensator (DSSC) on the other hand includes both series reactance and capacitance. Since the devices are small, a high level of compensation can be achieved by connecting several devices in series. The total effective impedance injected into the line would be as in **Figure 52**, [72], where N is the total number of devices switched. Control of the devices can be coordinated by designing an appropriate communication link among them and central operation point. Alternatively, the devices could be designed to work autonomously [70].

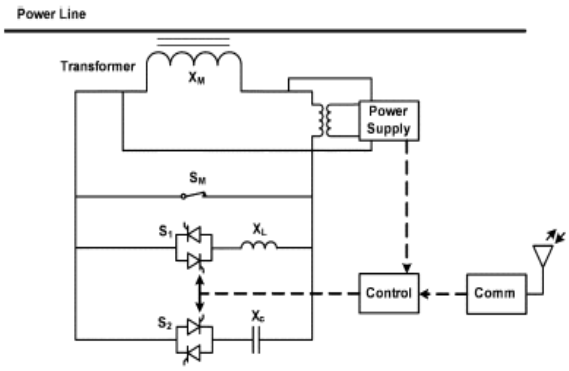

Figure 51. Circuit schematic of a DSI [71].

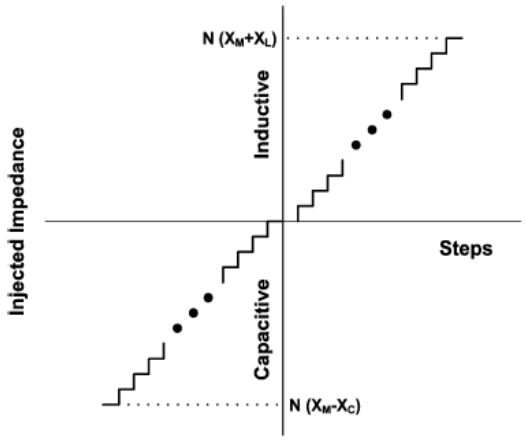

Figure 52. Profile of line impedance as modules are switched [72].

The automatic controls of line impedance from the FACTs devices aim at regulating line flows to improve reliability or line utilization. The impact of the changes in the line impedances on the voltage and stability controls needs to be considered.

(1) The impact of the D-FACTS on stability margin (considering line contingencies).

In a meshed network, changing the line impedances of alternative transmission paths will help release the unused transmission capacity. However, under contingency conditions, the loss of one transmission path may cause overload of the other alternative paths. If the FACTs devices react to increase the impedance of the overloaded transmission paths, the transmission losses will increase, causing deductions in stability margin. On the contrary, if the impedances of the lines in the vicinity of the location of the contingency defining disturbance could be decreased, voltage stability margin would increase.

In the IEEE-39 bus system shown in Figure 53, the power injection at bus 35 and 36 are dispatched through lines 23~24 and 21~22. The loss of line 21~22 would greatly

increase the current and power flow in line 22~23, 23~24 and 16~24, causing 31.6% or 1945.4MW drop in stability margin. Assuming that a FACTs device installed in line 23~24 detects the increase in current and reacts to increase the line impedance by 10% in an attempt to reduce line flow, the stability margin will drop by 34.9% or 2146.5MW because of the increased line losses. On the contrary, if the impedance of line 23~24 could be decreased by 10%, the, the drop in stability margin will decrease to 27.9% or 1719.7MW because of the decrease in losses. Decreasing the impedances of line 22~23, 23~24 and 16~24 by 10% leads to 27.1% or 1668.0MW post-contingency stability margin. Therefore, by changing the impedances of the lines in the vicinity of a contingency, the impact of the contingency on voltage stability could be decreased.

Since heavy loading (and overloads) in a line are usually associated with deep voltage drops on the nearby buses, the disturbance-affected control subsystem should include the overloaded lines. The controls of the DSIs on the overloaded lines, with proper control logic and coordination with other voltage control devices, could be an effective resource to increase stability margin. The design of the control logic for DSIs is out of the scope of this dissertation.

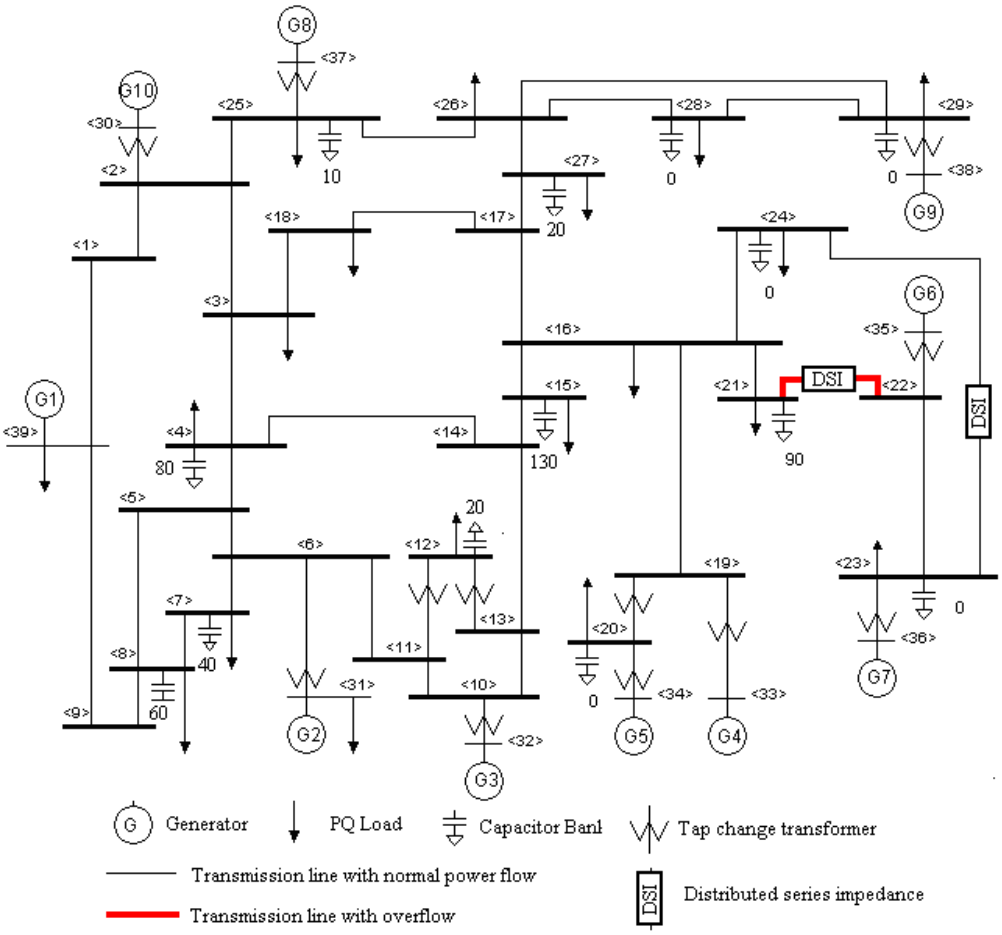

Figure 53. The IEEE 39-bus system installed with DSIs to reduce overflow in line 21~22.

(2) Use the D-FACTS to increase stability margin by solving line-flow constraints

Without considering line contingencies, increasing the impedance of an overloaded line would shift a portion of the line flows to the alternative paths, thereby avoiding the tripping of the overloaded line. By bypassing line-switching controls, the integrity of the network can be maintained. The increased stability margin, obtained by avoiding line-switching controls, could be larger enough to lower the utilization of other voltage stability controls.

In the IEEE-39 bus system shown in Figure 53, if the system load is gradually increased until the proximity to voltage instability is reached (165% loading factor), the

apparent power flow in 21~22 is 1025 MVA with 0.974 lagging power factor in the reverse direction. Assuming the instantaneous load-dump rating for line 21~22 is 1000 MVA, line 21~22 will be tripped by the protection relay to avoid overloading the line conductor. The critical loading factor for the 39-bus system without line 21~22 is 142%, which is less than the current system load. Assuming DSIs are installed on line 21~22 with the capability of increasing the line impedance up to 20%, the impact of the controls by the DSIs on stability margin are shown in Figure 54.

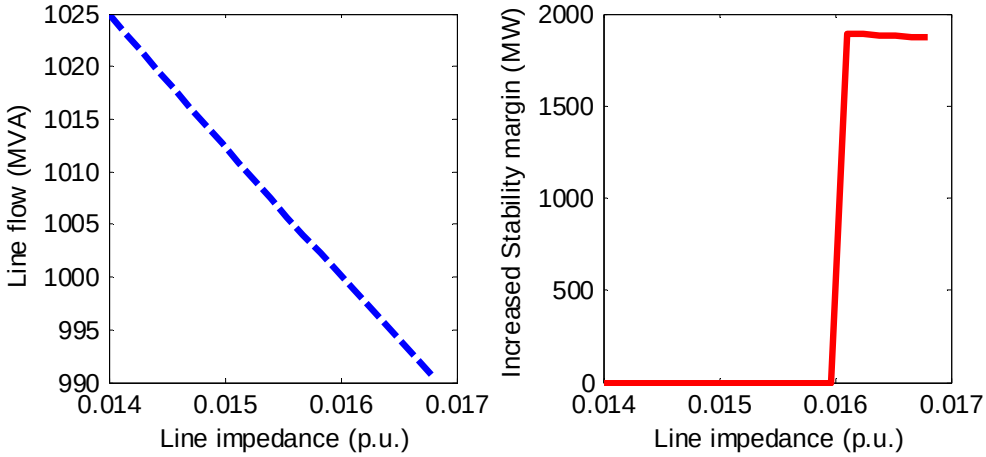

Figure 54. Use DSIs on line 21~22 to reduce line flow and increase stability margin.

At 165% loading level, the DSIs in line 21~22 kicks in because the line flow in 21~22 (1025 MVA) is higher that the instantaneous load-dump rating (1000 MVA). Assuming that the DSIs installed in branch 21~22 operate in 1% steps (increasing the line impedance by 1% at a time), the apparent power flow in line 21~22 will be reduced below 1000 MVA when the impedance of line 21~22 is increase by 14.3% (or from 0.014 p.u. to 0.016 p.u.). After the automatic controls of the DSIs, the tripping of line 21~22 is unnecessary. The remaining stability with line 21~22 in service is 541.2 MW. However, if line 21~22 were not equipped with DSIs, the tripping of line 21~22 would be conducted by protection relays due to the high line flow. The critical loading factor

after the contingency in line 21~22 would be only 142%, or 1774 MW less than the case when the DSIs are deployed. Increasing the line impedance above 0.016 p.u. will further reduce the apparent power flow in line 21~22, while slightly reducing the stability margin because of the increased reactive losses.

(3) The impact of the D-FACTS on choosing boundary models for the decentralized control subsystem

The selection of boundary equivalent models for the disturbance affected control subsystem depends on the ratio of voltage changes between the boundary bus and the immediate connected external bus caused by the detected contingency. The changing of line impedances between boundary buses and their adjacent external bus could improve the benefits obtained from the adopted boundary models. By increasing the impedance of a line, a voltage drop across the line will increase, and therefore increase the voltage difference between the two terminal buses of the line. The amplified voltage difference suggests the adoption of a PV model on the boundary of the control subsystem. By decreasing the impedance of a line, the voltage difference between the two terminal buses will decrease, which would favor the adoption of a PQ model on the boundary of the control subsystem.

Assuming the contingency in line 21~22 occurs at 140% of system base loading level, the voltage magnitude on bus 21 drops by 0.0813 p.u. The buses with more than 30% of the voltage drop on bus 21 include, bus 4 (0.028 p.u.), bus 14 (0.0317 p.u.), bus 17 (0.05 p.u.), and bus 26 (0.0268 p.u.). The buses with voltage violations (buses with voltage magnitudes in the range from 0.92 p.u to 0.95 p.u.) include bus 15, 16, 21, 24. PV equivalent models are adopted on bus 13 and 19 because of pronounced attenuation of

voltage drops from bus 14 to 13, and 16 to 19. PQ models are applied to represent bus 3 and bus 18, because of the close-to-unity attenuation ratio of the voltage drops from bus 3 to 4, and bus 17 to bus 18. VC models are applied on bus 5 and 26, because of the considerable attenuation of voltage drops from bus 4 to 5 and 27 to 26, as well as the installed shunt capacitor banks on bus 4.

The impact of the following FACTs control options on the boundary models as well as the stability margin is studied.

(1) Increase the impedance of line 23~24 by 10%;

(2) Decrease the impedance of line 23~24 by 10%;

(3) Decrease the impedance of line 23~24, 22~23, 16~24 by 10%;

(4) Decrease the impedance of line 23~24, 22~23, 16~24 by 10%; increase the impedance of line 13~14 by 10%; decrease the impedance of line 3~4 and 17~18 by 10%.

(5) Decrease the impedance of line 23~24, 22~23, 16~24 by 10%; increase the impedance of line 13~14 by 30%; decrease the impedance of line 3~4 and 17~18 by 30%.

The impact of FACTs control options on losses, stability margin and boundary models are compared in Table 12. The accuracy of the boundary models can be measured by the ratio of the voltage changes between the boundary bus and the adjacent external bus. A larger ratio for a PV model and a lower ratio close to “1” for a PQ model are desired for these models to more accurately represent the external network.

Table 12. The impact of FACTs control options on losses, stability margin and boundary models.

FACTs control options	Reactive losses (MVAr)	Active Power Losses (MW)	Remaining Stability Margin	$\frac{\Delta x_3}{\Delta x_4}$	$\frac{\Delta x_{14}}{\Delta x_{13}}$	$\frac{\Delta x_{17}}{\Delta x_{18}}$
Base case (no control)	2759.8	131.5	2.1%	1.135	1.366	1.157
1	n/a	n/a	Collapse	n/a	n/a	n/a
2	2637.6	128.9	5.7%	1.132	1.362	1.156
3	2615.2	128.4	6.6%	1.135	1.360	1.156
4	2616.8	128.4	6.6%	1.125	1.398	1.141
5	2619.5	128.4	6.4%	1.109	1.445	1.115

Reducing the impedances of the lines with pronounced high line flows in the control subsystem will reduce losses, and therefore increase the stability margin. The impact of control options 1~3 has negligible impact on the boundary models. Changing the impedance of the lines feeding the boundary models can improve the accuracy of the boundary models in representing the external network; while insignificantly affect the system-wide losses and stability margin. The design and coordination of FACTs with other voltage control devices is not covered in this dissertation.

The potential of integrating FACTs and secondary voltage control devices into a comprehensive and adaptive control system is promising. Because the controls of line impedances will change the pattern of power flow, the existing contracts of transmission services could be affected. A voltage-stability control with similar impact on transmission services is the transmission load relief (TLR). The adoption of TLR is usually considered after the exhaustion of available secondary voltage controls.

6.3 USE DECENTRALIZED VOLTAGE AND STABILITY CONTROLS TO SOLVE VOLTAGE CONSTRAINT VIOLATIONS AND REDUCE TRANSMISSION LOSSES

Based on the snapshot of the 39-bus system with 160% loading level shown in Figure 37, decentralized secondary voltage and stability controls will be evaluated in this section. The control variables include the LTC tap positions and the capacity of the switch shunt capacitor banks. The control objectives include (minimum active and reactive losses, minimum controls of shunt capacitor banks and LTCs):

$$\text{Minimize: } Q_{Loss} = \sum_{k=1}^{N_L}[-b_k V_{k,s}^2 \tau_k^2 - 2b_k V_{k,s} V_{k,r} \tau_k \cos(\theta_k) - b_k V_{k,r}^2];$$

$$\text{Minimize: } P_{Loss} = \sum_{k=1}^{N_L}[g_k V_{k,s}^2 \tau_k^2 - 2g_k V_{k,s} V_{k,r} \tau_k \cos(\theta_k) + g_k V_{k,r}^2];$$

$$\text{Minimize: } \sum_{k=1}^{N_C} \frac{\left| b_k^{Post} - b_k^{\Pr e} \right|}{B_k}; \text{ Minimize: } \sum_{k=1}^{N_L} \left| \tau_k^{Post} - \tau_k^{\Pr e} \right|;$$

Both equality and inequality constraints introduced in section 5.2.1 and 5.2.2 are now considered. The post-control voltages on all the buses should be maintained within their specified ranges. The limits of reactive power outputs from the generators are considered. The maximum allowable shunt susceptance on each bus is the total allocated capacity of the capacitor banks on the same bus. The initial allocation of the capacitor banks is performed using security-constrained OPF in order to pursue the reduction in active power losses and improvement in voltage profile.

The initial conditions of the overload 39-bus system are summarized as follows:

Buses with voltage violation: Bus 4, 5, 7, 8, 12;

Active power losses: 115.40 MW;

Reactive power losses: 2666.8 MVAr

Although the formats of secondary voltage controls vary between utilities and even between different zones of the same utility, their control philosophy can be summarized and emulated to the extent of providing useful benchmarks to validate the proposed decentralized secondary voltage and stability control.

1) Utility control practice 1

Philosophy of the secondary voltage control: rely on the automatic controls of LTCs and switched locally controlled shunt capacitor banks. If voltage violations still persist on certain buses after the automatic controls, the manual controls of the capacitor banks on the buses close to the faulted buses will be activated.

Using PSS/E power flow routine with automatic adjustment on Tap positions and switched shunt, the post-control system conditions are summarized as follows:

Active power loss: 114.9 MW.

Reactive power loss: 2633.6 MVAr.

Tap controls: Branch 11~12: change from 1.006 to 1.0481 p.u., totally 0.0421 p.u.

Capacitor bank controls (MVAr): Bus 4: add 20 MVAr,

Bus 7: add 30 MVAr,

Bus 8: add 40 MVAr, totally 90 MVAr.

Estimated time spent on automatic controls are in the range of 3~5 minutes.

2) Utility control practice 2

Philosophy of the secondary voltage control: coordinate the controls of the LTCs and the shunt capacitor banks to achieve minimum control actions. The capacitor banks which are beneficial to transfer capability and reliability should be kept in service.

In order to avoid redundant secondary voltage controls, the LTC and capacitor banks at the vicinity of the buses with voltage violations are controlled coordinately according to either the experience of the operator or the pre-defined control manual. Under ideal conditions, without considering possible incompatibility of the human decisions or the control manual to the actual system condition, the following control actions will correct all the voltage violations with a minimum amount of control resource.

Post-control active power loss: 114.8 MW;

Post-control reactive power loss: 2650.7 MVAr;

Tap controls: Branch 11~12: change from 1.006 to 1.0271 p.u.,

Branch 6~31: change from 1.07 to 1.10 p.u., totally 0.0511 p.u.

Capacitor bank controls (MVAr): Bus 7: add 10 MVAr,

Bus 8: add 20 MVAr, totally 30 MVAr.

Estimated time frame: According to the PJM transmission operation manual book, a maximum of 15 minutes delay is allowed for normal low voltage conditions (<0.95 p.u.), and 5 minutes for emergency low voltage conditions (<0.92 p.u.). Normal low voltage conditions are observed on the buses with voltage violations in this example.

3) Proposed decentralized control approach

Philosophy of the secondary voltage control: coordinate and minimize the controls of the LTCs and the shunt capacitor banks to achieve minimum local active and reactive power losses.

By following the system decomposition procedure introduced in section 6.2.2, an independent control subsystem can be constructed as shown in Figure 49.

Since the objectives are normalized by the normal constraint algorithm, the sum of the weight factors should be one. A greater weight factor represents higher emphasis on the corresponding objective. Different utilities may adopt different control objectives, whose priority could be represented by their weight factors. The population of the possible weight vectors (combinations of weight factors) could be large if each weight factor is finely graded between zero and one.

The control solutions and resulting objective values following several sets of weight vectors are shown in Table 13, which are all different but optimal. By increasing/decreasing a weighting factor, the optimality of the corresponding objective increases/decreases. Therefore, the system operator could conveniently translate his/her control interests into a weight vector to obtain the desired control solution. For utility with specific control objectives (such as the objective of minimum controls by PJM), a control solution similar to the conventional control solution should be provided by the proposed system within short time frame.

The estimated calculation time for evaluating each solution set is 4.24 seconds including the time spent on the normalization process.

Table 13. The decentralized voltage and stability control solutions for the 39-bus system.

Solutions Set	P Loss (MW)		Q Loss (MVAr)		Capacitor Control (MVAr)		LTC control (p.u.)	
	Weight	Obj.	Weight	Obj.	Weight	Obj.	Weight	Obj.
1	0.00	113.84	0.10	2644.2	0.80	0	0.10	0.0737
2	0.10	112.73	0.20	2611.9	0.60	70	0.10	0.0822
3	0.10	112.57	0.25	2606.5	0.55	80	0.10	0.0822
4	0.10	111.55	0.30	2575.9	0.50	150	0.10	0.0822
5	0.20	111.06	0.40	2558.6	0.20	200	0.20	0.0822
6	0.30	110.86	0.50	2544.9	0.10	270	0.10	0.0964
7	0.00	112.37	0.10	2583.0	0.10	170	0.80	0.0379
Utility 1	—	114.90	—	2633.6	—	90	—	0.0421
8	0.20	113.16	0.00	2615.2	0.40	110	0.40	0.0579
Utility 2	—	114.80	—	2650.7	—	30	—	0.0511
9	0.05	114.24	0.00	2635.6	0.65	70	0.30	0.0213

The objectives following solution set 8 is comparative to the results of utility practice 1; while the solution 9 is similar to utility practice 2. A system operator can conveniently chose a control solution which is suitable for the actual stability condition of the system or the operational goals of the utility. The proposed decentralized control approach has the advantage of providing a variety of suboptimal solutions, meeting different control objectives, while not requiring an excessive amount of time for evaluation. Decentralized control decisions are sensitive to the settings of the weight vector. By adjusting the weights on different objectives, not only can the conventional utility controls be emulated, but also more advanced controls with different objectives can be developed, such as pre- and post-contingency stability control, security-constrained voltage and stability control, and transmission loss optimization.

6.4 USE OF DECENTRALIZED VOLTAGE AND STABILITY CONTROL TO SOLVE VOLTAGE AND STABILITY CONSTRAINTS UNDER SEVERE CONTINGENCY CONDITIONS

The robustness of a power system relies on structural redundancy and security margins [73]. Traditionally, N-x contingency analysis is usually performed at both the planning and the operation stages, where "x" is the number of lost elements during the credible incidents. In order to satisfy an N-x criterion, a power system needs to remain in the range of its operational limits when any type of incidents causes the disconnection of "x" elements. Considering lower probability contingencies with *x* equals two or greater, the N-1 criterion is most commonly used to check the robustness of a power system.

When designing the infrastructure of a power system, probabilistic analysis is usually conducted to identify the contingencies with a high probability of occurrence. Defensive countermeasures and specific protection procedures are prepared to guarantee the security of the system against these contingencies. If certain credible contingencies could lead to stability concerns (such as sharp decrease in stability margin or even voltage collapse), automatic countermeasures are usually highlighted in the defense plan [36, 37, 55, 73]. However, the contingencies with lower probabilities are normally ignored during the planning stage.

During the operation of a power system, the system operator will possibly encounter more complex or even unexpected situations, especially with the presence of planned or unplanned outages and maintenances. When a stability problem emerges following a contingency incident, it is sometimes hard to be recognized by only monitoring the real-time voltage profile of the system. The classic approach to examine the N-1 criterion is to

use off-line load flows of the entire system model to check for the post-contingency voltage profiles and stability margins following each credible N-1 contingency.

Some utilities [17, 36, 37] use pre-contingency controls to raise the stability margin in anticipation of the occurrences of certain severe contingencies. The off-line contingency analysis uses the most recent state estimation results to evaluate the post-contingency system conditions following each monitored contingency. Once voltage violations (low voltages and voltage drops) are detected, non-cost voltage controls (capacitor and LTC controls) will be activated within the time frame (5~30 minutes by PJM) determined by the severity of the voltage violation.

When an actual contingency causes voltage violations, the voltage controls will be activated in the time frame (less than 15 minutes by PJM) determined by the severity of the voltage violation. Secondary voltage controls in the form of automatic adjustment or manual coordination are also used by different utilities. Severe voltage violations, such as low voltage level and big voltage drop, can be associated with stability problems. However, the correlation of the voltage violations does not guarantee sufficient improvement in the stability condition. Utilities (such as PJM, IESO, EDF) only emphasize the timing requirements of post-contingency voltage controls, but do not consider the improvement in stability conditions as a criterion to evaluate control options.

The urgency of stability controls can be illustrated by the contingency analysis performed on the 39-bus system. Based on the RRP scheme for 39-bus system presented in section 5.1, the loads in the entire 39-bus system are proportionally increased in 5% intervals starting from the base loading level, until a N-1 contingency is identified which will lead to less than 5% load margin in the post-contingency state (in line with the

WECC criterion). It has been discovered by the contingency analysis that the line contingency 21~22 will lead to 2.2% post-contingency load margin at 140% loading level, at which point appropriate voltage stability controls need to be applied immediately. With all the fixed capacitor banks switched on, the pre-contingency voltages at 140% loading level are all in normal condition (in the range of 0.95~1.05 p.u.). Figure 55 shows the post-contingency snapshot of the IEEE 39 bus system at 140% loading with all the fixed shunt capacitor banks switched on. In the post-contingency state, an emergency voltage-drop constraints are violated on four buses. The buses with post-contingency low-voltage (< 0.95 p.u.) or emergency voltage drop (> 0.05 p.u. drop) are listed in Table 14. The active power losses in pre- and post- contingency states are 84.52 MW and 131.54 MW, respectively. The reactive power losses are in pre- and post-contingency states 1926.6 MVAr and 2759.8 MVAr, respectively.

Table 14. Voltage violations for IEEE 39-bus system after the line contingency between bus 21 and bus 22 at 140% loading level.

Bus ID	Pre-Contingency V (p.u.)	Post-Contingency V (p.u.)	Voltage Drop (p.u.)
21	1.0167	***0.9354***	***0.0813***
24	1.02	***0.9407***	***0.0793***
16	1.0138	0.9505	***0.0633***
15	0.9998	***0.9446***	***0.0552***

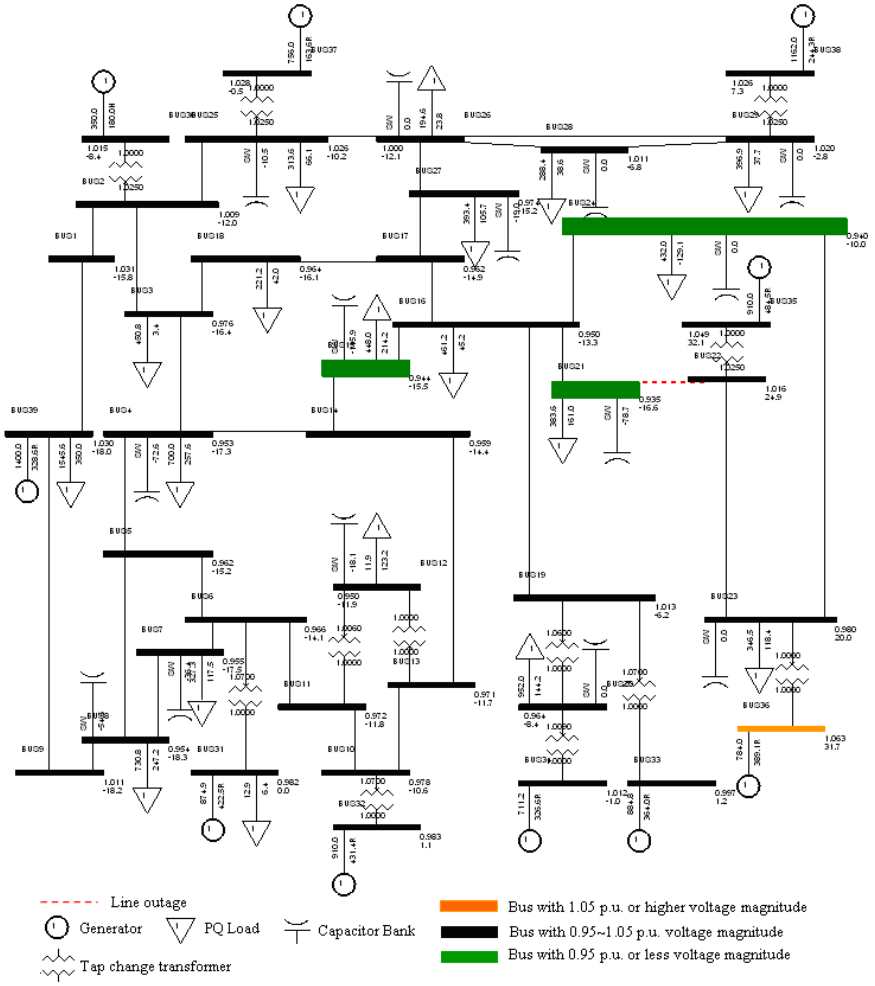

Figure 55. Snap shot of the 39-bus system following the contingency in branch 21~22.

In the following text, typical utility control practices will be reviewed. According to the control rules adopted by different utilities, the possible remedial controls for the 39-bus system example are designed. Assorted dynamic simulations will also be conducted in PSS/E to study the time-domain performance of the utility control actions.

6.4.1 Review and simulation of the utility secondary voltage controls

6.4.1.1 Type I Utility control practice: automatic LTC and shunt capacitor banks control.

Some utilities (in southeast United States, southwest China) rely on the automatic controls of LTCs and switched shunt capacitor banks to correct the voltage violations. In order to avoid control redundancy and possible conflicts between the voltage control devices, the LTCs with shorter time delays will operate first until either the voltages on the controlled buses are brought back to normal condition or the exhaustion of the available tap positions. Upon completion of the automatic LTC controls, the shunt capacitor banks on the remaining faulted buses will be switched on either under the supervision of a system operator or automatically after a time delay. The manual control of the shunt capacitor banks and LTCs at the vicinity of the faulted buses may be exercised after the exhaustion of the available control resources on the faulted buses.

In the post-contingency stage, if voltage limits are violated, the expected time to correct the voltage violation is strictly limited. For example, PJM requires a maximum of 15 minutes to exercise the possible secondary voltage controls actions (on LTCs, shunt capacitor banks, SVCs, etc.) to bring a bus under emergency low-voltage condition (usually 0.90 p.u. ~ 0.92 p.u.) to normal voltage condition (0.95 p.u. ~ 1.05 p.u.). Such control time frames will be reduced to 5 minutes if the voltage on the controlled bus is below load-dump limit (less than 0.90 p.u. by PJM). Post-contingency voltage drop is also used as an indicator to restrict the control time frame. Usually, a voltage drop of 5% or larger is considered to be a violation, which should be controlled within 15 minutes. Load shedding will be considered if the secondary voltage controls and generation re-

dispatches cannot bring the voltages on the controlled buses to normal condition within the scheduled time frame.

Dynamic simulation is performed to observe the control actions and the time frame following the automatic LTC and capacitor bank control approach. The 12 transformers in Figure 37 are all configured to be LTCs with discrete controllable tap positions in the range of 0.90 p.u. ~ 1.10 p.u. The adopted LTC model incorporates the most common type of timer, an integrator, which adds the total amount of time that the voltage is outside the preselected control band and subtracts the time it is inside the control band. When the voltage is outside more than inside by an amount greater than the time-delay setting, T_D, a tap signal will be sent to the tap changer motor. The tap changer motor operates T_C seconds later. The time constant T_D of the LTCs are set in the range from 30 to 50 seconds with slight differences between individual units so that the interaction of different LTCs can be observed. If the voltage on the controlled bus of LTC is still outside the control band following the first tap change, the next tap change will be performed after a fixed time delay T_{SD}, where $T_{SD}>T_C$. In the designed dynamic simulation, T_{SD} is set to be in the range of 10~20 seconds to shorten the total time delay caused by LTCs.

The allocation of the capacitor banks follows the same solution as shown in Table 10. The maximum block size of one capacitor bank is assumed to be 40MVAr, with four steps of 10MVAr switchable capacitors. Under low voltage (<0.95 p.u.) or large voltage drop condition (>0.05 p.u.), one block of 10 MVAr (or available capacity) capacitor bank will be switched on after a fixed time delay. Similar control models for the LTCs can be adopted to automatically control the shunt capacitor banks. However, the time constants

for the capacitor banks are longer than the LTCs'. For illustrative purposes, the time settings of the capacitor banks can be designed as: T_D = 100 seconds, T_{SD} = 50 seconds, T_C = 10~20 seconds.

Other dynamic models in the 39-bus system include 10 generators, 10 turbine governors, 10 excitation controllers, and 10 over excitation limiters. The parameters for the dynamic models are included in the Appendix II.

The time-domain changes of voltage magnitudes on the buses with pronounced voltage violations (buses 4, 12, 15, 21) are plotted in Figure 56. The adopted control actions using automatic control approach are listed in Table 15 according to ascending time sequence. The N-1 contingency in branch 21~22 are applied at 100 seconds. No LTC control is observed since the voltages on adjacent buses to the LTCs are all in the control band. The buses with voltage violations are buses 15, 21, 24. The shunt capacitor banks on these buses will be switched on in an order according to their switching time constants. The control sequence is shown in Table 15. Totally 90 MVAr of shunt capacitor banks are switched on. In post-control condition, the load margin is raised by 2%, while the active and reactive losses are 129.0 MW and 2709.0 MVAr, respectively. A summary of the post-control voltage constraints are listed in Table 16.

Table 15. Control actions following utility practice 1 for the 39-bus system example. Simulation starts at 0 s, and the contingency occurs at 100 s.

Control Event ID	Control Device	Device Location	Time Stamp (s)	Pre-control Status	Post-control Status
1	CAP	Bus 15	210.0	130 MVAr	140 MVAr
2	CAP	Bus 21	215.0	90 MVAr	100 MVAr
3	CAP	Bus 24	220.0	0 MVAr	10 MVAr
4	CAP	Bus 15	260.0	140 MVAr	150 MVAr

5	CAP	Bus 21	265.0	100 MVAr	110 MVAr
6	CAP	Bus 24	270.0	10 MVAr	20 MVAr
7	CAP	Bus 21	315.0	110 MVAr	120 MVAr
8	CAP	Bus 24	320.0	20 MVAr	30 MVAr
9	CAP	Bus 21	365.0	120 MVAr	130 MVAr

Table 16. Post-control voltage constraints following type I utility practice.

Bus ID	Pre-Contingency V (p.u.)	Pre-control V (p.u.)	Post-control V (p.u.)	Pre-control Voltage Drop (p.u.)	Post-control Voltage Drop (p.u.)
21	1.0167	***0.9354***	0.953	***0.0813***	***0.0637***
24	1.02	***0.9407***	0.9532	***0.0793***	***0.0668***
16	1.0138	0.9505	0.9622	***0.0633***	***0.0516***
15	0.9998	***0.9446***	0.9562	***0.0552***	0.0436

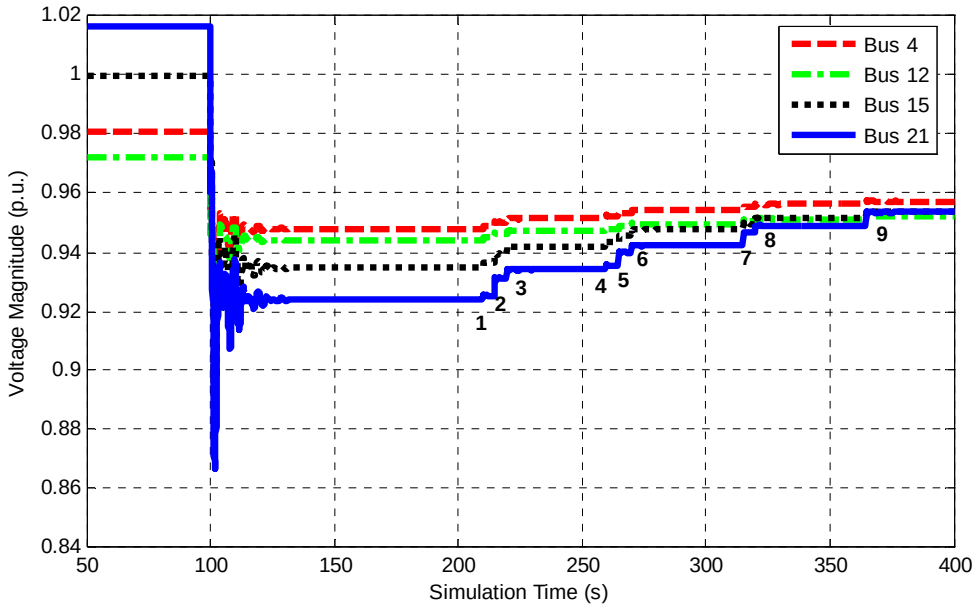

Figure 56. Time-domain voltage magnitudes on the buses with voltage violations before and after the automatic controls by LTCs and shunt capacitor banks.

With the automatic local secondary voltage controls, only low-voltage mitigation is performed. The voltage constraints in Table 16 indicate that the voltage-drop violations are very likely unsolvable through use of automatic voltage controls. Moreover, the 4% load margin in the post-control condition does not meet the 5% margin criterion.

From the simulation results, the challenges and limitations of the automatic secondary voltage controls can be summarized as follows:

(1) The automatic secondary voltage controls may not be sufficient to solve the existing voltage violations in the system. This will bring additional pressure to the system operator who must find an effective solution within a short time. Since the automatic controls have occupied a considerable amount of control resources, the system operator will face the options of whether or not to reverse some controls to allow better control solutions.

(2) Relying on voltage violations as the only indicator of stability condition is unreliable. The objective of the automatic secondary voltage controls is only to maintain desired voltage magnitudes, (not including mitigating voltage drops and stability conditions). Consequently, stability-oriented controls are postponed until the next scheduled off-line OPF and CPF analysis.

(3) The coordination of the secondary voltage controls is not considered. Consequently, the conflicts between different control devices can lead to redundant control actions and possible interlocks of the control devices.

(4) The time delays of the secondary voltage control devices constrain the capability of the automatic voltage controls under emergency conditions. If the voltage violations cannot be solved by the secondary voltage controls on time, load shedding or cancelation of transmission contract may have to be activated, which could inconvenience the load entities and create financial losses.

6.4.1.2 Type II Utility control practice: manually coordinated LTC and shunt capacitor bank control

In order to minimize the capacitor switching operation and transformer tap changes, manual coordinated controls of the LTCs and shunt capacitor banks are adopted by bulk system dispatchers (such as PJM). Local control centers need to periodically review and update their voltage control manual as a guideline to counteract possible severe voltage and stability problems. If a post-contingency simulated voltage violation indicates an emergency condition, the corresponding protection scheme from the control manual will be activated with the permission of the system dispatcher. The system dispatcher will monitor the system voltage profile and request LTC and capacitor operations in a timely manner.

In Figure 55, it can be observed that buses 15, 16, 21, 24 are experiencing either emergency low voltage (<0.92 p.u.) or voltage drop violations (>0.05 p.u.). It can be assumed that the special protection schemes related to this severe N-1 contingency have been designed by the system operator to counteract the emergency conditions on these buses in the 39-bus system.

Step 1: Starting from the most severely voltage-constrained bus, switch on four blocks of 10MVAr shunt capacitors. The switching of the shunt capacitor banks needs to be coordinated by the system dispatcher who can monitor the switching dynamics and the voltage constraints. In order to avoid redundant capacitor controls, LTC controls will be considered after 40 MVAr of shunt capacitors have been switched on each of the voltage-constrained buses.

Step 2: Increase the tap ratio in the LTC between bus 19 to 33 by 0.03 p.u. to boost the voltage support for bus 15 and bus 16. Adjust the tap ratio in the LTC between bus 22 and 35 by 0.02 p.u. to boost the voltage support for bus 21 and 24. Repeat Step 2 until either the disappearance of the voltage violations or the exhaustion of the available tap positions (tap limits are reached).

Since the voltage controls cross two control zones, the system dispatcher needs to coordinate the control actions by communicating with the two local control zones. Without considering the time delay caused by the communications, the timeline to apply the special protection scheme can be designed in Table 13. The voltage constraint violations on buses 15, 16, 21, and 24 are solved by voltage controls (as shown in Table 17). Both low-voltage and voltage-drop constraints are solved by manual controls of the system dispatcher, as shown in Table 18. The time-domain changes of voltage magnitudes on the buses with pronounced voltage violations are plotted in Figure 57.

The time delay between two adjacent control actions is optimistically assumed to be 30 seconds. Following the specified time delays, the system operator will evaluate the system condition, initiate the next control action, and communicate with local dispatchers in 30 seconds. In order to avoid a severe transient response, the tap change for any single LTC is set to be no more than 0.03 p.u. for each control action, which is in accordance to the limit on voltage drop warning adopted by PJM. The dead-band of the voltage controls is assumed to be in the range of ± 0.002 p.u. In the post-control condition, the load margin is raised by 3.2%, while the active and reactive losses are 126.4 MW and 2664.0 MVAr, respectively. The corrections of the voltage constraints are listed in Table 18.

Table 17. Control actions following utility practice 1 for the 39-bus system example. Simulation starts at 0 s, and the contingency occurs at 100 s.

Control Event ID	Control Device	Device Location	Time Stamp (s)	Pre-control Status	Post-control Status
1	CAP	Bus 21	160.000	90 MVAr	130 MVAr
2	CAP	Bus 24	190.000	0	40 MVAr
3	CAP	Bus 15	220.000	130 MVAr	170 MVAr
4	LTC	Bus 19 to 33	250.000	1.070 p.u.	1.100 p.u.
5	LTC	Bus 22 to 35	280.000	1.025 p.u.	1.045 p.u.
6	LTC	Bus 22 to 35	310.000	1.045 p.u.	1.065 p.u.

Table 18. Post-control voltage constraints following type I utility practice.

Bus ID	Pre-Contingency V (p.u.)	Pre-control V (p.u.)	Post-control V (p.u.)	Pre-control Voltage Drop (p.u.)	Post-control Voltage Drop (p.u.)
21	1.0167	***0.9354***	0.9690	***0.0813***	0.0477
24	1.02	***0.9407***	0.9694	***0.0793***	0.0506
16	1.0138	0.9505	0.9774	***0.0633***	0.0364
15	0.9998	***0.9446***	0.9711	***0.0552***	0.0287

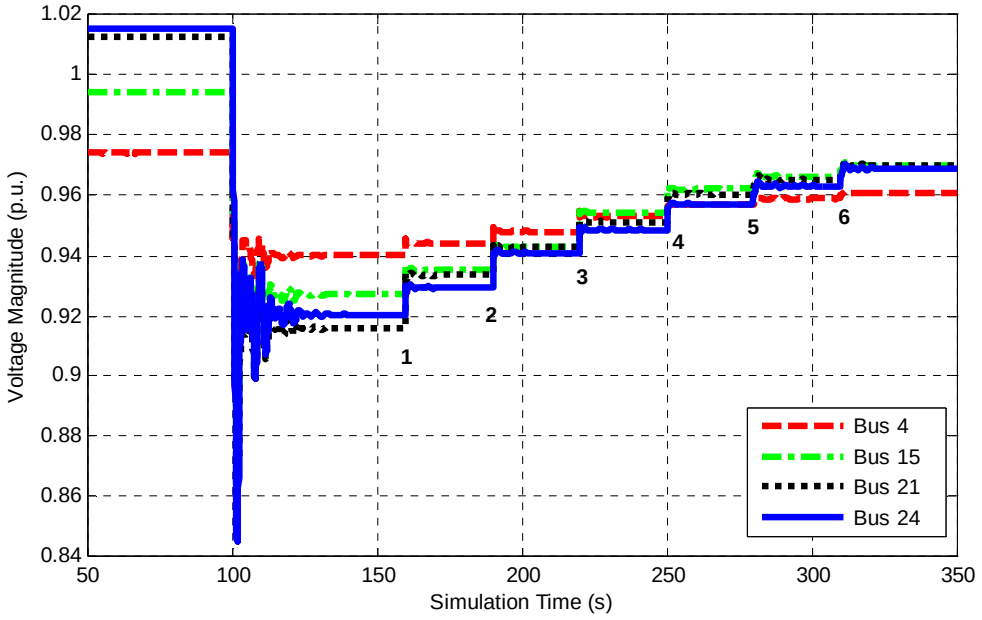

Figure 57. Time-domain voltage magnitudes on the buses with voltage violations before and after the manually coordinated control.

By performing the coordinated secondary voltage controls, both low voltage constraint violations and voltage-drop constraints are solved. The appropriate control

strategy is made by the system operator in accordance to the severities of the voltage constraint violations. The total time delay caused by the system operator making control decisions is optimistically assumed to be less than 60 seconds. During the approximately one minute time frame, the system operator is exposed to multiples challenges, because of the multiple tasks that he has to fulfill, such as evaluating voltage and stability conditions, determining control strategy, coordinating control actions, observing post-control system conditions, and communicating with local control centers. If multiple voltage violations occur at different control zones at the same time, the system operator may be overwhelmed by the amount of workload. The manual voltage controls are performed according to pre-designed protection scheme or purely human experience. It is unrealistic to design protection schemes to account for all possible circumstances. Under emergency conditions, it is very likely that a constrained contingency or disturbance is unexpected, which requires extensive human efforts to handle. The system dispatcher will face the challenges of tight control timelines, severe voltage constraint violations, limited control resources with uncertain impacts, limited information on stability margin, etc.

Finally, the system operator evaluates the system condition by the severity of the voltage violations. The control decisions aim at correcting voltage violations only. The stability margins of the system at both pre- and post-control stages are not considered by the system operator. It is implied, or rather expected, that stability problems will vanish with the mitigation of voltage constraint violations. The 39-bus example exposed the deficiency of the manual voltage controls in solving stability constraints. Despite the

correction of the voltage constraint violations on bus 15, 21 and 24, the post-control load margin is only 3.2%, which is less than the 5% desired load margin.

The weights on the control objectives can be adaptively changed with the stability condition of the post-contingency system. The proposed system can be embedded in any type of utility control systems to generate pre- and post- contingency voltage and stability control solutions. By adopting the proposed system, not only can the voltage violations caused by contingencies be corrected, but the stability condition can be monitored and improved in time without performing system-wide analysis.

6.4.2 Design the procedure for decentralized secondary voltage and stability controls under emergency conditions

Emergency low-voltage or voltage-drop conditions can be detected either in on-line by monitoring devices, or off-line by power flow analysis. Real-time voltage stability controls are performed in the time frame from 20 seconds to several minutes, depending on the control methods adopted by utilities. In order to monitor the stability constraints continuously, utilities usually rely on the real-time voltage measurements and line flows as indirect indicators to measure the voltage stability condition. Off-line periodic contingency and power flow analysis provide direct estimation of the actual load margins. When violations of voltage and stability constraints under emergency conditions are detected, immediate remedial control actions are needed because of the risk of voltage collapse. The secondary voltage control devices, despite their comparatively long time delays, are considered as a no-cost and effective way to solve emergency low voltage

constraint violations. However, since increasing voltage stability margin is not adopted as a direct control objective, the manually coordinated secondary voltage controls may be insufficient to relieve stability constraints. Moreover, both automatic and manual secondary voltage controls do not guarantee suitable time frame for stability control mitigations to be done. Consequently, more restrictive controls such as load shedding may be considered when no-cost controls do not solve the voltage constraint violations within the time limits set by the operation rules. In order to boost the capability and performance of the secondary voltage controls, two key factors need to be addressed: control time frame and control coordination. By adopting the decentralized controls, both of the two key factors could be satisfied. The control time will be shortened, because only local measurements and small-scale computation are used. The control coordination will be more efficient and flexible because a set of control objectives can be optimized to meet different control interests. Stability margin can be controlled directly through the objective of maximizing stability margin. The expected increase in stability margin can be quantified by the margin sensitivities of the available secondary voltage control devices.

During the real-time operation of a power system, severe contingencies leading to voltage and stability constraint violations can be identified by a few existing approaches, including power flow analysis for the pre-defined contingency group, monitoring of the line or interface flows associated with certain contingency events and off-line complete contingency ranking with respect to voltage stability. Parallel computations of the margin sensitivities for the secondary voltage control devices should be conducted for the

previously determined set of severe contingencies. These margin sensitivities would be used to calculate control decisions under both actual and simulated emergency conditions.

Figure 58 shows the flow chart of the decentralized voltage and stability controls under emergency conditions. System decomposition is performed first to construct the control subsystem(s). If the sum of the incremental stability margin obtained through use of all the secondary voltage control devices in the control subsystem(s) is higher than the target stability margin, decentralized secondary voltage and stability control problem(s) will be formulated to identify the suitable non-cost control solution. Otherwise, an emergency load shedding formulation will be deployed (the minimum load shedding scheme necessary to mitigate the impact of disturbances after the exhaustion of available secondary voltage controls). Normal constraint algorithm can be adopted to generate sparse Pareto solutions for each of the problem formulations. Finally, one suitable control solution from each sub-system will be selected. The synthesis of all the local control solutions will form a system-wide control decision.

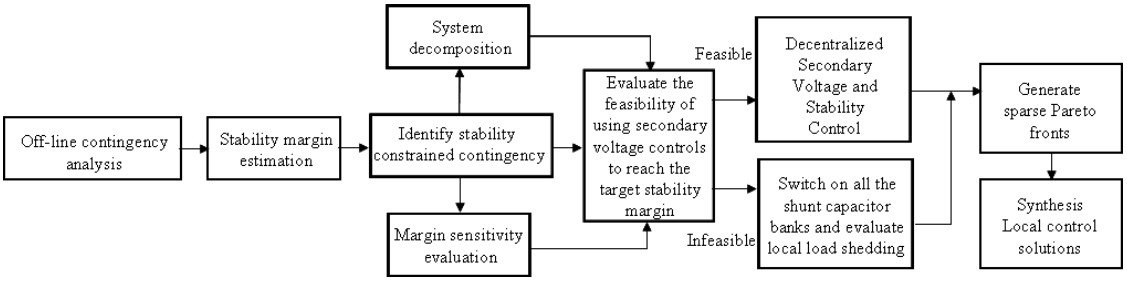

Figure 58. The flow chart of the decentralized voltage and stability controls under emergency condition.

Under emergency conditions, the formulation of the decentralized control is different from the control formulation for normal low-voltage conditions in the following ways:

(1) The objectives of minimum active and reactive power losses will be integrated as one objective to minimize MVA line consumption, considering active and reactive losses are highly correlated and not as important as the other objectives (such as maximum stability margin) during emergency conditions.

(2) The objective of maximum load margin for post-contingency state is added.

(3) The non-linear margin sensitivities of LTCs imply that stability margin could be affected by LTC controls in both positive and negative directions depending on the output limits of the nearby generators. LTCs controls may possibly aggravate stability margin by restoring voltage and load power, and therefore reduce generation reserve. Therefore, the control of LTCs needs to be blocked or restricted (by changing the relevant inequality constraints) to operate only within a narrow range under emergency conditions.

(4) The control variables and equality and inequality constraints are applied to both pre- and post-contingency states. If a constraint violation inducing contingency is actual, the control variables and equality and inequality constraints will only be evaluated under post-contingency system condition to reduce the time of control evaluation.

The objective of minimum secondary voltage controls should be replaced by the minimum load shedding objective, when the increased stability margin by the secondary voltage control devices is insufficient to meet the target stability margin under post-contingency conditions.

The problem formulation for the decentralized secondary controls under emergency condition is as follows:

Decentralized secondary voltage and stability control objective:

(1) Minimization of MVA line losses:

$$\text{Minimize } Q_{Loss} = \sum_{k \in N_C} \sum_{l \in N_{SUB}(l)} \sqrt{Q_{Loss,l}^{k}(V^{k}, \theta^{k})^{2} + P_{Loss,l}^{k}(V^{k}, \theta^{k})^{2}}$$

(2) Minimization of shunt capacitor controls:

$$\text{Minimize: } \sum_{n \in M_{SUB}(n)} \frac{\left| b_n^{Post} - b_n^{\Pr e} \right|}{B_n};$$

(3) Minimization of LTC controls:

$$\text{Minimize: } \sum_{l \in N_{SUB}(l)} \left| \tau_l^{Post} - \tau_l^{\Pr e} \right|;$$

(4) Maximization of stability margin

$$\text{Maximize } \sum_{k \in N_C} \left[\sum_{n \in M_{SUB}(n)} SC_n^{k}(b_n^{Post} - b_n^{\Pr e}) + \sum_{l \in N_{SUB}(l)} ST_n^{k}(\tau_l^{Post} - \tau_l^{\Pr e}) \right]$$

Decentralized load shedding control objective:

(1) Minimization of MVA line losses:

$$\text{Minimize } Q_{Loss} = \sum_{k \in N_C} \sum_{l \in N_{SUB}(l)} \sqrt{Q_{Loss,l}^{k}(V^{k}, \theta^{k})^{2} + P_{Loss,l}^{k}(V^{k}, \theta^{k})^{2}}$$

(2) Minimization of load shedding:

$$\text{Minimize: } \sum_{n \in M_{SUB}(n)} \left| P_{L,n}^{Post} - P_{L,n}^{Pre} \right|;$$

(3) Maximization of stability margin

$$\text{Maximize} \sum_{k \in N_C} \sum_{n \in M_{SUB}(n)} SL_n^k (P_{L,n}^{Post} - P_{L,n}^{Pre}))$$

The following constraints need to be accounted for during the optimization:

Active power injection at bus *i* in SUB following contingency k :

$$P_{SUB,G}^k(i) - P_{SUB,L}^k(i) - P_{SUB}^k(i, V^k, \theta^k) = 0$$

Reactive power flow equations for bus *i* in SUB following contingency k :

$$Q_{SUB,G}^k(i) + Q_{SUB,C}^k(i) - Q_{SUB,L}^k(i) - Q_{SUB}^k(i, V^k, \theta^k) = 0$$

Active power generation limits:

$$P_{SUB,G\min}^k(i) \le P_{SUB,G}^k(i) \le P_{SUB,G\max}^k(i)$$

Reactive power generation limits:

$$Q_{SUB,G\min}^k(i) \le Q_{SUB,G}^k(i) \le Q_{SUB,G\max}^k(i)$$

Voltage constraints:

$$V_{i,\min}^k \le V_i^k \le V_{i,\max}^k$$

Fixed voltage drop ratio from bus *n* to *m*:

$$\Delta V_m^k = r_{mn} \Delta V_n^k$$

LTC tap position ranges:

$$\tau_{l,\min} \le \tau_l^{Pre}, \tau_l^{Post} \le \tau_{l,\max}$$

The adjustable range of susceptances of shunt capacitor banks:

$$b_{n,\min} \le b_n^{Pre}, b_n^{Post} \le b_{n,\max}$$

The reactive power support from shunt capacitor banks:

$$Q^k_{SUB,C\min}(i) \le Q^k_{SUB,C}(i) \le Q^k_{SUB,C\max}(i)$$

Line flow limits:

$$\left|P^k_l\right| \le P^k_{l,max}$$

The following constraints are only applied in load shedding formulation:

Fixed LTC taps and switch on all shunt capacitor banks:

$$\tau^{Post}_l = \tau^{Pre}_l,\ b^{Post}_n = b_{n,\max}$$

The maximum portion of interruptible load on the load buses:

$$\frac{\left|P^{Post}_{L,n} - P^{Pre}_{L,n}\right|}{P^{Pre}_{L,n}} \le S_n;$$

Totally allowable amount of load shedding:

$$\sum_{n\in M_{SUB}(n)} \left|P^{Post}_{L,n} - P^{Pre}_{L,n}\right| \le \Psi_{max}$$

Notions:

$Q^k_{Loss,l}(V^k,\theta^k)$ —the reactive power losses in branch *l* following contingency *k*

N_c —the group of stability constrained contingencies

$P^k_{SUB}(i,V^k,\theta^k)$ —generator active power output on bus i for contingency *k*

$Q^k_{SUB,G}(i)$ —generator reactive power output on bus i for contingency *k*

$P^k_{SUB,L}(i)$ —load active power on bus *i*

$Q^k_{SUB,L}(i)$ —load active power on bus *i*

$P^k_{SUB}(i,V^k,\theta^k)$ —real power injection into bus *i*

$Q_{SUB}^{k}(i,V^{k},\theta^{k})$ —reactive power injection into bus *i*

V_i^k —voltage magnitude on bus *i* under contingency *k*. V_i^k should be a fixed variable if bus *i* is a PV bus under contingency *k*.

$V_{i,\min}^{k}, V_{i,\max}^{k}$ —minimum and maximum voltage magnitude on bus *i* for contingency *k*. Note $V_{i,\min}^{k} = \max(0.95, V_i^0 - 0.05)$.

ΔV_m^k —voltage change on bus m installed with a VC model;

ΔV_n^k —voltage change on bus n connecting bus *m*;

$r_{mn}^{Pre}, r_{mn}^{Post}$ — pre- and post-control ratio between ΔV_m^k and ΔV_n^k. r_{mn}^{Post} is limited in a small range around r_{mn}^{Pre}, such that $\left|r_{mn}^{Post} - r_{mn}^{Pre}\right| \le 0.1$,since a VC model is installed on bus *m*.

$\tau_l^{Pre}, \tau_l^{Post}$ —pre- and post-control LTC tap position in branch *l*

b_n^{Pre}, b_n^{Post} —pre- and post-control shunt susceptance on bus *n*

$Q_{SUB,C}^{k}(i)$ —Applied Var source on bus *i*

$Q_{SUB,C\min}^{k}(i), Q_{SUB,C\max}^{k}(i)$ —the minimum and maximum available capacity of the Var sources in the subsystem

P_l^k —Active load flow in branch *l*

$P_{l,max}^{k}$ —Maximum allowable Active load flow in branch *l*

$M_{SUB}(n)$ —the set of buses in the subsystem

$N_{SUB}(l)$—the set of branches in the subsystem

$P_{L,n}^{Pre}$, $P_{L,n}^{Post}$—the pre- and post-control active power load on bus *n*

Ψ_{max}—the maximum allowable load shedding across the entire the system

The suffix "SUB" indicates that the variable or parameter is defined for the control subsystem. The signs "$\big|_{pre}$" and "$\big|_{post}$" mean the corresponding quantities are evaluated before and after voltage and stability controls, respectively.

The proposed decentralized emergency voltage and stability control can be applied to the 39-bus example introduced in section 6.4.1. With the assumed contingency in branch 21~22 at 140% loading level, the remaining stability margin is only 2% with emergency low voltage or voltage drops detected on a few buses across two control zones. Since the voltage and stability constraints are actual, the decentralized controls will only be assessed under current system condition without considering other contingencies.

According to system decomposition procedures presented in section 6.2.2, a control subsystem (*SUB*) can be constructed from the set of buses enclosed in the dashed black curve as shown in Figure 59. SUB includes buses with voltage constraint violations (buses 15, 16, 21 and 24), 1st tier neighboring buses (14, 17, 19, 23). The buses with voltage constraint violations and the buses with voltage drops more than 30% of the voltage drop on bus 21 (largest voltage drop) are included in the set of buses {21, 24, 16, 15, 17, 23, 18, 27, 3, 14, 4}, all of which would constitute the disturbance-affected zone. Bus 3 and 18 are substituted by PQ models installed on bus 4 and 17 respectively since

the ratios $\left|\frac{\Delta x_4}{\Delta x_3}\right|$ and $\left|\frac{\Delta x_{17}}{\Delta x_{18}}\right|$ are close to unity. PV models are placed on bus 13 and bus 19 representing the external network as seen from bus 14 and 16, respectively, since the ratios $\left|\frac{\Delta x_{16}}{\Delta x_{19}}\right|$ and $\left|\frac{\Delta x_{15}}{\Delta x_{14}}\right|$ are significantly larger than 1. Voltage-controlled (VC) models are placed on bus 5 and 26 representing the external network as seen from bus 4 and 27, respectively, since both PQ and PV models are unsuitable. PV buses 35 and 36 are also included since they are connected to bus 23, where PV models are required because of the large ratio $\left|\frac{\Delta x_{23}}{\Delta x_{22}}\right|$.

The maximum boost in load margin by deployment of the capacitor banks in SUB is estimated to be 12%, which is about two times larger than the 5% margin criterion. Therefore, it is unnecessary to expand SUB to include additional capacitor banks. The one-line diagram of the independent control subsystem is shown in Figure 60.

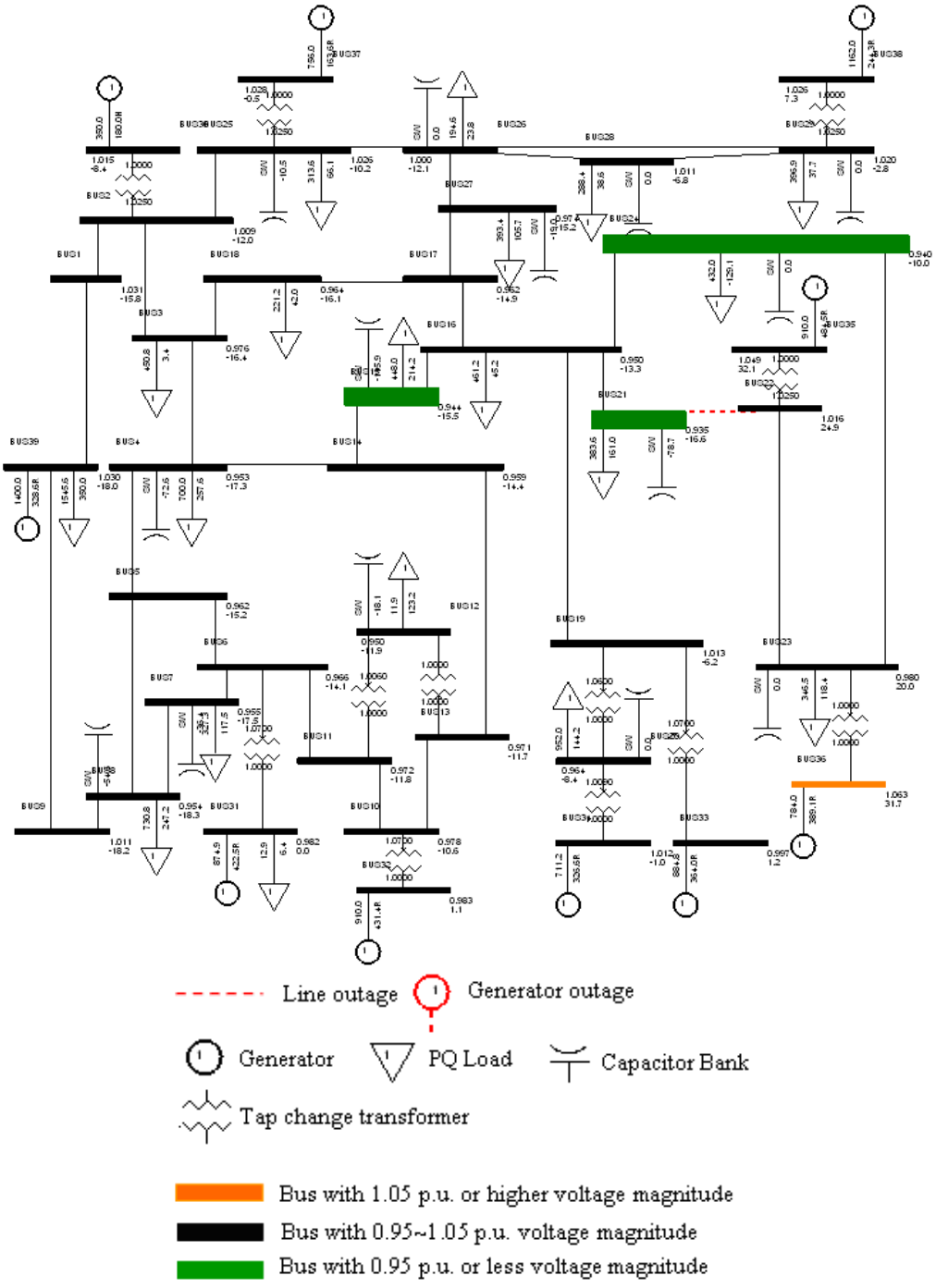

Figure 59. The decentralization of the control subsystems following the line contingency 21~22 at 140% loading.

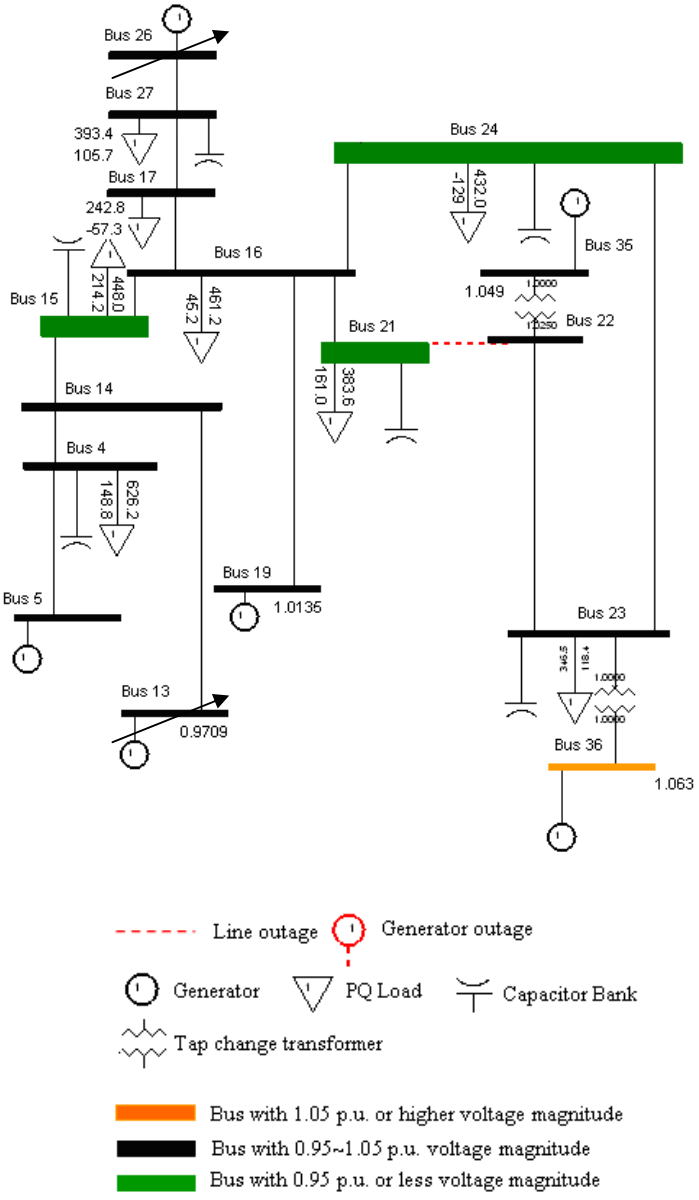

Figure 60. Decentralized control subsystem for evaluating voltage and stability controls to mitigate the impact of a severe N-1 contingency.

The emergency voltage and stability controls on SUB can be evaluated by solving the multiple-objective problem formulations introduced earlier in this section. Applying the normalized constraint algorithm to solve the multiple-objective problem formulations, 15 secondary voltage and stability control solutions are obtained in 24.4 seconds, while 27 load shedding solutions (corresponding to combinational loading shedding schemes at

the load buses in the control subsystem) are obtained in 22.6 seconds from a computer with 1.6 GHz dual core CQU and 1 GB RAM. The computation time is recorded for comparison purpose only. Shorter computation time could be achieved when specialized computer is used. These controls solutions, shown in Figure 61 and Figure 62, provide a variety of options for a system dispatcher to choose to meet different stability criteria. In Figure 61, three objective values (minimum capacitor control, minimum MVA line consumption, and maximum stability margin) of the decentralized secondary voltage and stability control solutions are plotted. The red dots represent the actual spatial locations of the three-objective solutions, while the grey dots are the projection of the three-objective solutions on the two-dimensional planes. Figure 62 compares the load margins estimated by margin sensitivities as a control objective with the load margin predicted by iterative power flow analysis. The reduction in reactive power losses is closely correlated with the increase in load margin. Therefore, minimizing reactive power losses is usually used as an indirect control objective to increase stability margin by utilities (such as EDF). The red and blue dots correspond to the secondary voltage and stability control solutions, while the black and green dots correspond to the load shedding solutions after switching on all the available shunt capacitor banks and blocking the LTCs in the decentralized control subsystem. The loading shedding solutions will only be reviewed when the secondary voltage controls are insufficient to achieve the desired stability margin. It can be observed in Figure 62 that the stability margin estimated by margin sensitivities of the control actions (red and green dots) and by iterative power flow method (black and blue dots) match closely with each other. Using power flow analysis as the benchmark, the accuracy of the load margins estimated by margin sensitivities can

be assessed. The reactive generation limits of the generators are considered in both power flow analysis and optimal control formulation.

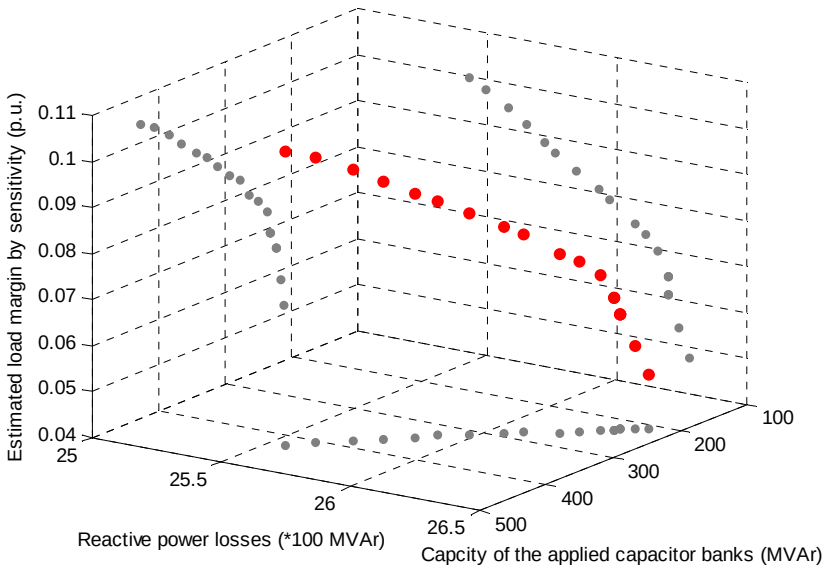

Figure 61. Pareto solutions for 39-bus contingency voltage and stability control example.

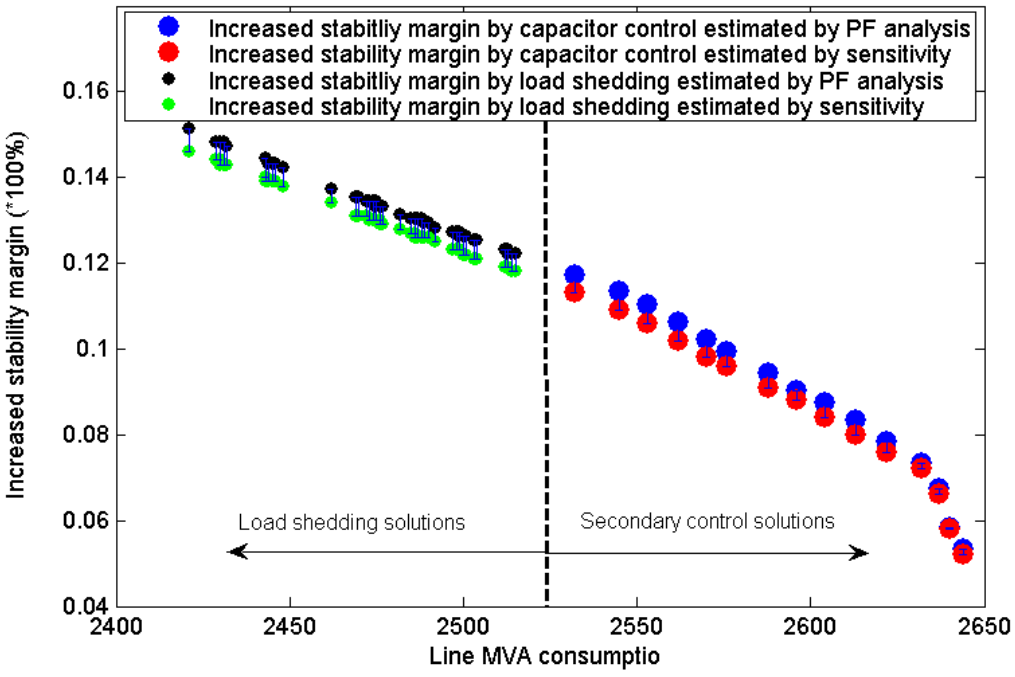

Figure 62. Comparison of the load margin estimated by margin sensitivity and power flow analysis following the optimal voltage and stability control and load shedding solutions.

Without performing the time-consuming power flow analysis on the entire system model, the decentralized control optimization is able to generate control solutions leading to predictable load margins. The selection of a suitable control solution could either be automated with specific expectation on the control objectives or determined by a system dispatcher after additional considerations on the actual operation environment. The following factors may be considered when selecting a suitable control solution:

(1). The minimum post-contingency voltage stability margin (such as the 5% WECC criterion [46]).

(2). Maximum allowable amount of load shedding.

(3). Minimum capacity of reactive reserve after voltage and stability control.

For example, under an emergency low voltage condition, a system operator may choose a control solution corresponding to 5% or high post-contingency voltage stability margin, minimum amount of applied reactive resource (or minimum amount of load shedding).

Assuming the desired post-control load margin is 6% or higher, a Pareto solution corresponding to 6.5% load margin can be promptly selected from Figure 62. The detailed control sequence following this Pareto solution is listed in Table 19. In order to avoid excessive transients, the simultaneous switching of the capacitor banks on the same bus is restricted. For illustrative purpose, the capacitor banks on bus 24 are divided into three groups to be switched on different times. Taking into account the possible delays consumed by dynamic monitoring (10 seconds), data transmission (5 seconds), and control evaluation (25 seconds), it can be assumed that the desired control decision is

automatically selected after 40 seconds following the contingency event. The switching time constant of the capacitor banks is typically in the range of 10~20 seconds. A 30 seconds time interval is adopted between two adjacent groups of switching commands on the same bus to avoid excessive transients.

Following the designed control sequence, the corrections of the voltage constraints are listed in Table 20. The post-control active and reactive power losses are 126 MW and 2632.8 MVAr respectively. The time-domain voltage magnitudes on the buses with significant voltage violations are plotted in Figure 63.

Table 19. The control sequence according to an optimal control solution leading to 6.5% increase in load margin. Simulation starts at 0 s, and the contingency occurs at 100 s.

Control Event ID	Control Device	Device Location	Time Stamp (s)	Pre-control Status	Post-control Status
1	CAP	Bus 24	150.0	0 MVAr	50 MVAr
2	CAP	Bus 21	155.0	90 MVAr	150 MVAr
3	CAP	Bus 23	160.0	0 MVAr	20 MVAr
4	CAP	Bus 24	180.0	50 MVAr	100 MVAr
5	CAP	Bus 24	210.0	100 MVAr	150 MVAr

Table 20. Post-control voltage constraints following an optimal control solution leading to 6.5% increase in load margin.

Bus ID	Pre-Contingency V (p.u.)	Pre-control V (p.u.)	Post-control V (p.u.)	Pre-control Voltage Drop (p.u.)	Post-control Voltage Drop (p.u.)
21	1.0167	***0.9354***	0.9735	***0.0813***	0.0433
24	1.02	***0.9407***	0.9760	***0.0793***	0.0440
16	1.0138	0.9505	0.9790	***0.0633***	0.0348
15	0.9998	***0.9446***	0.9694	***0.0552***	0.0304

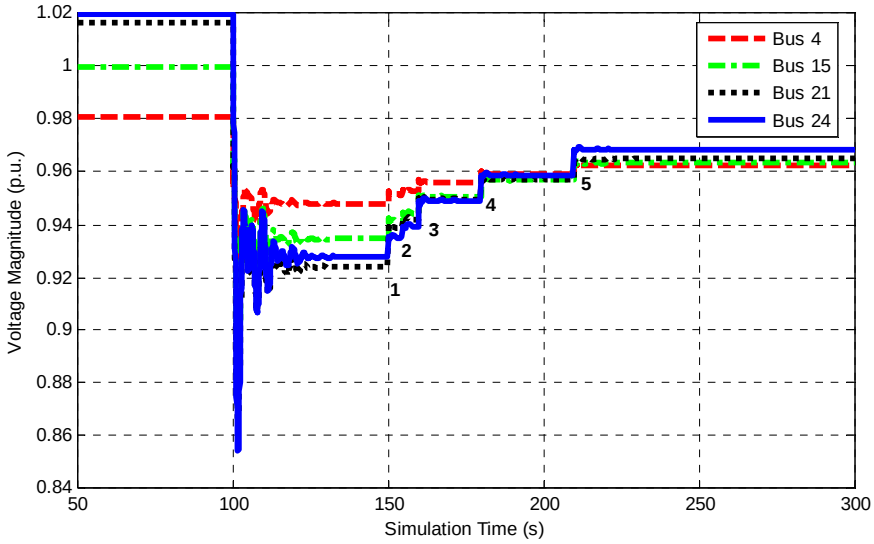

Figure 63. Time-domain voltage magnitudes on the buses with voltage violations before and after the optimal voltage and stability control leading to 6.5% load margin (PSS/E simulation).

Figure 63 shows a conservative dispatch pattern of the decentralized control decisions. A 30 seconds time delay is assumed between consecutive control orders so that the transients associated with secondary controls could die out completely. In fact, the switching transient could diminish much earlier that 30 seconds, and therefore the decentralized controls can be applied faster without jeopardize transient stability.

When control speed is the most important factor during critical system conditions, the decentralized control decisions can be dispatched together or in shorter time intervals. The capacitor banks at the same bus could be switched on together, if the resulting switching transients are not significant according to off-line analysis or field test. When a transient associated with a capacitor switching dies out (according to transient monitor), the next capacitor switching can be order immediately.

In Figure 64, the decentralized control decisions are all dispatched at 140 s to bus 21, 23 and 24, because the switching delays of the capacitor banks on these buses are

different by at least five seconds. The switching transients are assumed to vanish within five seconds. According to Figure 64, three groups of capacitor banks are switched on at 150 s, 155 s, and 160 s. No significant transient is discovered to be associated with capacitor controls.

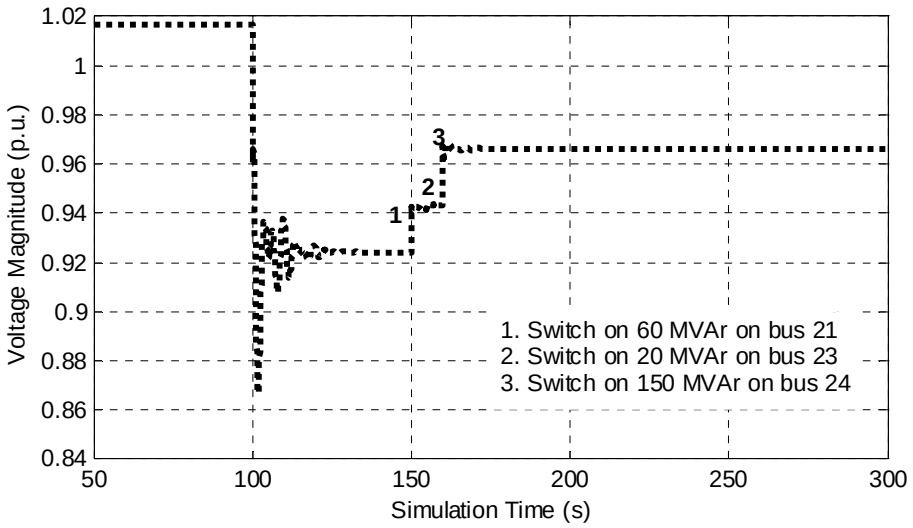

Figure 64. Time-domain voltage magnitudes on the bus 21 (largest voltage drop) when control decisions are dispatched at the same time to shorten control time delay

System-wide optimal power flow (OPF) is usually performed in 10~30-minutes time intervals by those utilities who use that tool. Assuming that voltage and stability control objectives are adopted in OPF, the Pareto solutions from OPF should closely match with the decentralized control solutions. From the Pareto front evaluated by OPF, a Pareto solution with similar objective values to the decentralized control solution is identified. The performance of different voltage and stability control solutions, including centralized and decentralized controls, type I and II utility controls, are compared in Table 21.

Table 21. Comparison of voltage and stability control solutions for the 39-bus example.

Items	Centralized Control Decision	Decentralized Control Decision	Type I Utility Control	Type II Utility Control
Control Solution	Bus 21: +50 MVAr Bus 23: +30 MVAr Bus 24: +130 MVAr	Bus 21: +60 MVAr Bus 23: +20 MVAr Bus 24: +150 MVAr	Details in Table 16	Details in Table 18
Total Applied Shunt Capacitor Banks	210 MVAr	230 MVAr	90 MVAr	120 MVAr
Post-control Voltage Constraints	None	None	Bus 21, 24 16	None
Post-control Reactive Loss	2644 MVAr	2633 MVAr	2709 MVAr	2664 MW
Post-control active Loss	125.9 MW	125.3 MW	129.0 MW	126.4 MW
Estimated Control time frame	> 10 minutes	< 120 s	265 s	210 s
Increase Stability Margin	6.3%	6.5%	2.0%	3.2%

Assuming the desired post-control load margin is 12.5%, a Pareto solution corresponding to 12.7% load margin can be promptly selected from Figure 62. Load shedding control has to be performed since the secondary voltage and stability controls are only capable of increasing stability margin by 11.9%. The selected load shedding solution suggests shedding 25.8MW load on bus 21, which is only 6.7% of the total monitored load on bus 21. The load shedding solutions can be obtained in half a minute up to several minutes, depending on the size of the studied system. The system dispatcher should review the load shedding suggestion from the Pareto front and compare it with other options, such as transmission loading relief (TLR) and generation re-dispatch, to make the final control decision. However, since the load shedding solution can be obtained in less time, the system operator will be given additional time to study the feasibility of other alternative options.

Compared with other control approaches, the proposed decentralized voltage and stability control system not only solves voltage constraint violations, but also helps to maintain acceptable stability margin under emergency conditions, when no other voltage control systems can be accounted for to provide similar support in the same time. The actuation time of decentralized control is shorter than typical utility voltage control methods, such as automatic voltage control and manually coordinated voltage control.

Because the proposed decentralized control system only generate sparsely distributed control solutions based on local system information, the performance of the decentralized control solutions falls shortly behind centralized control solutions. When the expectations on control objectives are specified, a centralized control solution can more accurately meet the control requirements without utilizing additional control resources. According to the example in this section, the centralized controls saved 20 MVAr of reactive reserve compared with the decentralized control. However, the centralized control solutions are generated by system-wide OPF, which are usually performed every 10~30 minutes.

Instead of the rigid voltage control schemes generated from automatic controllers or copied from control manual, a set of control solutions will be generated by the proposed decentralized control system to meet different control objectives by different utilities. The proposed system can quickly evaluate the sufficiency of the available secondary voltage resources in meeting the desired stability margin. In case of insufficient secondary voltage resources, load shedding schemes can be presented to the system dispatcher as back-up options. All of the above advantages suggest that the proposed system is an efficient voltage and stability control tool, to be seriously considered by the utilities.

6.5 COORDINATED DECENTRALIZED VOLTAGE AND STABILITY CONTROLS (INCLUDING LOAD SHEDDING) TO MAINTAIN VOLTAGE STABILITY FOR UNSECURED SINGLE CONTINGENCIES

Load shedding (LS) is the only solution to maintain the stability of a system when all the other accessible voltage and stability controls (such as secondary voltage controls, TLR, generation re-dispatch) have been exhausted. LS is even considered as a direct approach to avoid system instability under emergency conditions indicated by low voltages or high frequency offsets [39, 41]. The amount of load shedding in the LS program is usually defined in fixed steps corresponding to different voltage or frequency levels.

Optimal power flow (OPF) is adopted by some utilities to find out the minimum amount of load shedding that can sufficiently maintain the system stability margin. Feng [42] and Affonso [43] both used participation factors to identify the most adequate buses for load shedding purposes in their customized OPF formulation. However, the active and reactive load participation factors do not provide direct relation between the changes in stability margin and load shedding and therefore reduces the accuracy of the corresponding load shedding solutions. Also, singularity problems are often encountered when evaluating the participation factors close to the instability point. The complex calculation process causes long time delay, which may cause uncertainties in system stability condition.

Since OPF involves the system-wide optimization, the timeline of OPF-based load shedding can be as long as 15~30 minutes.

LS has also been coordinated with voltage controls [17, 36] to avoid unnecessary inconvenience to the end customers. Load shedding in PJM will only be conducted when other voltage controls are incapable of relieving an actual or simulated post-contingency violation. Therefore, the timeline for load shedding depends on the violations of the different ratings of the transmission facilities, such as 15 minutes for violating emergency rating (0.90~0.92 p.u.) and 5 minutes (<0.92 p.u.) for violating load dump rating. Limited by the timeline of the secondary voltage controls, load shedding could be conducted when the detected violations is solvable by alternative voltage controls. In order to avoid system instability caused by severe low probability contingencies, PJM [17] continuously monitors the severity of these contingencies and provides updated post-contingency control strategies to local control centers. For example, the loss of both Doubs #1 and #3 transformers [17] is a very severe contingency under heavy load conditions but with low probability. Instead of conducting pre-contingency controls, PJM performs off-line simulations to identify the need for load shedding after exhausting all available switching, effective generation re-dispatches, TLR and other emergency Procedure options. The off-line simulations rely on power-flow based methods. However, power flow will not converge when the simulated contingency brings the system directly into instability. Even if OPF could find a new system equilibrium point with a combination of changes in control parameters, the distance of the new equilibrium point may still be too close to a saddle node bifurcation (SNB) point.

In the previous section, the proposed decentralized secondary voltage and stability controls has been coordinated with load shedding to solve voltage constraint violations and enhance system stability condition for an actual N-1 contingency secure solution.

Similar control formulation can be used for coordinated load shedding and secondary controls considering simulated severe contingencies when the system may become unstable.

The flow chart of generating coordinated secondary control and load shedding solution for simulated severe contingencies are the same as in Figure 58. However, the stability margin estimated for the simulated contingencies could be negative. The estimations of the stability margins rely on power flow analysis. The negative stability margin can be estimated by consecutively decreasing the loads on all buses by a small proportion, such as 1%, until a new system equilibrium point is found. The margin sensitivities and target post-contingency stability margin need to be evaluated at the new system equilibrium point identified by power flow analysis. The simulated voltage drops between pre- and post-contingency conditions are recorded and used for performing system decomposition. If the sum of the incremental stability margins obtained by all the secondary voltage control devices in the control subsystem(s) is higher than the target stability margin objective, decentralized secondary voltage and stability control problem(s) will be formulated to identify the suitable non-cost control solution. If the available shunt capacitor banks in the control subsystem are insufficient to provide the desired stability margin, the decentralized control subsystem will be enlarged to cover additional reactive resources. The maximum increase in stability margin from the reactive resources can be quickly evaluated by margin sensitivity analysis. An emergency load shedding formulation will be adopted to identify the minimum load shedding scheme when the available secondary voltage control resources are insufficient to increase stability margin to the desired level. Normal constraint algorithm can be adopted

to generate sparse Pareto solutions for each of the problem formulations. Finally, one suitable control solution for each sub-system will be selected. The synthesis of all the local control solutions will form a system-wide control decision.

Under emergency conditions, the formulation of the decentralized control is different from the control formulation for normal low voltage condition in the following aspects:

(1) The objectives of minimum active and reactive power losses will be integrated as one objective to minimize MVA consumption of transmission lines, considering active and reactive losses are highly correlated and not as important as the other objectives (such as maximum stability margin) during emergency conditions.

(2) The objective of maximum load margin for post-contingency state is added.

(3) The non-linear margin sensitivities of LTCs imply that stability margin could be affected by LTC controls in both positive and negative directions depending on the output limits of the nearby generators. LTCs controls may possibly aggravate stability margin by restoring voltage and load power, and therefore reduce generation reserve. Therefore, the control of LTCs needs to be blocked or restricted to operate only within a narrow range (by changing the relevant inequality constraints) under emergency conditions.

(4) The control variables, equality and inequality constraints are applied for both pre- and post-contingency states. If a constraint violation inducing contingency is actual, the control variables, equality and inequality constraints will only be evaluated under post-contingency system condition to save the time of control evaluation.

(5) If a simulated contingency leads to zero or negative stability margin, the minimum voltage constraints are relaxed to 0.95 p.u. or other normal condition ratings adopted by the utilities.

The objective of minimum secondary voltage controls should be replaced by the minimum load shedding objective, when the increased stability margin through the secondary voltage controls meets the target stability margin under post-contingency condition.

The problem formulation for the decentralized secondary controls under emergency condition is as follows:

(1) Minimization of MVA line losses:

$$\text{Minimize } Q_{Loss} = \sum_{k \in N_c} \sum_{l \in N_{SUB}(l)} \sqrt{Q_{Loss,l}^{k}(V^{k}, \theta^{k})^2 + P_{Loss,l}^{k}(V^{k}, \theta^{k})^2}$$

(2) Minimization of shunt capacitor controls:

$$\text{Minimize: } \sum_{n \in M_{SUB}(n)} \frac{\left| b_n^{Post} - b_n^{\Pr e} \right|}{B_n};$$

(3) Minimization of LTC controls:

$$\text{Minimize: } \sum_{l \in N_{SUB}(l)} \left| \tau_l^{Post} - \tau_l^{\Pr e} \right|;$$

(4) Maximization of stability margin

$$\text{Objective A: Maximize: } \sum_{n \in M_{SUB}(n)} SC_n^k (b_n^{Post} - b_n^{Pr e})$$

Objective B: Maximize: $\sum_{n \in M_{SUB}(n)} SL_n^k (P_{L,n}^{Post} - P_{L,n}^{Pre}))$

Objective A will be adopted, if the increased stability margin through secondary voltage controls meets or exceeds the desired stability margin, or the following condition stands

$$\sum_{k \in N_C} \left[\sum_{n \in M_{SUB}(n)} SC_n^k (b_{n,max} - b_n^{Pre}) \right] \geq M_{min} .$$

Otherwise, objective B will be adopted and all shunt capacitor banks need to be switched on.

The following constraints need to be accounted for during the optimization:

Active power injection at bus *i* in SUB following contingency k :

$$P_{SUB,G}^k(i) - P_{SUB,L}^k(i) - P_{SUB}^k(i, V^k, \theta^k) = 0$$

Reactive power flow equations for bus *i* in SUB following contingency k :

$$Q_{SUB,G}^k(i) + Q_{SUB,C}^k(i) - Q_{SUB,L}^k(i) - Q_{SUB}^k(i, V^k, \theta^k) = 0$$

Active power generation limits:

$$P_{SUB,G\min}^k(i) \leq P_{SUB,G}^k(i) \leq P_{SUB,G\max}^k(i)$$

Reactive power generation limits:

$$Q_{SUB,G\min}^k(i) \leq Q_{SUB,G}^k(i) \leq Q_{SUB,G\max}^k(i)$$

Voltage constraints:

$$V_{i,\min}^k \leq V_i^k \leq V_{i,\max}^k$$

Fixed voltage drop ratio from bus *n* to *m*:

$$\Delta V_m^k = r_{mn} \Delta V_n^k$$

LTC tap position ranges:

$$\tau_{l,\min} \le \tau_l^{Pre}, \tau_l^{Post} \le \tau_{l,\max}$$

The adjustable range of susceptances of shunt capacitor banks:

$$b_{n,\min} \le b_n^{Pre}, b_n^{Post} \le b_{n,\max}$$

The reactive power support from shunt capacitor banks:

$$Q_{SUB,C\min}^k(i) \le Q_{SUB,C}^k(i) \le Q_{SUB,C\max}^k(i)$$

Line flow limits:

$$\left|P_l^k\right| \le P_{l,max}^k$$

The following Constraints are only applied in load shedding formulation:

Fixed LTC taps and switch on all shunt capacitor banks:

$$\tau_l^{Post} = \tau_l^{Pre},\ b_n^{Post} = b_{n,\max}$$

The maximum portion of interruptible load on the load buses:

$$\frac{\left|P_{L,n}^{Post} - P_{L,n}^{Pre}\right|}{P_{L,n}^{Pre}} \le S_n;$$

Totally allowable amount of load shedding:

$$\sum_{n \in M_{SUB}(n)} \left|P_{L,n}^{Post} - P_{L,n}^{Pre}\right| \le \Psi_{max}$$

Notions:

$Q_{Loss,l}^k(V^k, \theta^k)$ —the reactive power losses in branch *l* following contingency *k*

N_c —the group of stability constrained contingencies

$P_{SUB}^k(i,V^k,\theta^k)$ —generator active power output on bus i for contingency *k*

$Q_{SUB,G}^k(i)$ —generator reactive power output on bus i for contingency *k*

$P_{SUB,L}^k(i)$ —load active power on bus *i*

$Q_{SUB,L}^k(i)$ —load active power on bus *i*

$P_{SUB}^k(i,V^k,\theta^k)$ —real power injection into bus *i*

$Q_{SUB}^k(i,V^k,\theta^k)$ —reactive power injection into bus *i*

V_i^k —voltage magnitude on bus *i* under contingency *k*. V_i^k should be a fixed variable if bus *i* is a PV bus under contingency *k*.

$V_{i,\min}^k, V_{i,\max}^k$ —minimum and maximum voltage magnitude on bus *i* for contingency *k*. Note $V_{i,\min}^k = \max(0.95, V_i^0 - 0.05)$.

ΔV_m^k —voltage change on bus m installed with a VC model;

ΔV_n^k —voltage change on bus n connecting bus *m*;

$r_{mn}^{Pre}, r_{mn}^{Post}$ — pre- and post-control ratio between ΔV_m^k and ΔV_n^k. r_{mn}^{Post} is limited in a small range around r_{mn}^{Pre}, such that $\left|r_{mn}^{Post} - r_{mn}^{Pre}\right| \le 0.1$,since a VC model is installed on bus *m*.

$\tau_l^{Pre}, \tau_l^{Post}$ —pre- and post-control LTC tap position in branch *l*

b_n^{Pre}, b_n^{Post} —pre- and post-control shunt susceptance on bus *n*

$Q^k_{SUB,C}(i)$ —Applied Var source on bus i

$Q^k_{SUB,C\min}(i)$, $Q^k_{SUB,C\max}(i)$ —the minimum and maximum available capacity of the Var sources in the subsystem

P^k_l —Active load flow in branch l

$P^k_{l,max}$ —Maximum allowable Active load flow in branch l

$M_{SUB(n)}$ —the set of buses in the subsystem

$N_{SUB(l)}$ —the set of lines in the subsystem

$P^{Pre}_{L,n}$, $P^{Post}_{L,n}$ —the pre- and post-control active power load on bus n

Ψ_{max} —the maximum allowable load shedding across the entire system

The suffix "SUB" indicates that the variable or parameter is defined for the control subsystem. The signs "$\big|_{pre}$" and "$\big|_{post}$" mean the corresponding quantities are evaluated before and after voltage and stability controls, respectively.

The following example is similar to the 39-bus example introduced in section 6.4, where a contingency in line 21~22 at 140% loading level is applied. However, in this section, the contingency in line 21~22 is assumed to be an unsecured contingency when 50% of the generation on bus 39 is tripped due to unexpected outages. The off-line contingency analysis shows that the post-contingency stability margin is -11.2%. Voltage collapse could happen when the contingency in line 21~22 becomes actual. The target post-contingency stability margin is 5% or 307.5 MW, which matches with the WECC

criterion on minimum post-contingency stability margin. A suitable control solution is needed to increase the post-contingency stability margin from -11.2% to 5%. The minimum required increase in stability margin is 16.2% or 996.4 MW.

The largest voltage drop evaluated at 128% load level with the contingency (outage of line 21~22) is 0.0645 p.u. at bus 24. According to the system decomposition procedure presented in section 4.3.2, a control subsystem (*SUB*) can be constructed from the set of the buses with voltage violations and the buses with voltage drops more than 30% of the voltage drop on bus 24 in the set of buses {21, 24, 16, 15, 17, 23, 18, 27, 3, 14, 4}. Bus 3 and 18 are substituted by PQ models installed on bus 4 and 17, respectively, since the ratios $\left|\frac{\Delta x_4}{\Delta x_3}\right|$ and $\left|\frac{\Delta x_{17}}{\Delta x_{18}}\right|$ are close to unity. PV models are placed on bus 13 and 19 extended from bus 14 and 16, respectively, since the ratios $\left|\frac{\Delta x_{16}}{\Delta x_{19}}\right|$ and $\left|\frac{\Delta x_{15}}{\Delta x_{14}}\right|$ are significantly larger than 1. PV models are placed on bus 13 and bus 19, representing the external network as seen from bus 14 and 16, respectively, since the ratios $\left|\frac{\Delta x_{16}}{\Delta x_{19}}\right|$ and $\left|\frac{\Delta x_{15}}{\Delta x_{14}}\right|$ are significantly larger than 1. Voltage-controlled (VC) models are placed on bus 5 and 26 representing the external network as seen from bus 4 and 27, respectively, since both PQ and PV models are unsuitable. PV buses 35 and 36 are also included since they are connected to bus 23, where PV models are required because of the large ratio $\left|\frac{\Delta x_{23}}{\Delta x_{22}}\right|$. The one-line diagram of the independent control subsystem is shown in Figure 60.

Using the margin sensitivities evaluated at 128.9% load level with the contingency in line 21~22, the maximum boost in stability margin by the capacitor banks in SUB is estimated to be 11.0%, while the maximum possible increase in stability margin by the capacitor banks in the entire system is 12.7%. Therefore, additional stability margin from load shedding is necessary if no other control options (such as TLR and generation re-dispatch) are available. With all shunt capacitor banks in the entire system switched on, the decentralized load shedding control can be formulated to identify the optimal load shedding schemes. In the decentralized load shedding formulation, the maximum amount of total allowable load shedding is 250 MW (about 5% of the total system load), while the maximum fraction of load shedding on each load bus is 30%. The load shedding related constraints can be customized based on operation experience or regulatory rules by different utilities.

Applying the normalized constraint algorithm to solve the multiple-objective problem formulations, 33 optimal load shedding solutions are obtained in 26.1 seconds from a computer with 1.6 GHz dual core CQU and 1 GB RAM.

Figure 65 compares the increases in load margins estimated by margin sensitivities as a control objective with the load margin predicted by iterative power flow analysis. One load shedding solution corresponding to 16.5% or 1080.8MW of increase in stability margin can be picked out from Figure 65 (in the solid circle). According to the selected load shedding solution, 25 MW, 13 MW and 105 MW of load needs to be shed on bus 4, 15 and 21, respectively, to boost the stability margin to 16.5%.

The increase in stability margin is in near linear relation to the amount of load shedding. The difference in estimated stability margins (obtained by power flow

calculations) and margin sensitivity analysis lies in the aggregated estimation error (non-linearity effect) in the added stability margins by all the shunt capacitor banks. Since the interactions among control actions are ignored, the increased stability margin estimated by margin sensitivities is more conservative than the iterative power flow method. More important, the proposed decentralized control approach can generate control solutions with similar performance to the power flow method but within a much shorter time frame.

Dynamic simulations are performed in PSS/E to compare the performance of different control approaches in handling the simulated severe contingencies. The contingency in line 21~22 occurs at 360 seconds since the beginning of the disturbance, which is longer than the five minutes suggested by PJM under emergency conditions. The capacitor banks are allowed to be switched in groups at any bus as long as the system maintains stability after the switching of capacitor banks. Three types of controls approaches are simulated, including the automatic voltage controls (utility type I), manually coordinated controls (utility type II), and the proposed decentralized voltage and stability control. The time-domain voltage magnitudes on bus 21 (the location of the most severe voltage constraint violation) following different control approaches are shown in Figure 66. The detailed control sequences for different control approaches are explained in Table 22.

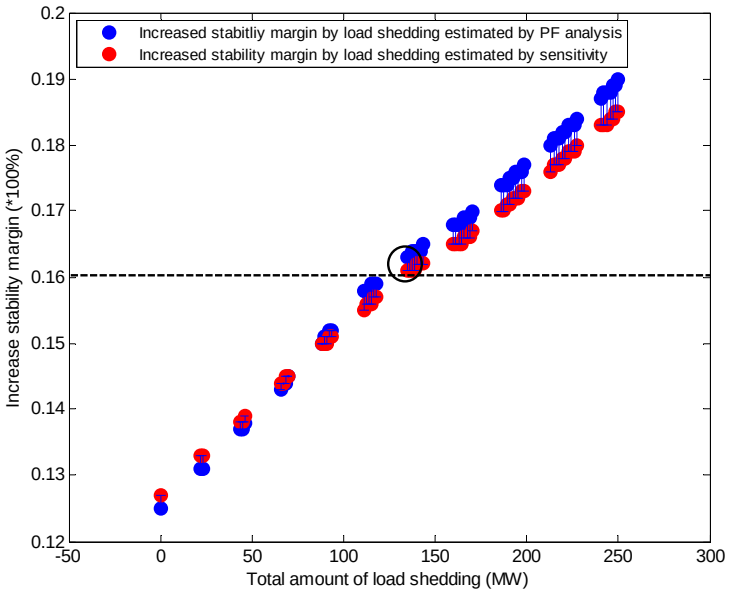

Figure 65. Comparison of the stability margin estimated by margin sensitivity and power flow analysis following the optimal load shedding solutions (a solution in the solid circle is adopted).

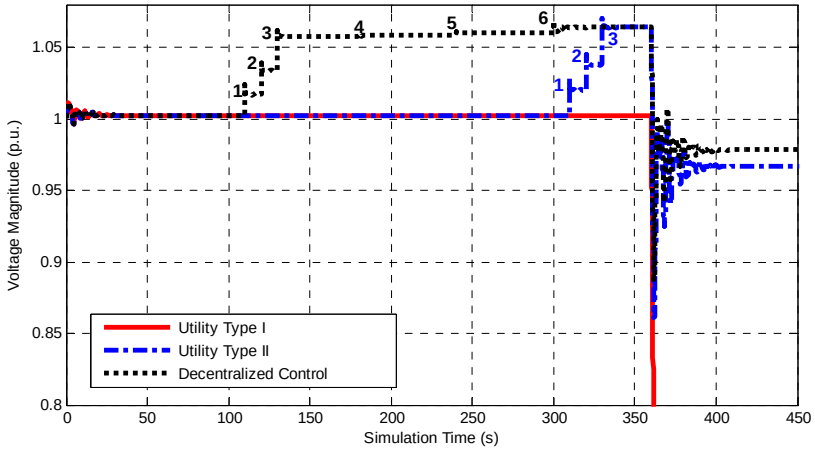

Figure 66. Time-domain voltage magnitudes on bus 21 following Type I and II utility control practices and decentralized control solution (PSS/E simulation).

Table 22. Control sequences according to Type I and II utility control approaches and the proposed decentralized control system. Simulation starts at 0 s, and the contingency occurs at 100 s.

Control Approach	Event ID	Time Frame (s)	Control Action
Type I Utility Control	1	360~370	Voltage collapse
Type II Utility Control	1	310	Switch on all shunt capacitors on bus 4, 12, 21, 25, 29
	2	320	Switch on all shunt capacitors on bus 7, 15, 23, 27
	3	330	Switch on all shunt capacitors on bus 8, 20, 24, 28
Decentralized Control Solution	1	110	Switch on all shunt capacitors on bus 4, 21, 25
	2	120	Switch on all shunt capacitors on bus 15, 23, 27
	3	130	Switch on all shunt capacitors on bus 20, 24
	4	180	Load shedding on bus 4: 25 MW
	5	240	Load shedding on bus 15: 13 MW
	6	300	Load shedding on bus 21: 105 MW

Figure 66 shows a conservative dispatch pattern of the decentralized control decisions. A 60 seconds time delay is assumed between consecutive load shedding controls so that the transients associated with load shedding could die out completely. In fact, the switching transient could diminish much earlier that 60 seconds, and therefore the decentralized controls can be applied faster without jeopardize transient stability.

When control speed is the most important factor during critical system conditions, the decentralized control decisions can be dispatched together or in shorter time intervals. When the transients associated with a group of controls die out (according to transient monitor), the next group of controls can be activated immediately.

In Figure 67, capacitor control decisions are dispatched to all buses in the system at 40 s, when the decentralized control system has finished computation and made load shedding decisions. Load shedding controls are activated at 80s on bus 4, 100s on bus 15, and 120 s on bus 21, respectively. According to Figure 67, all secondary controls and load shedding are finished within 120 seconds, which is much earlier that the

contingency at 360 s. The transients associated with decentralized controls did not cause any impact on stability, since the time interval between two consecutive controls are long enough for the transients to damp to a low level.

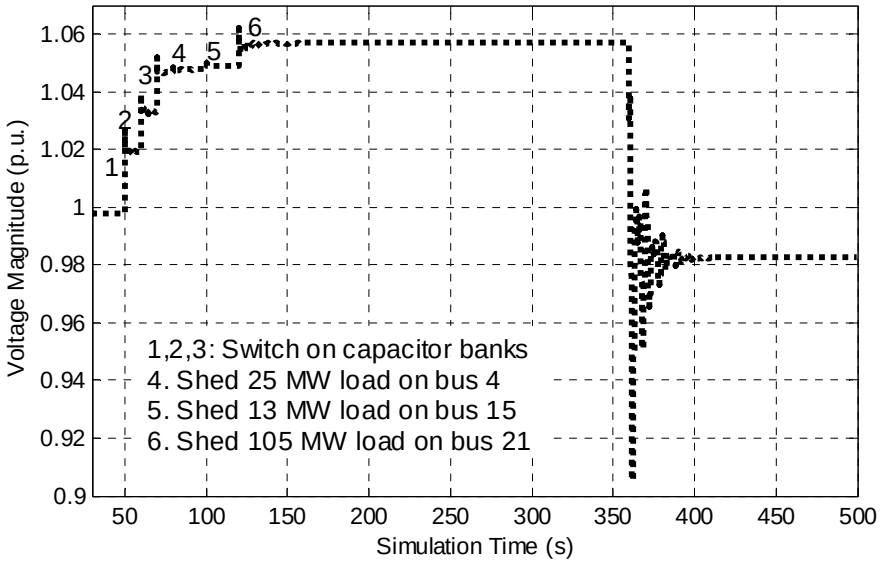

Figure 67. Time-domain voltage magnitudes on the bus 21 (largest voltage drop) when control decisions are dispatched in a compact format

1. Type I utility control—automatic secondary voltage controls

Since there is no voltage violation under the pre-contingency condition, the controls from the secondary voltage control devices are not observed until the contingency at 360 seconds causes emergency low voltages at most part of the system. During 360 seconds to 380 seconds, the load tap changer (LTC) and over-excitation limiter (OXL) at multiple locations operate to interact with the low voltages or overloads from generators. The controls of capacitor banks are not observed because of their low response time. In addition, the controls from LTC and OXL fail to improve the stability condition. Voltage collapse occurs and develops quickly between 360 seconds to 370 seconds after disturbance began.

2. Type II utility control—manually coordinated voltage controls

Assuming offline contingency analysis is available, the system operator is informed that the system could be unstable after the simulated contingency in line 21~22. Secondary voltage control decisions have to be made in five minutes before load shedding options are considered. The system operator may promptly run additional off-line power flow analysis to identify the amount of necessary reactive compensation to ensure stability. The power flow analysis will indicate that the maximum increase in the stability margin from the reactive resource is 12.7%. Finally, the system operator makes a decision to switch on all the capacitor banks in the entire system in order to maintain temporary system stability. Assuming the decision is made at 300 seconds, the capacitor banks are switched on between 310 seconds and 330 seconds following the moment of inception according to their different activation times. Because of the precautionary secondary voltage controls, the system is stable at 360 seconds after the actual contingency.

3. Decentralized voltage and stability control

The proposed decentralized voltage and stability control system will first examine the potential increases in stability margin from the available reactive resources in the control subsystem and then from the entire system. If the possible increase of stability margin from all the shunt capacitor banks is less than the target stability margin, decentralized load shedding control will be formulated with the assumption of full deployments of all shunt capacitor banks in the control subsystem. It can be assumed that the decision of switching on all the shunt capacitor banks is made at 200 seconds, which

could be much faster since the calculation of margin sensitivities only requires a few seconds. The shunt capacitor banks on bus 4, 15, 20, 21, 23, 24, 25, 27 are switched between 210 seconds and 230 seconds according to their different activation times. The load shedding solution is applied at 300 seconds, which is much longer than the sum of 26 seconds (computation time) and the necessary communication time. Because of the precautionary secondary voltage controls and load shedding, the system is stable at 360 seconds after the actual contingency.

OPF can also be used to identify the minimum amount of load shedding in order to achieve the target stability margin. An OPF solution can be obtained by adopting the following objective function and additional constraints:

Objective: (1) Minimum amount of load shedding,

(2).Achieve at least the target stability margin. Additional increase in stability margin above the target stability margin will cause unnecessary load shedding,

(3) Solve all the post-contingency voltage constraint violations.

The obtained system-wide OPF solution leads to 23 MW less of load shedding, but higher losses compared to the decentralized control solution.

The performance of the proposed voltage and stability control solutions is compared with the conventional control approaches in Table 34.

Table 23. Comparison of Decentralized control with other control approaches.

Items	Centralized Control Decision	Decentralized Control Decision	Type I Utility Control	Type II Utility Control
Control Solution	Switch on all the available capacitor banks in the entire system; Shed 3.3 MW load on bus 12; Shed 11.5 MW load on bus 15; Shed 105.2 MW load on bus 21	Switch on all the available capacitor banks in the entire system; Shed 25 MW load on bus 4; Shed 13 MW load on bus 15; Shed 105 MW load on bus 21	Mixed control of LTC and OXL at multiple locations under post-contingency condition	Switch on all the available capacitor banks in the entire system
Total Applied Shunt Capacitor Banks	870 MVAr	870 MVAr	0 MVAr	870 MVAr
Total Amount of Load Shedding	120 MW	143 MW	None	None
Post-control Voltage Constraints	None	None	Voltage collapse	None
Post-control Reactive Loss	2643 MVAr	2628 MVAr	N/A due to Voltage collapse	2771 MW
Post-control active Loss	137.2 MW	136.1 MW	N/A due to Voltage collapse	143.5 MW
Estimated Control time frame	> 10 minutes	< 300 s	N/A due to Voltage collapse	330 s
Actual Increased Stability Margin	16.3%	16.5%	-11.2%	12.7%

Compared with other control approaches, the proposed decentralized voltage and stability control system not only solves voltage constraint violations, but also helps to maintain acceptable stability margin under emergency conditions, when other voltage control systems could not provide sufficient stability margin in time. The actuation time

of decentralized control is shorter than typical utility voltage control methods, such as automatic voltage control and manually coordinated voltage control.

Because the proposed decentralized control system only generate sparsely distributed control solutions based on local system information, the performance of the decentralized control solutions falls shortly behind centralized control solutions. When the expectations on control objectives are specified, a centralized control solution can more accurately meet the control requirements without utilizing additional control resources. According to the example in this section, the centralized controls saved 23 MW of load shedding compared with the decentralized control. However, the centralized control solutions are generated in much longer time frame by system-wide OPF, which are usually performed every 10~30 minutes.

6.6 CONCLUSION

In this chapter, the motivation of designing a decentralized secondary voltage and stability control system was introduced, based on the review of the existing secondary voltage control systems. The general formulation for a voltage stability control problem is presented, which includes multiple control objectives, equality and inequality constraints, and variables representing the control settings of the secondary voltage control devices. A normal constraint algorithm is used to quickly obtain the Pareto solutions of for multiple-objective voltage stability control problems.

A decentralized voltage and stability control approach is designed to coordinate local secondary voltage controls and necessary load shedding without requiring information

about the entire system. A system decomposition procedure is designed to define the disturbance-affected zone as an independent control subsystem.

A reactive disturbance associated with an N-1 or N-1-1 contingency will cause voltage changes on a few buses electrically close to the contingency event. The propagation of a local reactive disturbance follows a pattern which can be described by a tier-wise structured network model. The voltage changes will decrease in the direction from a lower-ranking tier (closer to a disturbance) to a higher ranking tier (further away to a disturbance), and increase in the sub-tiers of a load pocket. In order to counteract the impact of a contingency, remedial voltage controls should first be considered in lower ranking tiers.

Based on the above assumptions, a system decomposition procedure can be designed. The basic idea is to identify the buses with voltage constraint violations and pronounced voltage drops, and substitute the external systems to these buses with suitable equivalent models.

Depending on the severity of the voltage constraint violations, causing either normal or emergency conditions, different control formulations can be established with emphasis on different objectives.

Typical utility practices in secondary voltage controls are reviewed and comparatively simulated on a number of disturbance scenarios to identify their limitations.

Finally, simulation examples are provided to demonstrate the ability of the proposed decentralized control in achieving similar control objectives as utility control practices.

Compared with other control approaches, the proposed decentralized voltage and stability control system not only solves voltage constraint violations, but also helps to maintain sufficient stability margin under emergency conditions, when no other voltage control systems can be accounted for to provide similar voltage and stability support in the same time frame. Because the proposed decentralized control system only generate sparsely distributed control solutions based on local system information, the performance of the decentralized control solutions falls shortly behind centralized control solutions. When the expectations on control objectives are specified, a centralized control solution can more accurately meet the requirements without utilizing additional control resources. According to the examples presented in section 6.4 and 6.5, the centralized controls saved 20 MAr of reactive reserve and 23 MW of load shedding compared with the decentralized controls. However, the centralized control solutions are generated in much longer time frame by system-wide OPF, which are usually performed every 10~30 minutes.

More simulation examples to achieve different control objectives using the proposed decentralized voltage and stability control system are presented in Appendix II.

CHAPTER VII

CONCLUSIVE REMARKS

The purpose of this research is to design a fast secondary voltage/stability monitoring and control system to counteract the voltage violations and the impact of contingencies on system voltage stability. The designed system can identify optimal voltage and stability control schemes to coordinate the secondary voltage controls and emergency load shedding to solve voltage constraint violations and maintain voltage stability margin without performing system-wide OPF. Different from the conventional automatic or manual secondary voltage controls adopted by utilities, the proposal control solutions are generated through multiple-objective optimization based on local measurements. Further more, the response time of the proposed secondary controls is shorter than the conventional secondary voltage controls, and therefore could be utilized to avoid voltage collapse or mitigate severe disturbances. In this chapter, the motivation and background of the proposed system is first reviewed. Research conclusions and achievements are summarized. Finally, future works as the continuation of the dissertation study are suggested.

7.1 OVERVIEW

Currently, the secondary voltage control practices in many power utilities only aim at maintaining desired voltage profile. The monitoring and optimizing of the voltage stability margin has not commonly been associated with routine secondary voltage

controls. The automatic operation of LTCs, an important secondary voltage control device, has been known as a potentially detrimental source to voltage stability. When a system component is faulted or operated outside its limits, protective relaying could be triggered and participate in the propagation of a cascaded disturbance. This situation could occur after the clearance of a very severe disturbance under stressful system conditions. It may also appear during the fast load growth.

The existing secondary voltage control applications [5-9] rely on the automatic/manual control of individual secondary voltage control devices. The response time of the secondary control devices, including LTCs and shunt capacitor banks, is approximately three minutes. Despite the long control time delays, the secondary voltage controls are automatically performed only to maintain the desired voltage profile in the local buses installed with secondary voltage control devices. Limited by the capacity of local voltage control resources (on the voltage controlled buses), voltage constraint violations may not be solved by automatic secondary voltage controls because of the lack of control coordination. Since voltage stability is not considered as a control objective, automatic voltage controls may not be sufficient to maintain the voltage stability of a power system. Consequently, system operators may consider loading shedding after secondary voltage controls, which is undesirable to customers.

Load shedding (LS), the ultimate stability control option, is usually considered when the available alternative control options are insufficient to achieve the desire system stability condition. LS has been applied world-wide to prevent power systems from blackout [38]. The prevailing LS programs either rely on simple control logics (fixed percentage of load shedding at pre-defined low voltage level) or time-consuming OPF to

decide the location and amount of load shedding to be conducted. The coordination between LS and secondary voltage controls are considered by utilities, such as PJM and MISO, but only through manual coordination within a limited time frame. PJM and MISO rely on voltage measurements as the indicator to measure the severity of a voltage constraint violation. Shorter control time (such as five minutes) is enforced for emergency low voltage violations. If voltage constraint violations can not be solved within the required time, more stringent controls (such as load shedding) could be conducted. System operators have to rely on their experience or control manual to make control decisions within the required time.

The proposed decentralized voltage and stability control system is flexible with respect to disturbances/contingencies by being able to change its control region. The coordination of voltage and stability controls is realized by solving a multi-objective optimization problem. The control objectives in the decentralized control region may include, but are not limited to, minimization of system transmission losses, maximization of the system stability margin, minimization of secondary voltage controls, and minimization of the necessary load shedding. The constraints of the optimization problem depend on the capacity of the actual system components. Because of the small scale of the decentralized control region, a set of Pareto voltage and stability control solutions can be generated in a shorter time frame than the current utility practices. Because of the control optimization mechanism, the decentralized control solutions can achieve the control objectives by occupying the minimum amount of control resources. The performance of the decentralized control solutions falls slightly behind the control solutions from the system-wide OPF, but superior to the automatic and manual secondary

voltage controls. The details of research conclusions are summarized in the proceeding section 7.2.

7.2 CONCLUSIONS

(1) The Voltage Instability Predictor (VIP), a fast load stability analysis method, relies on discrete phasor measurements to identify the equivalent Thevenin circuit of the entire power system connected to a load. Benchmark simulations of the VIP are conducted evaluate the performance of the VIP algorithms. The tradeoffs between the two representative VIP algorithms—the LS and recursive algorithms are discovered. Based on the characteristics of different VIP algorithms, an adaptive time-domain VIP routine is presented to make the VIP suitable for use in more complex operational environment. The proposed approach relies on actual system conditions (steady or dynamic state, slow changes or discontinuous changes) to activate or switch between the two VIP algorithms. The VIP routine is paused during severe dynamic processes when the VIP model is not valid. The performance of the dynamic VIP is examined by comparing with the result of quasi-steady state VIP algorithm. Dynamic 2-bus and 39-bus examples presented in Chapter 3 prove that the dynamic VIP can reflect the impact of severe disturbances (load increase or line tripping) on stability in dynamic environment. The relative error of the dynamic VIP is less than 5% bench-marked by the quasi-steady VIP when no transients are considered.

(2) The concept of using voltage-stability margin sensitivity to evaluate the post-control load margin improvement is presented as a fast and accurate way to assess potential voltage and stability control options. The linear combination of the margin

sensitivities of different control resources provides a tool for approximate estimation of the incremental load margin as a consequence of controls. The situations of redundant or insufficient stability controls could be avoided by adopting the margin sensitivity analysis. Benchmark simulations are conducted on the 39-bus system to compare the post-contingency stability margin evaluated by margin sensitivity analysis and the power flow based stability analysis. It has been shown that the voltage stability margin sensitivities of the shunt capacitor bank controls and load shedding can be accurately estimated by margin sensitivity analysis. However, the high non-linearity of the LTC model limits the usage of LTCs as a reliable stability resource. The increased stability margin by combinational shunt capacitor controls, as well as combinational load shedding on multiple buses, can be accurately predicted by margin sensitivity analysis without performing additional power flow analysis. The relative error of stability margin evaluated by margin sensitivity analysis for capacitor control is in the range from -3% to 3%. The relative error of stability margin evaluated by margin sensitivity analysis for load shedding varies with the percentage of interruptible load, but not more 12% when less than 10% of the total load is interruptible. Margin sensitivities of the voltage and stability controls could be introduced into the OPF or other optimization-based control formulations to achieve faster and more comprehensive evaluation of the control solutions for stability considerations.

(3) The general formulation for a voltage and stability control problem is presented, which includes multiple control objectives, equality and inequality constraints, and variables representing the control settings of the secondary voltage control devices. A

normal constraint algorithm is adopted to provide quick and sparse exploration of the Pareto front of the multiple-objective voltage and stability control problem. The partial Pareto front explored by the normal constraint algorithm matches with Pareto front obtained by solving decoupled optimizations with the exhaustive search over one of the solution dimension. Statistical analysis of the Pareto solutions for the 39-bus system shows that the optimal controls are usually conducted in the neighborhood of the buses with voltage violations with higher priority than the buses located three tiers or further to the buses with voltage violations. Therefore, control evaluation could be limited to these neighboring buses to reduce computation efforts and control time.

(4) A decentralized voltage and stability control approach is designed to coordinate the controls of the local secondary voltage control devices and necessary load shedding without requiring the information about the rest of the system.

A system decomposition procedure is designed to define the disturbance-affected zone as an independent control subsystem. A reactive disturbance associated with an N-1 or N-1-1 contingency will cause voltage changes on a few buses topologically close to the contingency event. The propagation of a local reactive disturbance follows a fixed pattern, which can be explained by a tier-wise structure network model. The voltage changes will decrease in the direction from a lower ranking tier to a higher ranking tier, and increase in the sub-tiers of a load pocket. In order to counteract the impact of the contingency, remedial voltage controls should first be considered in the lower-ranking tiers. The basic idea of the system decomposition is to identify the buses with voltage constraint violations and pronounced voltage drops, and terminate the interface of these buses to the external system. Different equivalent network models can be adopted to

represent the external system, which should have minimal impact on the patterns of power flow and disturbance propagation between the disturbance-affected zone and the external network. The ratio between the voltage drops on a boundary bus and its adjacent external bus is adopted to evaluate the accuracy of an equivalent network model in representing the external network. Analytical analysis proves that a PV, PQ or VC model should be adopted as the most suitable equivalent model when the ratio is larger than 1.5, in the range of 1~1.2, or in the range of 1.2~1.5.

Depending on the severity of voltage constraint violations, different control formulations can be established with emphases on different objectives. The proposed system can quickly evaluate the sufficiency of the available secondary voltage resources in meeting the desired stability margin. Compared with other conventional voltage and stability control approaches, the proposed decentralized voltage and stability control system can not only solve voltage constraint violations, but also achieve required stability margin (such as the minimum 5% load margin at post-contingency condition required by WECC) under emergency conditions. The performance of the control solutions generated by the decentralized control is better than the conventional voltage control solutions, such as automatic voltage controls and manually coordinated voltage controls. Compared with the optimal control solutions obtained by OPF with the same control objectives and constraints, the decentralized control solutions are generated in a much shorter time frame but with similar objective values. Table 24 summarizes the comparison results between centralized, decentralized, and utility voltage and stability controls. The proposed decentralized controls consistently possess validity and the fastest speed. Decentralized control requires more control resource utilization than centralized

control, such as 20 MVAr more capacitor bank in section 6.4 and 23 MW more load shedding in section 6.5. However, the control time of decentralized control (less than 200s for conservative estimation) is much shorter than centralized controls (>10 minutes), automatic controls (usually more than 300s), and manual coordinated controls (5~15 minutes).

Table 24. Summary of the comparison studies between centralized, decentralized, and utility controls.

	Valid solutions	Control time	Control resource utilization	Stability margin	Losses
Example in section 6.4	C, D	D>C	C>D	D>C	D>C
Example in section 6.5	C, D	D>C	C>D	D>C	D>C
App. II case 1	C, D	D>C	C=D	C=D	C=D
App. II case 2	C, D	D>C	C>D	D>C	D>C
App. II case 3	C, D	D>C	C>D	D>C	D>C
App. II case 4	C, D, T1	D>C>T1	C>D>T1	C>D>T1	C>D>T1
Note: Valid solutions means the listed solution meets all the constraints. C—centralized control; D—decentralized control, T1—type I automatic voltage control, T2—manual coordinated control. “>” means “better than”.					

7.3 CONTRIBUTIONS

The main contributions of this research are summarized as follows:

(1) An adaptive voltage and stability control system is designed as a convenient tool to provide a system operator with sub-optimal, security constrained, coordinated control solutions within 1 minute (for computation only). The coordinated control solutions involve the secondary voltage control devices within the adaptive control region, such as shunt capacitor banks and LTCs, as well as necessary load shedding at the buses prone to voltage instability. The performance of the control solutions from the designed system is assured by formulating and solving decentralized multi-objective optimizations without

time-consuming system wide analysis. The proposed system is characterized by short control time frame (30 seconds for computation, 1~2 minutes for control actuations) and direct evaluation of the impact of voltage controls on stability margin.

(2) The performance of the voltage instability predictor (VIP), a popular load stability analysis method, is studied in steady state, quasi-steady state, and dynamic environments considering the simulated slow load changes and fast dynamics caused by disturbances (such as line contingencies). A dynamic VIP routine is presented to adapt the VIP in complex operation environment. The proposed VIP routine relies on transient monitoring to switch between the two VIP algorithms, the least square and recursive algorithms, in order to optimize the performance of the VIP in stability monitoring.

(3) The concept of using margin sensitivity to evaluate the post-control load margin is presented as a fast (within a few seconds after stability margin sensitivities of controls are updated in parallel) and accurate (less than 3% error for capacitor bank, and less than 12% for load shedding) way to assess potential voltage and stability control options. The accuracy of the margin sensitivity algorithm is benchmarked with the iterative power flow method in evaluating stability margins after combined shunt capacitor controls or load shedding at multiple buses. The increased stability margin by combined shunt capacitor controls, as well as combined load shedding on different buses, can be accurately predicted by margin sensitivity analysis without performing additional power flow analysis. Margin sensitivities of the voltage and stability controls are introduced into

the formulation of optimal voltage and stability control as the parameters to achieve fast and direct evaluations of the control solutions for stability considerations.

(4) Analytical study of the propagation pattern of the local reactive disturbances following severe contingencies was performed. A tier-wise network model is introduced to explain the propagation of voltage disturbance. A system decomposition procedure is designed to define disturbance affected zones. Equivalent models, including PQ, PV and voltage-controlled models, are designed on the boundary of the disturbance affected zones. The equivalent models will not only represent the external network, but also represent the patterns of power flow and disturbance propagation between the disturbances affected region and the external network. By providing a mechanism for separation of the control zones and autonomous assessment of the control within the zones, we are effectively decoupling the system into independent subsystems.

5) The voltage stability related control routines in power utilities are reviewed. Comprehensive comparative studies between the proposed control system with the conventional voltages controls are conducted. The subjects of comparisons include an increase in stability margin, consumed time (measured from the moment of a disturbance to the completion of controls), active/reactive losses, and utilization of control resources. Compared with other conventional voltage and stability control approaches, the proposed decentralized voltage and stability control system can not only resolve voltage constraint violations, but also maintain a desired stability margin (such as a 5% post-contingency margin) under emergency conditions, while the utility controls failed to meet the voltage

and stability constraints in many of the simulation scenarios. The performance of the control solutions generated by the decentralized control is better than the conventional voltage control approaches, such as automatic voltage controls and manually coordinated voltage controls. Decentralized control requires more control resource utilization than centralized control, such as 20 MVAr more capacitor bank in section 6.4 and 23 MW more load shedding in section 6.5. However, the control time of decentralized control (less than 200s for conservative estimation) is much shorter than centralized controls (>10 minutes), automatic controls (usually more than 300s), and manual coordinated controls (5~15 minutes).

7.4 FUTURE WORK

With development of fast monitoring and communication technology (such as phasor measurement), conventional system control and operation methods are facing potential upgrades to embrace more comprehensive applications. Currently, there are about 80 PMUs installed across the U.S. power grid. It is anticipated that over the next five to 10 years over 500 PMUs will be deployed [8]. The design, communication and installation of PMUs have been thoroughly studied and documented in [6]. Some advanced functions, such as generator status monitoring, low-frequency oscillation analysis, and state estimation, have been proposed [6] to form a portfolio of applications in WAMS. As a major consideration in power system control and operation, voltage/stability control could be an ideal candidate application in WAMS. With the participation of PMU measurements, the proposed decentralized secondary voltage controls could be more

accurate, while the control time will be shortened because of the fast data processing mechanism of PMUs.

Distributed series impedance (DSI) has shorter control time (a few seconds) than the secondary voltage control devices (capacitor banks and LTCs). The controls of DSIs can avoid line overflow, and therefore increase voltage stability margin. The potential of integrating FACTs and secondary voltage control devices into a comprehensive and adaptive control system is promising.

The proposed decentralized voltage and stability control can be integrated to the EMS of utilities and act as a supplementary tool to provide control suggestions. More actual testing needs to be carried out to verify and improve the proposed system.

APPENDIX I
IEEE 39-BUS SYSTEM INFORMATION

I1. GENERAL INFORMATION AND SNAPSHOT OF THE IEEE 39-BUS SYSTEM WITH BASE LOAD

This IEEE 39-bus system is well known as 10-machine New-England Power System. The generators and loads in the system represent the aggregation of many generators and load feeders connection to the same nodes. Parameters shown below are adopted in the simulations in this dissertation and originally were presented in the book written by Pai [34].

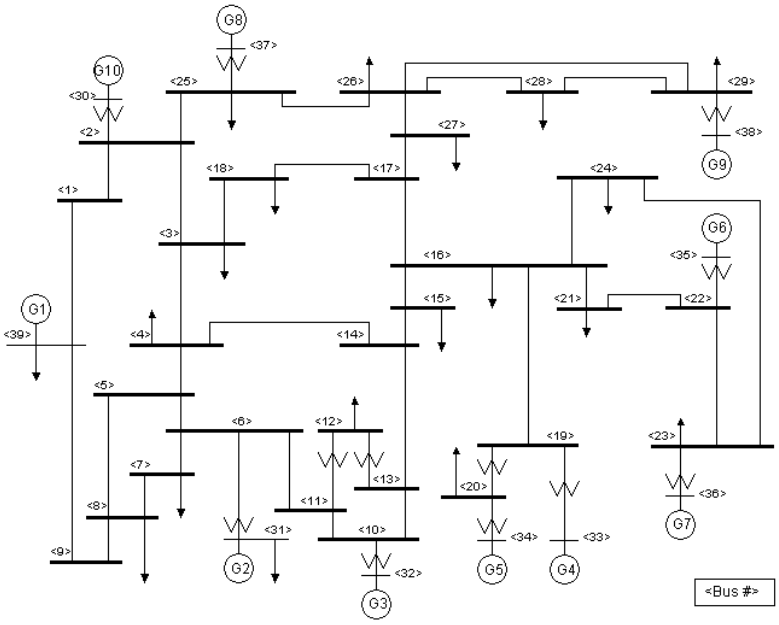

Figure 68. Snapshot of the IEEE 39-bus system with base load

I2. STEADY-STATE MODELING INFORMATION OF THE IEEE 39-BUS SYSTEM

A. Lines/transformers

The network data for this system is shown in the Table 25. All values are given on the same system base MVA.

Table 25. Steady-state line and transformer data for the 39-bus base case

Line Data					Transformer Tap	
From Bus	To Bus	R	X	B	Magnitude	Angle
1	2	0.0035	0.0411	0.6987	0.000	0.00
1	39	0.0010	0.0250	0.7500	0.000	0.00
2	3	0.0013	0.0151	0.2572	0.000	0.00
2	25	0.0070	0.0086	0.1460	0.000	0.00
3	4	0.0013	0.0213	0.2214	0.000	0.00
3	18	0.0011	0.0133	0.2138	0.000	0.00
4	5	0.0008	0.0128	0.1342	0.000	0.00
4	14	0.0008	0.0129	0.1382	0.000	0.00
5	6	0.0002	0.0026	0.0434	0.000	0.00
5	8	0.0008	0.0112	0.1476	0.000	0.00
6	7	0.0006	0.0092	0.1130	0.000	0.00
6	11	0.0007	0.0082	0.1389	0.000	0.00
7	8	0.0004	0.0046	0.0780	0.000	0.00
8	9	0.0023	0.0363	0.3804	0.000	0.00
9	39	0.0010	0.0250	1.2000	0.000	0.00
10	11	0.0004	0.0043	0.0729	0.000	0.00
10	13	0.0004	0.0043	0.0729	0.000	0.00
13	14	0.0009	0.0101	0.1723	0.000	0.00
14	15	0.0018	0.0217	0.3660	0.000	0.00
15	16	0.0009	0.0094	0.1710	0.000	0.00
16	17	0.0007	0.0089	0.1342	0.000	0.00
16	19	0.0016	0.0195	0.3040	0.000	0.00
16	21	0.0008	0.0135	0.2548	0.000	0.00
16	24	0.0003	0.0059	0.0680	0.000	0.00
17	18	0.0007	0.0082	0.1319	0.000	0.00
17	27	0.0013	0.0173	0.3216	0.000	0.00
21	22	0.0008	0.0140	0.2565	0.000	0.00
22	23	0.0006	0.0096	0.1846	0.000	0.00
23	24	0.0022	0.0350	0.3610	0.000	0.00
25	26	0.0032	0.0323	0.5130	0.000	0.00
26	27	0.0014	0.0147	0.2396	0.000	0.00
26	28	0.0043	0.0474	0.7802	0.000	0.00
26	29	0.0057	0.0625	1.0290	0.000	0.00
28	29	0.0014	0.0151	0.2490	0.000	0.00
12	11	0.0016	0.0435	0.0000	1.006	0.00
12	13	0.0016	0.0435	0.0000	1.006	0.00
6	31	0.0000	0.0250	0.0000	1.070	0.00
10	32	0.0000	0.0200	0.0000	1.070	0.00
19	33	0.0007	0.0142	0.0000	1.070	0.00
20	34	0.0009	0.0180	0.0000	1.009	0.00
22	35	0.0000	0.0143	0.0000	1.025	0.00
23	36	0.0005	0.0272	0.0000	1.000	0.00
25	37	0.0006	0.0232	0.0000	1.025	0.00
2	30	0.0000	0.0181	0.0000	1.025	0.00
29	38	0.0008	0.0156	0.0000	1.025	0.00

19	20	0.0007	0.0138	0.0000	1.060	0.00

B. Power and voltage setpoints

All values in Table 26 are given on the same system base MVA. Note that generator 2 is the swing node.

Table 26. Steady-state load and generator data for the 39-bus base case

Bus	Type	Voltage [PU]	Load		Generator		
			MW	MVar	MW	MVar	Unit No.
1	PQ	-	0.0	0.0	0.0	0.0	
2	PQ	-	0.0	0.0	0.0	0.0	
3	PQ	-	322.0	2.4	0.0	0.0	
4	PQ	-	500.0	184.0	0.0	0.0	
5	PQ	-	0.0	0.0	0.0	0.0	
6	PQ	-	0.0	0.0	0.0	0.0	
7	PQ	-	233.8	84.0	0.0	0.0	
8	PQ	-	522.0	176.0	0.0	0.0	
9	PQ	-	0.0	0.0	0.0	0.0	
10	PQ	-	0.0	0.0	0.0	0.0	
11	PQ	-	0.0	0.0	0.0	0.0	
12	PQ	-	7.5	88.0	0.0	0.0	
13	PQ	-	0.0	0.0	0.0	0.0	
14	PQ	-	0.0	0.0	0.0	0.0	
15	PQ	-	320.0	153.0	0.0	0.0	
16	PQ	-	329.0	32.3	0.0	0.0	
17	PQ	-	0.0	0.0	0.0	0.0	
18	PQ	-	158.0	30.0	0.0	0.0	
19	PQ	-	0.0	0.0	0.0	0.0	
20	PQ	-	628.0	103.0	0.0	0.0	
21	PQ	-	274.0	115.0	0.0	0.0	
22	PQ	-	0.0	0.0	0.0	0.0	
23	PQ	-	247.5	84.6	0.0	0.0	
24	PQ	-	308.6	-92.0	0.0	0.0	
25	PQ	-	224.0	47.2	0.0	0.0	
26	PQ	-	139.0	17.0	0.0	0.0	
27	PQ	-	281.0	75.5	0.0	0.0	
28	PQ	-	206.0	27.6	0.0	0.0	
29	PQ	-	283.5	26.9	0.0	0.0	
30	PV	1.0475	0.0	0.0	250.0	-	Gen10
31	PV	0.9820	9.2	4.6	-	-	Gen2
32	PV	0.9831	0.0	0.0	650.0	-	Gen3
33	PV	0.9972	0.0	0.0	632.0	-	Gen4
34	PV	1.0123	0.0	0.0	508.0	-	Gen5
35	PV	1.0493	0.0	0.0	650.0	-	Gen6
36	PV	1.0635	0.0	0.0	560.0	-	Gen7
37	PV	1.0278	0.0	0.0	540.0	-	Gen8
38	PV	1.0265	0.0	0.0	830.0	-	Gen9
39	PV	1.0300	1104.0	250.0	1000.0	-	Gen1

I3. DYNAMIC MODELING INFORMATION OF THE IEEE 39-BUS SYSTEM

A. Generators

Parameters for the two-axis model of the synchronous machines are shown in Table 27. All values are given on the same system base MVA (100MVA).

Table 27. Data of the generator models adopted in the 39-bus system

Unit No.	H	R_a	x'_d	x'_q	x_d	x_q	T'_{do}	T'_{qo}	x_l
1	500.0	0	0.006	0.008	0.02	0.019	7.0	0.7	0.003
2	30.3	0	0.0697	0.170	0.295	0.282	6.56	1.5	0.035
3	35.8	0	0.0531	0.0876	0.2495	0.237	5.7	1.5	0.0304
4	28.6	0	0.0436	0.166	0.262	0.258	5.69	1.5	0.0295
5	26.0	0	0.132	0.166	0.67	0.62	5.4	0.44	0.054
6	34.8	0	0.05	0.0814	0.254	0.241	7.3	0.4	0.0224
7	26.4	0	0.049	0.186	0.295	0.292	5.66	1.5	0.0322
8	24.3	0	0.057	0.0911	0.290	0.280	6.7	0.41	0.028
9	34.5	0	0.057	0.0587	0.2106	0.205	4.79	1.96	0.0298
10	42.0	0	0.031	0.008	0.1	0.069	10.2	0.0	0.0125

B. Excitation control and over-excitation limiter

An excitation control model IEEET1 and an over-excitation limiter model MAXEX1 from the library of PSS/E are adopted. The definitions of the parameters in the IEEET1 and MAXEX1 models can be found in [74].

Table 28. Data of the IEEET1 models adopted in the 39-bus system

Bus ID	T_R	K_A	T_A	V_{RMAX}	V_{RMIN}	K_E	T_E	K_F	T_F	E_1	$S_E(E1)$	E_2	$S_E(E2)$
39	0	5	0.06	1	-1	-0.0485	0.25	0.04	1	0.75	0.08	1.1	0.26
38	0	6.2	0.05	1	-1	-0.633	0.405	0.057	0.5	0.75	0.66	1.1	0.88
37	0	5	0.06	1	-1	-0.0198	0.5	0.08	1	0.75	0.13	1.1	0.34
36	0	5	0.06	1	-1	-0.525	0.5	0.08	1	0.75	0.08	1.1	0.314
35	0	40	0.02	10	-10	1	0.785	0.03	1	0.75	0.67	1.1	0.91
34	0	5	0.02	1	-1	-0.0419	0.471	0.0754	1.246	0.75	0.064	1.1	0.251
33	0	40	0.02	6.5	-6.5	1	0.73	0.03	1	0.75	0.53	1.1	0.74
32	0	5	0.02	1	-1	-0.047	0.528	0.0845	1.26	0.75	0.072	1.1	0.282
31	0	40	0.02	10.5	-10.5	1	1.4	0.03	1	0.75	0.62	1.1	0.85
30	0	40	0.02	10	-10	1	0.785	0.03	1	0.75	0.67	1.1	0.91

Table 29. Data of the MAXEX1 models adopted in the 39-bus system

Bus ID	EFD_{RATED}	EFD_1	$TIME_1$	EFD_2	$TIME_2$	EFD_3	$TIME_3$	EFD_{DES}	K_{MX}	V_{LOW}
30	1	1	1	1.1	1	1.15	1	0.7	1.5	-0.1
32	1	1.5	50	1.2	30	1.3	5	0.7	1.5	-0.1
33	1	1.7	120	1.3	90	1.5	30	0.8	1.5	-0.5
34	1.7	1.2	120	1.3	60	1.5	15	0.8	0.6	-0.2
35	1.6	1.1	100	1.2	50	1.25	15	0.7	1.5	-0.3
36	1.7	1.1	120	1.2	40	1.25	15	0.8	0.6	-0.3
37	1.31	1.2	120	1.3	40	1.5	15	0.8	0.8	-0.1
38	1.3	1.2	120	1.3	40	1.5	15	0.8	0.8	-0.1
39	1.04	1.2	120	1.3	40	1.5	15	0.8	0.6	-0.1

C. LTCs and Shunt capacitor banks

The automatic LTC control model, adopted in the time-domain simulations in this dissertation, is the same model as OLTC1 from the library of PSS/E. The definitions of the parameters in the OLTC1 model can be found in [74]. The time constants of the adopted LTC model vary in different simulation scenarios to differentiate the operation of individual LTCs. The range of the time constants are listed in Table 30.

Table 30. Data of the OLTC1 models adopted in the 39-bus system

Time constant	Definition	Range
T_D	Time constant for triggering control request when the voltage is outside the preselected control band.	20~40 seconds
T_C	Time delay for the operation of tap changer motors	10~20 seconds
T_{SD}	Subsequent delay for sending further signals to the tap changer motor after the first motor operation	10~20 seconds

The automatic shunt capacitor control model, adopted in the time-domain simulations in this dissertation, is the same model as SWCAP from the library of PSS/E. The definitions of the parameters in the SWCAP model can be found in [74]. The time constants of the adopted SWCAP model vary in different simulation scenarios. The range of the time constants are listed in Table 31.

Table 31. Data of the SWCAP models adopted in the 39-bus system

Time constant	Definition	Range

T_D	Time constant for triggering control request when the voltage is outside the preselected control band.	80~140 seconds
T_C	Time delay for the operation of tap changer motors	10~20 seconds
T_{SD}	Subsequent delay for sending further signals to the tap changer motor after the first motor operation	10~20 seconds

D. Turbine governor

A turbine governor model TGOV1 from the library of PSS/E is adopted. The definitions of the parameters in the TGOV1 model can be found in [74].

Table 32. Data of the TGOV1 models adopted in the 39-bus system

Bus ID	R	T_1	V_{MAX}	V_{MIN}	T_2	T_3	D_t
30	0.05	0.4	1	0	1.5	5	0
31	0.05	0.4	1	-0.05	1.5	5	0
32	0.05	0.4	1	-0.05	1.5	5	0
33	0.05	0.4	1	-0.05	1.5	5	0
34	0.05	0.4	1	-0.05	1.5	5	0
35	0.05	0.4	1	-0.05	1.5	5	0
36	0.05	0.4	1	-0.05	1.5	5	0
37	0.05	0.4	1	-0.05	1.5	5	0
38	0.05	0.4	1.2	-0.05	1.5	5	0
39	0.1	0.8	1.5	-0.05	1.5	5	0

APPENDIX II

EXAMPLES OF THE DECENTRALIZED VOLTAGE AND STABILITY CONTROLS ON THE IEEE 39-BUS SYSTEM

The following examples are selected to demonstrate the applications of the decentralized secondary voltage controls in the dynamic environment of the IEEE 39-bus system. Different combinations of disturbances, such as N-1 and N-2 contingencies, generator outages, are simulated to force voltage constraint violations at different buses. Type I utility control (automatic secondary voltage control), type II utility control (manual coordinated voltage control), and OPF based control are compared with the proposed decentralized control in each example.

II.1 TRIP OF LINE 13~14 DURING A PLANNED OUTAGE IN LINE 4~5

A. System Snapshot

Line 4~5 is assumed to be open due to a planned outage for a few days. Line 13~14 is likely to be overloaded, since it is the alternative line feeding power from generator 31 and 32 to load buses 4 and 14. In the system snapshot in Figure 69, the N-1 contingency in line 13~14 causes voltage constraint violations on several buses (including bus 4~9, 12) at 137% loading level. Generators on bus 31 and 32 are assumed to be running at the voltage setpoint of 0.99 p.u.

B. Shift of system conditions from pre- to post-contingency states

Table 33. Comparison of system conditions under pre- to post-contingency conditions.

Conditions	Pre-contingency	Post-contingency
Active power Loss (MW)	82	139
Reactive Power Loss (MVAr)	1848	2861
Stability Margin	34.2%	4.6%
Low Voltage Constraints (p.u.)	None	Bus 5 (0.943), bus 6 (0.948), bus 7 (0.928), bus 8 (0.924), bus 12 (0.945)
Voltage Drop Constraints (p.u.)	None	Bus 5 (0.0577), bus 6 (0.0544), bus 7 (0.0644), bus 8 (0.0718), bus 9 (0.0542)

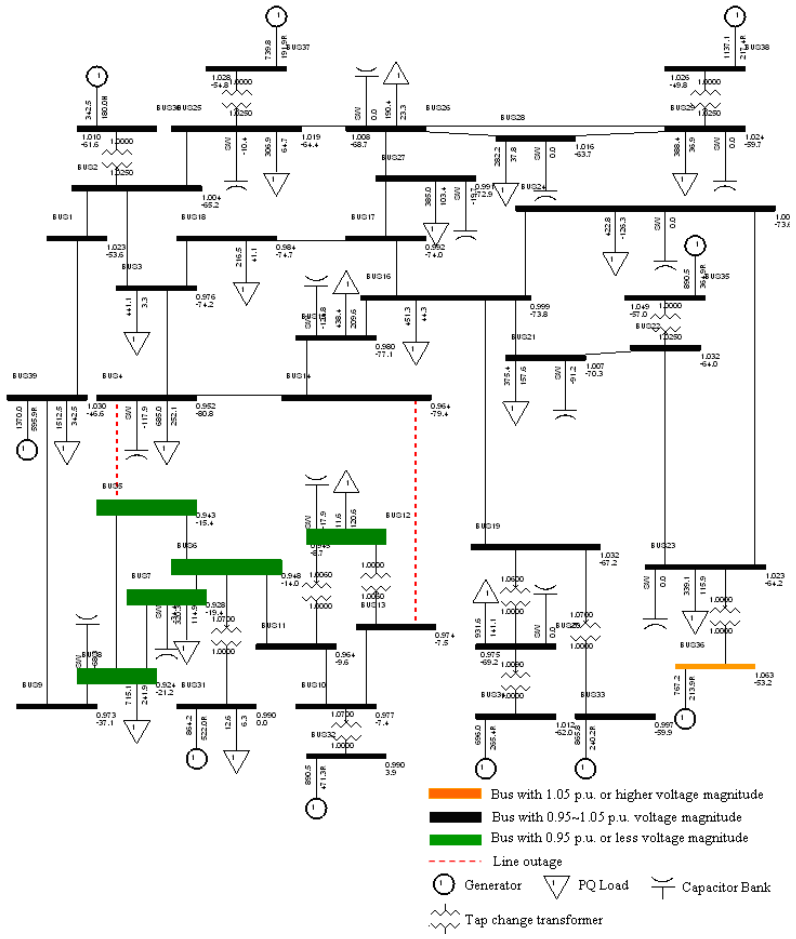

Figure 69. Snapshot of the 39-bus system with double line contingencies in line 4~5 and 13~14.

C. Decentralized Control Sub-system

According to the system decomposition procedure presented in section 4.3.2, a control subsystem (*SUB*) can be constructed as shown in Figure 70. The largest voltage drop is 0.0718 p.u. on bus 8. The buses with voltage violations and the buses with voltage drops more than 30% of the voltage drop on bus 8 include bus 5~13, 31, 32, 39, which should be included in the disturbance-affected zone. A PQ model is applied on bus 39 to represent the external network as seen from bus 2.

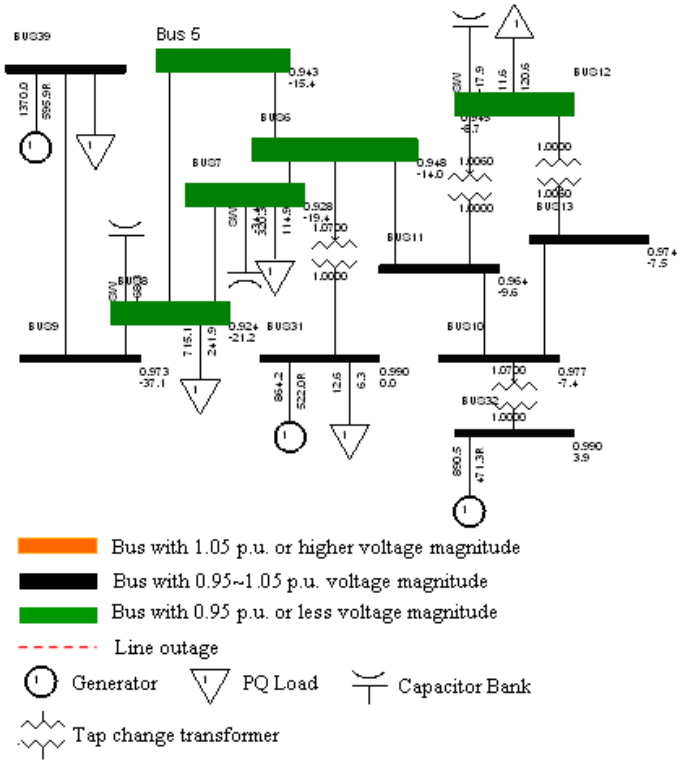

Figure 70. Decentralized voltage and stability control sub-system for case 1.

D. Control Resources in the decentralized control sub-system:

Shunt Capacitor Banks (busID/MVAr: 7/50, 8/60, 12/50 with linearized margin sensitivities;

LTC Transformers: Line 6~31 in the range of 0.90~1.10 p.u. and 0.01 p.u. automatic control step,

Disabled Control Devices: line 10~32 due to generator on bus 32 running at its reactive limit (490 MVAr); line 11~12 and 12~13 due to possible control conflicts and negligible margin sensitivities.

E. Control Objectives:

(1) 10% or higher stability margin, or at least 5.4% increase in stability margin because of the 4.6% remaining stability margin under post-contingency and pre-control condition;

(2) Minimum capacity of the applied shunt capacitor banks;

(3) Minimum MVA line consumption.

(4) Solve all the low voltage and voltage drop constraint violations.

By performing decentralized control optimization on the subsystem in Figure 70, seven Pareto solutions are obtained in 22 seconds. Figure 71 compares the stability margins corresponding to the Pareto solutions evaluated by margin sensitivity calculation and iterative power flow method. One control solution corresponding to 10% or higher post-control stability margin and minimum utilization of control resource will be selected. The details of the control solution are presented in Table 35.

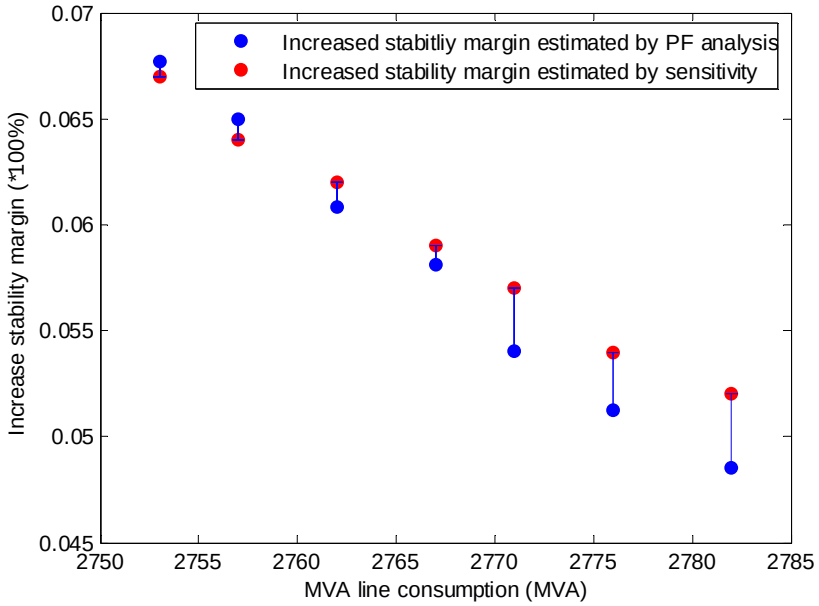

Figure 71. Pareto solutions obtained by the decentralized control system.

F. Comparison of Decentralized control with other control approaches

Conventional secondary voltage control approaches include automatic voltage control (Type I utility control), manually coordinated voltage control (Type II utility control), OPF based voltage and stability control (centralized control). The proposed decentralized voltage and stability control is compared with the conventional control approaches in achieving the control objectives presented in E. The comparison results are listed in Table 34.

Table 34. Comparison of Decentralized control with other control approaches.

Items	Centralized Control Decision	Decentralized Control Decision	Type I Utility Control	Type II Utility Control
Control Solution	Bus 7: +40 MVAr Bus 8: +60 MVAr LTC 6~31: 1.10 p.u.	Bus 7: +40 MVAr Bus 8: +60 MVAr LTC 6~31: 1.10 p.u.	LTC 6~31: 1.085 p.u. Bus 7: +40 MVAr Bus 8: +60 MVAr Bus 12: +10 MVAr	LTC 6~31: 1.10 p.u. LTC 10~32: 1.10 p.u.
Total Applied Shunt Capacitor Banks	90 MVAr	90 MVAr	110 MVAr	0 MVAr

Post-control Voltage Constraints	None	None	Bus 8: 0.947 p.u.	None
Post-control Reactive Loss	2786 MVAr	2786 MVAr	2788 MVAr	2821 MW
Post-control active Loss	135.6 MW	135.6 MW	136.1 MW	136.5 MW
Estimated Control time frame	> 10 minutes	< 100 s	245 s	180 s
Increased Stability Margin	5.4%	5.4%	4.8%	1.7%

The time-evolution of voltage magnitudes on bus 8 (the location of the most severe voltage constraint violation) following different control approaches are shown in Figure 72. The detailed control sequences for different control approaches are explained in Table 35. The step-size of the automatic capacitor controls is assumed to be 10MVAr. The time constants for the shunt capacitor banks are as follows: T_D = 80 seconds, T_{SD} = 20 seconds, T_C = 10~20 seconds. The step-size of the automatic LTC controls is assumed to be 0.01 p.u. The time constants for the LTCs are as follows: T_D = 20 seconds, T_{SD} = 10 seconds, T_C = 20 seconds. The time delays for the automatic capacitors and LTCs controls are set shorter than the practical values to get an optimistic estimation of the control time.

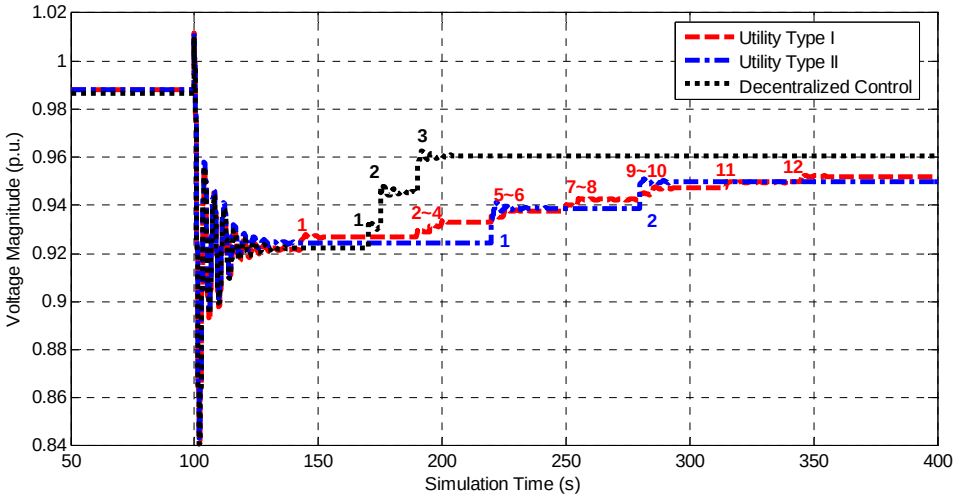

Figure 72. Time-domain voltage magnitudes on bus 8 following Type I and II utility control practices and decentralized control solution (PSS/E simulation).

Table 35. Control sequences according to Type I and II utility control approaches and the proposed decentralized control system. Simulation starts at 0 s, and the contingency occurs at 100 s.

Control Approach	Event ID	Time Frame (s)	Control Action
Type I Utility Control	1	140	LTC 6~31: 1.08 p.u
	2~4	190~200	Bus 7, 8, 12: +10 MVAr
	5~6	220~225	Bus 7, 8: +10 MVAr
	7~8	250~255	Bus 7, 8: +10 MVAr
	9~10	280~285	Bus 7, 8: +10 MVAr
	11	320	Bus 8: +10 MVAr
	12	345	Bus 8: +10 MVAr
Type II Utility Control	1	220	LTC 6~31: 1.10 p.u
	2	280	LTC 10~32: 1.10 p.u.
Decentralized Control Solution	1	170	Bus 7: +40 MVAr
	2	175	Bus 8: +60 MVAr
	3	190	LTC 6~31: 1.10 p.u

1. Type I utility control—automatic secondary voltage controls

Because of the low voltage constraint violation on bus 6, LTC 6~31operates in 0.01 p.u. steps until it reaches the highest position of 1.10 p.u. Shunt capacitor bank on bus 7 and 8 operate after the LTC control by switching on 10MVAr at a time until the voltage

constraint violations are solved. The estimated control time frame is 365 seconds or longer.

2. Type II utility control—manually coordinated voltage controls

In order to solve the emergency low voltage constraint violations on bus 8 (<0.92 p.u.), a system operator will be involved in making control decisions in 5~15 minutes. Assuming the system operator acknowledges the capability of LTC 6~31 in boosting the voltage and stability supports for bus 5~14, the first control decision for the system operator to consider would be to raise the tap position of LTC 6~31 to 1.10 p.u. Additional voltage supports can be obtained by raising the tap position of LTC 10~32, which could be exercised as an alternative mean to capacitor controls. By only tuning the LTC in line 6~31 and 10~32, all existing voltage constraint violations can be solved, and the control of the capacitor banks is minimized. During the dynamic simulation, two minutes time delay is considered for the system operator to collect necessary monitoring data and make control decision. One minute of time delay is considered for the system operator to follow up the impact of the previous control action and make subsequent control decisions. The estimated control time frame is 310 seconds or longer.

3. Decentralized voltage and stability control

From the Pareto solutions shows in Figure 71, a control solution corresponding to 5.4% increases in stability margin is selected, which uses minimum amount of control resources and leads to minimum losses since the solution is picked from the Pareto front. The selected control solution suggests switching on a total of 100 MVAr shunt capacitor

banks on bus 7 and 8, and the increase of 0.03 p.u. tap in LTC 6~31. During the dynamic simulation, a one-minute time delay is considered for the decentralized control system to perform system decomposition, collect local monitoring data, and obtain control solutions. The estimated control time frame is 200 seconds or less, including 60s for data collection and system decomposition, 40s for computation, and 100 for control actuation.

4. OPF based centralized voltage and stability control

An OPF solution can be obtained by adopting the following objective functions and additional constraints:

Objective: (1) Minimum capacity of applied shunt capacitor banks;

(2). Achieve at least the same increased stability margin as the decentralized control solution;

(3) Resolve all the low voltage and voltage drop constraint violations.

The obtained OPF solution is identical to the decentralized control decision except for a much long time delay. The simulation double contingency isolates the disturbance affected zone from the external network. The controls from the external network can not efficiently increase the voltages in the disturbance affected zone. Therefore, the system-wide OPF solution suggests the controls inside the disturbance affected zone to resolve the voltage constraints. Under such special condition, the centralized control solution is identical to the decentralized control solution.

G. Summary

The decentralized voltage and stability control system can generate optimal or suboptimal control decisions in a shorter frame time than all the other control approaches. Both the automatic and coordinated secondary voltage controls lead to unsatisfying stability margin and higher losses. The control solution obtained by the decentralized control system is identical to the solution obtained by system-wide OPF. However, the centralized control solutions are generated in much longer time frame by system-wide OPF, which are usually performed every 10~30 minutes.

II.2 TRIP OF LINE 15~16 DURING A PLANNED OUTAGE OF LOSING 75% GENERATION ON BUS 39

A. System Snapshot

Due to scheduled maintenance, the power plant on bus 39 is only providing 25% of its rated capacity. The lost generation on bus 39 is proportionally compensated by the other generators in the system. At 125% loading level, an N-1 contingency occurs in line 15~16, causing voltage constraint violations in several buses (including bus 4~8, 11~15) and a low load margin of 5.9%. The post-contingency system snapshot is shown in Figure 73.

B. Shift of system conditions from pre- to post-contingency states

Table 36. Comparison of system conditions under pre- to post-contingency conditions.

Conditions	Pre-contingency	Post contingency
Active power Loss (MW)	140.3	176.3
Reactive Power Loss (MVAr)	2623.4	3029.1
Stability Margin	16.8%	5.9%
Low Voltage Constraints (p.u.)	None	Bus 4 (0.926), 5 (0.937), 6 (0.943), 7 (0.929), 8 (0.928), 11 (0.948), 12 (0.929), 13 (0.945), 14 (0.928), 15 (0.896)
Voltage Drop Constraints (p.u.)	None	Bus 15 (0.0929)

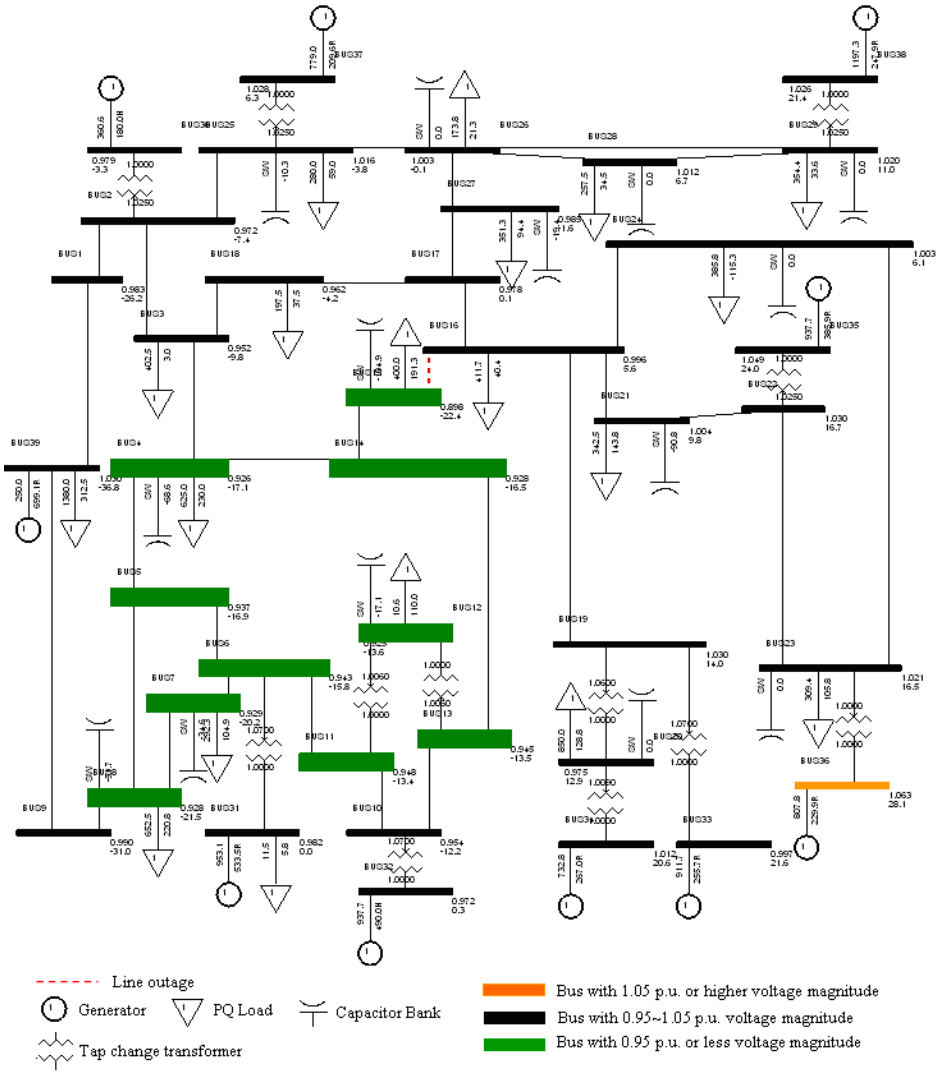

Figure 73. Snapshot of the 39-bus system with the loss of 75% generation in bus 39 and an N-1 contingency in line 15~16.

C. Decentralized Control Sub-system

According to the system decomposition procedure presented in section 4.3.2, a control subsystem (*SUB*) can be constructed as shown in Figure 74. The largest voltage drop is 0.0929 p.u. on bus 15. The buses with voltage violations and the buses with voltage drops more than 30% of the voltage drop on bus 15 include 3~15, 31, 32. PV

models are applied on bus 3 and 9, because of the high disturbance attenuation ratios from bus 4 and 8 to 3 and 9 respectively.

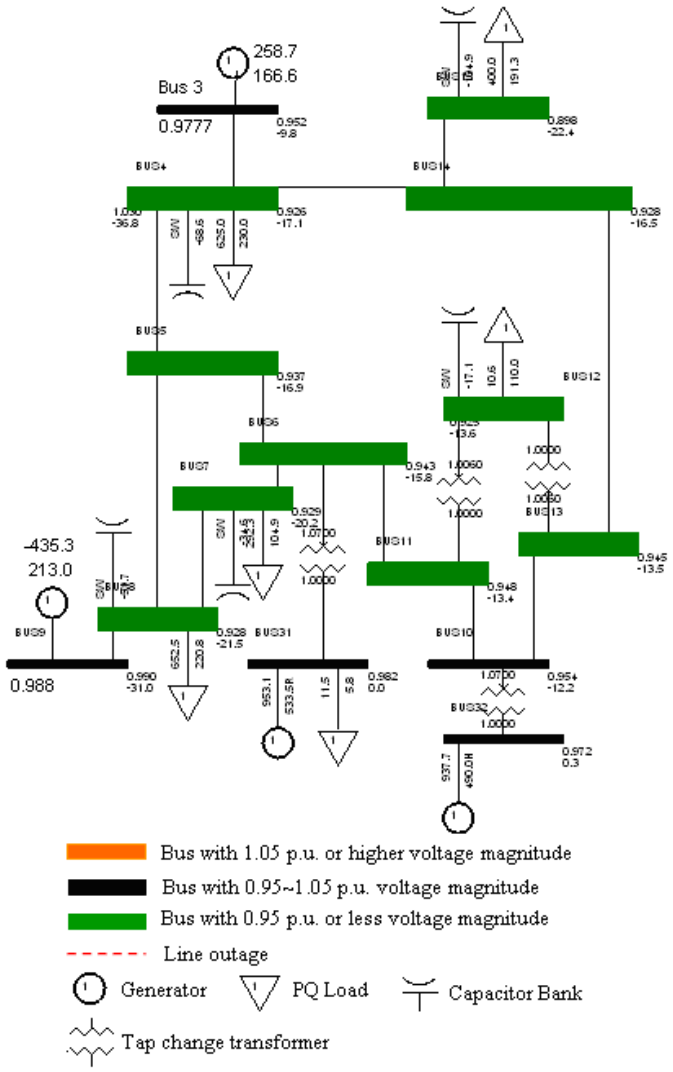

Figure 74. Decentralized voltage and stability control sub-system for case 2.

D. Control Resource in the decentralized control sub-system:

Shunt Capacitor Banks (bus ID/MVAr): 4/80, 7/50, 8/60, 12/50, 15/70 with linearized margin sensitivities;

LTC Transformers: Line 6~31 in the range of 0.90~1.10 p.u. and 0.01 p.u. automatic control step,

Disabled Control Devices: line 10~32 due to generator on bus 32 running close to its reactive limit (2.1 MW margin); line 11~12 and 12~13 due to possible control conflicts and negligible margin sensitivities.

E. Control Objectives:

(1) 10% or higher stability margin, or at least 4.1% increase in stability margin because of the 5.9% remaining stability margin under post-contingency condition;

(2) Minimum capacity of applied shunt capacitor banks;

(3) Minimum MVA line consumption.

(4) Resolve all the low voltage and voltage drop constraint violations.

By performing decentralized control optimization on the subsystem in Figure 74, 24 Pareto solutions are obtained in 26 seconds (for computation only). Figure 75 compares the stability margins corresponding to the Pareto solutions evaluated by margin sensitivity calculation and iterative power flow method.

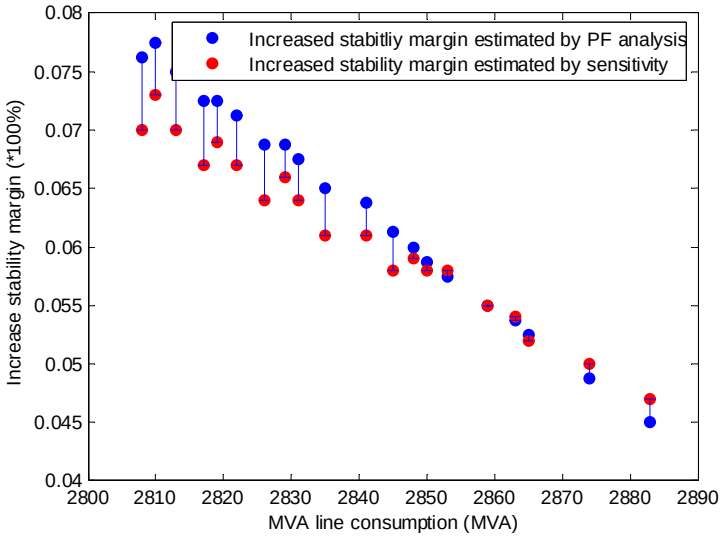

Figure 75. Pareto solutions obtained by the decentralized control system.

F. Comparison of Decentralized control with other control approaches

Conventional secondary voltage control approaches include automatic voltage control (Type I utility control), manually coordinated voltage control (Type II utility control), OPF based voltage and stability control (centralized control). The proposed decentralized voltage and stability control is compared with the conventional control approaches in achieving the control objectives presented in E. The detailed comparison results are listed in Table 37.

Table 37. Comparison of Decentralized control with other control approaches.

Items	Centralized Control Decision	Decentralized Control Decision	Type I Utility Control	Type II Utility Control
Control Solution	Bus 4: +60 MVAr Bus 15: +70 MVAr LTC 6~31: 1.10 p.u.	Bus 4: +80 MVAr Bus 15: +60 MVAr LTC 6~31: 1.10 p.u.	LTC 11~12: 1.056 p.u. LTC 12~13: 1.016 p.u. LTC 6~31: 1.09 p.u. Bus 4: +20 MVAr Bus 7: +20 MVAr Bus 8: +20 MVAr Bus 15: +60 MVAr	LTC 6~31: 1.10 p.u. LTC 10~32: 1.10 p.u. Bus 8: +10 MVAr Bus 15: +40 MVAr
Total Applied Shunt	130 MVAr	140 MVAr	120 MVAr	50 MVAr

Capacitor Banks				
Post-control Voltage Constraints	None	None	None	None
Post-control Reactive Loss	2886.1 MVAr	2886.2 MVAr	2957.3 MVAr	2971.6 MW
Post-control active Loss	169.3 MW	169.1 MW	172.5 MW	172.3 MW
Estimated Control time frame	> 10 minutes	< 100 s	265 s	260 s
Increased Stability Margin	4.12%	4.25%	3.40%	1.90%

The time-evolution voltage magnitudes on bus 15 (the location of the most severe voltage constraint violation) following different control approaches are shown in Figure 72. The detailed control sequences for different control approaches are explained in Table 35. The step-size of the automatic capacitor controls is assumed to be 10MVAr. The time constants for the shunt capacitor banks are as follows: T_D = 100 seconds, T_{SD} = 20 seconds, T_C = 10~40 seconds. The step-size of the automatic LTC controls is assumed to be 0.01 p.u. The time constants for the LTCs are as follows: T_D = 20 seconds, T_{SD} = 0 seconds, T_C = 16s.

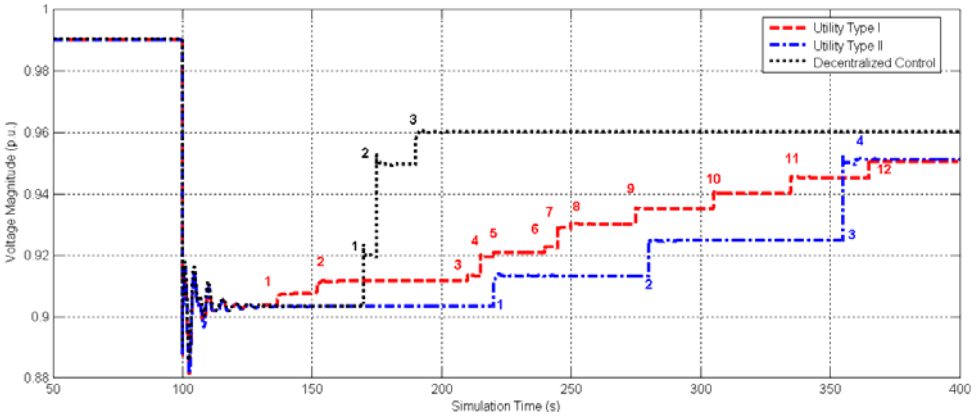

Figure 76. Time-domain voltage magnitudes on bus 15 following Type I and II utility control practices and decentralized control solution (PSS/E simulation).

Table 38. Control sequences according to Type I and II utility control approaches and the proposed decentralized control system. Simulation starts at 0 s, and the contingency occurs at 100 s.

Control Approach	Event ID	Time Frame (s)	Control Action
Type I Utility Control	1	136.6	LTC 6~31: 1.080 p.u
	2	152.2	LTC 6~31: 1.090 p.u
	3	210.0	Bus 4: +10 MVAr
	4	215.0	Bus 7: +10 MVAr Bus 15: +10 MVAr
	5	220.0	Bus 8: +10 MVAr
	6	240.0	Bus 4: +10 MVAr
	7	245.0	Bus 7: +10 MVAr Bus 15: +10 MVAr
	8	250.0	Bus 8: +10 MVAr
	9	275.0	Bus 15: +10 MVAr
	10	305.0	Bus 15: +10 MVAr
	11	335.0	Bus 15: +10 MVAr
	12	365.0	Bus 15: +10 MVAr
Type II Utility Control	1	220	LTC 6~31: 1.10 p.u
	2	280	LTC 10~32: 1.10 p.u.
	3	355	Bus 15: +40 MVAr
	4	360	Bus 8: +10 MVAr
Decentralized Control Solution	1	180	Bus 4: +80 MVAr
	2	185	Bus 15: +60 MVAr
	3	190	LTC 6~31: 1.10 p.u

1. Type I utility control—automatic secondary voltage controls

Because of the low voltage constraint violation on bus 6, LTC 6~31operates in 0.01 p.u. steps until reaching 1.09 p.u when the voltage constraint violation in bus 6 disappears. Shunt capacitor bank on bus 7 and 8 operate after the LTC control by switch on 10MVAr at a time until the voltage constraint violations are solved. The estimated control time frame is 365 seconds or longer. The added stability margin by the voltage controls is 4.5% according to the off-line iterative power flow analysis.

2. Type II utility control—manually coordinated voltage controls

In order to solve the emergency low voltage constraint violations on bus 15 (<0.92 p.u.), a system operator will be involved in making control decisions in 15 minutes. By tuning the tap changers in 6~31 and 10~32 to their upper limit of 1.10 p.u. (similar situation as example 1), as well as switching on 10 MVAr and 40 MVAr shunt capacitor banks on bus 8 and 15, all the voltage constraint violations in the 39-bus system disappear. The amount of applied shunt capacitor bank on bus 8 and 15 is decided by monitoring the voltage magnitudes on these two buses. During the dynamic simulation, two minutes time delay is considered for the system operator to collect necessary monitoring data and make control decision. A one-minute time delay is considered for the system operator to follow up the impact of the previous control action and make subsequent control decisions. The estimated control time frame is 310 seconds or longer. The estimated control time frame is 310 seconds or longer, while the increased stability margin is 2.4%.

3. Decentralized voltage and stability control

From the Pareto solutions shows in Figure 71, a control solution corresponding to a 4.91% increase in stability margin is selected, which uses minimum amount of control resources and leads to minimum losses since the solution is picked from the Pareto front. The selected control solution suggests switching on a total of 150 MVAr shunt capacitor banks on bus 7, 8, 12, 15, and increasing 0.03 p.u. tap in LTC 6~31. During the dynamic simulation, a one-minute time delay is considered for the decentralized control system to perform system decomposition, collect local monitoring data, and obtain control solutions. At 150 seconds, the selected control solution is executed in the form of batched

control actions in 5s intervals. The estimated control time frame is 200 seconds or less, including 60s for data collection and system decomposition, 40s for computation, and 100 for control actuation.

4. OPF based centralized voltage and stability control

An OPF solution can be obtained by adopting the following objective functions and additional constraints:

Objective: (1) Minimum capacity of applied shunt capacitor bank;

(2). Achieve at least the same increased stability margin as the decentralized control solution;

(3) Resolve all the low voltage and voltage drop constraints.

The obtained OPF solution leads to 10 MVAr less of utilized capacitor bank and achieves the exact expected 4.1% increase in stability margin. Although the resulting active losses is 0.2 MW higher than the decentralized control, the saved reactive resource could be helpful towards future stability problems.

G. Summary

The decentralized voltage and stability control system can generate optimal or suboptimal control decisions in a shorter frame time than all the other control approaches. Both the automatic and coordinated secondary voltage controls lead to unsatisfying stability margin and higher losses. Because the utility controls do not recognized the needs for stability controls, only limited control resources are utilized to increase voltages.

The control solution obtained by the decentralized control system is similar to the solution obtained by system-wide OPF. Because the proposed decentralized control system only generate sparsely distributed control solutions based on local system information, the performance of the decentralized control solutions falls shortly behind centralized control solutions. When the expectations on control objectives are specified, a centralized control solution can more accurately meet the control requirements without utilizing additional control resources. According to the example in this section, the centralized controls saved 10 MVAr reactive reserves compared with the decentralized control. However, the centralized control solutions are generated in much longer time frame by system-wide OPF, which are usually performed every 10~30 minutes.

II.3 TRIP OF LINE 16~17 DURING A PLANNED OUTAGE OF LOSING 100% GENERATION ON BUS 38

A. System Snapshot

Due to scheduled maintenance, the power plant on bus 38 is shunt down. The lost generation on bus 38 is proportionally compensated by the other generators in the system. In order to boost the voltage support for buses 6~13, LTC 6~31 is tapped to 1.10 p.u. At 116% loading level, an N-1 contingency occurs in line 16~17, causing voltage constraint violations in several buses (including bus 17, 18, 26~29, 38) and a low load margin of 3.0%. The post-contingency system snapshot is shown in Figure 77.

B. Shift of system conditions from pre- to post-contingency states

Table 39. Comparison of system conditions under pre- to post-contingency conditions.

Conditions	Pre-contingency	Post contingency
Active power Loss (MW)	75.4	125.8
Reactive Power Loss (MVAr)	1684	2378
Stability Margin	22.7%	3.0 %
Low Voltage Constraints (p.u.)	None	Bus 17 (0.941), 18 (0.947), 26 (0.934), 27 (0.930), 28 (0.913), 29 (0.913), 38 (0.913)
Voltage Drop Constraints (p.u.)	None	Bus 17 (0.0801), 18 (0.0757), 26 (0.0829), 27 (0.0820), 28 (0.0927), 29 and 38 (0.0931)

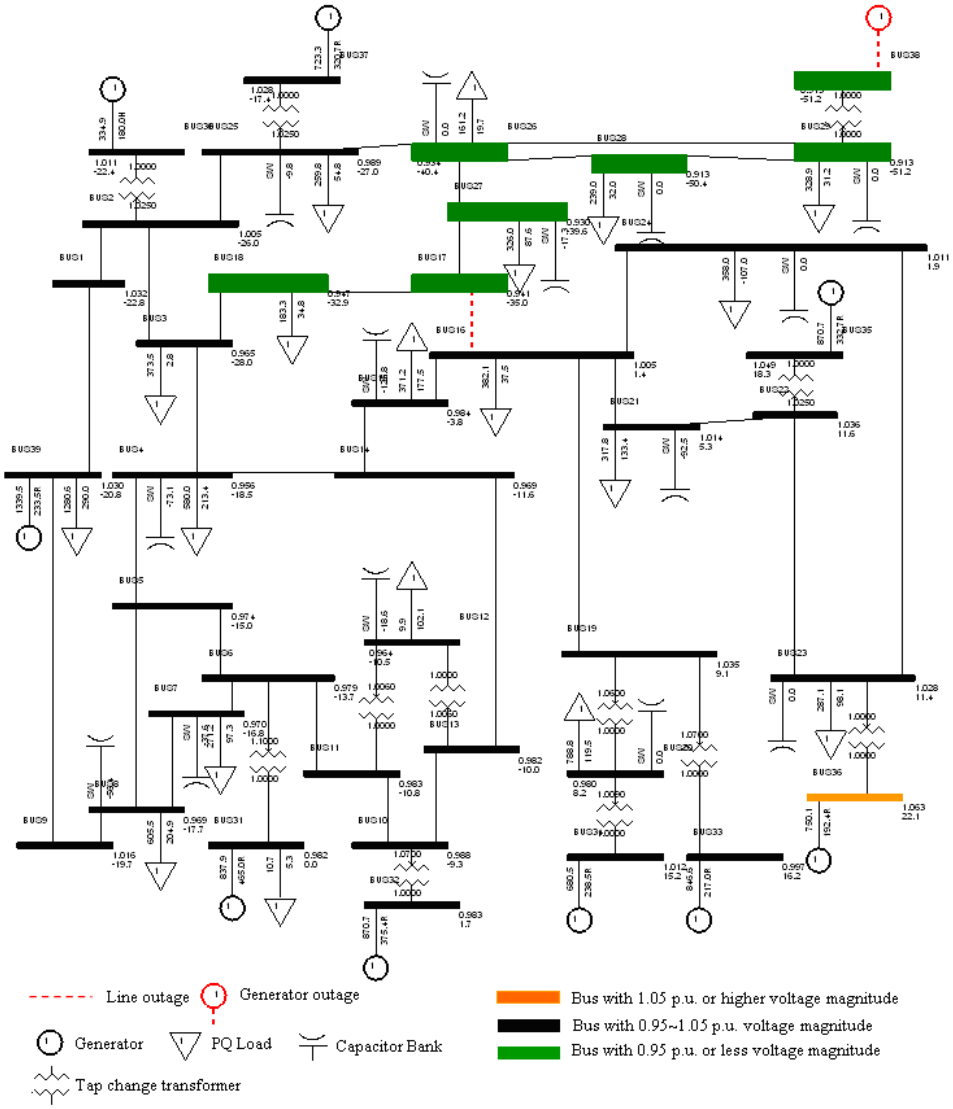

Figure 77. Snapshot of the 39-bus system with the loss of 100% generation in bus 38 and an N-1 contingency in line 16~17.

C. Decentralized Control Sub-system

According to the system decomposition procedure presented in section 4.3.2, a control subsystem (*SUB*) can be constructed as shown in Figure 78. The largest voltage drop is 0.0931 p.u. on bus 29. The buses with voltage violations and the buses with

voltage drops more than 50% of the voltage drop on bus 29 include bus 2~4, 14, 17~18, 25~29, 38. Using 40% or 30% as the threshold to define the buses affected by the disturbance will lead to the coverage of much larger area, which will reduce the flexibility of the decentralized control system. A PV model is placed on bus 5 to represent the external network as seen from bus 4, because of the large attenuation ratio from bus 4 to 5 (1.39). Bus 14 is represented as a PQ model to represent the external network as seen from bus 14, because of the small attenuation ratio from bus 4 to 14 (1.13). Bus 1 is represented as a PV model and integrated with PV bus 30 to represent the external network as seen from bus 2, because of the large attenuation ratio from bus 2 to 1 (26.0).

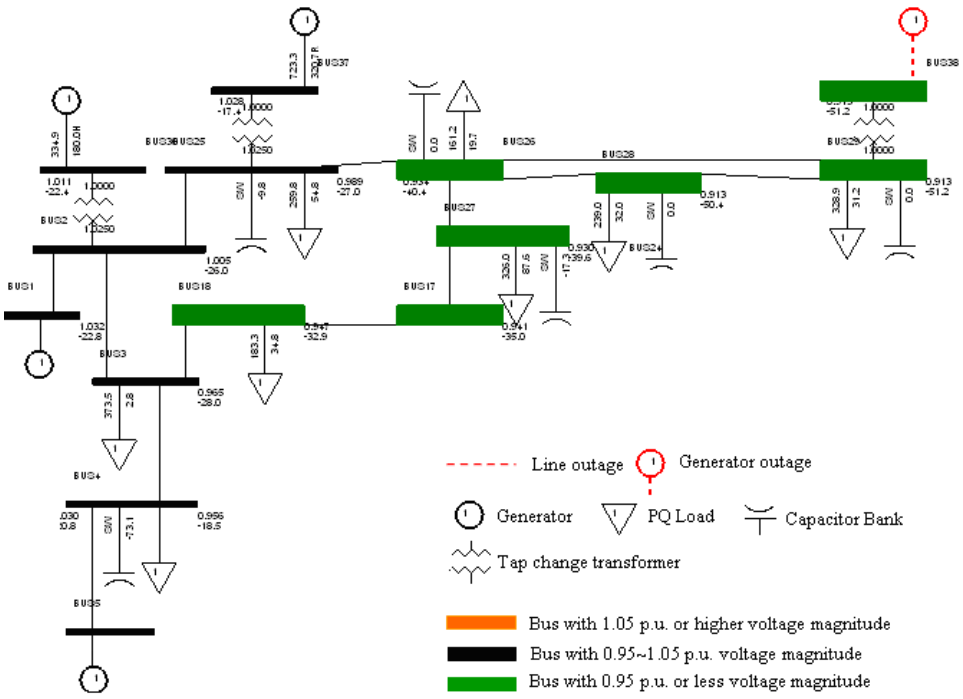

Figure 78. Decentralized voltage and stability control sub-system.

D. Control Resource in the decentralized control sub-system:

Shunt Capacitor Banks (busID/MVAr): 4/80, 25/110, 27/110, 28/10, 29/30 with linearized margin sensitivities;

LTC Transformers: line 29~38 fixed at 1.00 p.u. position;

Disabled Control Devices: The control of LTC 2~30 is locked due to generator on bus 30 running at its reactive limit (180 MVAr). The control of LTC 25~37 is locked due the highly nonlinear margin sensitivity.

E. Control Objectives:

(1) 10% or higher stability margin, or at least 7.0% increase in stability margin because of the 3.0% stability margin under post-contingency condition.

(2) Minimum capacity of applied shunt capacitor bank;

(3) Minimum MVA line consumption.

(4) Resolve all the low voltage and voltage drop constraints.

By performing decentralized control optimization on the subsystem in Figure 78, 19 Pareto solutions are obtained in 24 seconds. Figure 79 compares the stability margins corresponding to the Pareto solutions evaluated by the margin sensitivity calculation and the iterative power flow method.

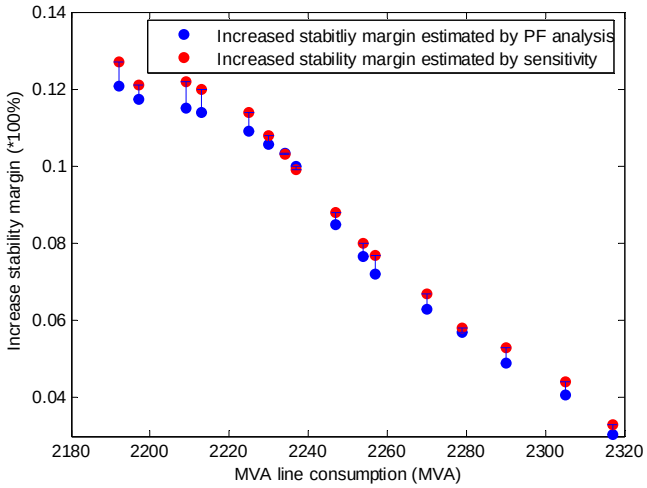

Figure 79. Pareto solutions obtained by the decentralized control system.

F. Comparison of Decentralized control with other control approaches

Conventional secondary voltage control approaches include automatic voltage control (Type I utility control), manually coordinated voltage control (Type II utility control), OPF based voltage and stability control (centralized control). The proposed decentralized voltage and stability control is compared with the conventional control approaches in achieving the control objectives presented in E. The detailed comparison results are listed in Table 40.

Table 40. Comparison of Decentralized control with other control approaches.

Items	Centralized Control Decision	Decentralized Control Decision	Type I Utility Control	Type II Utility Control
Control Solution	Bus 25: +10 MVAr Bus 27: +110 MVAr Bus 28: +10 MVAr Bus 29: +30 MVAr	Bus 25: +20 MVAr Bus 27: +110 MVAr Bus 28: +10 MVAr Bus 29: +30 MVAr	Bus 27: +10 MVAr Bus 28: +10 MVAr Bus 29: +20 MVAr	Bus 28: +10 MVAr Bus 29: +30 MVAr
Total Applied Shunt Capacitor Banks	160 MVAr	170 MVAr	40 MVAr	40 MVAr
Post-control Voltage Constraints	None	None	None	None

Post-control Reactive Loss	2241 MVAr	2237 MVAr	2319 MVAr	2318 MW
Post-control active Loss	116.5 MW	116.1 MW	121.5 MW	121.4 MW
Estimated Control time frame	> 10 minutes	< 100 s	150 s	140 s
Increased Stability Margin	7.0%	7.4%	2.0%	2.1%

The time-evolution voltage magnitudes on bus 29 (the location of the most severe voltage constraint violation) following different control approaches are shown in Figure 80. The detailed control sequences for different control approaches are explained in Table 41. The step-size of the automatic capacitor controls is assumed to be 10MVAr. The time constants for the shunt capacitor banks are as follows: T_D = 100 seconds, T_{SD} = 30 seconds, T_C = 10~20 seconds.

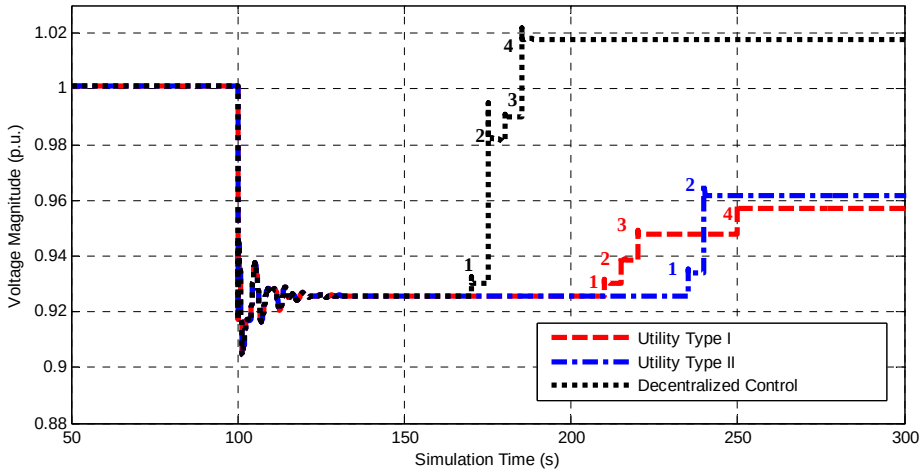

Figure 80. Time-domain voltage magnitudes on bus 29 following Type I and II utility control practices and decentralized control solution (PSS/E simulation).

Because Type I and II utility controls do not aim at increasing stability margin, the utilization of control resource is less than decentralized or centralized controls (40

MVAr vs. 160 MVAr). The decentralized and centralized controls resolved both voltage and stability requirements by utilizing minimum amount of control resource. System operators can choose other control solutions from Figure 79 to obtain more stability margin.

Table 41. Control sequences according to Type I and II utility control approaches and the proposed decentralized control system. Simulation starts at 0 s, and the contingency occurs at 100 s.

Control Approach	Event ID	Time Frame (s)	Control Action
Type I Utility Control	1	210	Bus 27: +10 MVAr
	2	215	Bus 28: +10 MVAr
	3	220	Bus 29: +10 MVAr
	4	250	Bus 29: +10 MVAr
Type II Utility Control	1	235	Bus 28: +10 MVAr
	2	240	Bus 29: +30 MVAr
Decentralized Control Solution	1	170	Bus 25: +30 MVAr
	2	175	Bus 27: +110 MVAr
	3	180	Bus 28: +10 MVAr
	4	185	Bus 29: +30 MVAr

1. Type I utility control—automatic secondary voltage controls

Because of the low voltage constraint violations on bus 27, 28 29 under post-contingency condition, 10MVAr of shunt capacitor bank on these three buses will be switched on automatically after fixed time delays of 110 seconds, 115s, 120 seconds respectively. Additional 10MVAr shunt capacitor bank will be switched on bus 29 after 30 seconds of subsequent delay to boost the voltage magnitude on bus 29 to be above 0.95 p.u. The estimated total control time frame is 250 seconds. The added stability margin by the voltage controls is 2.0% according to the off-line iterative power flow analysis.

2. Type II utility control—manually coordinated voltage controls

In order to solve the emergency low voltage constraint violations on bus 29 (<0.92 p.u.), a system operator will be involved in making control decisions in 15 minutes. Assuming no applicable control manual is available, the system operator has to evaluate the severity of the disturbance and assess control actions one after another until all voltage constraint violations are solved. Utilities such as PJM requires as long as 5~15 minutes to handle emergency low voltage constraint violations. Since the emergency low-voltage constraint violations are located on bus 28 and 29, it is reasonable for a system operator to switch on available shunt capacitor banks on bus 28 and 29 as the first control option to exercise. During the dynamic simulation, a two-minute time delay is considered for the system operator to collect necessary monitoring data and make control decision. After the switching of the shunt capacitor banks on bus 28 and 29 at 235 and 240 seconds, the post-contingency voltage constraint violations are solved. The increase in stability margin is 2.1%.

3. Decentralized voltage and stability control

From the Pareto solutions shows in Figure 71, a control solution corresponding to 7.7% increases in stability margin is selected, which uses minimum amount of control resources and leads to minimum losses since the solution is picked from the Pareto front. The selected control solution suggests switching on a total of 170 MVAr shunt capacitor banks on bus 25, 27, 28, 29. During the dynamic simulation, a one-minute time delay is considered for the decentralized control system to perform system decomposition, collected local monitoring data, and obtain control solutions. At 160 seconds, the selected

control solution is executed in the form of batched control actions. The estimated control time frame is 200 seconds or less, including 60s for data collection and system decomposition, 40s for computation, and 100 for control actuation.

4. OPF based centralized voltage and stability control

An OPF solution can be obtained by adopting the following objective functions and additional constraints:

Objective: (1) Minimum capacity of applied shunt capacitor bank;

(2).Achieve at least the same increased stability margin as the decentralized control solution;

(3) Resolve all the low voltage and voltage drop constraint violations.

The obtained OPF solution leads to 10 MVAr less of utilized capacitor bank and achieves the exact expected 7.0% increase in stability margin. Although the resulting active losses is 0.4 MW higher than the decentralized control, the saved reactive resource could be helpful towards future stability problems.

G. Summary

The decentralized voltage and stability control system can generate optimal or suboptimal control decisions in a shorter frame time than all the other control approaches. Both the automatic and coordinated secondary voltage controls lead to unsatisfying stability margin and higher losses. The control solution obtained by the decentralized control system is similar to the solution obtained by system-wide OPF. Because the proposed decentralized control system only generate sparsely distributed control

solutions based on local system information, the performance of the decentralized control solutions falls shortly behind centralized control solutions. When the expectations on control objectives are specified, a centralized control solution can more accurately meet the control requirements without utilizing additional control resources. According to the example in this section, the centralized controls saved 10 MVAr reactive reserves compared with the decentralized control. However, the centralized control solutions are generated in much longer time frame by system-wide OPF, which are usually performed every 10~30 minutes.

II.4 OPTIMAL VOLTAGE CONTROL TO SOLVE THE VOLTAGE CONSTRAINT VIOLATIONS CAUSED BY THE CONTINGENCY IN LINE 2~3 WHEN GENERATOR 35 IS OUT OF SERVICE

A. System Snapshot

To reduce the risk and severity of the contingency in line 21~22, the system operator decides to take the generator on bus 35 out of service based on a day-ahead security study. The loss of generation on bus 35 will be proportionally compensated by all the other generators in the system according to their committed generation capacities. During the peak hours, the load in the 39-bus system increases to 135% of the base load level, at which point the off-line contingency analysis indicates that the contingency in line 2~3 would cause normal low-voltage constraint violations on bus 3, 4, 7, 8, 18, and 27. The post-contingency stability margin is 11.6%, which is higher than the 5% minimum allowable stability margin for N-1 contingencies. The post-contingency system snapshot is shown in Figure 81.

B. Shift of system conditions from pre- to post-contingency states

Table 42. Comparison of system conditions under pre- to post-contingency conditions.

Conditions	Pre-contingency	Post contingency
Active power Loss (MW)	94.1	120.4
Reactive Power Loss (MVAr)	1961	2433
Stability Margin	25.5%	11.6%
Low Voltage Constraints (p.u.)	None	Bus 3 (0.940), 4 (0.940), 7 (0.949), 8 (0.948), 18 (0.944), 27 (0.942)
Voltage Drop Constraints (p.u.)	None	Bus 3 (0.0552)

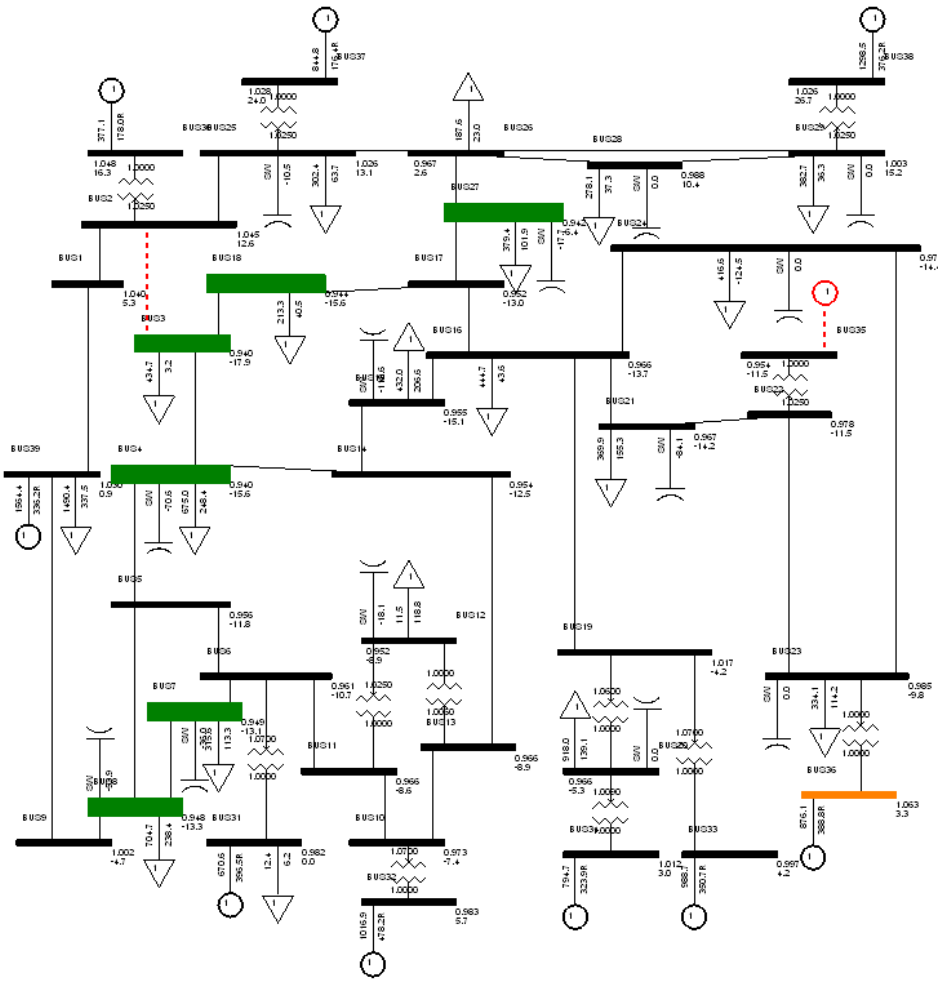

Figure 81. Snapshot of the 39-bus system with the loss of 100% generation in bus 35 and an N-1 contingency in line 2~3.

C. Decentralized Control Sub-system

According to the system decomposition procedure presented in section 4.3.2, a control subsystem (*SUB*) can be constructed as shown in Figure 82. The largest voltage drop is 0.0552 p.u. on bus 3. The buses with voltage violations and the buses with voltage drops more than 50% of the voltage drop on bus 3 include bus 3~9, 14~18, 26~27, 31. Using 40% or 30% as the threshold to identify the disturbance affected buses will lead to

the coverage of much larger area, which will reduce the flexibility of the decentralized control system. A PV model is placed on bus 9 to represent the external network as seen from bus 8, because of the large attenuation ratio from bus 8 to 9 (1.71). Bus 14 is represented as a PQ model to represent the external network as seen from bus 4, because of the small attenuation ratio from bus 4 to 14 (1.26). VC models are placed on bus 16 and 26 to represent the external network as seen from bus 15 and 27.

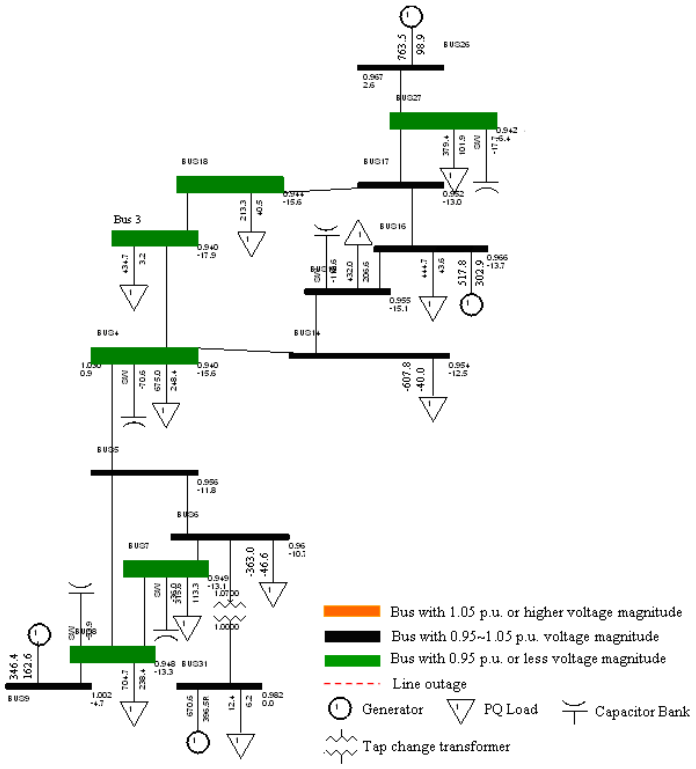

Figure 82. Decentralized voltage and stability control sub-system.

D. Control Resource in the decentralized control sub-system:

Shunt Capacitor Banks (busID/MVAr): 4/80, 7/50, 8/60, 15/70, 27/110 with linearized margin sensitivities;

LTC Transformers: Line 6~31 in the range of 0.90~1.10 p.u. and 0.01 p.u. automatic control step,

E. Control Objectives:

(1) Minimum capacity of the applied shunt capacitor bank;

(2) Minimum apparent-power losses;

(3) Minimum changes in the tap positions of the LTCs;

(4) Solve all the low voltage and voltage drop constraints.

By performing decentralized control optimization on the subsystem in Figure 78, 35 Pareto solutions are obtained in 90 seconds.

Figure 83 compares the objective values corresponding to the Pareto solutions obtained by the solving a multiple-objective optimal control problem.

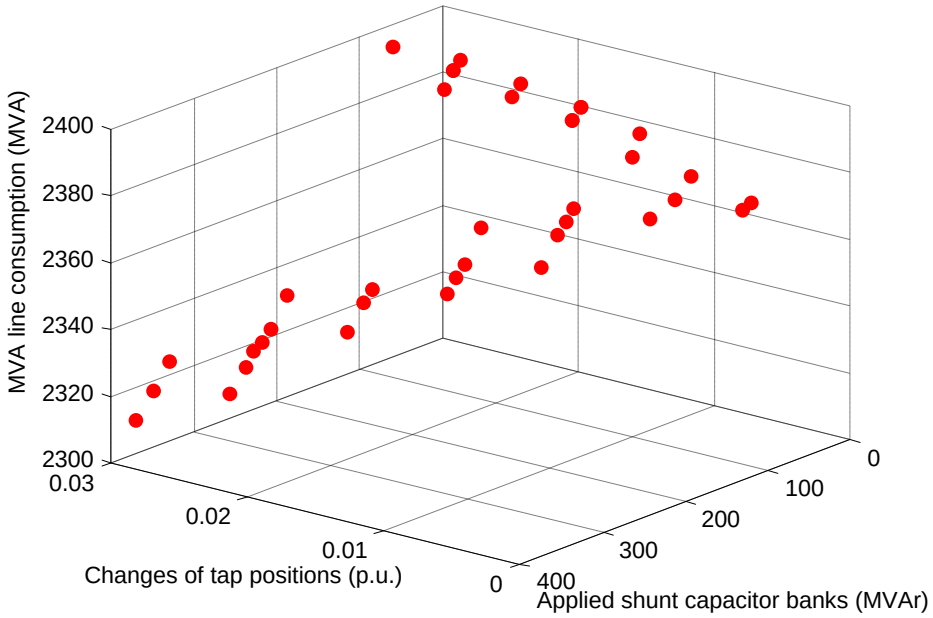

Figure 83. Pareto solutions obtained by the decentralized control system.

F. Comparison of Decentralized control with other control approaches

Conventional secondary voltage control approaches include automatic voltage control (Type I utility control), manually coordinated voltage control (Type II utility

control), OPF based voltage and stability control (centralized control). The proposed decentralized voltage and stability control is compared with the conventional control approaches in achieving the control objectives presented in E. The detailed comparison results are listed in Table 43.

Table 43. Comparison of Decentralized control with other control approaches.

Items	Centralized control decision / Type II Utility control	Decentralized control decision	Type I Utility control
Control Solution	LTC 6~31: +0.01 p.u. Bus 4: +40 MVAr Bus 27: +50 MVAr	LTC 6~31: +0.01 p.u. Bus 4: +80 MVAr Bus 7: +10 MVAr	Bus 4: +50 MVAr Bus 7: +20 MVAr Bus 8: +20 MVAr Bus 27: +50 MVAr
Total applied shunt capacitor banks	90 MVAr	90 MVAr	140 MVAr
Post-control voltage constraints	None	None	None
Post-control reactive loss	2400 MVAr	2402 MVAr	2384 MVAr
Post-control active loss	118.2 MW	118.7 MW	117.8 MW
Estimated control timeline	>10 minutes	< 270 s	360 s
Increased stability margin	2.0%	2.1%	2.5%

The time-evolution voltage magnitudes on bus 4 (the location of the most severe voltage constraint violation) following different control approaches are shown in Figure 84. The detailed control sequences for different control approaches are explained in Table 44. The step-size of the automatic capacitor controls is assumed to be 10MVAr. The time constants for the shunt capacitor banks are as follows: T_D = 110~140 seconds, T_{SD} = 30 seconds, T_C = 10 seconds.

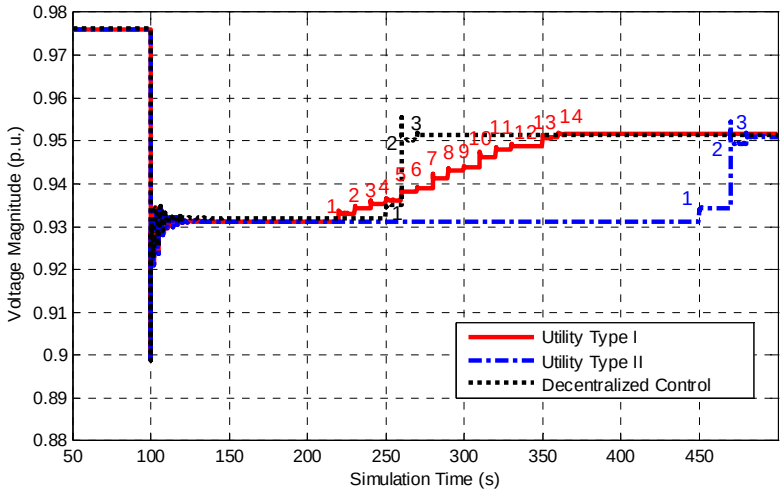

Figure 84. Time-domain voltage magnitudes on bus 29 following Type I and II utility control practices and decentralized control solution (PSS/E simulation).

Table 44. Control sequences according to Type I and II utility control approaches and the proposed decentralized control system. Simulation starts at 0 s, and the contingency occurs at 100 s.

Control approach	Event ID	Time frame (s)	Control action
Type I Utility control	1	220	Bus 4: +10 MVAr
	2	230	Bus 7: +10 MVAr
	3	240	Bus 8: +10 MVAr
	4	250	Bus 27: +10 MVAr
	5	260	Bus 4: +10 MVAr
	6	270	Bus 7: +10 MVAr
	7	280	Bus 8: +10 MVAr
	8	290	Bus 27: +10 MVAr
	9	300	Bus 4: +10 MVAr
	10	310	Bus 27: +10 MVAr
	11	320	Bus 4: +10 MVAr
	12	330	Bus 27: +10 MVAr
	13	350	Bus 4: +10 MVAr
	14	360	Bus 27: +10 MVAr
Type II Utility control	1	450	LTC 6~31: 1.08 p.u.
	2	470	Bus 4: +40 MVAr
	3	480	Bus 27: +50 MVAr
Decentralized control solution	1	250	LTC 6~31: 1.08 p.u.
	2	260	Bus 4: +80 MVAr
	3	270	Bus 7: +10 MVAr

1. Type I utility control—automatic secondary voltage controls

Because of the low-voltage constraint violations on bus 4, 7, 8, 27 under post-contingency condition, 10MVAr of shunt capacitor bank on these three buses will be switched on automatically during 120 seconds to 150 seconds according to their time constants. Additional 10MVAr shunt capacitor bank will be switched on these four buses after subsequent time delays during 260 seconds to 290 seconds. Additional 30MVAr shunt capacitor banks are switched on bus 4 and 27 respectively during 300 seconds~360 seconds to solve the low-voltage constraint violations on these two buses. The estimated control timeline for type I utility control is 360 seconds. The added stability margin by the voltage controls is 2.0% according to the off-line iterative power flow analysis.

2. Type II utility control—manually coordinated voltage controls

In order to solve the normal low-voltage constraint violations (0.92~0.95 p.u.) on multiple buses (bus 3, 4, 7, 8, 18, 27), a system operator will be involved in making control decisions in 15 minutes. Assuming no applicable control manual is available, the system operator could wait for the next round of OPF to decide a system-wide optimal-control solution when no immediate voltage stability issue has been discovered.

An OPF solution can be obtained by adopting the following objective functions and additional constraints:

Objective: (1) Minimum total MVA line consumption;

(2) Resolve all the low voltage and voltage drop constraints.

Additional constraints besides the equality and inequality constraints:

(1) The amount of applied shunt capacitor bank is no more than the decentralized control solution;

(2) The total amount of tap changes in the LTCs is no more than the decentralized control solution.

During the dynamic simulation, the OPF control solution is executed during 450 seconds to 480 seconds, which is shorter than the typical 10~15 minutes timeline of the OPF function. The obtained OPF solution is similar to the decentralized control decision in achieving control objectives, but demands much longer time for control evaluation.

3. Decentralized voltage and stability control

From the Pareto solutions shows in Figure 83, a control solution corresponding to minimum capacitor and LTC controls is selected, which also leads to minimum losses since the solution is picked from the Pareto front. The selected control solution suggests switching on a total of 80 and 10 MVAr shunt capacitor banks on bus 4 and 7 respectively, while increase 0.01 p.u. of tap position on LTC 6~31. During the dynamic simulation, 150 seconds of time delay is considered for the decentralized control system to perform system decomposition, collected local monitoring data, and obtain control solutions. After 150 seconds, the selected control solution is executed in the form of batched control actions. The estimated control time is 270 seconds.

G. Summary

The decentralized voltage and stability control system can generate optimal or suboptimal control decisions in a shorter frame time than all the other control approaches. The

automatic secondary voltage controls (Type I utility control) lead to 50 MVAr additional utilization of reactive resources compared with the decentralized and centralized controls. The control time of Type I utility controls is 90 seconds longer than the decentralized controls. Although Type I utility controls lead to more loss reduction, the waste of reactive resources may cause future stability problems. The centralized controls utilize the same among of reactive resource as the decentralized control, but lead to more loss reductions (additional 0.5 MW). However, the centralized control solutions are generated in much longer time frame by system-wide OPF, which are usually performed every 10~30 minutes.

REFERENCES

[1] D. Karlsson, L. Broski, and S. Ganesan, "Maximizing Power System Stability through Wide Area Protection," in *57th Annual Conference for Protective Relay Engineers*, 2004, p. 15.

[2] D. Kirschen and G. Strbac, "Why investments do not prevent blackouts," *The Electricity Journal* vol. 17, p. 7, Mar, 2004 2004.

[3] T. V. Cutsem and C. Vournas, "Voltage Stability of electric Power Systems," Kluwer Academic Publishers, 1998.

[4] D. P. Kothari and I. J. Nagrath, *Modern Power System Analysis*, 4th edition ed.: McGraw Hill Higher Education, 2007.

[5] S. Greene, I. Dobson, and F. L. Alvarado, "Sensitivity of the loading margin to voltage collapse with respect to arbitrary parameters," *IEEE Transaction on Power Systems,* vol. 12, p. 11, Feb, 1997 1997.

[6] X. R. Xie and Y. Z. Xin, "WAMS Applications in Chinese Power System," *IEEE Power and Energy Magazine,* vol. 4, p. 9, Jan, 2006 2006.

[7] B. Ingelsson and D. Karlsson, "Wide Area Protection Against Voltage Collapse," *IEEE Computer Applications in Power,* vol. 10, p. 5, Oct, 1997 1997.

[8] C. W. Taylor and D. C. Erickson, "WACS-Wide-Area Stability and Voltage Control System: R&D and Online Demonstration," *Proceedings of IEEE,* vol. 93, p. 15, May, 2005 2005.

[9] I. Kamwa and R. Grondin, "Wide-Area Measurement Based Stabilizing Control of Large Power Systems-A Decentralized/Hierarchical Approach," *IEEE Transaction on Power Systems,* vol. 16, p. 17, Feb 2001.

[10] F. Okou and L. A. Dessaint, "Power Systems Stability Enhancement Using a Wide-Area Signals Based Hierarchical Controller," *IEEE Transaction on Power Systems,* vol. 20, p. 13, Aug, 2005 2005.

[11] T. Hiyama and M. Kawakita, "Multi-Agent Based Wide Area Stabilization Stability Evaluation Agent Control of Power Systems Using Power System Stabilizer," *POWERCON 2004,* p. 5, Nov 2004 2004.

[12] J. Q. Venkatasubramanian, "A Real-Time Wide-Area Control Framework for Mitigating Small-Signal Instability in Large Electric Power System," *Proceedings of the 38th Hawaii International Conference on System Sciences* p. 10, 2005.

[13] H. Ni and G. T. Heydt, "Power System Stability Agents Using Robust Wide Area Control," *IEEE Transaction On Power Systems,* vol. 17, p. 9, Nov, 2002 2002.

[14] B. Milosevic and M. M. Begovic, "Voltage-Stability Protection and Control Using a Wide-Area Network of Phasor Measurement," *IEEE Transaction on Power Systems,* vol. 18, p. 7, Feb, 2003 2003.

[15] K. Vu and M. M. Begovic, "Use of Local Measurements to Estimate Voltage-Stability Margin," *IEEE Transaction on Power Systems,* vol. 14, p. 6, Aug, 1999 1999.

[16] M. Zima and M. Larsson, "Design Aspects for Wide-Area Monitoring and Control Systems," *Proceeding of the IEEE,* vol. 93, p. 16, May 2005 2005.

[17] "PJM Manual 03: Transmission Operations," 30th ed System Operations Division: PJM Interconnection, 2008.

[18] S. Mandal and V. S. Kolluri, "Coordinated Capacitor Bank Switching Using SVC Controls," *IEEE PES General Meeting,* p. 7, July 2008.

[19] H. Lefebvre and D. Fragnier, "Advantages of Coordinated Secondary Voltage Control in A Deregulated Environment," in *21, rue d'Artois, F-75008* E.-R. a. D. Division, Ed. Paris,France, 2000, p. 7.

[20] H.Vu, P.Pruvot, and C.Launay, "AN IMPROVED VOLTAGE CONTROL ON LARGE SCALE POWER SYSTEM," *IEEE Transactions on Power Systems,* vol. 11, p. 9, Aug, 1996 1996.

[21] M. D. Ilic and X. Liu, "Improved Secondary and New Tertiary Voltage Control," *IEEE Transactions on Power Systems,* vol. 10, p. 12, Nov, 1995 1995.

[22] "Voltage and reactive power management ": Midwest independent system operator, 2008.

[23] M. M. Begovic and A. *G.* Phadke, "CONTROL OF VOLTAGE STABILITY USING SENSITMTY ANALYSIS," *Transactions on Power Systems,* vol. 7, p. 10, Feb, 1992 1992.

[24] D. E. Julian, K. T. Vu, and R. P. Schulz, "Quantifying Proximity To Voltage Collapse Using The Voltage Instability Predictor (VIP)," 2000 2000.

[25] M. Begovic and D. Novosel, "A Novel Method for Voltage Instability Protection," in *Proceedings of the 35th Hawaii International Conference on System Sciences* Hawaii IEEE Computer Society, 2002.

[26] L. Warland and A. T. Holen, "A Voltage Instability Predictor Using Local Area Measurements (VIP++)," in *2001 IEEE Porto Power Tech Conference* Porto, Portugal, 2001, p. 6.

[27] B. Milosevic, *On Voltage Stability Monitoring and Control Using Multiagent Systems* 2002.

[28] A. Leirbuk and K. Vu, "Voltage Monitoring and Control for Enhanced Utilization of Power Grids," 2004 2004.

[29] G. Verbiˇ and F. Gubina, "A New Concept of Voltage-Collapse Protection Based on Local Phasors," *IEEE Transaction on Power Systems,* vol. 19, p. 6, Apr, 2004 2004.

[30] T. Alzahawi and M. S. Sachdev, "A Special Protection Scheme For Voltage Stability Prevention," *IEEE CCECE/CCGEI,* p. 4, 2005.

[31] I. ˇSmon and G. Verbiˇc, "Local Voltage-Stability Index Using Tellegen's Theorem," *IEEE Transaction on Power Systems,* vol. 21, p. 9, Aug, 2006 2006.

[32] S. Corsi and M. Pozzi, "The Coordinated Automatic Voltage Control of the Italian Transmission Grid-Part II: Control Apparatuses and Field Performance of the Consolidated Hierarchical System," *IEEE Transaction on Power Systems,* vol. 19, p. 9, Nov, 2004 2004.

[33] L. Ljung, *System identification : theory for the user*, 2nd ed.: Upper Saddle River, NJ : Prentice Hall PTR, c1999., 1999.

[34] M. A. Pai, *Energy Function Analysis for Power System Stability*: Kluwer Academic Publishers, 1989.

[35] David F.Walnut, *An introduction to wavelet analysis* Boston : Birkhäuser, c2002., 2002.

[36] C. K. Tang, "Voltage Security Management and Reactive Power Procurement in Ontario," in *IEEE PES General Meeting* Pittsburg: IEEE, 2008.

[37] H. Chen, "Practices of Reactive Power Management and Compensation," in *IEEE PES General Meeting*, I. P. E. Society, Ed. Pittsburg, 2008, p. 4.

[38] R. Faranda and A. Pievatolo, "Load Shedding: A New Proposal," *IEEE TRANSACTIONS ON POWER SYSTEMS,* vol. 22, p. 8, 2007.

[39] "Protection Against Voltage Collapse," CIGRE Task Force 34.08, 1998.

[40] J. V. Heche and J. Deuse, "COORDINATED VOLTAGE CONTROL EXPERIENCE IN BELGIUM," in *21, rue d'Artois, F-75008*. vol. Session 2000 Paris. France: CIGRE, 2000, p. 6.

[41] G. Trudel, S. Bernard, and G. Scott, "Hydro-Quebec's defence plan against extreme contingencies," *IEEE Transactions on Power Systems,* vol. 14, p. 9, Aug., 1999.

[42] Z. Feng, V. Ajjarapu, and D. J. Maratukulam, "A Practical Minimum Load Shedding Strategy To Mitigate Voltage Collapse," *IEEE TRANSACTIONS ON POWER SYSTEMS,* vol. 13, p. 7, Nov. 1998.

[43] C. M. Affonso, L. C. P. d. Silva, F. G. M. Lima, and S. Soares, "MW and MVar Management on Supply and Demand Side for Meeting Voltage Stability Margin Criteria," *IEEE TRANSACTIONS ON POWER SYSTEMS,* vol. 19, p. 8, Aug. Aug., 2004.

[44] S. Greene, I. Dobson, and F. L. Alvarado, "Sensitivity of Transfer Capability Margins With a Fast Formula," *IEEE TRANSACTIONS ON POWER SYSTEMS,* vol. 17, p. 7, Feb. Feb. 2002.

[45] P. Lagonotte and J. C. Sabonnadiere, "STRUCTURAL ANALYSIS OF THE ELECTRICAL SYSTEM : APPLICATION TO SECONDARY VOLTAGE CONTROL IN FRANCE," *IEEE TRANSACTIONS ON POWER SYSTEMS,* vol. 4, p. 8, May, 1989 1989.

[46] "Guide to WECC/NERC Planning Standards I.D: *Voltage Support and Reactive Power* " in *Technical Studies Subcommittee* Reactive Reserve Working Group 2006, p. 35.

[47] W. C. Merritt, C. H. Saylor, and R. C. Burchett, "Security constrained optimization-a case study," *IEEE Transaction on Power Systems,* vol. 3, p. 7, 1988.

[48] W. Qiu, A. J. Flueck, and F. Tu, "A new parallel algorithm for security constrained optimal power flow with a nonlinear interior point method," *IEEE Power Engineering Society General Meeting,* p. 6, Jun. 12-16 2005.

[49] L. G. Dias and M. E. El-Hawary, "Security-constrained OPF: Influence of fixed tap transformer fed loads," *IEEE Transaction on Power Systems,* vol. 6, p. 6, Nov. 1991.

[50] V. C. Ramesh and X. Li, "A fuzzy multi-objective approach to contingency constrained OPF," *IEEE Transaction on Power Systems,* vol. 12, p. 6, Aug. 1997.

[51] R. C. Dageneff, W. Neugebauer, and C. Saylor, "Security constrained optimization: An added dimension in utility systems optimal power flow technology," *IEEE Computer. Applications in PowerSystem,* p. 4, Oct. 1988.

[52] W. R. Thomas and A. M. Dixon, "Optimal reactive planning with security constraints," *IEEE Power Industry Computer Application Conf.,* p. 5, May. 1995.

[53] Y. T. Hsiao, C. C. Liu, and H. D. Chiang, "A new approach for optimal Var sources planning in large scale electric power systems," *IEEE TRANSACTIONS ON POWER SYSTEMS,* vol. 8, p. 8, Aug. 1993.

[54] T. Gomez and I. J. Perez-Arriaga, "A security-constrained decomposition approach to optimal reactive power planning," *IEEE Transaction on Power Systems,* vol. 6, p. 7, 1991.

[55] B. Cova, "Contingency constrained optimal reactive power flow procedures for voltage control in planning and operation," *IEEE Transaction on Power Systems,* vol. 10, p. 6, May 1995.

[56] A. P. S. Meliopoulos, *Power System Modeling, Analysis and Control* Georgia Institute of Technology 2004.

[57] H. G. K. Frauendorfer, "Optimization in Planning and Operation of Electric Power System," *Physica-Verlag Heidelberg,* vol. Physica-Verlag Heidelberg, 1993.

[58] A. K. Osyczka, "New method to solve generalized multicriteria optimization problems using the simple genetic algorithm," *Struct. Optim.,* vol. 10, p. 6, 1995.

[59] I. Das and J. E. Dennis, "A closer look at drawbacks of minimizing weighted sums of objectives for Pareto set generation in multicriteria optimization problems.," *Struct. Optim.,* vol. 14, p. 7, 1997.

[60] I. Das and J. E. Dennis, "Normal-boundary intersection: a new method for generating the Pareto surface in nonlinear multicriteria optimization problems," *SIAM J. Optim.,* vol. 8, p. 27, 1998.

[61] A. Messac and A. Ismail-Yahaya, "The Normalized Normal Constraint Method for Generating the Pareto Frontier," *Structural and Multidisciplinary Optimization,* vol. 25, p. 14, 2003 2003.

[62] *R. Fourer*, "*AMPL: A Modeling Language for Mathematical Programming*," *Northwestern University, AT&T Bell Laboratories,* 2007.

[63] I. Stanford Business Software, "Using AMPL/MINOS," *Supplement to AMPL: A Modeling Language for Mathematical Programming,* 2008.

[64] J. L. Sancha and J. L. Fesn, "Secondary Voltage Control: Analysis, Solutions and Simulation Results For the Spanish Transmission System," *IEEE Transaction on Power Systems,* vol. 11, p. 9, May, 1996 1996.

[65] H. F. Wang, H. Li, and H. Chen, "Coordinated Secondary Voltage Control to Eliminate Voltage Violations in Power System Contingencies," *IEEE TRANSACTIONS ON POWER SYSTEMS,* vol. 18, p. 8, May, 2003 2003.

[66] A. Conejo, "Pilot Bus Selection for Secondary Voltage Control," *European Transactions on Electrical Power*

Engineering (ETEP), vol. 3, p. 7, Sep,1993 1993.

[67] A.Conejo and M. J. Aguilar, "Secondary voltage control: Nonlinear selection of pilot buses, design of an optimal control law, and simuIatioil resuIts," *IEE ProcGener. Transm. Distrib.,,* vol. 145, p. 5, Jan,1998 1998.

[68] M. Ilic-Spong, "The no-gain Theorem and Localized Response for the Decoupled P- ˙ Network with Active Power Losses Included," *IEEE Transaction On Circuits and Systems,* vol. 32, p. 7, Feb, 1985 1985.

[69] M. Ilic-Spong and J. S. Thorp, "Localized Response Performance of the Decoupled Q-V Network," *IEEE Transactions on Circuits and Systems,* vol. Cas-33, p. 6, Mar, 1986 1986.

[70] D. M. Divan, W. E. Brumsickle, R. S. Schneider, B. Kranz, R. W. Gascoigne, D. T. Bradshaw, M. R. Ingram, and I. S. Grant, "A Distributed Static Series Compensator System for Realizing Active Power Flow Control on Existing Power Lines," *IEEE Transactions on Power Delivery,* vol. 22, p. 8, Jan. 2007.

[71] D. Divan, "Improving power line utilization and performance with D-FACTS devices," *IEEE Power Engineering Society General Meeting,* vol. 3, p. 5, June 2005 2005.

[72] J. Harjeet and D. Divan, "Design considerations for series connected distributed FACTS converter " *IEEE Transactions oon Industry Applications,* vol. 43, Dec. 2007.

[73] J. Deuse, K. Karoui, A. Bihain, and J. Dubois, "Comprehensive approach of power system contingency analysis," *2003 IEEE Bologna PowerTech Conference,* p. 6, June 2003.

[74] *PSS/E Program application guide* vol. 2: Shaw Power Technologies, Inc., 2004.